UCLouvain

École polytechnique de Louvain

Assessment of reliability in seismic design of reinforced concrete structures according to the 2nd generation of Eurocode 8

Author: **Yerald Caballero**
Supervisors: **João Saraiva Esteves Pacheco De Almeida, António Correia**
Readers: **Humberto Varum, Pierre Latteur**
Academic year 2021–2022
Master [120] in Civil Engineering

Abstract

The recent extreme seismic events recorded throughout the world have brought with them numerous questions to structural engineering; among them, knowing reliably if a structure already built has sufficient capacity to withstand large-scale events. Furthermore, there is a need to know the degree of overdesign or under-design in which recent structures have been designed, taking into account the seismic zone in which it is located, the type of structural system and the design concept used.

It is here where novel approaches, such as the probabilistic criterion, take place. The reliability evaluation developed in this project, established in the new generation of Eurocode 8 (EC8), is based on the modelling of a determined reinforced concrete structure (designed with the current version of EC8), in which non-linear response-history analyzes are performed in order to represent the seismic action and therefore, the required seismic demand. In this case, the seismic hazard defined for Belgium will be evaluated.

On the other hand, the method here developed with this second version of EC8 allows defining the limit values of the parameters that affect the annual probability of exceedance of a seismic event of a given limit state, when compared with the target annual probability of exceedance of a limit state for a given consequence class.

ACKNOWLEDGEMENTS

The preparation of this project was achieved thanks to the support of many people, including family and friends who were always supporting me in the last year.

First of all, I want to thank my parents, Octavio and Elena, who were supporting me every week from Panama and who knew how to perceive when a mood boost was necessary. I also want to recognize the encouragement from my sisters Lourdes and Eylyn, and my brother Osman. In the same way, I want to include my friends who are in my native country, for motivating me to continue despite the obstacles.

Since I arrived in Louvain-la-Neuve I knew that I would be living in a very special place, despite the pandemic situation that we have been going through. Proof of this are the great friends with whom I have been able to interact during the last two years, from all over the world, where I highlight the Italian friends who included me in their group as if I were one of them. These and many more moments have contributed to this wonderful experience of living and studying in Louvain-la-Neuve.

I thank my closest colleagues who welcomed me in a very human way and guided me in the process of completing the master's degree, including the introduction of Louvain-la-Neuve's life from Belgians viewpoint, which is one of the best experiences in my life.

Finally, I would like to thank my thesis supervisors Prof. João P. De Almeida and Dr. António Correia, for the patience shown and the trust placed in me to finish my thesis. Their continuous presence in the investigative process, as well as their organization, were essential to achieve short-term goals that were fundamental in achieving the project's objectives.

List of Figures

List of Tables

Contents

Part I

Contextualization

CHAPTER I-A

INTRODUCTION

I-A.1. Motivation

Only a few decades have passed since seismic action was taken into account in the design of structures within the European Union; in addition, the time in which it has been implementing truly reliable and accurate methods for seismic demand calculations in different sites is even less. For example, the first edition of Eurocode 8 (EC8) was released less than twenty years ago, with verified and acceptable design criteria, but at the same time with several somewhat conservative assumptions.

That is why the obligation to evaluate the behavior of recently designed structures and analyze if they require reinforcement structures, and the necessity to design structures with more complex and precise methods, reducing a possible overdesign or ensuring its integrity more adequately, are essentials.

It is here where the new (second) generation of EC8 takes place, methods such as non-linear response history analysis, but more demanding than the one described in the first edition of the normative, for the design of structures; and also presents in its annexes a method to evaluate the reliability of existing structures through a probabilistic approach.

The concept of reliability is commonly known as the probability that a product, system, or service will perform its intended function adequately for a specified period, or will operate under defined conditions without failure. The main components to establish the reliability of a product or service are the likelihood of mission success, the intended function, the performance level, the period, and the specific conditions. In the context of this project, the previous definition can be adapted as the assessment of the probability of failure in seismic design conditions of a reinforced concrete building according to the second generation of EC8, which will be specifically considered for the Near Collapse limit state.

I-A.2. Objectives

The need to evaluate the behavior and real capacity of a structure, as well as the probability of failure or collapse, is one of the most important challenges in seismic engineering and, therefore, in structural design. This project seeks to evaluate the probability of failure in seismic design of a reinforced concrete (RC) building designed according to the current generation of EC8, using a method proposed on the second generation.

Initially, the considered building will be designed taking into account the seismic hazard with a moderately seismic region, then it will be modeled and analyzed through different methods to

more accurately represent the seismic action to which the building will be subjected in that area. Finally, the full methodology provided by the second generation of EC8 to assess the reliability of the RC structure will be implemented.

The main aims of the project can be stated as follows:

1. To design a RC building using the current version of the EC8.
2. Examine the performance of the RC structure, in terms of displacement, subjected to a certain seismic force demand according to the second generation of EC8 and compare it to the current generation.
3. To evaluate the different procedures outlined in the second generation of EC8 to calculate the performance point in a given structure subjected to a certain seismicity level.
4. Assess the reliability (i.e., probability of failure) of the RC structure presented, according to second generation of EC8, and compare it to the target reliability for the Near-Collapse limit state (NC).
5. To analyze the evolution of the annual probability of exceedance depending on variations in the structure displacement capacity, the seismicity, and the spectral acceleration dispersion; to finally define the limit values of these three parameters for non-exceedance.

I-A.3. Structure of the document

The structure of this document is composed of five parts:

- Part I related to the contextualization, where the introduction, the motivation, and objectives of the work are described.
- Part II defines all the characteristics of the case-study structure including the structure elements predimensioning, design, and verifications that are followed according to EC8 current version.
- Part III focused on numerical modelling of the building, where the procedure adopted in each analysis (i.e., modal analysis, pushover analysis, and time history analysis) are conceptually developed and the results are explained within the corresponding chapters.
- Part IV contains the assessment provisions in terms of the simplified reliability-based verification format stated in the second generation of EC8, the results of the building reliability evaluation, and some parametric studies associated with the annual probability of exceedance.
- Finally, part V depicts the results of the analysis and verifications made for the current structure. Conclusions regarding the existing methods to consider seismic actions in newly designed structures are also covered in this section.

Part II

Characteristics of case-study structure

CHAPTER II-B

BUILDING STRUCTURE

II-B.1. Material properties

The analyzed structure is designed and modelled in reinforced concrete with principles and rules given in [14].

II-B.1.1 Concrete

The concrete considered is C30/37, which satisfies the material requirement stated in [16],where the minimum concrete class for Ductility Class Medium (DCM) is C16/20. The mechanical properties of concrete are enlisted in section III-D.3.1.

II-B.1.2 Reinforcing steel

Similarly, the steel used for longitudinal and transversal reinforcement is BE500S. To comply the specification for primary seismic elements, at least class B reinforcing steel shall be used. Mechanical properties of steel are also enlisted in section III-D.3.1.

II-B.1.3 Partial factors

Finally, throughout this project the partial factors used were $\gamma_c = 1.50$ for concrete and $\gamma_s = 1.15$ for steel, corresponding to ultimate limit state [14].

II-B.2. Seismic zone, soil type and other characteristics of the case-study structure

The structure to be studied is conceived as Residential building, which is defined as Importance class II for ordinary buildings according to EC8.

To identify the ground type of the structure under analysis, it is assumed a foundation ground soil classified as type B, according to [16]. It particularly means *Deposits of very dense sand, gravel, or very stiff clay* characterised by a gradual increase of mechanical properties with depth.

Furthermore, the seismic zone of the structure is assumed in a region with a peak ground acceleration PGA on rock: $a_{gR} = 2.5\ m/s^2$ for Type 1 and $a_{gR} = 1.7\ m/s^2$ for Type 2.

II-B.3. Structural systems

The building analyzed is composed by lateral load resisting systems identified as *Wall-Equivalent Dual System* (walls shear resistance is higher than 50% of the whole structural system resistance) in both directions according [16].

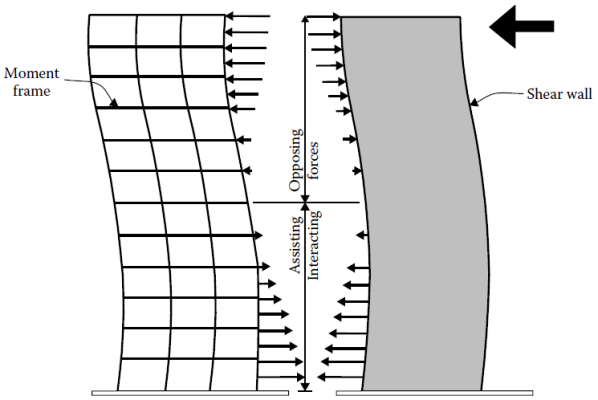

Figure II-B.1: Wall-equivalent dual system interaction. Adapted from [18]

II-B.3.1 Geometry in plan and elevation

The general dimensions of the building structure shown below (figure II-B.2 and II-B.3), represent a clear symmetric distribution of the lateral load resisting system in both horizontal directions of the building. In each direction, the building counts with two wall equivalent dual system which has one ductile wall and four columns per system.

In plan geometry, the building has four bays of 6m span in the X direction and two bays of 7m span in the Y direction, as depicted in figure II-B.4. In a complementary, see the 3D view of the building in figure II-B.5.

The dimensions of the sections are estimated in the next session within the pre-dimensioning procedure of the frame elements, walls, and slabs.

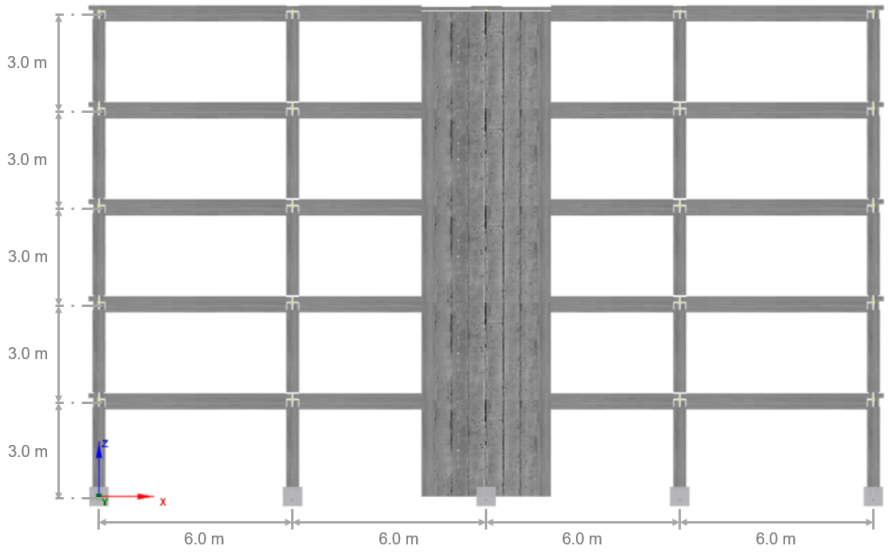

Figure II-B.2: Frontal elevation (X-Z) of the building

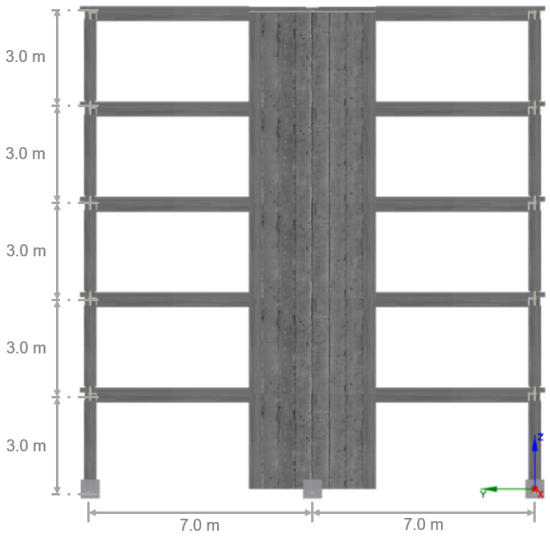

Figure II-B.3: Lateral elevation (Y-Z) of the building.

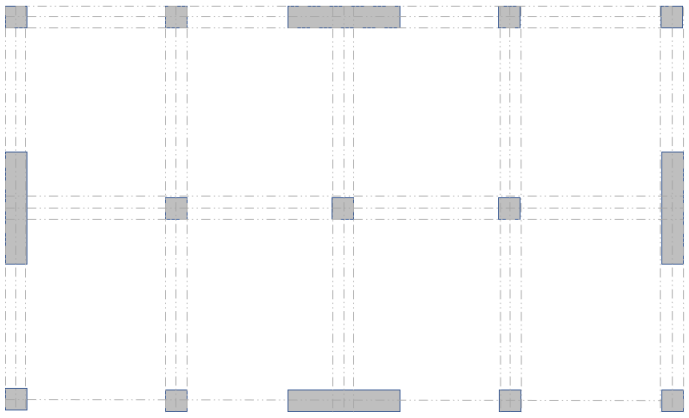

Figure II-B.4: Plan view of the building.

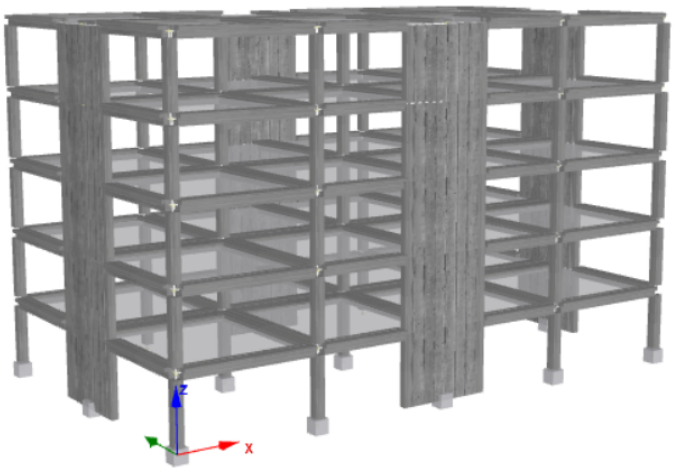

Figure II-B.5: Perspective view of the building.

II-B.4. Pre-dimensioning of RC frames

II-B.4.1 Loads

II-B.4.1.1 Self-weight and other permanent loads G_k

The permanent loads applied in the building are the addition of the external walls and partitions, and the loads associated with the reinforced concrete elements self-weights (wall, beams, columns, and slabs). Floor finishing is also part of the permanent loads per each building storey.

II-B.4.1.2 Variable loads Q_k

The corresponding variable loads depend on the building use, in this case civil dwellings. For this particular building, the roof is not accessible except for normal maintenance and repair.

Table II-B.1: Gravity loads summary

Storey	Permanent load G_k	Variable load Q_k
Roof	1 $\frac{KN}{m^2}$	1 $\frac{KN}{m^2}$
4	2.5 $\frac{KN}{m^2}$	2 $\frac{KN}{m^2}$
3	2.5 $\frac{KN}{m^2}$	2 $\frac{KN}{m^2}$
2	2.5 $\frac{KN}{m^2}$	2 $\frac{KN}{m^2}$
1	2.5 $\frac{KN}{m^2}$	2 $\frac{KN}{m^2}$

II-B.4.2 Load combinations

II-B.4.2.1 Fundamental combination

The structure is designed for the combinations of actions for persistent or transient design situations (fundamental combinations) according to [15].

$$\gamma_{G,j} G_{k,j} + \gamma_{Q,1} Q_{k,1} \tag{II-B.4.1}$$

where $\gamma_{G,j} = 1.35$ and $\gamma_{Q,1} = 1.50$

Wind, snow and thermals actions are not taken into account in the present structure.

II-B.4.2.2 Seismic combinations

Following [15], the design values of bending moments and forces are obtained from the structural analysis with seismic design situation calculated as follows:

$$\sum G_{K,j} + E_d + \psi_{2,i} Q_{K,i} \tag{II-B.4.2}$$

- $G_{k,j}$ is the characteristic value of a permanent action j;
- $Q_{K,i}$ is the characteristic value of a live-load action i;
- E_d is the design value of the seismic action;
- $\psi_{2,i} = \varphi\psi_1$ are the live load factors depending on building categories according to [15]. For residential areas $\psi_1 = 0.3$, φ is 0.8 for storeys with occupancy and 1.0 for roofs.

II-B.4.3 Dimensioning of elements

The sizing of frame members is mostly conceived to avoid different problems which affect either the element's behaviour or the reinforcement detailing. Three of the most important problems that can occur if the conceptual design is not appropriate are:

- Members with smaller dimensions than the required to meet the ULS verification leading to failure in shear or flexure, regardless of the reinforcement amount.
- Reinforcement congestion in undersized members.
- In the case of oversized members, a poor utilization of materials properties (with minimum longitudinal reinforcement only), with an undesirable distribution of overstrength over the structures, causing an inelasticity concentration in members which are not oversized.

II-B.4.3.1 Beams: for fundamental combination

It is known that in frame buildings with shear walls, beam depth is generally controlled by gravity loads. In addition, to facilitate continuity of the beam top and bottom bars across a column, the cross-section should be the same along each frame on a single storey level

Beam web should be sufficiently wide for the following reasons:

- To avoid inappropriate congestion of longitudinal bars. Preferably placed in one layer.
- Minimum concrete cover of stirrups needs to be provided at the sides of the beam.
- To provide a minimum axial distance of longitudinal bars to the concrete surface.

Moreover, as the seismic action is not taken into account at this phase, a good practice is to limit the bending moment and shear force ratios for the strength of the section, using the design bending moments and shear forces from the fundamental combination.

For bending moment:

$$\mu = \frac{M_{Ed}}{bd^2 f_{cd}} < 0.20 \tag{II-B.4.3}$$

For shear force:

$$\mu = \frac{V_{Ed}}{bdf_{cd}} < 0.30 \tag{II-B.4.4}$$

- V_{Ed}, M_{Ed} are design values from fundamental combination

- b is the beam width
- d is the effective depth of the beam
- L is the beam length

II-B.4.3.2 Columns: for seismic design situation

For this building, the column dimensions are kept constant in all storeys. This is a result of field experience and tests where was observed that a reduction in the column section, from the base to the roof of the buildings, produces a detriment in the seismic performance of columns at intermediate or upper storeys. Additionally, the changes in dimensions limit the detailing in the transition of column rebars through the joint.

Furthermore, for the building analyzed the column sections were designed as square and following the minimum length established in [16] for DCM columns: 200mm.

Upper limit on normalized axial load

In the same way, as in the beams, where the bending moment and shear force ratio were limited, the flexural ductility in columns plays an important role in the response of the structure. Therefore, EC8 sets upper limits on the column's axial load ratio for DCM, as follows:

$$\nu_d = \frac{N_d}{A_c f_{cd}} \leq 0.65 \tag{II-B.4.5}$$

- N_d column axial load in the seismic design situation
- A_c column cross section area

II-B.4.4 Equivalent Lateral Force (ELF) method

For the pre-dimensioning of elements, the seismic action is estimated using the *Equivalent Lateral Force Method*. This analysis assumes a dynamic behaviour of the structure mainly controlled by the fundamental period, and does not imply a substantial influence of higher vibration modes.

Base shear force

For each horizontal direction the base shear force is determined using the following expression:

$$F_b = V_b = S_d(T_1) m \lambda \tag{II-B.4.6}$$

- $S_d(T_1)$ is the ordinate(acceleration) of the design spectrum at period T_1 (see design spectrum in section III-D.3);
- T_1 is the fundamental period of vibration of the building for lateral motion in the direction considered;
- m is total mass of the building including selfweight of the elements;
- λ is the correction factor: 0.85 or 1.00.

The estimation of the natural period of the structure T_1 is approximated by the expression given in EC8:

$$T_1 = C_t H^{3/4} \tag{II-B.4.7}$$

$C_t = 0.075$ for moment resistant space concrete frames and H represents the height of the building.

Coefficient of repartition for reinforced concrete frames and structural walls

In dual systems, the proper distribution of the base shear force in the shear wall and the moment frames is necessary for structural analysis. To carry out this, the base shear force is distributed proportionally to their stiffness (shear wall and frames).

It is important to add that this procedure can be done if an equal lateral displacement is assumed in each storey as a result of the rigid diaphragm action, which is the case.

To express this distribution of the base shear force is used:

$$C_{walls} = \frac{K_{walls}}{K_{walls} + K_{frames}} \tag{II-B.4.8}$$

$$C_{frames} = \frac{K_{frames}}{K_{walls} + K_{frames}} \tag{II-B.4.9}$$

- K_{frames} is the frames stiffness
- K_{walls} is the walls stiffness

Finally, once the coefficients of distribution are determined, the corresponding lateral load can be computed so:

$$F_{frames/walls} = C_{frames/walls} F_b \tag{II-B.4.10}$$

Forces distribution per storey

Taking the fundamental period mode shape as approximated horizontal displacements increasing linearly along the height, the force distribution of the base shear in each storey can be taken as [9]:

$$F_j = F_b \frac{z_i * m_i}{\sum z_j * m_j} \tag{II-B.4.11}$$

- z_i,z_j represents the heights of the masses m_i,m_j above the application of the seismic action i.e. ground level.

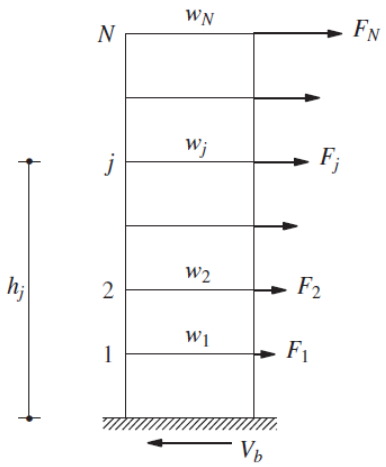

Figure II-B.6: Forces distribution in Equivalent Lateral Force method. Adapted from [5]

II-B.4.4.1 Preliminary structural analysis

For the preliminary design, the following assumptions in the structural analysis were taken for fast hand-calculations:

- The shear force at each frame storey is distributed homogeneously in each column.
- Moment equal to zero at the half-span of the beam.
- Moment equal to zero at the middle of the column height.
- The beam shear force and column axial force are obtained by static analysis in the nodes.

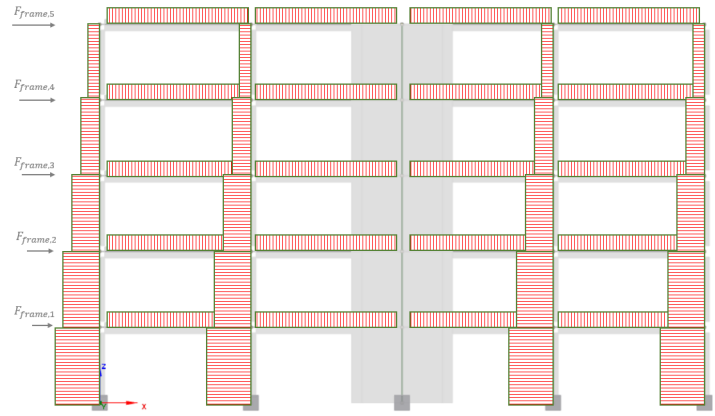

Figure II-B.7: Shear Force distribution-ELF

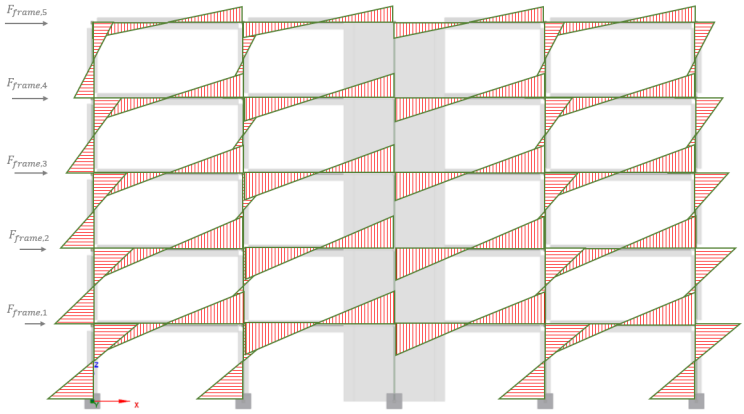

Figure II-B.8: Moments distribution-ELF

Recapping the gravity loads in each storey and applying the expressions mentioned in section II-B.4.3, the following dimensions are obtained:

Table II-B.2: Gravity loads and dimensions of frame elements.

Storey	Fundamental combination	Seismic design situation	Beam	Column
Roof	2.85 $\frac{KN}{m^2}$	1.30 $\frac{KN}{m^2}$	0.35m x 0.45m	0.40m x 0.40m
4	6.38 $\frac{KN}{m^2}$	2.98 $\frac{KN}{m^2}$	0.35m x 0.45m	0.40m x 0.40m
3	6.38 $\frac{KN}{m^2}$	2.98 $\frac{KN}{m^2}$	0.35m x 0.45m	0.40m x 0.40m
2	6.38 $\frac{KN}{m^2}$	2.98 $\frac{KN}{m^2}$	0.35m x 0.45m	0.40m x 0.40m
1	6.38 $\frac{KN}{m^2}$	2.98 $\frac{KN}{m^2}$	0.35m x 0.45m	0.40m x 0.40m

Besides, the wall dimensions of the dual system are those that satisfy the dimensions criteria of the ductile walls (i.e. the ratio length to web thickness is at least 4) according Eurocode 8. The walls of this building have 4m length and 0.30m width.

Subsequently, once we have the selfweight of the whole structure we can compute the total masses in each storey, and in this way the Equivalent Lateral Force method can be applied correctly. See table II-B.3.

Table II-B.3: Storey masses and forces for the Equivalent lateral force method in the entire building.

Storey	z_i(m)	m_i(ton)	$z_i m_i$(tonm)	F_j(KN)	Storey shear V_j (KN)
Roof	15	255.04	3825.57	440.16	440.16
4	12	337.65	4051.87	466.20	906.36
3	9	337.65	3038.90	349.65	1256.01
2	6	337.65	2025.94	233.10	1489.11
1	3	337.65	1012.97	116.55	1605.66
Total	-	1605.66	13955.25	1605.66	-

As already explained, the distribution of storey shear can be carried out then with the coefficient of repartition calculated for the frame structures and walls: $C_{walls} = 0.966$ and $C_{walls} = 0.028$. Finally, the structural analysis is developed with the assumptions pointed out at the beginning of this section.

II-B.4.5 Final verification

II-B.4.5.1 Beams verification for bending and shear: seismic action combined with gravity loads

As the last verification, the use of equations (II-B.4.3) and (II-B.4.4) considering the internal forces from the combined action of seismic forces and gravity loads described in equation (II-B.4.2)

II-B.4.5.2 Columns verification for axial load ratio: seismic action combined with gravity loads and fundamental combination

Similar to the beams, for columns some limitations regarding the axial load ratio are adopted.

For seismic action combined with gravity loads:

$$\frac{N_{qp}}{A_{col}} \leq 0.65 f_{cd}$$

For fundamental combination:

$$\frac{N_{Ed}}{A_{col}} \leq 0.8 f_{cd}$$

II-B.5. Reinforced concrete frames design and detailing for Ultimate Limit State (ULS)

II-B.5.1 Resistance condition

The resistance condition needs to be verified from the global response of the structure to the seismic design action, for each direction of analysis (X and Y), which must consider the vertical loads, modal analysis and the effect of the accidental eccentricities [19].

The steel reinforcements in beams, columns, and joints are calculated according to the specific design and detailing requirements in EC8.

The latter means reinforcement ratios adopted in design $\rho = 1\%$ for columns, $\rho = (0.3 - 0.5)\%$ for bottom reinforcement in beams and $\rho = (0.5 - 1.0)\%$ for upper reinforcement in beams. Additionally, a balanced reinforcement in both faces of the beams was adopted.

For the Ultimate Limit State (ULS), the following relation between design values of the action effect E_d and design resistances R_d shall be satisfied for all structural elements:

$$E_d \leq R_d$$

II-B.5.1.1 Beams

Bending moment resistance

The required longitudinal steel reinforcement $A_{s,req}$ area and the resistant moment are calculated according to the rectangular stress block distribution assumption. Design and detailing followed the requirements of [14].

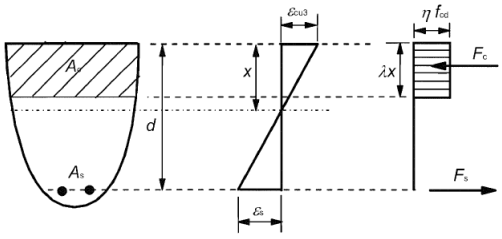

Figure II-B.9: Rectangular stress distribution. Adapted from [14].

Reduced moment:

$$\mu = \frac{M_{Ed}}{bd^2 f_{cd}} \tag{II-B.5.1}$$

Mechanical percentage of reinforcement:

$$w = 1 - \sqrt{1 - 2\mu} \tag{II-B.5.2}$$

Steel reinforcement area:

$$A_s = \frac{wbdf_{cd}}{f_{yd}} \tag{II-B.5.3}$$

Shear resistance
In the presented design, only the stirrups perpendicular to the axis of the beam are considered in the calculation of the shear resistance:

$$V_{Rd} = V_{Rd,s} = \frac{A_{sw} z f_{ywd} \cot\theta}{s} \tag{II-B.5.4}$$

Also, the concrete strut strength verification according with [14] needs to be checked:

$$V_{Rd,max} = \frac{\alpha_{cw} b_w z \nu_1 f_{cd}}{\cot\theta + \tan\theta} \tag{II-B.5.5}$$

θ represents angle between the concrete compression strut and the beam axis perpendicular to the shear force, for all beams $\theta = 45°$ was adopted

II-B.5.1.2 Columns

Bending moment resistance [6]

Symmetrical reinforcement distribution in column sections and equal in the four faces were adopted. The required steel reinforcement area A_{req} was calculated according to the following model and meeting the criteria of [14].

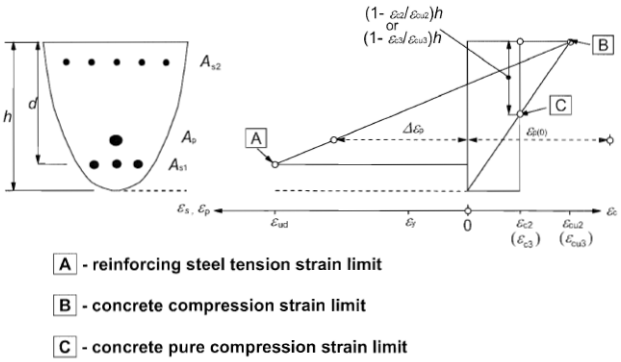

Figure II-B.10: Possible strain distributions in the ULS. Adapted from [14]

Reduced moment:

$$\mu = \frac{M_{Ed}}{bh^2 f_{cd}} \tag{II-B.5.6}$$

Normalized axial force:

$$\nu = \frac{N_{Ed}}{bhf_{cd}} \leftrightarrow \nu_c = 1 - \nu \tag{II-B.5.7}$$

Mechanical reinforcement ration:

$$w = \frac{A_{s,total}f_{yd}}{bhf_{cd}} \leftrightarrow A_{s,total} = A_{s1} + A_{s2} \tag{II-B.5.8}$$

Neutral axis ratio:

$$k = \frac{x}{d} \tag{II-B.5.9}$$

Also $\beta = \frac{h}{d}$ and $\lambda_s = 0.5 - \frac{d_c}{h}$. And since $w_1 = w_2 = \frac{w}{2}$ then $\frac{k}{\beta} = 1.25\nu$

$$\begin{cases} w = \frac{\mu - 0.5\nu\nu_c}{\lambda_s} & 0 \leq \nu \leq 1 \\ w = \frac{\mu}{\lambda_s} - \nu_c & 1 \leq \nu \\ w = \frac{\mu}{\lambda_s} - \nu & \nu < 0 \end{cases}$$

Shear resistance

For the column shear resistance, the same criteria and assumptions are applied as the one for beam shear resistance. See section II-B.5.1.1.

II-B.5.1.3 Beam-column joints

For the horizontal confinement reinforcement in joints, established requirements for primary seismic beams with columns according to [16] are applied.

II-B.5.2 Second-order effects revision

Fundamental combination

Second-order effects in the analysis for the fundamental combinations (i.e., for the factored gravity loads) are allowed to be neglected if the column exigencies for the slenderness limits are checked and ensured as stated in [16].

$$\lambda_{lim} = \frac{20ABC}{\sqrt{n}} \tag{II-B.5.10}$$

For this verification, the following values were assumed: $A = 0.7$, $B = 1.1$ and $C = 0.7$. $n = \nu$ named as relative normal force [19].

The slenderness ratio is defined as follows:

$$\lambda = \frac{I_0}{i}$$

where I_0 is the effective length (see figure II-B.11) and i is the radius of gyration of the uncracked concrete section.

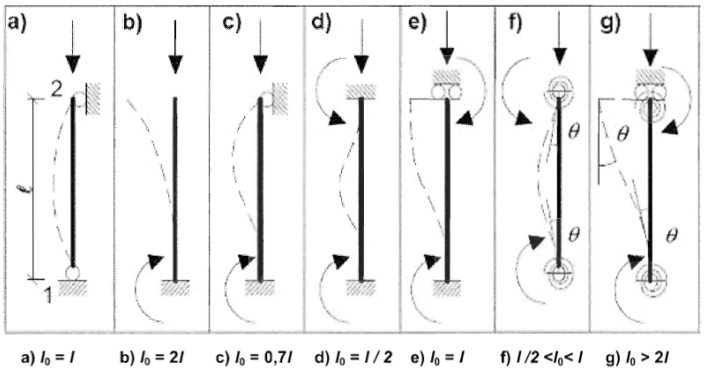

Figure II-B.11: Buckling modes and corresponding effective lengths for isolated members. Adapted from [14]

Seismic design situation

Correspondingly, the second-order effects resulting from the seismic situation analysis need not be taken into account following [16], if the following limitation is verified and ensured:

$$\theta = \frac{P_{tota} d_r}{V_{tot} h} \tag{II-B.5.11}$$

where:

- θ is the interstorey drift sensitivity coefficient;
- P_{tot} is the total gravity load at and above the storey considered in the seismic design situation;
- d_r is the design interstorey drift, evaluated as the difference of the average lateral displacement d_s at the top and bottom of the storey (see next section);
- V_{tot} is the total seismic storey shear; and h is the storey height

Average lateral displacement d_s according EC8

After a linear analysis is performed, displacements induced by the seismic action are calculated based on elastic deformation of the structural systems, using the following expression:

$$d_s = q_d d_e \tag{II-B.5.12}$$

with:

- d_s as the displacement of a point of the structural system induced by the design seismic action;
- q_d as the behaviour factor q unless otherwise specified;
- d_e as the displacement of the same point of the structural system, obtained from design response spectrum analysis.

II-B.5.3 Capacity design rule

Concrete members are inherently brittle in shear: if they reach their shear resistance before yielding in flexure, they suffer a drastic drop in resistance right after their peak. This shows that shear failure of members before flexural yielding must be avoided.

Eurocode 8 accomplishes this goal by enforcing the "capacity design" of all members in shear. Furthermore, designing against this "capacity design" shear, instead of the one obtained from the analysis for the seismic design situation, prevents a shear failure of the beams or the column for any level of earthquake [9].

II-B.5.3.1 Beams

Under EC8, the design shear force shall be determined based on equilibrium of the beam under:

1. the transverse load acting on it in the seismic design situation and
2. end moments $M_{i,d}$, corresponding to plastic hinge formation for positive and negative directions of seismic loading. See figure II-B.12.

$$M_{i,d} = \gamma_{Rd} M_{Rb,i} min\left(1, \frac{\sum M_{Rc}}{\sum M_{Rb}}\right)$$

with:

- $\gamma_{Rd} = 1.0$ for DCM beams;
- $M_{Rb,i}$ is the design value of the beam moment of resistance at end i in the sense of the seismic bending moment under the considered sense of the seismic action;
- $\sum M_{Rc}$ and $\sum M_{Rb}$ are the sum of the design values of the moments of resistance of the columns and the sum of the design values of the moments of resistance of the beams framing into the joint.

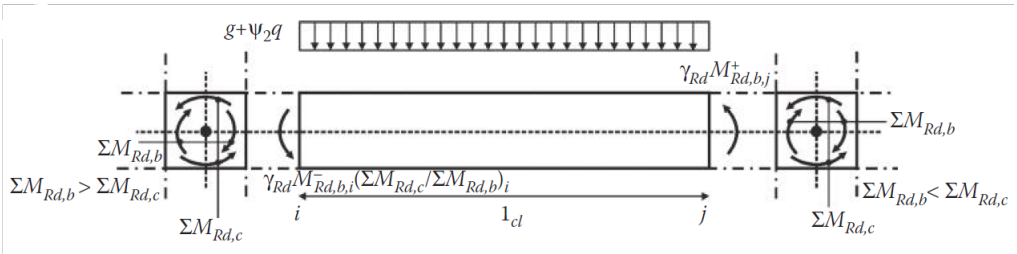

Figure II-B.12: Static representation of design shear force for capacity design rules on beams. Adapted from [16]

II-B.5.3.2 Columns

In the same way, for columns the design value of shear force shall be determined based on the equilibrium of the column under end moments M_{id}, corresponding to plastic hinge formation for positive and negative directions of seismic loading, as established in [16]. See figure II-B.13.

$$M_{i,d} = \gamma_{Rd} M_{Rc,i} min\left(1, \frac{\sum M_{Rb}}{\sum M_{Rc}}\right)$$

with:

- $\gamma_{Rd} = 1.1$ for DCM columns;
- $M_{Rc,i}$ is the design value of the column moment of resistance at end i in the sense of the seismic bending moment under the considered sense of the seismic action;
- $\sum M_{Rc}$ and $\sum M_{Rb}$ are as defined in subsection II-B.5.3.1
- $M_{Rc,i}$ and $\sum M_{Rc}$ should correspond to the column axial force(s) in the seismic design situation for the considered sense of the seismic action.

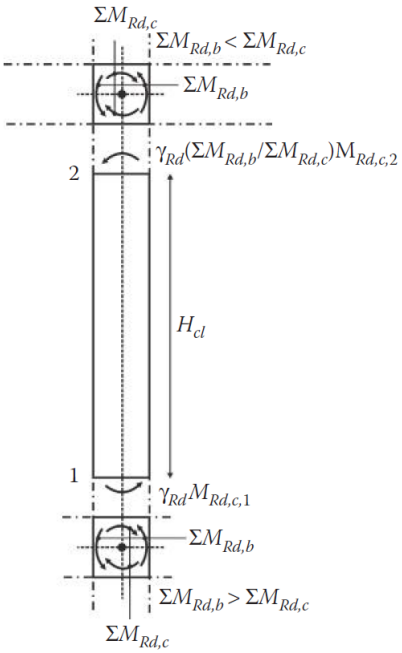

Figure II-B.13: Static representation of design shear force for capacity design rules on columns. Adapted from [16]

II-B.5.4 Geometrical constraints and detailing rules

Beams

Some limitations in beams geometry specified in EC8 are:

- Eccentricity of the beam axis relative to that of the column should be limited to less than $b_c/4$, where b_c is the largest cross-sectional dimension of the column normal to the longitudinal axis of the beam.
- The width b_w of a primary seismic beam shall satisfy:

$$b_w \leq min\{b_c + h_w; 2b_c\}$$

Columns

The main geometrical constraints adopted for columns are:

- Minimum cross-section dimension shall be not less than 200mm.
- Unless $\theta \leq 0.1$, calculated with equation (II-B.5.11), the cross-sectional dimension of primary seismic columns should not be smaller than one tenth of the larger distance between the point of contraflexure and the ends of the columns; and $250mm$.

II-B.5.4.1 Local ductility in beams

In the detailing for local ductility in beams, the requirements in the critical regions $l_{cr} = h_w$ (where h_w is the beam depth) of primary seismic, a value of the curvature ductility factor was used according to these expressions [19]:

$$\mu_\phi = 2q_0 - 1 \leftrightarrow T_1 \geq T_c$$
$$\mu_\phi = 1 + \frac{2(q_0 - 1)T_c}{T_1} \leftrightarrow T_1 \leq T_c$$

where: T_1 is the fundamental period of a building and q_0 the basic value of the behaviour factor.

Also, the following rules regarding the reinforcement at both flanges of the beam need to be verified:

- The compression zone reinforcement must be at least equal to half of the reinforcement provided at the tension zone.
- Reinforcement ratio in tension zone does not exceed:

$$\rho_{max} = \rho' + \frac{0.0018 f_{cd}}{\mu_\phi \cdot \epsilon_{sy,d} \cdot f_{yd}}$$

- Along the entire length of the beams, reinforcement ratio of the tension zone shall be at least equal to:

$$\rho_{min} = 0.5 \frac{f_{ctm}}{f_{yk}}$$

II-B.5.4.2 Local ductility and adequate confinement in columns

For the detailing of primary seismic columns for local ductility the following requirements established in [16] are satisfied:

- Longitudinal reinforcement ratio ρ_l between 0.01 and 0.04.
- At least one intermediate bar provided between corner bars
- Critical region length l_cr computed from: $l_{cr} = max\left(h_c; b_c; \frac{l_{cl}}{6}; 0.45m\right)$

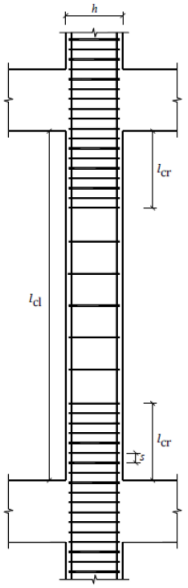

Figure II-B.14: Critical regions in columns. Adapted from [16]

- Minimum diameter for hoops within the critical region of the primary column: 6mm.
- Maximum hoops spacing does not exceed:

$$s = min\left(\frac{b_o}{2}; 175; 8d_{bL}\right)$$

- Maximum consecutive longitudinal bars engaged by hoops or cross-ties spacing does not exceed 200mm.
- Ductility factor μ_ϕ should be estimated similarly to section II-B.5.4.1.
- Also, the effective mechanical αw_{wd} ratio of confinement hoops shall satisfy:

$$\alpha \cdot w_{wd} \geq 30 \cdot \mu_\phi \cdot \nu_d \cdot \epsilon_{sy,d} \cdot \frac{b_c}{b_o} - 0.035$$

II-B.6. Reinforced concrete frames design and detailing for Service Limit State (SLS)

II-B.6.1 Damage limitation

Following the Eurocode 8 requirement for damage limitation, it needs to be ensured that the structure under a certain seismic action having a larger probability of occurrence than the design seismic action corresponding to the "No-collapse requirement", the interstorey drifts (i.e., relative translational displacement between two consecutive storeys divided by the storey height) can be limited in accordance with [16]:

$$d_r \cdot \nu \leq 0.005 \cdot h$$

where d_r is the design interstorey drift and h is the storey height, ν is the reduction factor which takes into account the lower return period of the seismic action associated with the damage limitation requirement (recommended value of ν for important class II is equal to 0.5 [19]).

The previous limitation corresponds to buildings having *non-structural elements of brittle materials attached to the structure*, this assumption has been made for the current building.

Furthermore, verifications of interstorey drifts for each floor caused by the considered seismic level were carried out, thus complying with interstorey drifts less than the limit of 0.5%. Therefore, is important to mention that this criterion has not controlled the design of the frame elements.

Part III

Numerical Modelling

CHAPTER III-C

INTRODUCTION TO SEISMOSTRUCT

Description of the software

Seismostruct is a finite element software part of SEISMOSOFT group capable of predicting large displacement behaviour of structures under static or dynamic loading, and very efficient in performing nonlinear inelastic analysis through a fiber discretization approach. It takes into account both geometric nonlinearities and material inelasticity, and linear analysis can also be performed.

Furthermore, is particularly suited and validated for seismic analysis especially for structural assessment and structural retrofitting. Additionally, its interface is user-friendly.

Using this software, the user can execute several analysis types such as eigenvalue analysis, response spectrum analysis, static pushover, static adaptive pushover, static/dynamic time-history analysis, incremental dynamic analysis, and others.

Figure III-C.1: Seismosoft logo. Adapted from *www.seismosoft.com*

Adaptation for case-study structure

Recalling the use of the Lateral Equivalent Force method (LEF) for the estimation of the internal forces in the frame elements, a more complex structural analysis needs to be carried out to have a better approximation of those forces taking into account the dynamic response of the structure. In this case, and as often, Response Spectrum Analysis (RSA) also known as *modal analysis* is executed to evaluate that dynamic solicitation of the structure within the linearity of the materials.

On the other hand, to assess the non-linear response of the structure pushover analysis and time history analysis are performed for static and dynamic loading scenarios respectively. The following sections describe the analysis carried out with the different parameters and assumptions taken for the numerical modelling.

CHAPTER III-D

RESPONSE SPECTRUM ANALYSIS (RSA)

III-D.1. Description of RSA method

Response Spectrum Analysis is a linear (pseudo) dynamic analysis method that provides the peak values of response quantities, such as forces and deformations, of structures under seismic excitation. It is called (pseudo) dynamic because the response quantities for certain ground motion can be estimated by static analysis rather than time-history dynamic analysis [9].

To implement the above, equivalent static forces is applied to the support of the structure, those forces are distributed to all free degree of freedom of the structure, and they represent the contribution from each natural vibration mode.

III-D.1.1 Dynamics of multiple degrees of freedom system

The dynamic equilibrium condition of a multi-degree of freedom system with N (numbers of vibration modes) uncoupled equations subjected to a ground motion is:

$$\mathbf{M}\ddot{U} + \mathbf{P}_r(\dot{U}(t), U(t)) = -\mathbf{M}\mathbf{J}\ddot{u}_g(t) \tag{III-D.1.1}$$

where **M** is the mass matrix, **Pr** the resisting forces of the system which can be dependent on velocity $U(t)$ and/or displacement $U(t)$ of the system. The right side of the equation is known as *effective earthquake forces* where **J** is the ground motion influence factor of each degree of freedom and $\ddot{u}_g$ is the ground acceleration.

The equation (III-D.1.1) can also be written in terms of the damping matrix **C** and the stiffness matrix **K** as follows:

$$\mathbf{M}\ddot{U} + \mathbf{C}\dot{U} + \mathbf{K}U(t) = -\mathbf{M}\mathbf{J}\ddot{u}_g(t) \tag{III-D.1.2}$$

III-D.1.2 Modal participation factor Γ

However, a very common loading case, applicable to many practical situations (including earthquake excitation), is given by the assumption that the external loading does not vary with time. That is to say for our particular case the effective earthquake forces, right side of expression (III-D.1.2), can be represented as the product of a load pattern P_{ref} that does not depend on time and a scalar loading parameter $\lambda(t)$ that depends on time.

Taking $P_{ref} = \mathbf{MJ}$ and $\lambda(t) = -\ddot{u}_g(t)$, the *modal participation factor* is defined as:

$$\Gamma_j = \frac{\phi_j^T P_{ref}}{\phi_j^T M \phi_j} = \frac{\phi_j^T M J}{\phi_j^T M \phi_j} \tag{III-D.1.3}$$

It should be recalled from dynamic of structures concepts, ϕ_j is the natural mode shape of the j vibration mode, obtained from the corresponding natural frequency W_n (or natural periods $T_n = 2\pi/W_n$) that represent the dynamic characteristics of the structure. Those features can be calculated from the eigenvalues of the characteristic equation, also known as *frequency equation* [1].

III-D.1.3 Effective modal mass

On the other hand, an important quantity called *effective modal mass* depicts the part of the total mass of the structure responding to the ground excitation in mode j. This quantity is a good indicator to know the direction of the seismic action that most excites a certain vibration mode. The sum of the effective modal mass for all modes in a given direction is equal to the total mass of the structure.

Equally important is the contribution of different vibration modes ϕ_j to the total dynamic response of the structure, commonly normalized by the total mass of the structure excited in the relevant direction. Is denoted then as the *participating mass ratio*. The sum of the participating mass ratios for all modes and a given direction is equal to 1, as suspected [7].

III-D.1.4 Response spectrum

The seismic response of a single degree of freedom system can be obtained through numerical procedure as a function of a time, this is called "response-history" analysis. In practice, the dimensioning of a structure is conceived considering the maximum response values, which may be determined from a *response spectrum*.

The response spectrum is a central concept in Earthquake Engineering. It gives the maximum absolute values of a response quantity (typically acceleration, velocity, and/or displacement) as a function of the natural vibration period T_n. This plot is normally computed by performing a response-history analysis of several single degree of freedom systems with different natural periods (figure III-D.1), subjected to the same ground motion. The damping ratio ξ is also fixed.

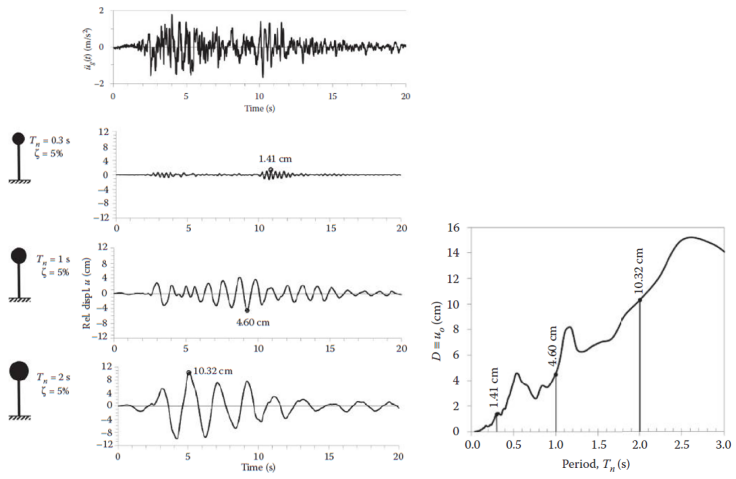

(a) **(b)**

Figure III-D.1: (a) Ground motion and displacement response of 3 single degree of freedom systems (b) Example of displacement response spectrum. Adapted from [5]

In terms of seismic analysis, once the dynamic response of a structure is evaluated, the internal forces are estimated by applying a static analysis of the structure subjected to the equivalent forces mentioned at the beginning of this section. Those forces shall satisfy the following expression in each time t:

$$P_{eq} = k \cdot u(t) = m \cdot w^2 \cdot u(t) = m \cdot S_{pa}(t) \tag{III-D.1.4}$$

where S_{pa} is the pseudo-acceleration that represents the product between the square natural frequency w^2 and the displacement response history $u(t)$ of the structure.

III-D.1.5 Combination of modal responses

As mentioned before the total structure response is a contribution of several modes. Therefore, the determination of the peak value response represented by the combined contribution of all relevant vibration modes is essential. In the analysis by means of response spectra, only the maximum values of the response for individual modes are known and is almost impossible that they can occur simultaneously in all vibration modes.

Nonetheless, several approaches have been developed for the combination of responses in different vibration modes. Below is the description of some combination rules.

Sum of the Maximum Absolute Values (ABSSUM)
The assumption that all maxima occur at the same instant and in the same direction produces an upper bound value for the response quantity. One can induce that it is an assumption too conservative.

$$E_E = \sum_{j=1}^{N} |\phi_{i,j}\, q_{j,max}|$$

Square-root-of Sum-of-Squares (SRSS)
The SRSS combination is intended to represent the expected value of the peak response for a set of ground motions, which are typically defined by a (smooth) response spectrum. It provides very close estimates of peak responses if the natural frequencies of the relevant modes are well separated. The main drawback of this rule is when the frequencies are closely spaced. According to Eurocode 8, it can be used if the periods of two relevant vibration modes accomplish (with $T_j \leq T_i$) the condition $T_j \leq 0.9\dot{T}_i$.

The resulting value of any response quantity is obtained as the square root of the sum of the squared values of this response quantity for all the relevant modes as follows:

$$E_E = \sqrt{\sum_{j=1}^{N} (\phi_{i,j}\, q_{j,max})^2} \tag{III-D.1.5}$$

Complete Quadratic Combination (CQC)
Another combination rule, which takes into account the correlation between different vibration modes and is applicable also for closely spaced natural frequencies, is the *Complete Quadratic Combination* (Der Kiureghian 1981; Wilson et al. 1981) defined as follows:

$$E_E = \sqrt{\sum_{n=1}^{M} \sum_{r=1}^{M} \rho_{nr}\, E_{En}\, E_{Er}} \tag{III-D.1.6}$$

with n and r as the indexes of vibration modes, ρ_{nr} is the correlation coefficient. For the case where the damping ratio ξ is the same for all modes, ρ_{nr} can be determined as:

$$\rho_{nr} = \frac{8\xi^2(1+\beta_{nr})\beta_{nr}^{3/2}}{(1-\beta_{nr}^2)^2 + 4\xi^2\beta_{nr}(1+\beta_{nr})^2}$$

where β_{nr} is the ratio of the frequencies of the modes n and r: $\beta_{nr} = \frac{w_n}{w_r} = \frac{T_r}{T_n}$.

An important remark to notice is in the case of well-separated natural frequencies the CQC rule reduces to the SRSS combination rule.

Equally important as the combination rules are the number of vibration modes to be taken into account, to obtain reasonably accurate results. In earthquake engineering analysis the influence of higher modes is typically small for displacements and increases for more local response quantities. Following EC8, to apply the modal Response Spectrum Analysis one needs to consider: (i) all modes, from the lowest, until the sum of the effective modal masses corresponds to at least 90% of the total mass; (ii) all modes with effective modal masses greater than 5% of the total mass are considered [9].

III-D.2. Applied loads and distribution of masses

In the spatial representation of the building required to perform Response Spectrum Analysis, the gravity (vertical) loads and the masses of the concrete elements used in section II-B.4.4.1 have been divided into horizontal and vertical elements unlike the ELF analysis of the mentioned section before. As a reminder, the vertical loads need to be applied using the expression II-B.4.2 for the seismic combination.

III-D.2.1 Horizontal elements

To consider the horizontal elements, the masses of slabs and beams are converted into loads, and using superposition with the external loads, they can be directly imposed on the beams.

Table III-D.1: Vertical loads applied on beams per storey.

Storey	Beams(perimeter)-Y	Beams(interior)-Y	Beams(perimeter)-X	Beams(interior)-X
Roof	14.7 KN/m	21.4 KN/m	12.6/18.6 KN/m	25.2 KN/m
4	18.4 KN/m	26.7 KN/m	15.7/23.2 KN/m	31.5 KN/m
3	18.4 KN/m	26.7 KN/m	15.7/23.2 KN/m	31.5 KN/m
2	18.4 KN/m	26.7 KN/m	15.7/23.2 KN/m	31.5 KN/m
1	18.4 KN/m	26.7 KN/m	15.7/23.2 KN/m	31.5 KN/m

Table III-D.1 shows the applied forces in the horizontal elements (i.e., beams) taking into account the offsets within the interception of the beams with the columns, walls, and slabs. At this point the weight distributed for horizontal elements is $W_{horizontal} = 13537.5\,KN$ which corresponds to $M_{horizontal} = 1380\,ton$.

III-D.2.2 Vertical elements

Similar to the horizontal elements, the masses of the columns and walls are transformed into weight, and then using a uniform distribution in each node, the loads are applied.

Table III-D.2: Vertical loads applied in nodes per storey.

Storey	Total weight	Load in nodes
Roof	246 KN	16.4 KN
4	492 KN	32.8 KN
3	492 KN	32.8 KN
2	492 KN	32.8 KN
1	492 KN	32.8 KN

Weight of the columns and walls: $W_{vertical} = 2214\ KN$ corresponding to $M_{vertical} = 225.69\ ton$. The total weight and total mass of the building result as:

$$W_{total} = W_{horizontal} + W_{vertical} = 15751.5\ KN$$

$$M_{total} = M_{horizontal} + M_{vertical} = 1605.7\ ton$$

A better representation of the applied loads for this analysis can be found in figure III-D.9.

III-D.2.3 Seismic action representation

As described in section III-D.1.4, the response spectrum defines the peak responses of all possible single-degrees-of-freedom systems for a particular ground motion. However, for the design of new structures or the seismic safety evaluation of existing structures, one needs a *design spectrum* more representative of ground motions recorded at a given site during past earthquakes [2].

The (smooth) design spectrum is a specification of the level of seismic design force, or deformation, as a function of natural vibration period and damping ratio.

To compute the design seismic action according to Eurocode 8, the following parameters need to be defined:

- Reference return period for the design seismic action, chosen by the National Authorities;
- Peak ground acceleration (PGA) on rock, resulting from probabilistic seismic hazard analysis;
- Important class of the building, defined from the use and occupancy of the building;
- Representative ground type, depending on the local soil conditions;
- Predominant surface wave magnitude of earthquakes that contribute to the seismic hazard.

Eurocode 8 defines the ground type in terms of the average shear wave velocity, $V_{s,30}$, in the top 30m below the ground surface. If the $V_{s,30}$ is not available, other parameters like the SPT blow

count, N, or the soil undrained shear strength, c_u, may be used.

Elastic response spectrum

Finally, the horizontal component of the seismic action, the (pseudo) acceleration elastic response spectrum A, which in EC8 is denoted as $S_e(T)$ is defined by the following equations:

$$\begin{cases} 0 \leq T \leq T_B & S_e(T) = a_g\, S\, [1 + \frac{T}{T_B}(2.5\eta - 1)] \\ T_B \leq T \leq T_C & S_e(T) = 2.5\, a_g\, S\, \eta \\ T_C \leq T \leq T_D & S_e(T) = 2.5\, a_g\, S\, \eta\, [\frac{T_C}{T}] \\ T_D \leq T \leq 4s & S_e(T) = 2.5\, a_g\, S\, \eta\, [\frac{T_C T_D}{T^2}] \end{cases}$$

where:

- T is the vibration period of a linear single-degree-of-freedom system;
- a_g is the design acceleration on rock;
- T_B is the lower limit of the constant acceleration branch;
- T_C is the upper limit of the constant acceleration branch;
- T_D is the value defining the beginning of the constant displacement response branch;
- S is the soil factor;
- η is the damping correction given by $\eta = \sqrt{10/(5+\xi)} \geq 0.55$ with the damping ratio of the structure ξ expressed as percentage.

Statistical analyses of recorded events have shown that the spectral shape is dependent on the magnitude and almost independent of distance (from source to the site). This is the reason why the parameters S, T_B, T_C, and T_D are defined for two different spectral shapes that depend on the area seismicity: Type 1 defines areas of high intensity characterized by earthquakes with a surface wave magnitude larger than 5.5; Type 2 defines areas of low intensity characterized by earthquakes with a surface wave magnitude smaller than 5.5. See figure (III-D.2).

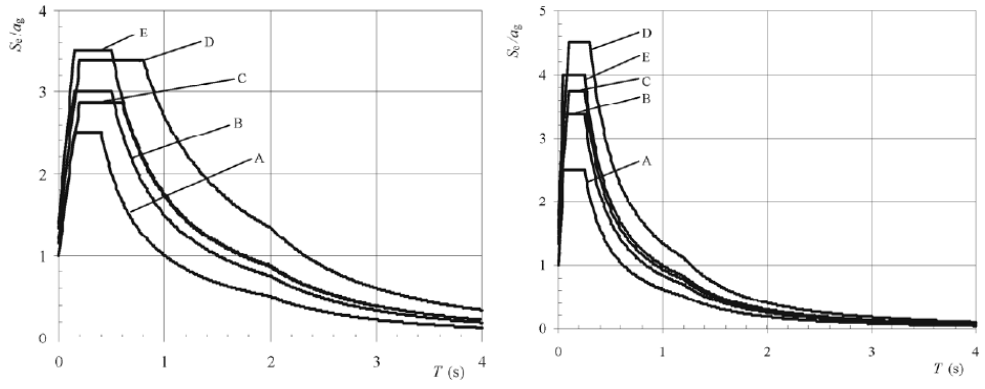

(a) **(b)**

Figure III-D.2: (a)Type 1 elastic response spectra for all ground types (b)Type 2 elastic response spectra for all ground types. Adapted from [16]

Using the characteristics of the building described in section (II-B.2) and applying the expression for $S_e(T)$, the elastic response spectrum in function of the natural period of the structure for low and high intensity is depicted in figure (D.11)

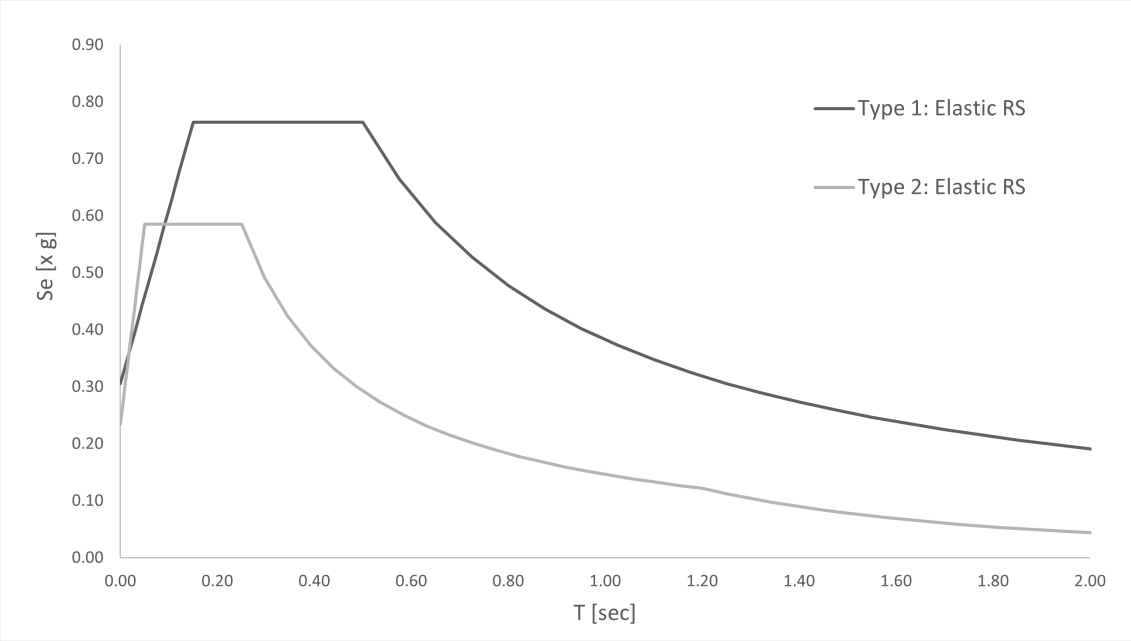

Figure III-D.3: Elastic response spectrum type 1 and type 2.

Design spectrum

The design spectrum results from the reduction of the elastic response spectrum by a factor called behaviour factor q. The purpose of this reduction is to avoid explicit inelastic structural analysis during structures design, taking into consideration structure capacity to dissipate energy (i.e., non-linear response of a structure, associated with the material, structural system, and the design procedures) [2].

For the horizontal components of the seismic action, the design spectrum $S_d(T)$, is defined by the following expressions [16]:

$$\begin{cases} 0 \leq T \leq T_B & S_d(T) = a_g\, S\, [\frac{2}{3} + \frac{T}{T_B}(\frac{2.5}{q} - \frac{2}{3})] \\ T_B \leq T \leq T_C & S_d(T) = a_g\, S\, \frac{2.5}{q} \\ T_C \leq T \leq T_D & S_d(T) = a_g\, S\, \frac{2.5}{q}\, [\frac{T_C}{T}]\ \ and\ \ \geq \beta\, a_g \\ T_D \leq T \leq 4s & S_d(T) = a_g\, S\, \frac{2.5}{q}\, [\frac{T_C T_D}{T^2}]\ \ and\ \ \geq \beta\, a_g \end{cases}$$

where:

- T, a_g,T_B,T_C,T_D,S have same definitions as elastic response spectrum;
- $S_d(T)$ represents the design spectrum;
- q is the behaviour factor;
- β is the lower bound factor for the horizontal design spectrum, the recommended value is 0.2

The value of the behaviour factor q_o for systems regular in elevation are given in *Table 5.1* B.3 of EC8. This factor depends on the structural system type and its ductility level. For the building under analysis, it corresponds to the first category: the dual systems with Ductility Class Medium (DCM). This category follows the expression $3.0\,\alpha_u/\alpha_1$ where the last term has a value equal to 1.2 for *Wall equivalent dual system.*

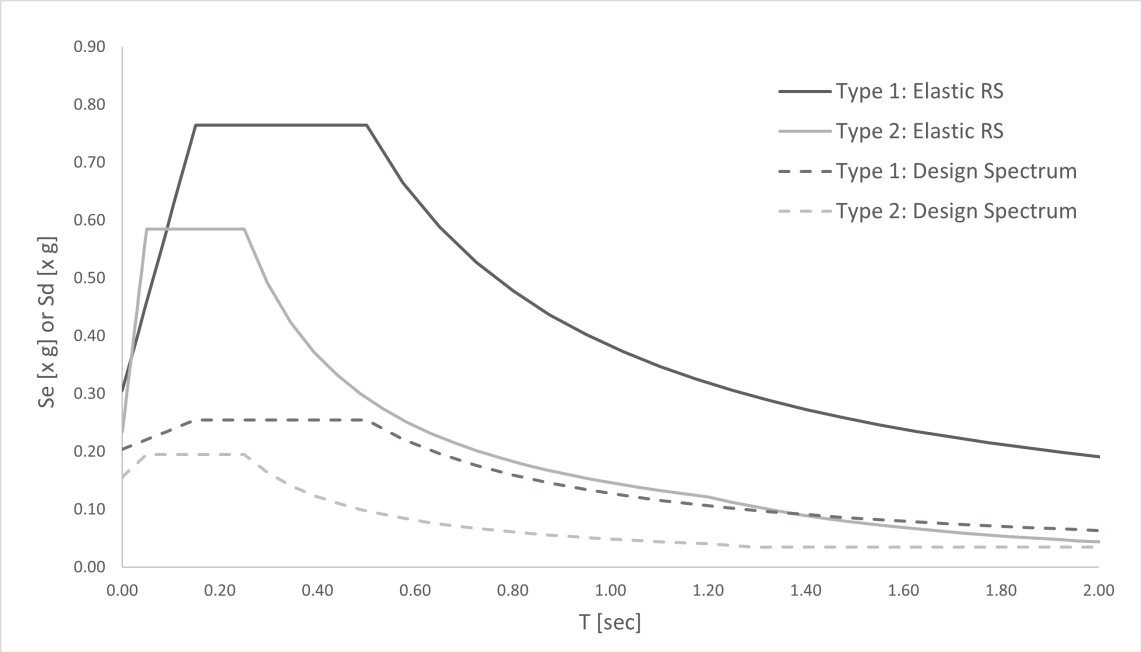

Figure III-D.4: Elastic and design spectrum representation for type 1 and type 2.

III-D.3. Description of Seismostruct model

III-D.3.1 Materials

The concrete and reinforcing steel properties are enlisted in tables III-D.3 and III-D.4, and the representation of the materials within the Seismostruct model is shown in figure III-D.5

Table III-D.3: Mechanical properties of concrete according EC2

Mechanical properties of concrete		
Characteristic compressive cylinder strength of concrete	f_{ck}	30 MPa
Mean value of concrete cylinder compressive strength	f_{cm}	38 MPa
Design value of concrete compressive strength	f_{cd}	20 MPa
Mean value of axial tensile strength of concrete	f_{ctm}	2.9 MPa
Characteristic axial tensile strength of concrete	$f_{ctk,0.05}/f_{ctk,0.95}$	2 MPa/ 3.8 MPa
Design value of tensile strength	f_{ctd}	1.35 MPa
Young Modulus	E_{cm}	32.8 GPa
Compressive strain in the concrete at the peak stress f_c	ϵ_{c1}	2.2 %
Ultimate compressive strain in the concrete	ϵ_{cu1}	3.5 %
Density	ρ_c	2500 kg/m^3

Table III-D.4: Mechanical properties of steel according EC2

Mechanical properties of steel		
Characteristic yield strength of reinforcement	f_{yk}	500 MPa
Mean strength of reinforcement	f_{ym}	575 MPa
Design yield strength of reinforcement	f_{yd}	434.8 MPa
Young modulus	E_s	200 GPa
Yielding strain	ϵ_y	0.25%
Ultimate strain	ϵ_u	5%

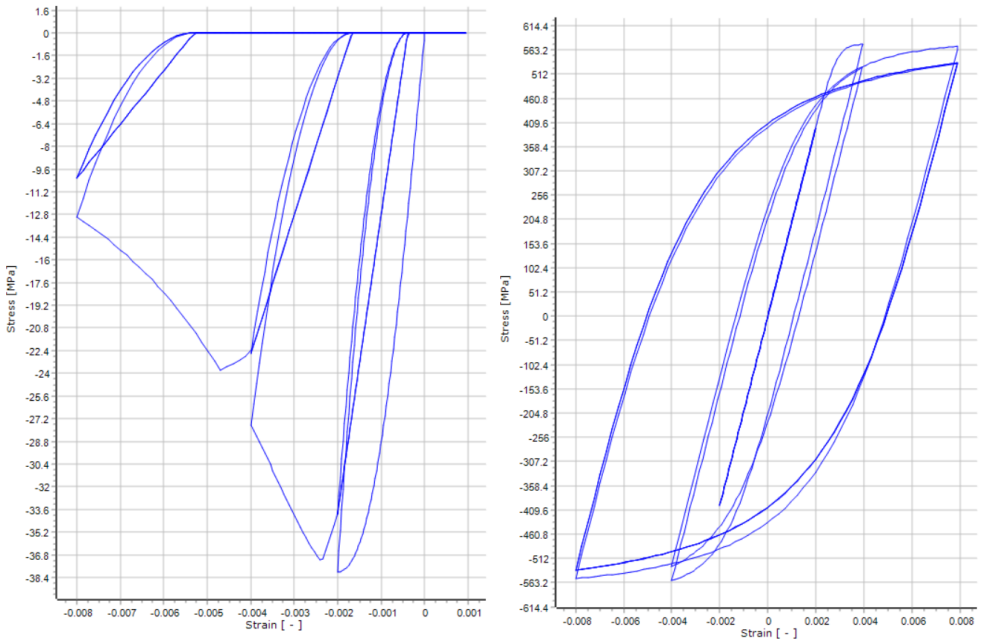

(a) Concrete C30/37 **(b)** Reinforcing steel S500

Figure III-D.5: Constitutive laws of the reinforcing steel and concrete in terms of stress σ and deformation ϵ.

III-D.3.2 Reinforced concrete sections

The modal analysis (or RSA) is performed with the initial dimensions obtained after the final verifications described in section II-B.4.5. The properties and assumptions developed in this chapter are also included to finally obtain the correct cross-sections and steel reinforcements that can resist the internal forces resulting from the RSA. The following tables describe all the cross-sections with the corresponding longitudinal and transversal reinforcements of the frame elements.

Table III-D.5: Sections of perimeter beams per storey in X direction.

Storey	Section	Longitudinal reinforcement		Transversal reinforcement
		Upper (No. ϕ)	Lower (No. ϕ)	($\phi/s\ cm$)
Roof	0.35m x 0.45m	3ϕ16	5ϕ16	ϕ8/11.3
4	0.35m x 0.45m	3ϕ16	6ϕ16	ϕ8/11.3
3	0.35m x 0.45m	4ϕ16	6ϕ16	ϕ8/11.3
2	0.35m x 0.45m	3ϕ16	5ϕ16	ϕ8/11.3
1	0.35m x 0.45m	3ϕ16	5ϕ16	ϕ8/11.3

Table III-D.6: Sections of interior beams per storey in X direction.

Storey	Section	Longitudinal reinforcement		Transversal reinforcement
		Upper (No. ϕ)	Lower (No. ϕ)	($\phi/s\ cm$)
Roof	0.35m x 0.45m	3ϕ16	3ϕ16	ϕ8/11.3
4	0.35m x 0.45m	5ϕ16	4ϕ16	ϕ8/11.3
3	0.35m x 0.45m	4ϕ16	4ϕ16	ϕ8/11.3
2	0.35m x 0.45m	3ϕ16	3ϕ16	ϕ8/11.3
1	0.35m x 0.45m	3ϕ16	2ϕ16	ϕ8/11.3

Table III-D.7: Sections of perimeter beams per storey in Y direction.

Storey	Section	Longitudinal reinforcement		Transversal reinforcement
		Upper (No. ϕ)	Lower (No. ϕ)	($\phi/s\ cm$)
Roof	0.35m x 0.45m	3ϕ16	3ϕ16	ϕ8/11.3
4	0.35m x 0.45m	5ϕ16	4ϕ16	ϕ8/11.3
3	0.35m x 0.45m	4ϕ16	4ϕ16	ϕ8/11.3
2	0.35m x 0.45m	3ϕ16	3ϕ16	ϕ8/11.3
1	0.35m x 0.45m	3ϕ16	2ϕ16	ϕ8/11.3

Table III-D.8: Sections of interior beams per storey in Y direction.

Storey	Section	Longitudinal reinforcement		Transversal reinforcement
		Upper (No. ϕ)	Lower (No. ϕ)	($\phi/s\ cm$)
Roof	0.35m x 0.45m	3ϕ16	3ϕ16	ϕ8/11.3
4	0.35m x 0.45m	3ϕ16	3ϕ16	ϕ8/11.3
3	0.35m x 0.45m	3ϕ16	3ϕ16	ϕ8/11.3
2	0.35m x 0.45m	3ϕ16	3ϕ16	ϕ8/11.3
1	0.35m x 0.45m	3ϕ16	2ϕ16	ϕ8/11.3

Table III-D.9: Sections of corner columns per storey.

Storey	Section	Longitudinal reinforcement	Transversal reinforcement	Confinement hoops
		No. Φ	(ϕ/s cm)	(No./s)
4-roof	0.40m x 0.40m	12ϕ20	ϕ8/15	4/15
3-4	0.40m x 0.40m	8ϕ20	ϕ8/15	3/15
2-3	0.40m x 0.40m	8ϕ20	ϕ8/15	3/15
1-2	0.40m x 0.40m	8ϕ20	ϕ8/13	3/13
0-1	0.40m x 0.40m	8ϕ20	ϕ8/11	3/11

Table III-D.10: Sections of edge columns per storey.

Storey	Section	Longitudinal reinforcement	Transversal reinforcement	Confinement hoops
		No. Φ	(ϕ/s cm)	(No./s)
4-roof	0.40m x 0.40m	16ϕ20	ϕ8/15	3/15
3-4	0.40m x 0.40m	8ϕ20	ϕ8/15	3/15
2-3	0.40m x 0.40m	8ϕ20	ϕ8/13	3/13
1-2	0.40m x 0.40m	8ϕ20	ϕ8/10	3/10
0-1	0.40m x 0.40m	8ϕ20	ϕ8/9	3/9

Table III-D.11: Sections of interior columns per storey.

Storey	Section	Longitudinal reinforcement	Transversal reinforcement	Confinement hoops
		No. Φ	(ϕ/s cm)	(No./s)
4-roof	0.40m x 0.40m	8ϕ20	ϕ8/15	3/15
3-4	0.40m x 0.40m	8ϕ20	ϕ8/14	3/14
2-3	0.40m x 0.40m	8ϕ20	ϕ8/10	3/10
1-2	0.40m x 0.40m	8ϕ20	ϕ8/8	3/8
0-1	0.40m x 0.40m	8ϕ20	ϕ8/6.5	3/6.5

III-D.3.3 Element classes

Currently in SEISMOSTRUCT, a large number of element types are available, such as *inelastic force-based frame element (infrmFB), inelastic displacement-based frame element (infrmDB), inelastic force-based plastic hinge frame element (infrmFBPH), inelastic displacement-based plastic hinge frame element (infrmDBPH)* among others.

For the simplicity of modelling in the elements to carry out modal analysis, the type of elements adopted are inelastic force-based frame element (infrmFB). In section III-E.2.1, the reasons for selection will be further expanded upon.

III-D.3.4 Type of nodes

Throughout the whole building in the intersection of the elements whether they are beams, columns or walls, the type of node defined in the model is *structural node*.

III-D.3.5 Constraints and restraints

In buildings, the floors act as horizontal diaphragms that collect and transmit the inertial forces to the vertical structural systems and ensure that those systems act together in resisting the horizontal seismic action. One of the cases where the action of the floors is especially relevant occurs when systems with different horizontal deformability characteristics are used together [9] (i.e., dual systems). Another aspect to consider is that diaphragms should have sufficient in-plane stiffness for the distribution of horizontal inertial forces to the vertical structural systems, mobilizing them with fairly similar displacements, this is depicted in figure III-D.6.

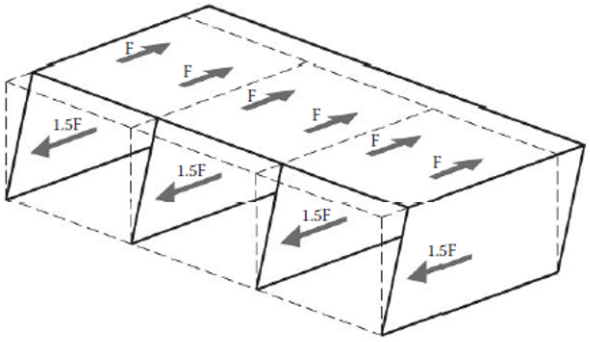

Figure III-D.6: Effect of rigid diaphragm. Adapted from [9]

For the above, rigid diaphragms to restrain the horizontal degree of freedoms in each storey are defined as the constraint type of the building model. The master nodes that control the horizontal displacements, whose position coincides with the center of gravity of the building, are also designated.

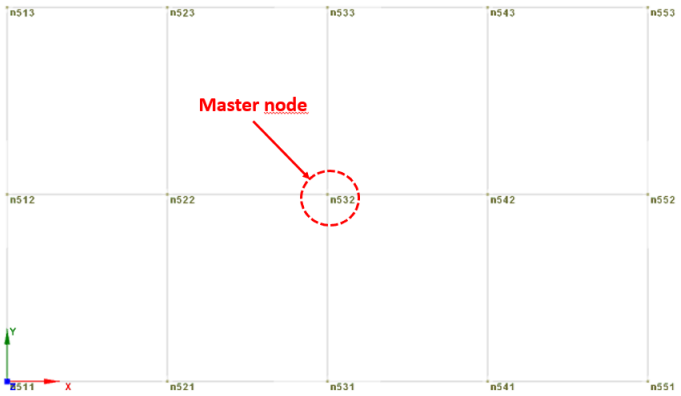

Figure III-D.7: Master node location in plan view.

Concerning the restraints, all the supports in the columns and structural walls are modelled fixed, which means *fully restrained* and zero degrees of freedom in the corresponding nodes. See figure III-D.8.

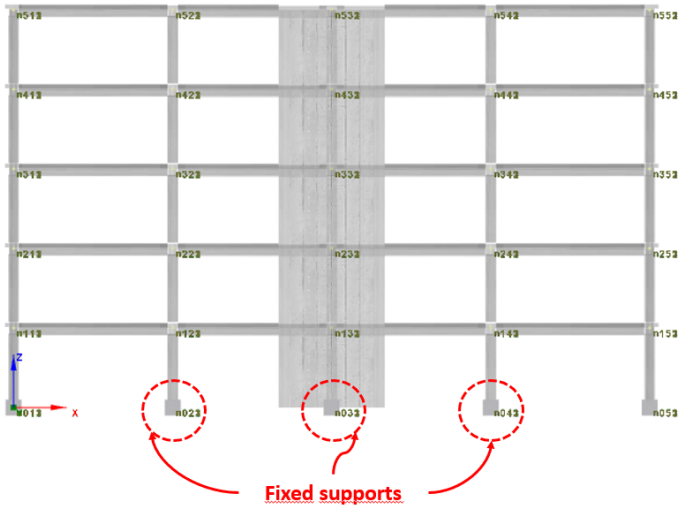

Figure III-D.8: Fixed supports in columns and walls representation.

III-D.3.6 Combination of seismic action components and accidental torsion

EC8 describes how the action effects due to the combination of the three components of the seismic action may be calculated:

$$E_X" + "\lambda\, E_Y" + "\lambda\, E_Z \tag{III-D.3.1}$$

$$\lambda\, E_X" + "E_Y" + "\lambda\, E_Z \tag{III-D.3.2}$$

$$\lambda\, E_X" + "\lambda\, E_Y" + "E_Z \tag{III-D.3.3}$$

where E_X, E_Y, and E_Z represent the total values (considering all the relevant modes) of the response quantity of interest due to the application of the seismic action. (Vertical direction of the seismic action E_Z is rarely taken into account). $\lambda = 0.3$ and "+" means "to be combined with".

These separate combinations should be superimposed separately with the gravity load effects in the "seismic design situation" (equation II-B.4.2), each combination with an alternating sign.

Accidental torsion

In structural models in 3D, fully symmetric in plan, the horizontal components of the ground motion do not produce any torsion. Nevertheless, seismic response analysis cannot capture possible variations in the stiffness and/or mass distributions from their nominal values. Furthermore, the possible components of torsional ground motion are not considered in the seismic analyses. The last two effects may produce torsional response even in nominally fully symmetric buildings [9].

In contemplation of these uncertainties and to ensure minimum torsional resistance, as well as to limit the possible effects of an unforeseen torsional response, the concept of *accidental eccentricity* has been used in seismic codes, including EC8.

Eurocode 8 states that accidental torsional effects can be introduced by shifting the masses from their nominal positions by a distance equal to the accidental eccentricity e_{ai}, taken as 5% of the dimension of the floor in storey i:

$$e_{ai} = \pm 0.05\, L_j$$

where L_j represents the floor-dimension perpendicular to the direction of the seismic action.

In Seismostruct, the accidental eccentricity is considered by adding additional torsional moments about the vertical axis for each storey according to EC8, which are defined as follows:

$$M_{ai} = e_{ai}\, F_i$$

where the F_i is the horizontal force acting on storey i, as derived in table II-B.3.

Finally, converting this moment to a pair of forces with respect to each floor- dimension the applied forces are equal to (figure III-D.10):

$$F_{ecc,a} = \frac{M_{ai}}{L_j}$$

The internal forces for the seismic design situation are calculated using the following combinations, which include the fundamental combination and eight more seismic combinations that take into account the three components of the seismic action in each direction. Additionally, each seismic combination needs to be split into four combinations taken E_X and E_Y with the accidental eccentricities effects $F_{ecc,a}$. In conclusion, the structure is designed for the envelope of 33 combinations (1 fundamental combination + [4 × 8] seismic combinations).

$$\begin{aligned}
&\text{Combination 1: } (G_{\mathrm{k},1} + G_{\mathrm{k},2}) + \psi_2 \cdot Q_{\mathrm{k}} \\
&\text{Combination 2: } (G_{\mathrm{k},1} + G_{\mathrm{k},2}) + E_{\mathrm{x}} + 0.3 \cdot E_{\mathrm{y}} + \psi_2 \cdot Q_{\mathrm{k}} \\
&\text{Combination 3: } (G_{\mathrm{k},1} + G_{\mathrm{k},2}) - E_{\mathrm{X}} + 0.3 \cdot E_{\mathrm{y}} + \psi_2 \cdot Q_{\mathrm{k}} \\
&\text{Combination 4: } (G_{\mathrm{k},1} + G_{\mathrm{k},2}) + E_{\mathrm{X}} - 0.3 \cdot E_{\mathrm{y}} + \psi_2 \cdot Q_{\mathrm{k}} \\
&\text{Combination 5: } (G_{\mathrm{k},1} + G_{\mathrm{k},2}) - E_{\mathrm{x}} - 0.3 \cdot E_{\mathrm{y}} + \psi_2 \cdot Q_{\mathrm{k}} \\
&\text{Combination 6: } (G_{\mathrm{k},1} + G_{\mathrm{k},2}) + 0.3 \cdot E_{\mathrm{x}} + E_{\mathrm{y}} + \psi_2 \cdot Q_{\mathrm{k}} \\
&\text{Combination 7: } (G_{\mathrm{k},1} + G_{\mathrm{k},2}) - 0.3 \cdot E_{\mathrm{x}} + E_{\mathrm{y}} + \psi_2 \cdot Q_{\mathrm{k}} \\
&\text{Combination 8: } (G_{\mathrm{k},1} + G_{\mathrm{k},2}) + 0.3 \cdot E_{\mathrm{x}} - E_{\mathrm{y}} + \psi_2 \cdot Q_{\mathrm{k}} \\
&\text{Combination 9: } (G_{\mathrm{k},1} + G_{\mathrm{k},2}) - 0.3 \cdot E_{\mathrm{x}} - E_{\mathrm{y}} + \psi_2 \cdot Q_{\mathrm{k}}
\end{aligned}$$

III-D.3.7 Graphical representation of the model

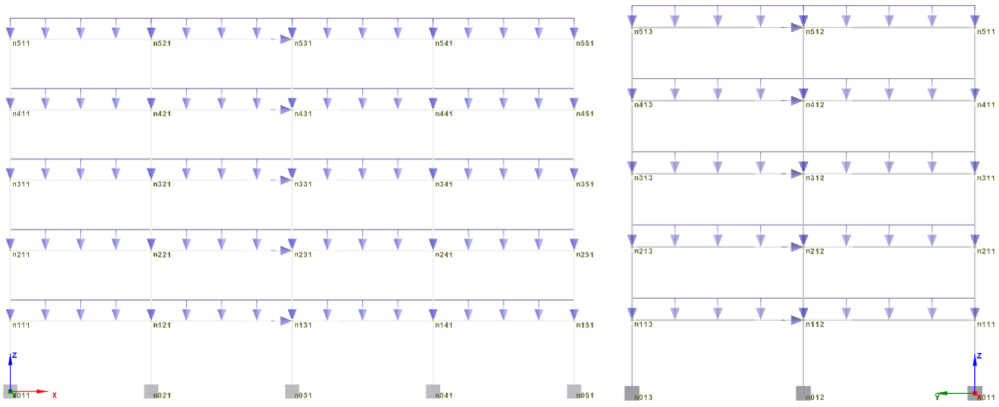

(a) X-Z elevation **(b)** Y-Z elevation

Figure III-D.9: Building elevations with applied loads for RSA.

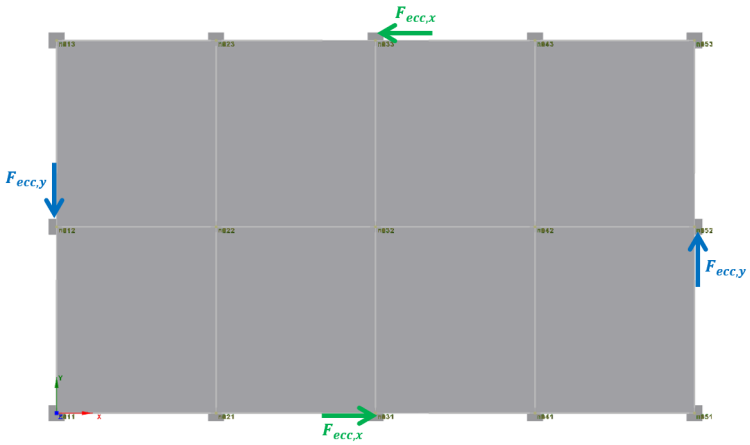

Figure III-D.10: Accidental eccentricity representation in a given storey of the building.

III-D.4. Response Spectrum Analysis results

Once the RSA is performed, the dynamic properties of the whole structure (e.g. natural frequencies, modal masses, modal participation factor, etc), nodal displacements, and internal forces of the elements are obtained. Figures III-D.11 and III-D.12 illustrate the mentioned dynamic properties for each vibration mode except for the nodal displacements that are found in the annexes.

MODAL PERIODS AND FREQUENCIES

Mode	Period (sec)	Frequency (Hertz)	Angular Frequency (rad/sec)
1	0.44809274	2.23168088	14.02206449
2	0.41783498	2.39328933	15.03748035
3	0.30500246	3.27866211	20.60044158
4	0.09272025	10.7851303	67.76497204
5	0.09064157	11.0324659	69.31902747
6	0.03535394	28.285387	177.7223278
7	0.03512345	28.4710083	178.8886209
8	0.01881365	53.1528872	333.96944
9	0.01877721	53.2560489	334.6176239
10	0.01278427	78.221141	491.477924

MODAL PARTICIPATION FACTORS

For Unit Acceleration Loads in Global Coordinates

Mode	Period	[Ux]	[Uy]	[Uz]	[Rx]	[Ry]	[Rz]
1	0.44809274	0	33.4945	0	-80.1878	0	0
2	0.41783498	-33.6567	0	0	0	-79.1669	0
3	0.30500246	0	0	0	0	0	302.8295
4	0.09272025	0	17.321	0	107.7075	0	0
5	0.09064157	-17.0489	0	0	0	108.8168	0
6	0.03535394	0	-10.5375	0	-72.5307	0	0
7	0.03512345	-10.4832	0	0	0	72.0812	0
8	0.01881365	0	-7.3186	0	-54.7177	0	0
9	0.01877721	7.2979	0	0	0	-54.6513	0
10	0.01278427	4.4094	0	0	0	-33.7075	0

EFFECTIVE MODAL MASS PERCENTAGES

[Individual Mode]

Mode	Period	[Ux]	[Uy]	[Uz]	[Rx]	[Ry]	[Rz]
1	0.44809274	0.00%	69.85%	-	15.61%	0.00%	0.00%
2	0.41783498	70.53%	0.00%	-	0.00%	6.90%	0.00%
3	0.30500246	0.00%	0.00%	-	0.00%	0.00%	69.48%
4	0.09272025	0.00%	18.68%	-	28.17%	0.00%	0.00%
5	0.09064157	18.10%	0.00%	-	0.00%	13.04%	0.00%
6	0.03535394	0.00%	6.91%	-	12.78%	0.00%	0.00%
7	0.03512345	6.84%	0.00%	-	0.00%	5.72%	0.00%
8	0.01881365	0.00%	3.34%	-	7.27%	0.00%	0.00%
9	0.01877721	3.32%	0.00%	-	0.00%	3.29%	0.00%
10	0.01278427	1.21%	0.00%	-	0.00%	1.25%	0.00%

[Cumulative Mass]

Mode	Period	[Ux]	[Uy]	[Uz]	[Rx]	[Ry]	[Rz]
1	0.44809274	0.00%	69.85%	-	15.61%	0.00%	0.00%
2	0.41783498	70.53%	69.85%	-	15.61%	6.90%	0.00%
3	0.30500246	70.53%	69.85%	-	15.61%	6.90%	69.48%
4	0.09272025	70.53%	88.53%	-	43.79%	6.90%	69.48%
5	0.09064157	88.63%	88.53%	-	43.79%	19.94%	69.48%
6	0.03535394	88.63%	95.45%	-	56.56%	19.94%	69.48%
7	0.03512345	95.47%	95.45%	-	56.56%	25.67%	69.48%

Figure III-D.11: Natural frequencies and natural periods from Seismostruct

EFFECTIVE MODAL MASSES							
					[Individual Mode]		
Mode	Period	[Ux]	[Uy]	[Uz]	[Rx]	[Ry]	[Rz]
1	0.44809274	0	1121.882306	0	6430.083225	0	0
2	0.41783498	1132.77069	0	0	0	6267.396901	0
3	0.30500246	0	0	0	0	0	91705.70258
4	0.09272025	0	300.017034	0	11600.90092	0	0
5	0.09064157	290.664806	0	0	0	11841.09299	0
6	0.03535394	0	111.039009	0	5260.69532	0	0
7	0.03512345	109.897612	0	0	0	5195.703683	0
8	0.01881365	0	53.562603	0	2994.027368	0	0
9	0.01877721	53.259109	0	0	0	2986.760869	0
10	0.01278427	19.44238	0	0	0	1136.198056	0
					[Cumulative Mass]		
Mode	Period	[Ux]	[Uy]	[Uz]	[Rx]	[Ry]	[Rz]
1	0.44809274	0	1121.882306	0	6430.083225	0	0
2	0.41783498	1132.77069	1121.882306	0	6430.083225	6267.396901	0
3	0.30500246	1132.77069	1121.882306	0	6430.083225	6267.396901	91705.70258
4	0.09272025	1132.77069	1421.89934	0	18030.98415	6267.396901	91705.70258
5	0.09064157	1423.4355	1421.89934	0	18030.98415	18108.48989	91705.70258
6	0.03535394	1423.4355	1532.938348	0	23291.67947	18108.48989	91705.70258
7	0.03512345	1533.33311	1532.938348	0	23291.67947	23304.19357	91705.70258
8	0.01881365	1533.33311	1586.500951	0	26285.70684	23304.19357	91705.70258
9	0.01877721	1586.59222	1586.500951	0	26285.70684	26290.95444	91705.70258
10	0.01278427	1606.0346	1586.500951	0	26285.70684	27427.1525	91705.70258

Figure III-D.12: Effective modal masses from Seismostruct

Recalling that the internal forces from the RSA results have been used for the design of the RC elements. The bending moments, the shear forces, and the axial forces acting in a given element can be computed by using the local axes system depicted in figure III-D.13, and their corresponding internal forces magnitudes that are shown in the annexes.

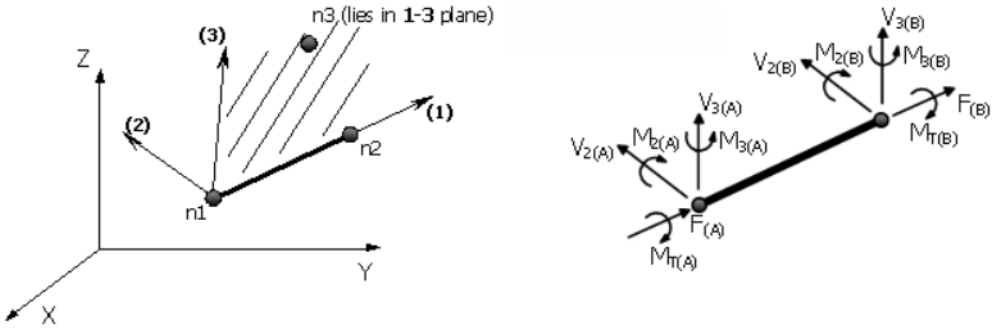

Figure III-D.13: Local axes of the elements

In Annex C, a table enlisting the internal forces of the elements according to their nodes (A and B using III-D.13) is displayed. The figures III-D.14, III-D.15c, and III-D.16b allow identifying the element nodes of a given frame element for the X and Y direction.

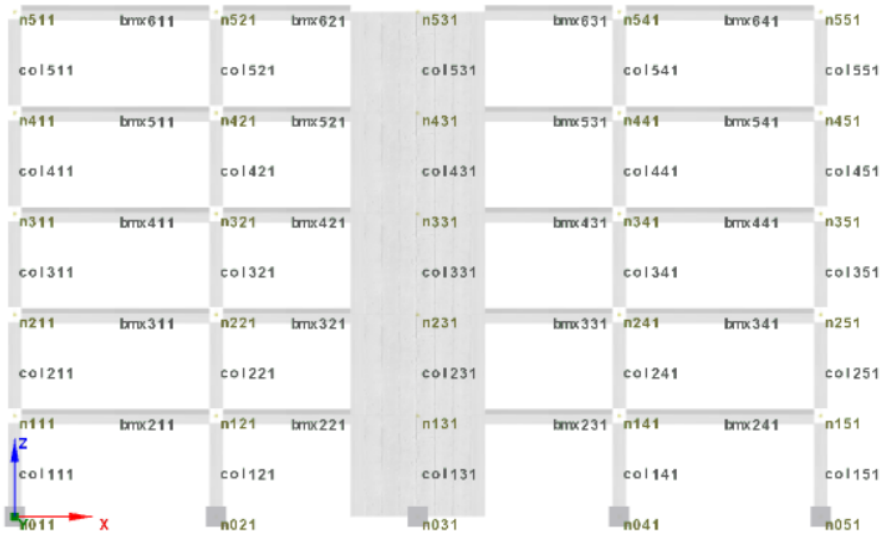

(a) Frame at $Y = 0m$

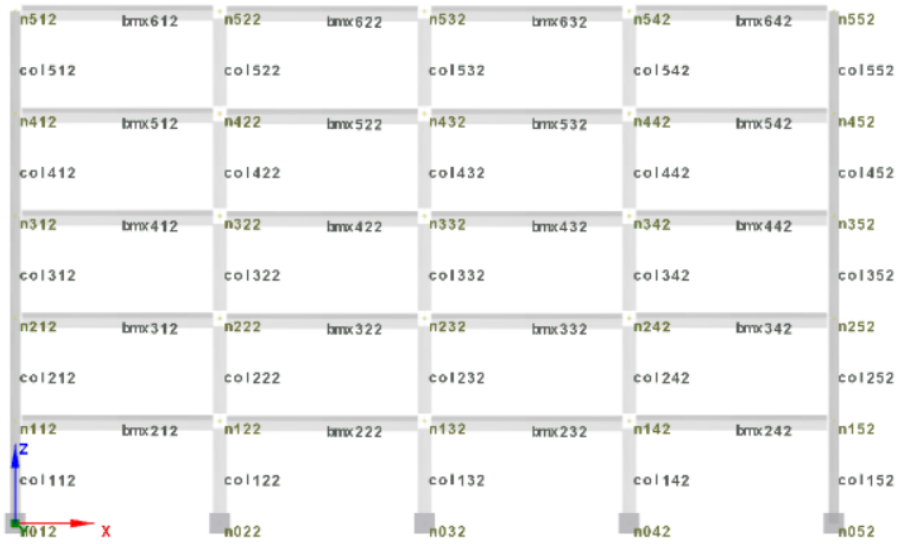

(b) Frame at $Y = 7m$

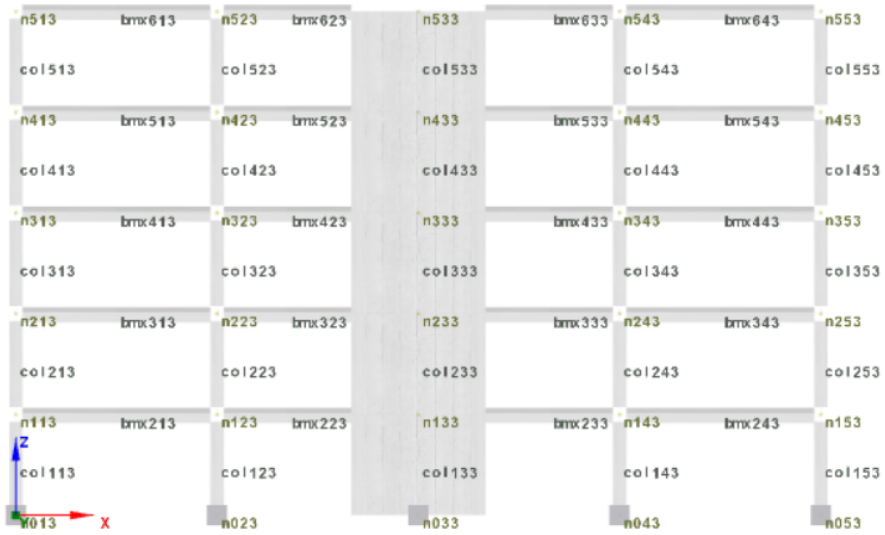

(c) Frame at $Y = 14m$

Figure III-D.14: Elements and nodes for frames in the X direction

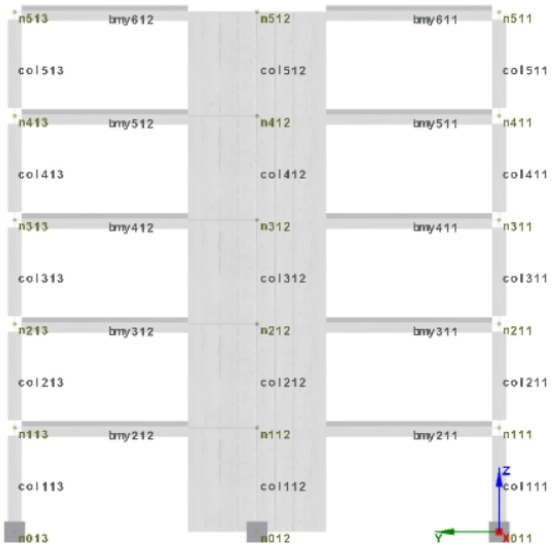

(a) Frame at $X = 0m$

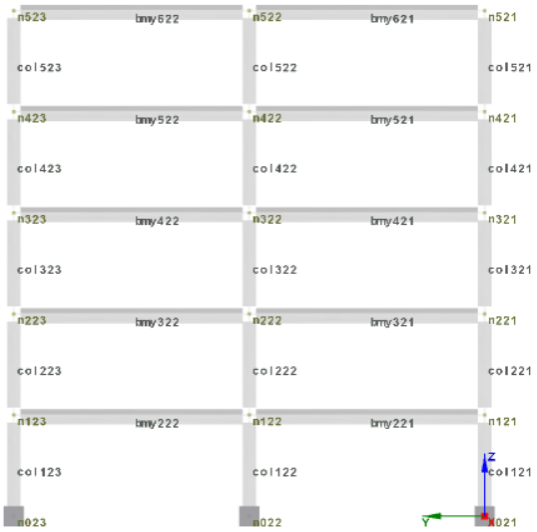

(b) Frame at $X = 6m$

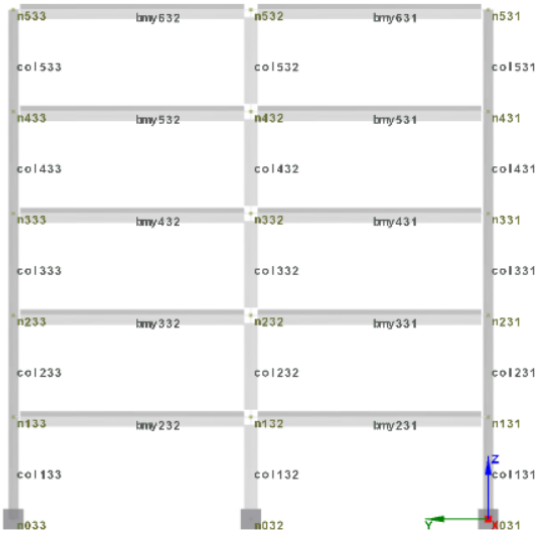

(c) Frame at $X = 12m$

Figure III-D.15: Elements and nodes for frames in the Y direction (1/2)

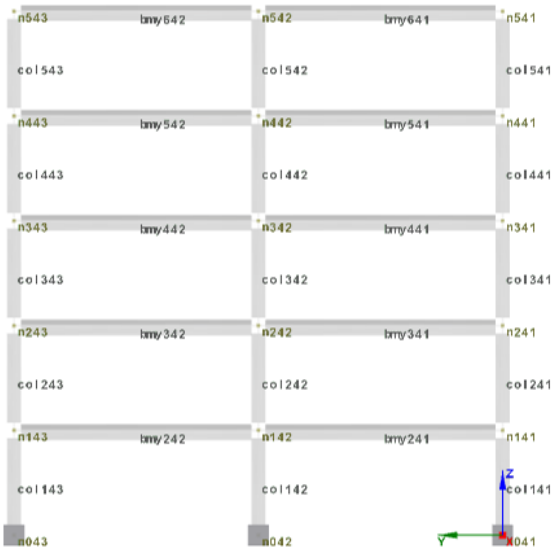

(a) Frame at $X = 18m$

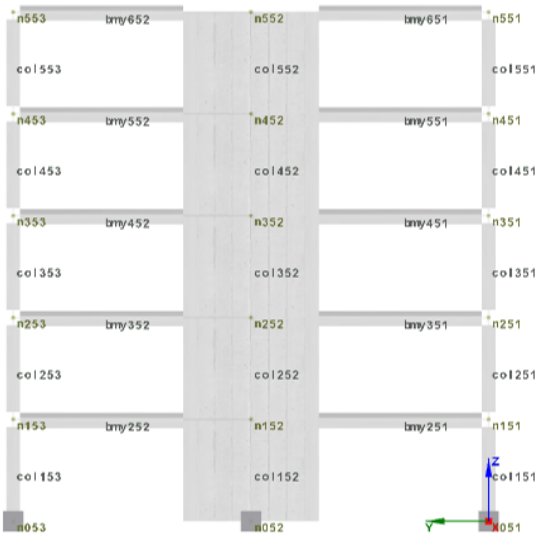

(b) Frame at $X = 24m$

Figure III-D.16: Elements and nodes for frames in the Y direction (2/2)

CHAPTER III-E

NON-LINEAR STATIC ANALYSIS

III-E.1. Description of the method

III-E.1.1 Non-linear analysis of structures

The structure's behaviour during the rupture or ductile response of its elements cannot be well depicted through linear elastic analysis, therefore the need to perform the non-linear analysis is then fundamental to show a more realistic behaviour of structures. The first non-linear source of a structure is the result of the nonlinearity of the materials, they cannot respond for a moderate to large ground motion according to Hooke's law anymore. The second one is due to the geometric non-linearity, where the displacements are not linearly proportional to the loads [9].

III-E.1.2 Pushover analysis

The non-linear static analysis procedure, commonly called "the pushover analysis", uses an idealization of the structure by an assembly of component models capable of representing the non-linear monotonic load-deformation characteristics. In the simplified pushover, an invariant lateral load pattern is applied to the structure and the structure is monotonically pushed under this load pattern to large inelastic deformations until a target value is reached at a reference point, which normally refers at the roof level. During the load pattern application, the constant gravity loads are also present.

The objective is to evaluate drift demands and component deformations and force demands when the structure is pushed to the displacement expected under the design earthquake, called target displacement.

For structures that vibrate primarily in the fundamental mode, such analysis provides good estimates of global as well as local inelastic demands. Pushover analysis is a useful tool for assessing inelastic deformation demands and for exposing design weaknesses that may remain hidden in an elastic analysis, such as story mechanisms, excessive deformation demands, strength irregularities, and overloads on potentially brittle columns and/or connections.

Implementing with caution, the pushover analysis is a great improvement over elastic evaluation procedures. This applies particularly to the seismic evaluation of existing structures whose element behavior cannot be evaluated in the context of q-factors method used in the presentEC8 [4].

III-E.2. Description of the Seismostruct model

III-E.2.1 Type of elements

Concentrated versus distributed plasticity
In recent years, elements with distributed plasticity are more often used during modelling phases. One of the main advantages is the non-essential definition of the effective inelastic regions (i.e. plastic hinge length), opposite to the concentrated plasticity elements. Furthermore, with distributed plasticity elements the inelastic deformations can spread along the entire elements but with a longer computational time, [3].

Displacement-based vs force-based elements
There are two types of elements in which the distributed plasticity can be implemented: Displacement-based elements (DB) and Force-based elements (FB).

Displacement-based elements express the relation between basic displacements and sectional deformations through displacement interpolation functions. The solution of this element is only exact for a linear elastic beam, for the inelastic behaviour is approximate. On the other hand, the Force-based elements depict the relation between basic forces and sectional forces through force interpolation functions, and its solution is always exact regardless of the material behaviour [3].

Based on the description and concepts above, the choice of Force-based elements with distributed plasticity, identified in Sismostruct as *inelastic force-based frame element (infrmFB)*, is the most appropriate type of element for the different analyses to be carried out.

III-E.2.2 Materials

For this model, the material properties are the same already mentioned in section (II-B.1). As a reminder, the non-linear behaviour of the materials is considered and also their mean strength.

III-E.2.3 Applied loads

In pushover analysis, the applied loading usually consists of permanent gravity loads in the vertical direction and incremental loads in one or both transversal(lateral) directions.

Appropriate lateral load distribution is fundamental in the pushover analysis. EC8 describes two different load patterns that should be applied: one with uniform distribution, based on lateral forces proportional to mass; the other one with a "modal" pattern consistent with lateral force distribution based on the elastic analysis used (i.e. Equivalent Lateral Force method or Modal Analysis). In other words, the second load pattern follows the fundamental vibration mode distribution.

In Seismostruct software, the applied incremental load P is kept proportional to the pattern of nominal loads P_0 initially defined: $P = \lambda P_0$. Where λ is the load factor and is increased by the program until a user-defined limit, or numerical failure, is reached.

Generally, the application of forces is preferred to the employment of displacement incremental loads, since constraining the structure deformation to a predefined shape may conceal its true response characteristics (e.g. soft-storey). For this reason, the most common loading strategy and best option is a force-based pushover with response control.

Response control loading type implies that the response of a particular node in the structure is controlled. It is requested to define the node and the corresponding degree-of-freedom to be controlled by the algorithm, together with the target displacement at which the analysis is to be terminated. In addition, the number of increments, in which the target displacement is to be subdivided for incremental application, should be specified. Furthermore, with this loading strategy, users can capture the irregular response features, the softening post-peak branch of the response, and obtain an even distribution of force-displacement curve points.

Besides, accidental eccentricity does not need to be taken into consideration for the pushover analysis, contrary to response spectrum analysis (RSA) (Figure III-E.1)

III-E.2.4 Graphical representation of the model

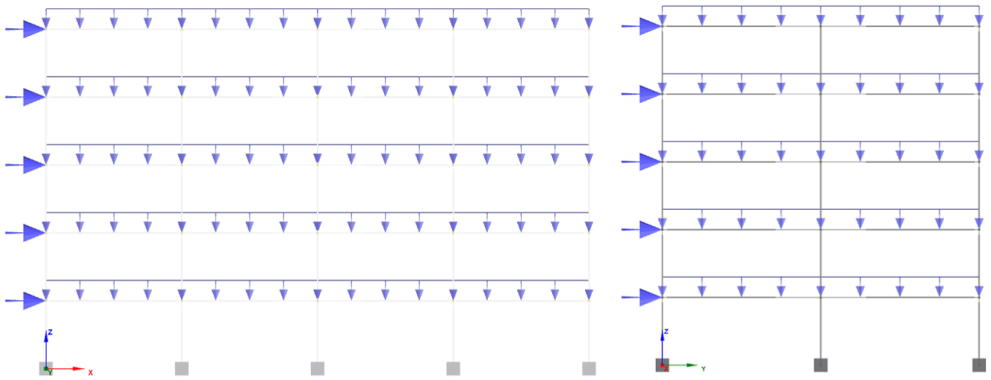

(a) X-Z elevation **(b)** Y-Z elevation

Figure III-E.1: Gravity and incremental loads for each direction

III-E.3. Pushover analysis results

The capacity curves or pushover curves in terms of base shear force and (control node) displacement are computed using the reinforced concrete sections enunciated before in section (III-D.3.2) and under the conditions explained in (III-E.2).

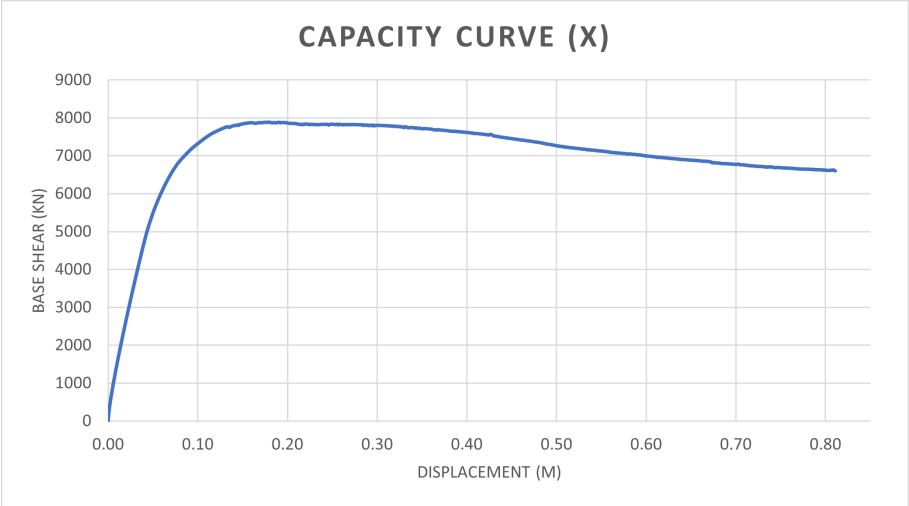

Figure III-E.2: Pushover curve in X direction

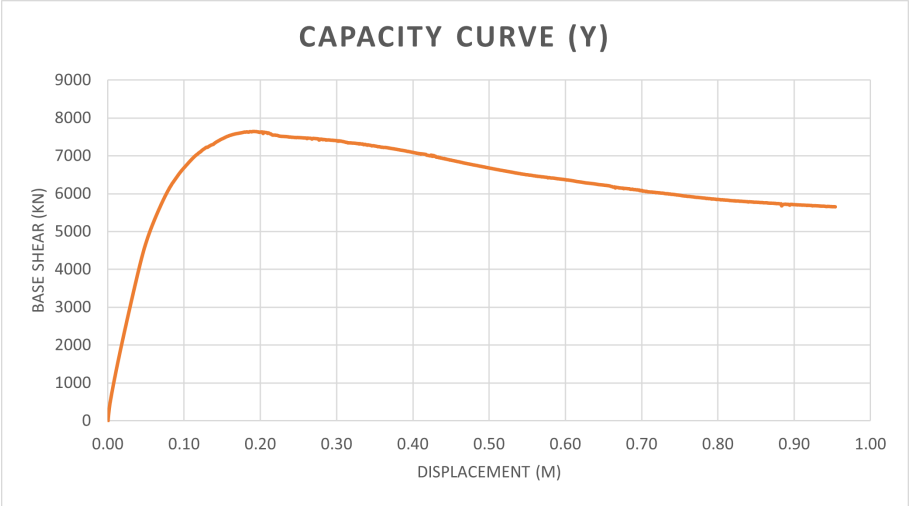

Figure III-E.3: Pushover curve in Y direction

It is clearly shown that the long direction (X) of the building corresponds to the strongest direction in terms of strength, although the ductility of the orthogonal direction (Y) is higher. However, in terms of seismic design, the difference between both directions is not important. It may be a result of the greater number of columns in the X direction or the different lengths, since the numbers and dimensions of the structural walls are the same.

III-E.4. N2 method

In the N2 method, seismic demand is determined by using response spectra, and the inelastic behaviour is taken into account explicitly. The structure shall be represented as a single-degree-of-freedom (SDoF) system, therefore to determine the characteristics of an equivalent SDoF system is done by the N2 method.

III-E.4.1 Transformation to an equivalent single-degree-of-freedom system

By introducing the procedure described in Annex B of EC8 current version, the equivalent SDoF system transformation is based on:

The relation between normalized lateral forces F_i and normalized displacements ϕ_i is taken as:

$$F_i = m_i \phi_i$$

The effective mass is equal to:

$$m^* = \sum m_i \phi_i$$

And the transformation factor is given by:

$$\Gamma = \frac{m^*}{\sum m_i \phi_i^2}$$

The transformation factor is the equivalent of expression III-D.1.3, which is commonly known as the modal participation factor. It is necessary to compute this factor for each direction, X and Y, to obtain the corresponding force and equivalent displacement of the equivalent system. The m_i is the mass in i-th storey; the displacements are normalized for $\phi_n = 1$, with n as the control node. And so, the $F_i = m_i$.

Therefore the force F^* and displacement d^* of the SDoF system is calculated as [16]:

$$F^* = \frac{F_b}{\Gamma} \tag{III-E.4.1}$$

$$d^* = \frac{d_n}{\Gamma} \tag{III-E.4.2}$$

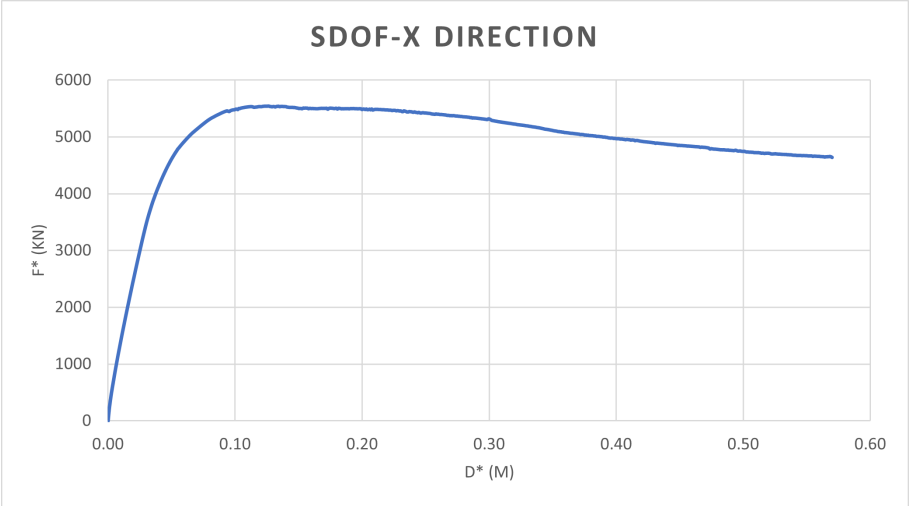

(a) X direction

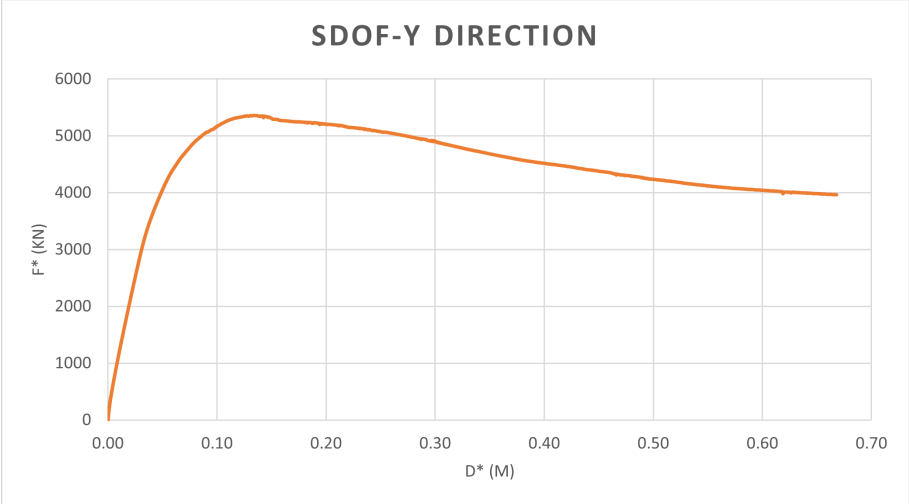

(b) Y direction

Figure III-E.4: Capacity curve of the equivalent SDoF system in each direction

III-E.4.2 Idealisation of the Capacity spectrum

III-E.4.2.1 Procedure according EN1998-1:2004 [16]

In EC8 the bilinear/multilinear idealization is based on the equal-energy principle at the SDoF level, although is possible to be performed at the level of the entire building (i.e. multi-degree-of-freedom system). Below the procedure for the idealization of the pushover curves using the same principle is explained.

The current version suggests an idealization of the pushover curve as a perfectly elasto-plastic force-displacement relation. This implies two main assumptions: firstly, the yield force F_y^* also represents the ultimate strength of the idealized system (i.e. post-yield stiffness equal to zero); and second, the initial stiffness of the idealization is determined in such a way that the areas under the actual and idealized force-deformation curves are equal.

The above assumes the yield displacement d_y^* of the system as:

$$d_y^* = 2 \left[d_m^* - \frac{E_m^*}{E*_y} \right] \tag{III-E.4.3}$$

where E_m^* is the deformation energy up to the formation of the plastic mechanism (point A in figure III-E.5).

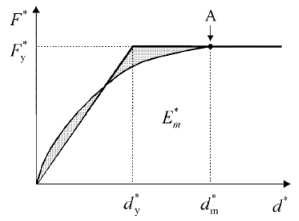

Figure III-E.5: Bilinear idealisation of the pushover curve according current version of Eurocode 8. Adapted from [16]

Additionally, to carry the N2 method out correctly it is also necessary to convert the force of the equivalent SDoF in terms of acceleration to superpose it with the seismic demand, dividing by the effective mass.

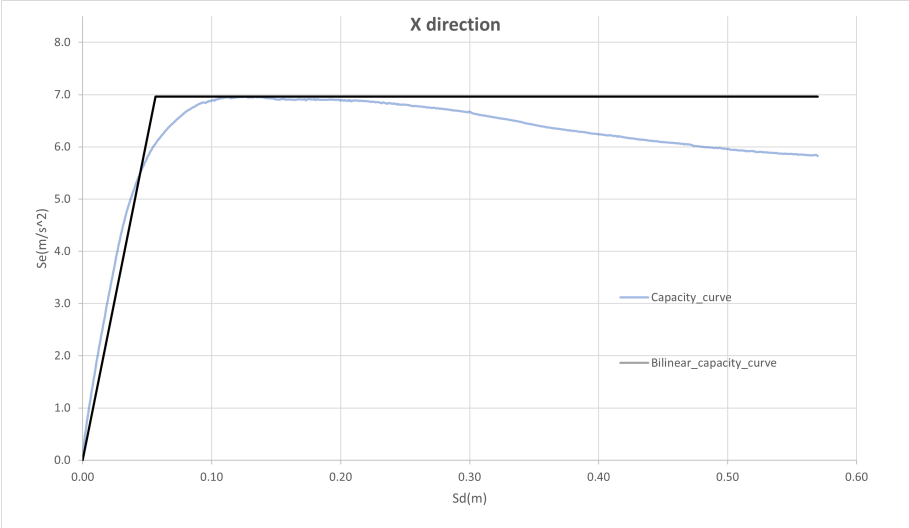

(a) X direction

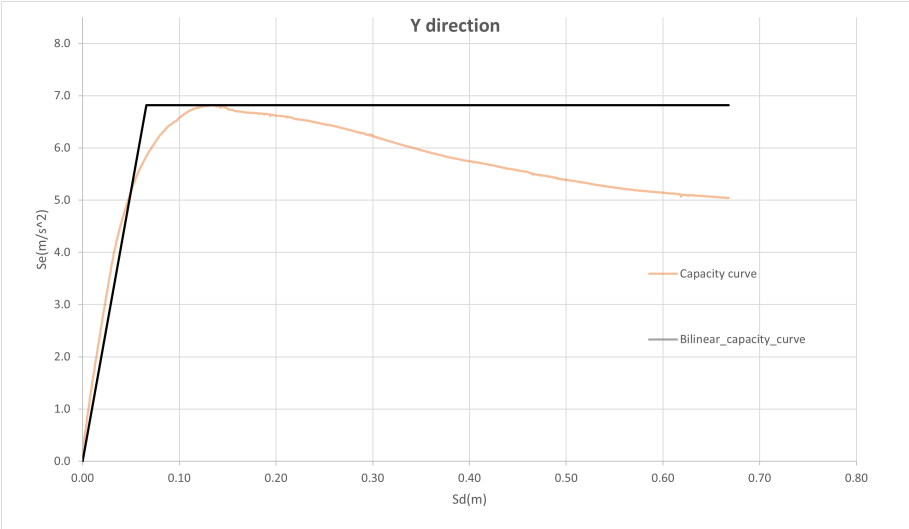

(b) Y direction

Figure III-E.6: Idealised pushover curve in terms of accelerations and displacement for each direction according EN1998:1 2004

Determination of the period

The period T^* of the idealized equivalent SDoF system in the X direction is determined by the following expression:

$$T^* = 2\pi\sqrt{\frac{m^*\, d_y^*}{F_y^*}} = 0.565s \tag{III-E.4.4}$$

Determination of target displacement

To determine the displacement demand for MDoF system (i.e. target displacement) is necessary firstly, to compute the one of the SDoF system with period T^* and unlimited elastic behaviour given by the equation:

$$d_{et}^* = S_e(T^*)\left[\frac{T^*}{2\pi}\right] = (6.65)\cdot\left[\frac{0.565}{2\pi}\right] = 0.054m \tag{III-E.4.5}$$

where $S_e(T^*)$ is the elastic acceleration response spectrum at the period T^*

Secondly, as the period $T^* \geq T_C$, the target displacement d_t^* for the SDoF system is within the long-period range and is also equal to the target displacement d_{et}^*.

$$d_t^* = d_{et}^* = 0.054m \tag{III-E.4.6}$$

Therefore, the displacement demand for the building in the X direction, which is defined as the control node displacement in Seismostruct, is obtained as follows:

$$d_t = \Gamma \, d_t^* = (1.423) \cdot (0.054) = 0.076m$$

Applying the same procedure for the orthogonal (Y) direction with $T^* = 0.618s$, $S_e(T^*) = 6.09m/s^2$ and $\Gamma = 1.428$, the target displacement for the building is: $d_t = 0.084m$. A graphical representation for the N2 procedure is depicted in figure (D.11)

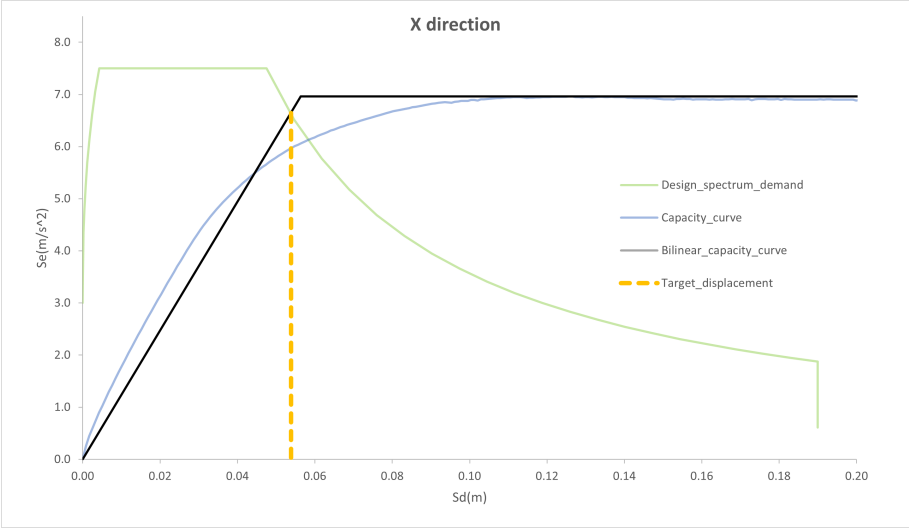

(a) X direction

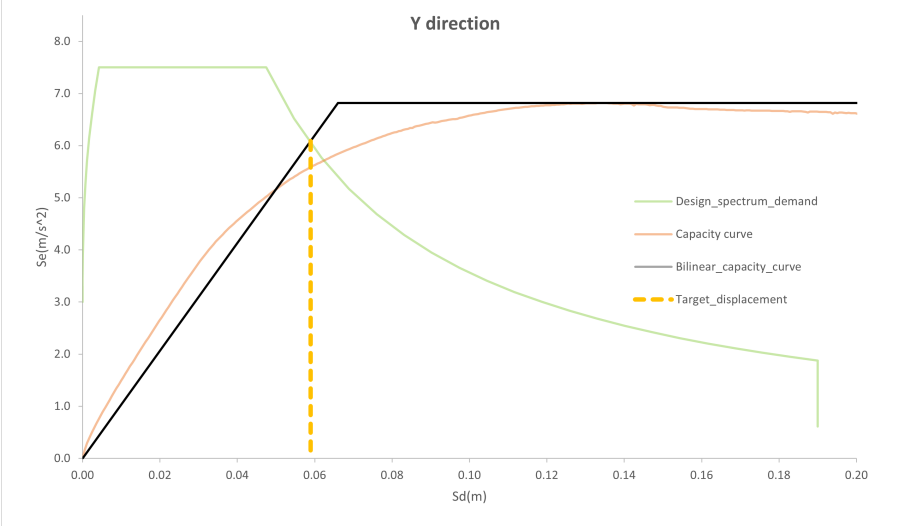

(b) Y direction

Figure III-E.7: N2 method representation for X and Y direction of the building (EN1998-1:2004)

Note that N2 method is performed just with the elastic design spectrum in AD (acceleration vs displacement) format, which in this case corresponds to the code spectrum described in figure (III-D.3). The construction of inelastic spectra is not needed in the computational procedure.

III-E.4.2.2 Idealisation of the Pushover curve according prEN1998-1-1: 2022 [12]

In the next version of EC8, two cases are explained for the idealization of the force-deformation relationship for new structures, one as bilinear if the capacity curve is non-decreasing; and the other if a post-peak negative stiffness branch is exhibited in the capacity curve. However, as one of the objectives of this project is to evaluate the different procedures provided by the second generation of EC8 to determine the target displacement of the structure, and the Dynamic Time History Analysis (DTHA) will be performed in the following chapter, then is suitable to use the multi-linear idealization.

In the procedure described, the idealized $F^*(d^*)$ relationship should be at least trilinear. The multi-linear idealisation of the capacity curve is depicted graphically below.

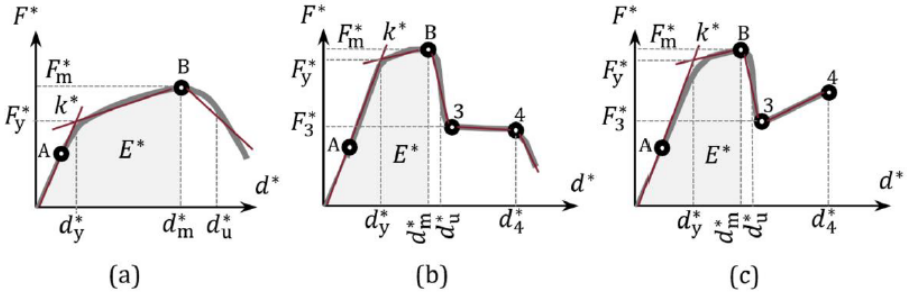

Figure III-E.8: Graphical repesentation of the multi-linear idealisation of the capacity curve: (a) Trilinear idealisation; (b) and (c) multi-linear. Adapted from [12]

To achieve this trilinear idealization, the first step is to define the elastic stiffness k^* as the secant to the point of the capacity curve where the first yielding of the primary structure occurs (point A of figure III-E.8) unless a different value is given in the relevant part of EN1998. In the presented structure, this situation occurs when the first reinforcing rebar in the structural wall yields (further explanation in section III-E.5.2). As second step, the yield displacement (d_y^*) of the SDoF model may be calculated as [12]:

$$d_y^* = \frac{2E^* - F_m^*\, d_m^*}{k^*\, d_m^* - F_m^*} \tag{III-E.4.7}$$

where: F_m^* is the point of maximum force; d_m^* is the displacement corresponding to the maximum force, and E_m^* is the area under the transformed capacity curve up to the point of the maximum force F_m^*.

The ultimate displacement d_u^* of the force-displacement curve is given as the maximum value of equivalent displacement d^* of the SDoF system, using equation III-E.4.2.

Finally, the negative post-capping stiffness (starting at point B) should be determined in such a way that the sum of the squares of the differences between $F^*(d^*)$ and its idealization after point B is minimized.

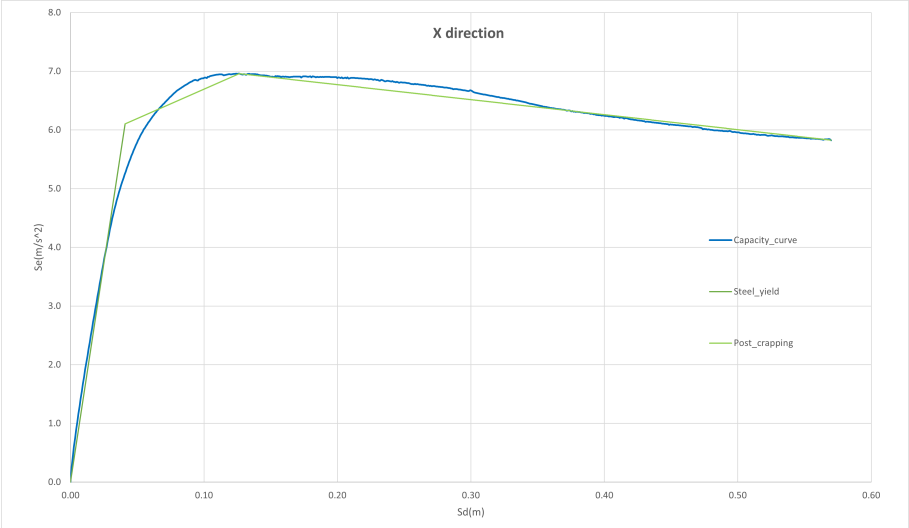

(a) X direction

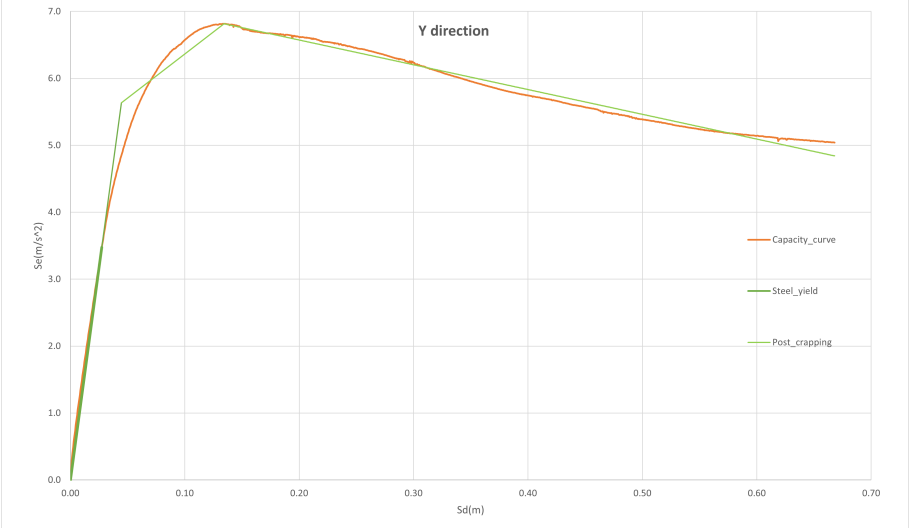

(b) Y direction

Figure III-E.9: Idealised pushover curve in terms of accelerations and displacement for each direction according prEN1998:-1-1 2022

Determination of the period

Using the same expression III-E.4.4, the period T^* of the SDoF system can be determined, resulting $0.514s$ and 0.558 for X and Y direction respectively.

Determination of target displacement

The target displacement for the SDoF system in both directions in the case of period T^* greater than T_C, is equal to the elastic displacement response spectrum S_{De} in terms of AD format at that period, for the limit state under verification. In X direction results:

$$d_t^* = d_{et}^* = S_{De}(T^*) = S_{De}(0.514s) = 0.049m \tag{III-E.4.8}$$

Therefore, the target displacement d_t of the entire structure is equal to $0.069m$ and $0.076m$ in the X and Y direction, respectively.

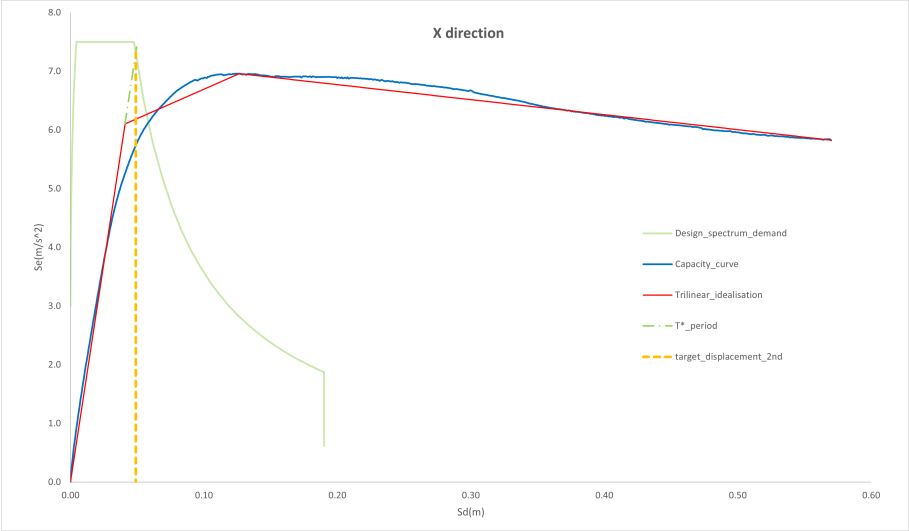

(a) X direction

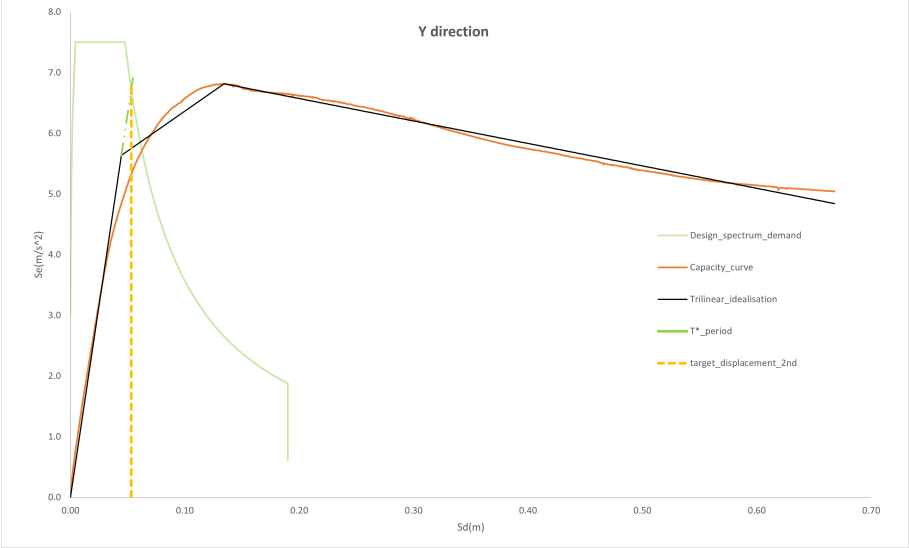

(b) Y direction

Figure III-E.10: N2 method representation for X and Y direction of the building (prEN1998-1-1: 2022)

Comparing both linear idealizations, it seems that the 2nd generation method under the same design spectrum demand gives smaller values of the target displacement. However, the difference is so minimal that is not convenient to ensure that the current version of Eurocode 8 is non conservative.

III-E.5. Performance criteria

During the pushover, in Seismostruct, performance evaluation of the structural elements throughout each time step of the analysis, for different situations, can be executed. Among the different criterion types that can be examined there are chord rotation yielding, chord rotation capacity, shear capacity, bending moment capacity for frame elements; strains in concrete; section curvatures; and reinforcement and/or steel strains. The user also defines strength degradation if

exists, the material type to be analyzed and the elements to be evaluated for each performance criteria.

III-E.5.1 Criteria for material strains

Crushing of core concrete: to identify when the elements concrete core crushes, defined as a negative strain larger than the ultimate crushing strain of confined concrete material, in this case, is equal to -0.8%. This value comes out from the definition that the ultimate compression strain in confined concrete occurs when transverse confining steel fractures, which may be estimated by equating the strain-energy capacity of the transverse steel at fracture to the increase in energy absorbed by the concrete [13]. The last is depicted in figure III-E.11.

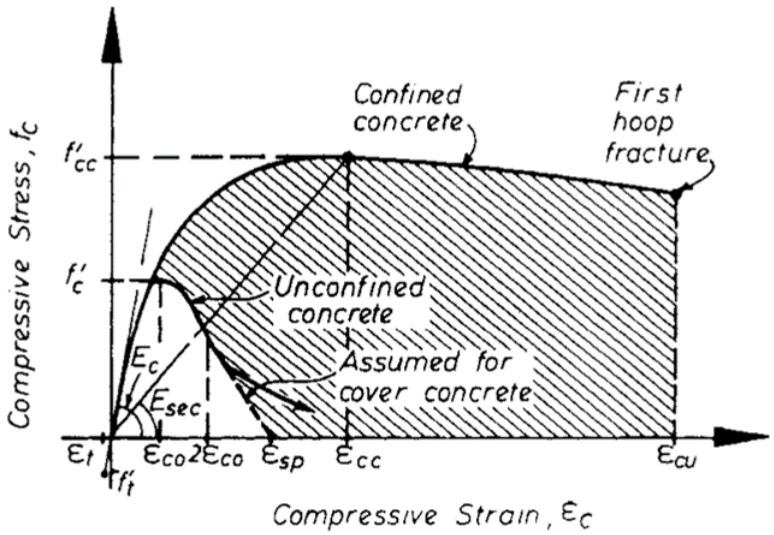

Figure III-E.11: Stress-strain model for monotonic loading of confined and unconfined concrete in compression. Adapted from [13]

Another criterion to determine the point of unconfined concrete spalling is defined, corresponding to negative strains larger than the ultimate crushing limit, equal to -0.35% (strain value used from the concrete properties of the unconfined concrete in table III-D.3).

Reinforcement strain: used to detect when the reinforcing steel yields, having steel strains larger than the ratio between yield strength and elasticity modulus, according to steel properties the value is equal to 0.002875. Similarly, a criterion to identify the steel rupture is when the steel strain is larger than the value of fracture strain, in this case, 0.20 is the defined value. Values used from the steel properties enlisted in III-D.4.

III-E.5.2 Criteria for frame elements

For the calculations of frame elements capacity, whether chord rotation capacity or shear capacity, the mean material values without safety factors are used. The last is stated in [17].

Shear capacity
Shear strength V_R of the beams, columns, and walls are computed with the following expression named (A.12) in [17]:

$$V_{\mathrm{R}} = \frac{1}{\gamma_{\mathrm{el}}}\left[\frac{h-x}{2L_{\mathrm{V}}}\min\left(N; 0,55A_{\mathrm{c}}f_{\mathrm{c}}\right) + \left(1 - 0,05\min\left(5; \mu_{\Delta}^{\mathrm{pl}}\right)\right)\right] \left[0,16\max\left(0,5; 100\rho_{\mathrm{tol}}\right)\left(1 - 0,16\min\left(5; \frac{L_{\mathrm{V}}}{h}\right)\right)\sqrt{f_{\mathrm{c}}}A_{\mathrm{c}} + V_{\mathrm{w}}\right]\right] \quad \text{(III-E.5.1)}$$

where γ_{el} is equal to 1.5 for primary seismic elements; h is the depth of the cross section; x is the compression zone depth; N is the compressive axial force; $L_V = \frac{M}{V}$ as the moment/shear ration at the end section; A_c is the cross-section area; f_c is the concrete compressive strength; ρ_{tot} as total longitudinal reinforcement ration; V_w contribution of transverse reinforcement to shear resistance.

Chord rotation at yielding

In current generation of Eurocode 8, part 3, the deformation capacity is defined in terms of the chord rotation θ_y, which is defined as *"the angle between the tangent to the axis at the yielding end and the chord connecting that end with the end of the shear span, that is the inflection point. The chord rotation is also equal to the element drift ratio, that is, the deflection at the end of the shear span with respect to the tangent to the axis at the yielding end, divided by the shear span"* [17]. There are two sets of expressions to evaluate the chord rotation at yielding θ_y, where equations with label [A.10] are used to beams and columns, and with label [A.11] for the walls.

The first set of equations is:

$$[A.10a] \quad \theta_y = \phi_y\frac{L_V + a_V z}{3} + 0.0014\left(1 + 1,5\frac{h}{L_V}\right) + \frac{\varepsilon_y}{d - d'}\frac{d_{bL}f_y}{6\sqrt{f_c}} \quad \text{(III-E.5.2)}$$

$$[A.11a] \quad \theta_y = \phi_y\frac{L_V + a_V z}{3} + 0.0013 + \frac{\varepsilon_y}{d - d'}\frac{d_{bL}f_y}{6\sqrt{f_c}} \quad \text{(III-E.5.3)}$$

and the second one:

$$[A.10b] \quad \theta_y = \phi_y\frac{L_V + a_V z}{3} + 0.0014\left(1 + 1.5\frac{h}{L_V}\right) + \phi_y\frac{d_{bL}f_y}{8\sqrt{f_c}} \quad \text{(III-E.5.4)}$$

$$[A.11b] \quad \theta_y = \phi_y\frac{L_V + a_V z}{3} + 0.0013 + \phi_y\frac{d_{bL}f_y}{8\sqrt{f_c}} \quad \text{(III-E.5.5)}$$

where:
L_V has the same definition as expression (III-E.5.1),
ϕ_y is the yield curvature of the end section (i.e. point of the moment-curvature curve in reinforces concrete section where the section starts to yield),
$a_V z$ is the tension shift of the bending moment diagram,
f_y and f_c steel yield stress and the concrete strength,
$\epsilon_y = f_y/E_s$,
d and d' are the depths to the tension and compression reinforcement, respectively, and
d_{bL} is the mean diameter of the tension reinforcement.

Both sets are basically the same expression and the only difference is regarding the calculation of the third component. In the second generation of EC8 just one set of equation is given for the calculation of the chord rotation at yielding: equation III-E.5.6 for rectangular columns and equation III-E.5.7 for walls and members with hollow rectangular section

$$[7.1]\quad \theta_{\mathrm{y}} = \phi_{\mathrm{y}} \frac{L_{\mathrm{V}} + a_1}{3} + \frac{\phi_{\mathrm{y}} d_{\mathrm{bL}} f_{\mathrm{y}}}{8\sqrt{f_{\mathrm{c}}}} + 0,0019 \left(1 + \frac{h}{1,6 L_{\mathrm{v}}}\right) \tag{III-E.5.6}$$

$$[7.2]\quad \theta_{\mathrm{y}} = \phi_{\mathrm{y}} \frac{L_{\mathrm{V}} + a_1}{3} + \frac{\phi_{\mathrm{y}} d_{\mathrm{bL}} f_{\mathrm{y}}}{8\sqrt{f_{\mathrm{c}}}} + 0,0011 \left(1 + \frac{h}{3 L_{\mathrm{v}}}\right) \tag{III-E.5.7}$$

To be consistent with the expressions of the next generation of EC8 to evaluate this chord rotation at yielding, and the fact that Seismostruct includes only the equations of the first version of EC8, the second set of equations (III-E.5.4 and III-E.5.5) can be considered convenient. These expressions for chord rotation at yielding contain three different contributions [17]. Some of them are neglected for simplicity in the modelization and to be conservative.

- First term: flexural contribution. The tension shift of the bending moment diagram a_V within this component is not taken into in the model.
- Second term: shear deformation contribution. With the fiber elements (i.e. infrmFB) is not possible to contemplate it, plastic hinge elements must be used instead.
- Third term: anchorage slips component. Is not considered in the model (may be added with springs located at the base of the elements).

The expressions computed analytically from EC8 (III-E.5.4 and III-E.5.5), where the three contributions are considered, give a much larger value compared with the results in Seismostruct. EC8 considers the plastic hinge (elements) approach for the walls, columns, and beams where you defined the moment rotation behaviour at the plastic hinges, instead fiber elements used in this model.

From the three contributions, only the first term associated with the flexure component is used as the point where the first yielding in a primary structure occurs, which defines the elastic stiffness during the multi-linear idealization of the SDoF in section III-E.4.2.2. In other words, the use of this component without the tension shift factor a_1 is equivalent to saying the point where the first yielding of the reinforcement occurs in a certain element.

The chord rotation at yielding is then reduced to:

$$\theta_y = \phi_y \frac{L_V}{3} \tag{III-E.5.8}$$

Chord rotation capacity:
Similar to the chord rotation at yielding, part 3 of the current EC8 gives two alternatives to compute the chord rotation capacity. The first one avoids the calculation of the chord rotation at yielding explicitly (equation III-E.5.9); the other is given by the sum of the elastic part (yielding) and the inelastic part (can be derived from equation III-E.5.10).

$$\theta_{um} = \frac{1}{\gamma_{el}} \cdot 0.016 \cdot (0.3^{v}) \left[\frac{\max(0.01;\omega')}{\max(0.01;\omega)} f_c\right]^{0.225} \cdot \left(\min\left(9, \frac{L_V}{h}\right)\right)^{0.35} \cdot 25^{\left(\alpha \rho_{sx} \frac{f_{yd}}{f_c}\right)} \cdot \left(1.25^{100\rho_d}\right) \tag{III-E.5.9}$$

$$\theta_{\mathrm{um}}^{\mathrm{pl}} = \theta_{um} - \theta_y = \frac{1}{\gamma_{\mathrm{el}}} 0.0145 \cdot (0.25^{v}) \left[\frac{\max(0.01;\omega')}{\max(0.01;\omega)}\right]^{0.3} \cdot f_{\mathrm{c}}^{0.2} \cdot \left(\min\left(9; \frac{L_V}{h}\right)\right)^{0.35} \cdot 25^{\left(\alpha \rho_{sx} \frac{f_{yw}}{f_c}\right)} \cdot \left(1.275^{100\rho_{\mathrm{d}}}\right) \tag{III-E.5.10}$$

where:
γ_{el} is equal to 1.8 for primary seismic elements,
α is the confinement effectiveness factor,
$\nu = N/bhf_c$ is the axial force ratio,
w,w' is the mechanical reinforcement ratio of the tension and compression longitudinal reinforcement, respectively,
ρ_d is the steel ratio of diagonal reinforcement (if any),
others variables have the same definition as the previous expression.
In the case of structural walls, the value given by (III-E.5.10) needs to be multiplied by 0.6

However, the 2nd generation of EC8 gives just the second alternative as the superposition of the elastic and the plastic part (equation III-E.5.11), which is similar to equation III-E.5.10.

$$[7.4] \quad \theta_{\mathrm{u}} = \theta_{\mathrm{y}} + \theta_{\mathrm{u}}^{\mathrm{pl}} \tag{III-E.5.11}$$

Therefore, been consistent with the assumptions taken for yielding chord rotation, the assumption of definition for chord rotation capacity as the superposition of the elastic and the inelastic part is considered the most appropriate. The elastic part that corresponds to the chord rotation yielding θ_y given by equation III-E.5.8. Whereas the plastic part of the chord rotation capacity follows the equation III-E.5.10:
In conclusion, the ultimate chord rotation capacity of concrete members is given by:

$$\theta_{um} = \theta_y + \theta_{\mathrm{um}}^{\mathrm{pl}} \tag{III-E.5.12}$$

III-E.5.3 Near collapse limit state (NC) comparison

The Near collapse limit state (NC) of a structural element is usually defined as the point where its capacity curve drops by 20%, relative to the maximum previously attained. At the level of an entire structure, this quantitative definition of the NC limit state does not exist. In some cases, a similar definition as in the case of individual elements, at a 20% drop of the lateral resistance of the structure. However, this definition, cannot be applied in non-linear dynamic analysis, or pushover analyses with simplified models (e.g. models without strength degradation) [9].

A more appropriate and practical definition of the NC limit state for entire structures is that it is reached when the first important vertical element (i.e. a column or a wall) reaches the NC [9]. In other words, the flexural deformation capacity of those structural elements will control their NC limit state and therefore that of the structure. In the case of ductile components and/or mechanisms, that is, beams, columns, and walls under flexure with and without axial forces, the deformation capacity is defined in terms of chord rotation θ.

The following figures depict the most important structural element scenarios in terms of chord rotation at yielding (θ_y) and chord rotation failure (θ_{um}), and their corresponding absolute lateral displacements of the building (d_t) per storey.

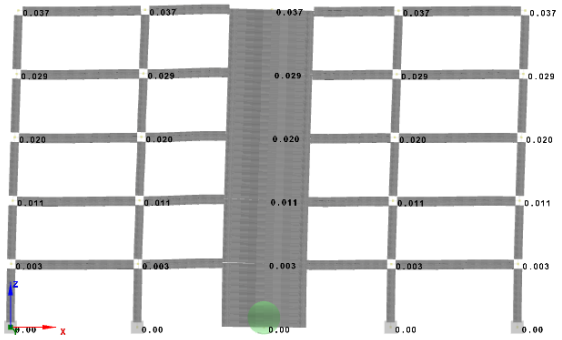

(a)

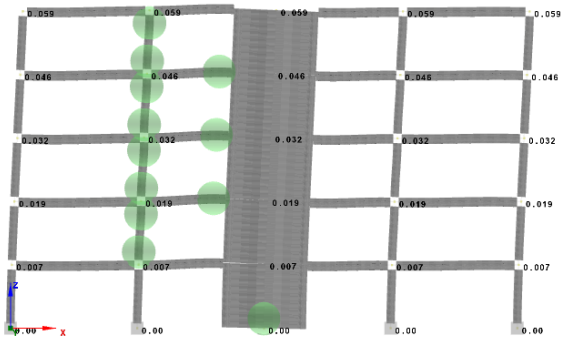

(b)

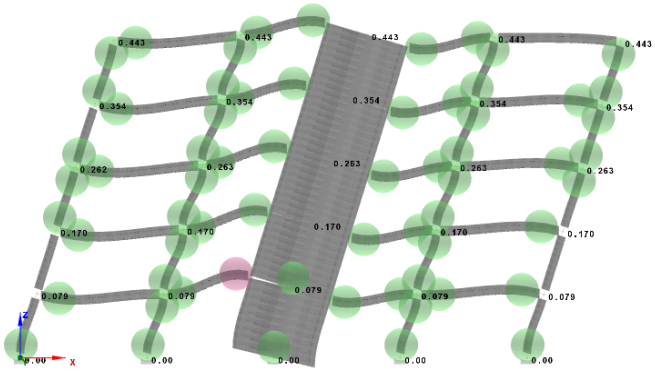

(c)

Figure III-E.12: The green and purple colors represent the chord rotation at yielding (θ_y) and chord rotation failure (θ_{um}), respectively, in the elements. (a) Chord rotation at yielding (θ_y) in the structural walls; (b) Yielding point (d_y) of equivalent SDoF system obtained in (III-E.4.2.2); (c) First chord rotation failure (θ_{um}) in beams. Extracted from Seismostruct model. (1/2)

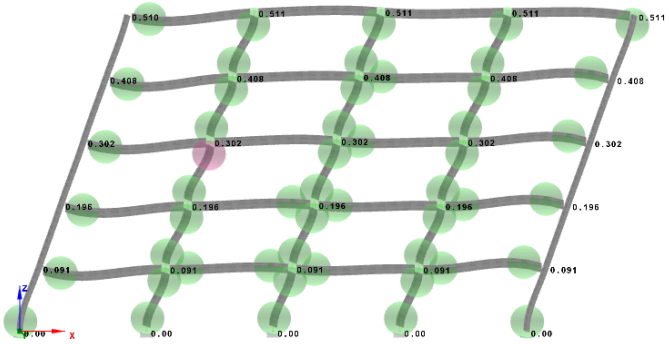

(a)

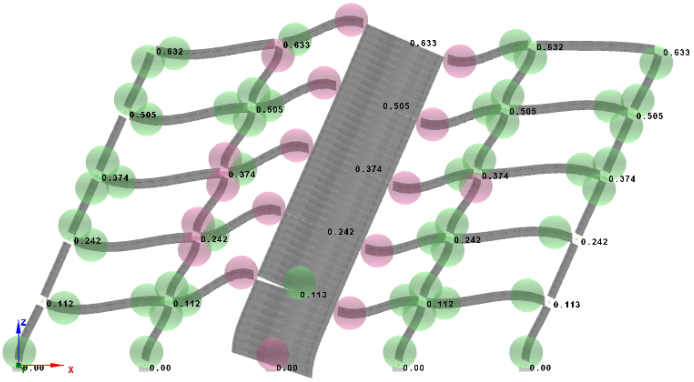

(b)

Figure III-E.13: The green and purple colors represent the chord rotation at yielding (θ_y) and chord rotation failure (θ_{um}), respectively, in the elements. (a) First chord rotation failure (θ_{um}) in columns (middle frame); (b) Chord rotation failure (θ_{um}) in structural walls. Extracted from Seismostruct model. (2/2)

Some remarks related to the previous scenarios can be done using the capacity curve for both directions (figure III-E.14 and III-E.15):

- Chord rotation at yielding in the structural wall (III-E.12a): displacement depicted with yellow dashed line by which the elastic stiffness (k^*) of the equivalent SDoF is obtained.
- Yielding horizontal displacement (III-E.12b): illustrated with the pink dashed line which represents the beginning of the inelastic zone of the equivalent SDoF system.
- Chord rotation failure in the first beam (III-E.12c): displacement in light blue dashed line in the capacity curve that shows where the first beam (next to the wall) reaches the chord rotation failure. Being located next to the structural wall, it is expected to be subjected to a high-stress demand and therefore large chord rotations.
- Chord rotation failure in column (III-E.13a): displacement in purple dashed line which evidences the chord rotation failure in the first column, occurring after beams as expected. The column reaches its capacity after the adjacent beams have already undergone large deformations and therefore are transmitted to the column throughout the node.
- Chord rotation failure in the wall (III-E.13b): displacement in green dashed line which indicates the wall failure by chord rotation. This failure occurs after some beams and columns have already reached the chord rotation failure, this behaviour can be also predicted within wall-equivalent dual systems.

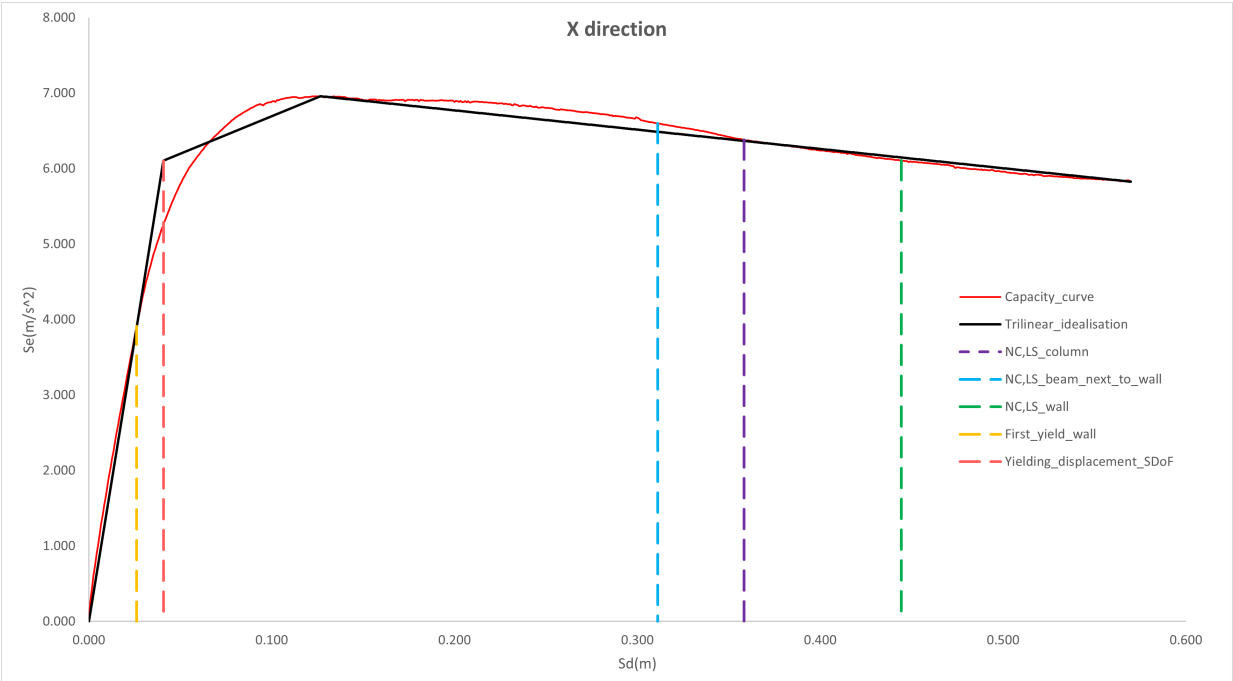

Figure III-E.14: Chord rotation failure comparison for different members in X direction

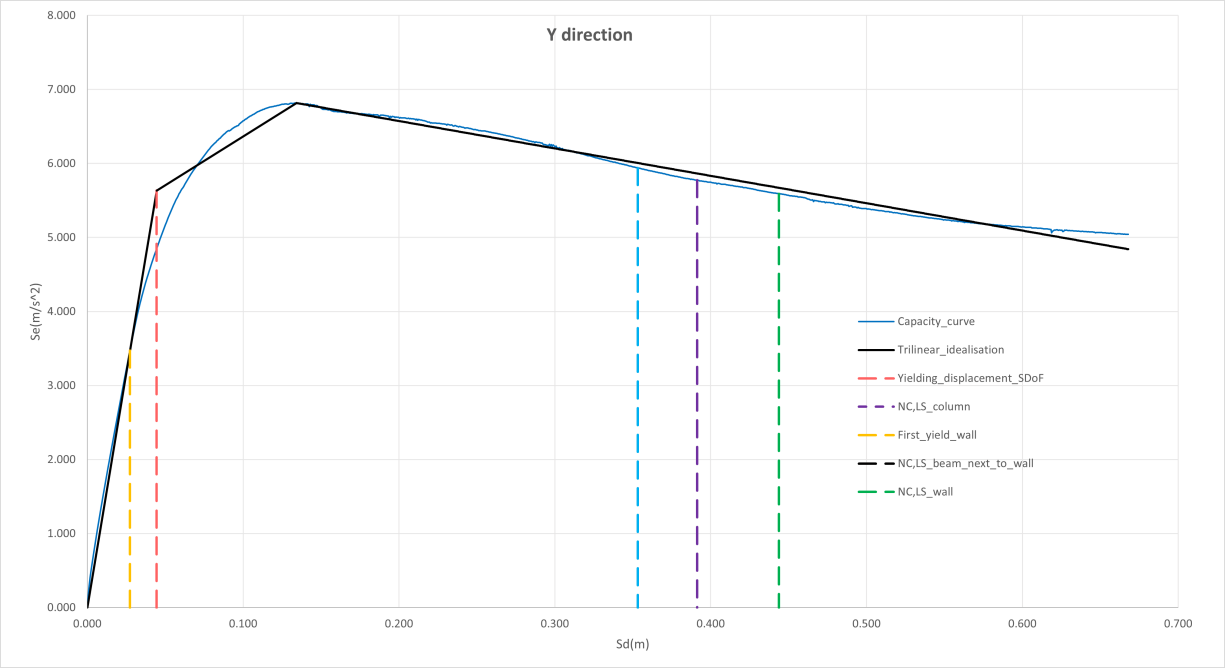

Figure III-E.15: Chord rotation failure comparison for different members in Y direction

CHAPTER III-F

NON-LINEAR DYNAMIC ANALYSIS (DTHA)

Many structural engineers use non-linear dynamic analysis for earthquake-resistant design, especially for retrofit, and to assess the behaviour of existing structures. It is also commonly used to predict the non-linear inelastic response of structures subjected to an earthquake.

In Dynamic Time History Analysis (DTHA), the modelling of the seismic action is achieved by introducing acceleration loading curves (i.e. accelerograms) at the supports of the structure. Among the positive effects of inducing ground motions in the model are better information obtained if significant non-linear behavior is expected in a structure; a more accurate manner to predict the amount of damage, and hence for assessing earthquake risk.

Nonetheless, additional inelastic properties are needed due to the possibility of yielding in some components, as well as the non-linear behavior type. These inelastic properties include such parameters as the yield strength, the post-yield behavior, the stiffness degradation under cyclic loading, and residual strength. It is important to highlight the difference between dynamic and static time history analysis, (DTHA and STHA, respectively) which is the inclusion of the inertia and damping parameters in the first one.

The steps to run a standard DTHA can be summarized as follows:

- Definition of structure geometry.
- Define the gravity loads.
- Definition of the properties of the structural components.
- Selection of the earthquake ground motions.
- Run a non-linear dynamic analysis for each accelerogram.
- Evaluate the performance, using both deformation and strength demand/capacity (D/C) ratios.
- If necessary revise the design and re-analyze.

III-F.1. prEN1998-1-1: 2022: Annex D

In the next generation of EC8, Annex D is called: *Criteria for selection and scaling of input motions*, and as its name says, it provides additional provisions for selection and scaling of accelerograms to run response-history analyses [12].

In the modelling, analysis, and verification section of the mentioned edition is stated that the minimum number of input motions should be at least seven, for the case of Response-history analysis. However, will be seen later in section (III-F.2) that this number is larger for specific cases when one needs to determine the target displacement or limit-state spectral acceleration through non-linear response history analyses.

III-F.1.1 Recorded accelerograms

This Annex also describes different ways to obtain such ground motions: recorded, simulated, and artificial accelerograms; and within each kind of accelerogram certain provisions must be satisfied. It is expressed in Annex D that recorded ground motions should be the preferred representation of the seismic action for analyses in the time domain, and naturally, they shall be obtained from qualified strong-motion databases.

Besides, the following requirements for the use of recorded accelerograms, including their scaling, must be satisfied:

- The spectral acceleration of each ground motion should approach the elastic response spectrum in the following period range: $0.2\,T_1$ to $1.5\,T_1$, where T_1 is the fundamental period of the structure in the direction in which the accelerogram is applied.
- The recorded accelerograms may be scaled to improve their compatibility with the target spectrum according to one of these methods: constant-amplitude scaling or spectra-matching scaling. The scaling factor should not be larger than 2 and smaller than 0.5.
- The compatibility of the ground motions after scaling is considered satisfied if in the previous period range: the ratio average 5%-damped response spectrum of the set to the target spectrum falls within the band from 0.75 to 1.3 and has an average value larger than 0.95, and the response spectrum of each accelerogram of the suite does not fall below 50% of the target spectrum.

III-F.1.2 Selection of recorded accelerograms with Seismoselect

As an earthquake engineering software solutions group, SEISMOSOFT, has software focused on finding, scaling, and downloading real earthquake accelerograms that are matched to a specific target response spectrum, called Seismoselect. It is an easy and efficient way to search, select, scale and download ground motion data from different strong-motion databases.

The software allows you to define a target response spectrum; different ground motion parameters such as peak ground acceleration (PGA) and intensity; information regarding the event (e.g. magnitude, date, location), and the recording site (e.g. $\nu_{s,30}$, epicentral distance). Based on these parameters the software finds sets of compatible records and provides ways to easily

download the selected records.

Using Seismoselect software and matching with the provisions enunciated in the previous section, the following criteria are defined to select the best set of accelerograms:

- Database: Engineering Strong-Motion Database v2.0 (ESM).
- Earthquake magnitude: from 5.5 to 7.5 on the Richter scale.
- Average shear wave velocity $\nu_{s,30}$: although the corresponding range for Ground type B is 360-800 (m/s), it is selected a range between 200 and 1000 (m/s) to be less restrictive.
- Peak ground acceleration (PGA): based on the characteristics of the site (II-B.2), the PGA range selected is within 0.15(g) and 0.5(g).
- Maximum numbers of records per event: two.
- Target response spectrum parameters: single horizontal component of the ground motions and the average spectral acceleration corresponding to the required range $0.2\,(0.5s) = 0.1s$ and $1.5\,(0.5s) = 0.75s$.
- Selection of 15 records as defined in Annex E.
- Scaling factor limits: lower limit 0.5 and upper limit 2.

III-F.1.3 Scaling of accelerograms

Once the set of accelerograms has been obtained from Seismoselect, the scaling factor (using the constant-amplitude scaling method) for each accelerogram is displayed. Then, those records can be downloaded as they are original and with a spreadsheet, the direct scaling can be done. Figure III-F.1 shows the response spectrum of the ground motions after the scaling factor obtained from the software is applied.

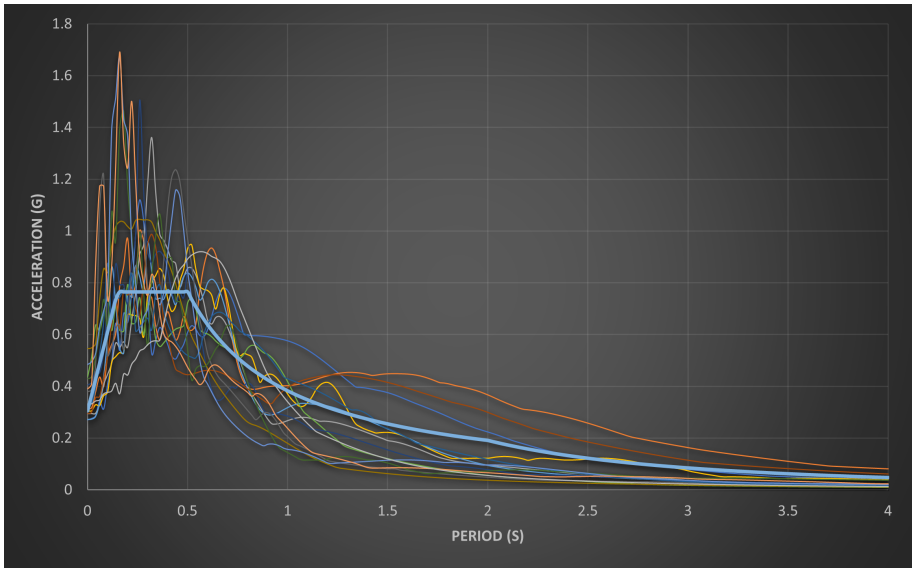

(a)

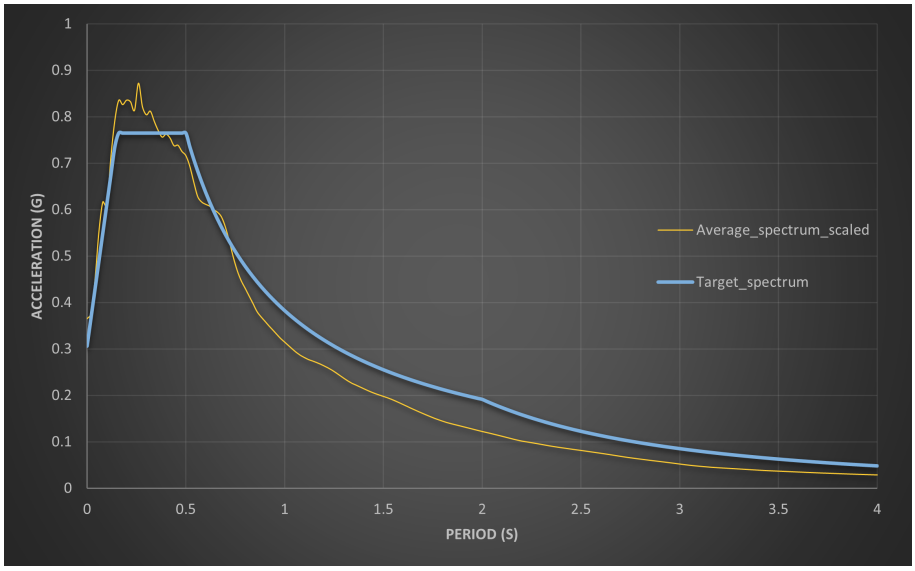

(b)

Figure III-F.1: (a) Response spectrum per ground motion after first scaling and target response spectrum (b) Average response spectrum of the ground motions after first scaling and target response spectrum

Knowing that the ground motions selected have different duration, about 13 to 130 seconds, by cutting all of them to the most important and/or significant lapse, a better representation of the average response spectrum can be obtained, and thus a better fit of the accelerograms. The last is depicted in figure III-F.2

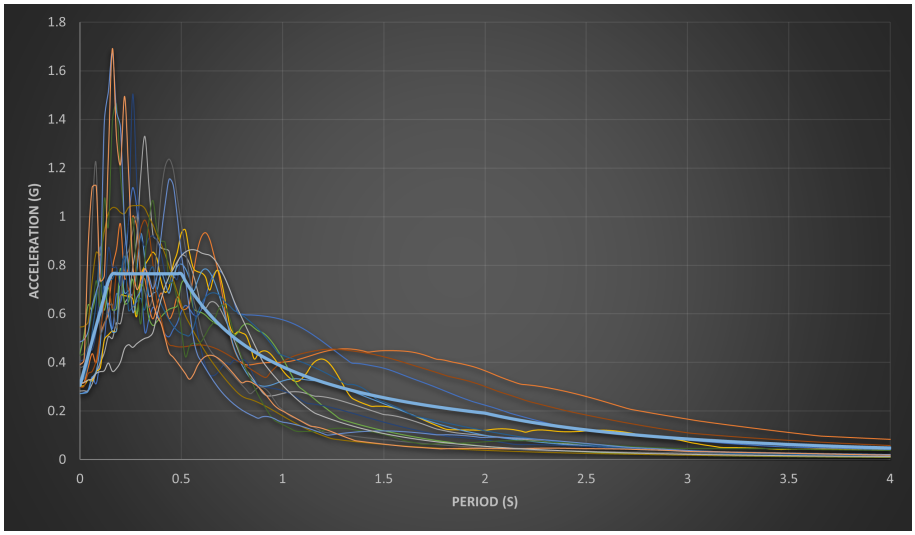

(a)

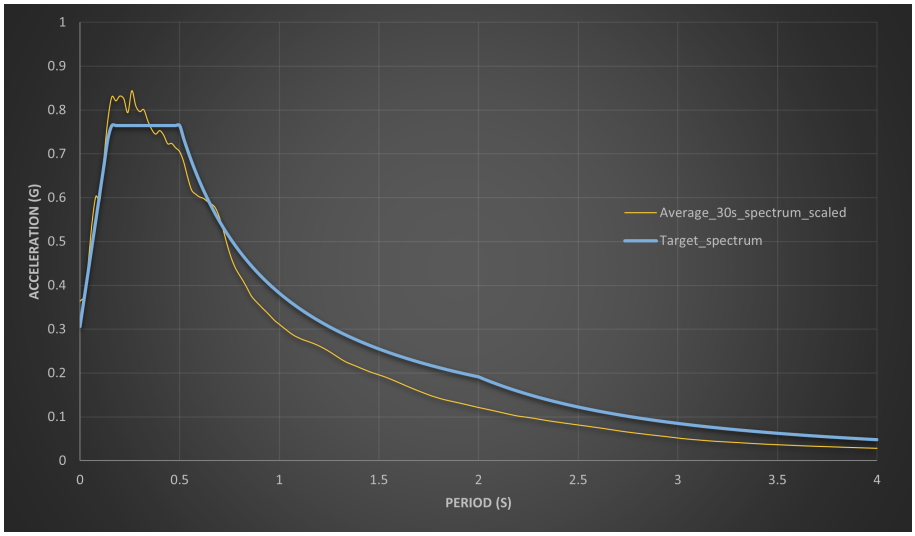

(b)

Figure III-F.2: (a) Response spectrum per ground motion cut to 30s and target response spectrum (b) Average response spectrum of the ground motions cut to 30s and the target response spectrum

Finally, following the provisions in Annex D, the spectral of each ground motions spectrum needs to be fitted in $0.2\,T_1$ to $1.5\,T_1$ in amplitude by a constant factor if the constant-amplitude scaling method is used. However, the lower limit of the period range specified before ($0.2\,T_1$) takes into account the higher vibration modes of the structure and since the response history analysis will be carried on for an equivalent SDoF system is not necessary to be considered. On the other hand, to ensure that the scaling includes properly the fundamental period of the system ($T_1 \approx 0.5s$), lower limit $T_L = 0.4s$ and upper limit $T_U = 1.75s$ is then used.

For better understanding, the steps to obtain the scaling factors for each accelerogram can be expressed as follows:

- Compute the geometric mean of the response spectrum for each accelerogram $GM_{fs,i}$ and for mean accelerogram $GM_{fs,mean}$ within T_L and T_U for the first scaling.
- Calculate the geometric mean of the response spectrum for each accelerogram $GM_{cut,i}$ and for mean accelerogram $GM_{cut,mean}$ within T_L and T_U for the cut of 30s.

- Determine the geometric mean of the target spectrum for the same range: GM_t
- Calculate the correction scaling factor for each accelerogram $SF_{corr,i} = \frac{GM_{fs,i}}{GM_{cut,i}}$ and for mean accelerogram $SF_{corr,i} = \frac{GM_{fs,mean}}{GM_{cut,mean}}$
- Obtain the final scaling factor for each accelerogram as: $SF_{final,i} = [SF_{corr,i}] * \left[\frac{GM_t}{GM_{fs,mean}}\right]$
- Compute the final response spectrum for each accelerogram by multiplying the final scaling factor and the corresponding spectral acceleration (cut of 30s):

$$S_{a,i} = S_{a,cut} * SF_{final,i}$$

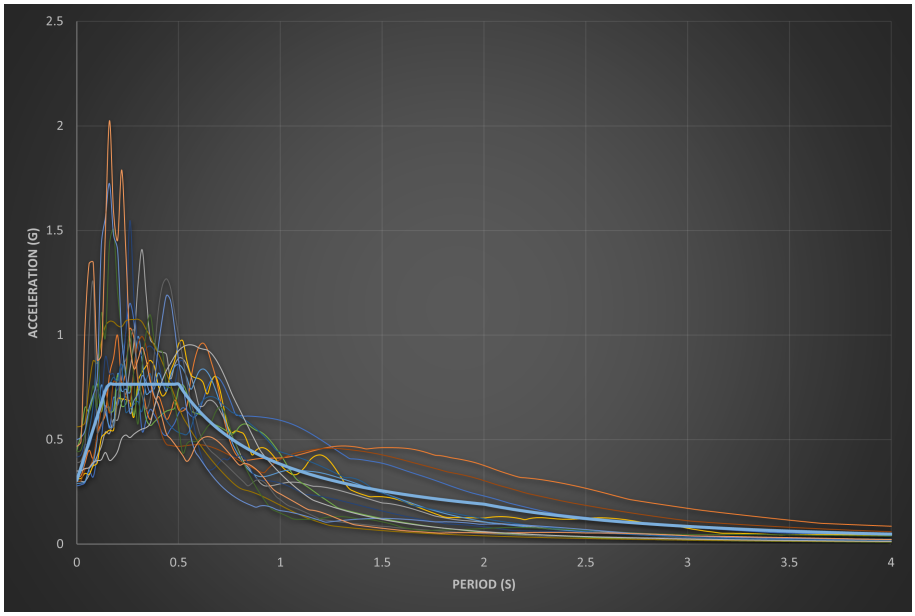

(a)

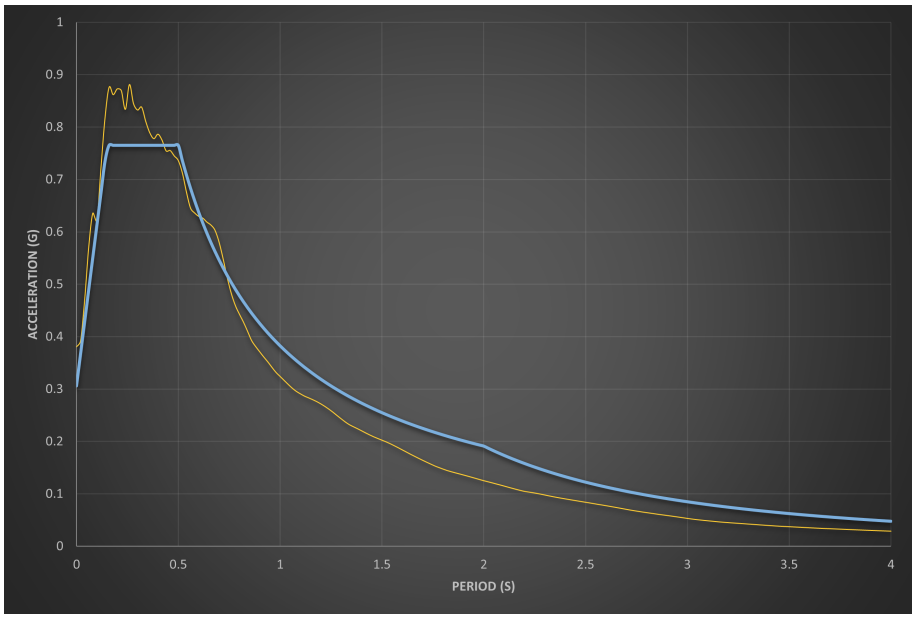

(b)

Figure III-F.3: (a) Final response spectrum per ground motion and target spectrum (b) Final average response spectrum and target response spectrum

To recap, the target response spectrum used in this ground motion selection is the elastic response spectrum type 1 depicted in figure III-D.3. Initially, in the design procedure of the structure, this code spectrum represents the seismic action corresponding to the No-Collapse limit state (NC) with a probability of exceedance $P_{NCR} = 10\%$ in 50 years for a reference return period $T_{NCR} = 475$ years, as defined in EN1998-1-1:2004. Since the limit state of Significant Damage (SD) for assessing structures ascribed, in EN1998-1-3:2004, to the seismic action associated with reference return period $T_R = 475$ years, corresponding to a probability of exceedance of $P_R = 10\%$ in 50 years, they are considered roughly equivalent.

III-F.2. prEN1998-1-1: 2022: Annex E

This annex gives additional provisions to determine target displacement (beside the procedure showed in III-E.10) and limit-state spectral acceleration by using non-linear response-history analysis of an equivalent SDoF model [12].

As will be seen in the next sections, Annex E provides detailed procedures to define an equivalent SDoF model based on a multi-linear force-displacement relationship, and estimate the target displacement and the limit-state spectral acceleration by using non-linear response-history analyses of an equivalent SDoF model.

III-F.2.1 Definition of a multi-linear equivalent SDoF model according prEN 1998-1-1:2022

To obtain the force-displacement relationship $F^*(d^*)$ of the equivalent SDoF model it should be determined from the capacity curve of the entire building, with at least a trilinear curve when a non-linear response-history analysis is necessary, exactly as explained in section III-E.4.2.2.

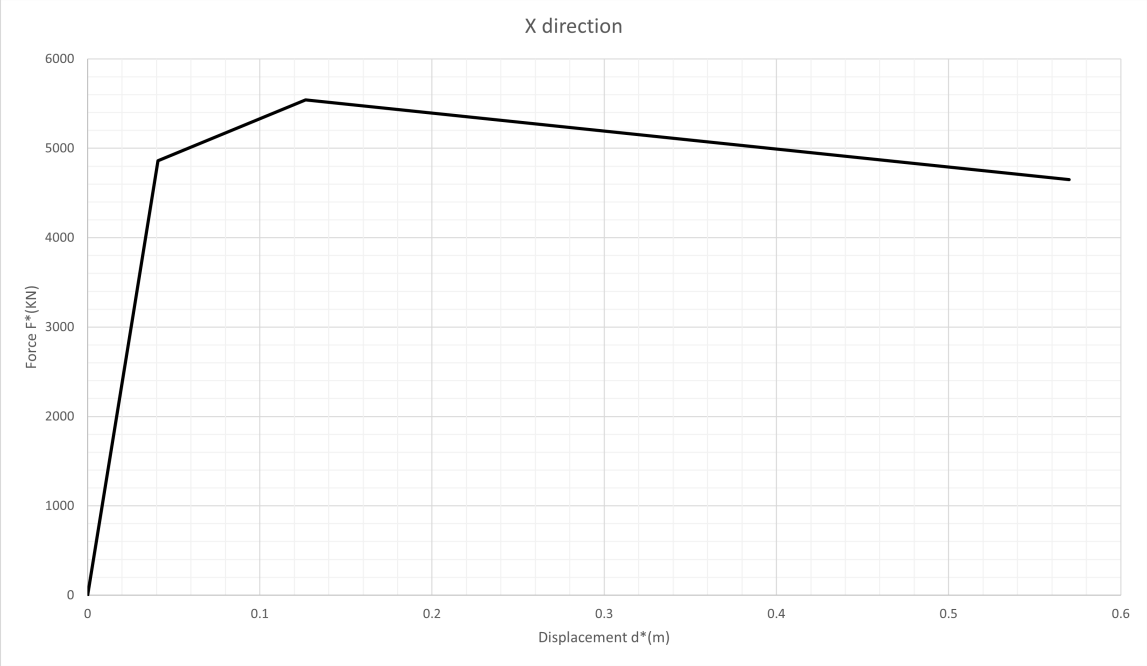

Figure III-F.4: Capacity curve in terms of equivalent SDoF $F^*(d^*)$

III-F.2.2 Description of Seismostruct model

Once the building is represented in the equivalent SDof model and the corresponding capacity curve, the definition in Seismostruct software can be done with special elements called *link elements*.

The link element is equivalent to saying that it is a non-linear spring that follows the response of the trilinear approximation obtained in the equivalent SDoF system. At the same time, this

link element connects two initially coincident structural nodes with the same coordinates, and require the definition of an independent force-displacement response (hysteretic) curve, for each of its six degrees of freedom that reflect the cyclic behaviour of the system. Moreover, the mass acting for each degree of freedom needs to be defined. In this case, the effective mass to be defined is just acting in the X direction where the ground motions are applied ($m^* = 796.17ton$)

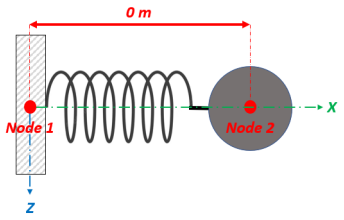

Figure III-F.5: Free body diagram of equivalent SDoF model

Since the analysis needs to be performed for 15 different ground motions and the model is quite simple, an efficient solution is to parallel replicate a link model 15 times so that all responses from each ground motion applied in the same direction can be associated with a different link element.

III-F.2.2.1 Hysteretic behaviour of the equivalent SDoF model

Seismostruct presents twenty-nine response curves that can be selected for the representation of the model hysteresis. All options(curves) include different characteristics, among them: strength degradation, stiffness degradation, pinched hysteretic loops, symmetric or asymmetric elastic-plastic behaviour, unloading stiffness deterioration, accelerated loading stiffness deterioration, and others.

For the definition of the hysteretic behaviour, Annex E gives the following provisions:

- The hysteretic behaviour of the SDoF model should be representative and it should also reflect the response of the whole structure and not only a single structural element behaviour. This is the reason why the capacity curve of the entire building is used.
- It is not necessary to include the deterioration of the cyclic force in the hysteretic behavior since this effect is considered in the nonlinear model of the entire structure.
- A peak-oriented behaviour of the hysteretic model needs to be implemented.

Initially, several models that meet previous provisions including the trilinear envelope of the capacity curve have been tested, such as *multi-linear curve, simplified bilinear Takeda curve, Ibarra-Medina-Krawinkler deterioration model with peak-oriented hysteretic response, trilinear symmetric curve* and *pinched asymmetric curve*. However, just the *pinched asymmetric curve* model adapted to the requirements results in a proper representation of the equivalent SDoF system against input ground motions.

Pinched asymmetric model

This hysteretic curve is a uniaxial force-displacement model characterized by non-linear stiffness and strength deterioration rules and also by pinching of force and displacement. It is also able to add the damage deterioration due to ductility and energy [11]. The envelope curve of this model is defined by supplying three force-displacement pairs for the positive branch and three force-displacement pairs for the negative branch (left side in figure III-F.6).

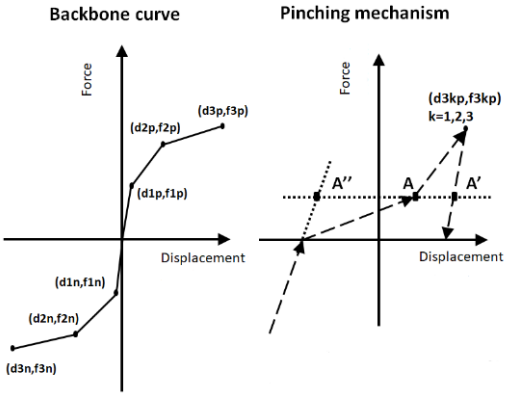

Figure III-F.6: Backbone (envelope) curve and characteristics of the pinched asymmetric model. Adapted from Seismostruct help system

The envelope curve, or backbone curve, of this model can be described as the capacity curve (showed in figure III-F.4) with the following slopes:

- The first slope represents the elastic (initial) stiffness, with points $f1p$ and $d1p$ as the yield strength and yield displacement respectively.
- The second one is called strain-hardening stiffness, which its final coordinate called capping (peak) point $f2p$ and $d2p$.
- The last slope or softening branch shows the post-capping stiffness which usually has a negative slope defined as the ultimate point with coordinates $f3p$ and $d3p$.

Although the envelope curve of the hysteretic model is defined in six different pairs of points, the equivalent SDoF model is symmetric for each direction, so the magnitude of those pairs of points is the same.

Table III-F.1: Displacements and forces for the envelope curve

Coordinates	Displacement d^* (m)	Force F^* (KN)
Positive 1	d1p = 0.041	f1p = 4860
Positive 2	d2p = 0.126	f2p = 5540
Positive 3	d3p = 0.570	f3p = 4650
Negative 1	d1n = -0.041	f1n = -4860
Negative 2	d2n = -0.126	f2n = -5540
Negative 3	d3n = -0.570	f3n = -4650

The right side in figure III-F.6 illustrates the characteristics called pinching hysteretic loops that are usually the results of crack closures in the reinforced concrete and could be taken into account for the displacement and/or force during reloading phases of the cyclic loads. The pinching

model is similar to the peak-oriented one, except that reloading consists of a first part when the reloading path is directed towards a "breakpoint" (point A in figure III-F.6) and a second one, when the reloading path is directed towards the maximum deformation of earlier cycles in the direction of reloading [10]. However, according to Annex E, it is not necessary for the modelling to include this behaviour, so by disabling the pinching in this curve the simple peak-oriented hysteretic model can be obtained directly.

Finally, the restraints of the model need to be defined as fixed in all degrees of freedom except the X direction where the accelerograms are applied. Also, the link element (spring) is defined to have a stiffness-proportional damping (Rayleigh damping) type according to the first vibration mode which corresponds to the period ($T^* = 0.51s$ for the X direction) of the equivalent SDoF system, with a damping ratio equal to 2% and a tangent stiffness variation.

An example of the SDoF model represented by this peak-oriented hysteretic behaviour model is depicted in the following figure III-F.7:

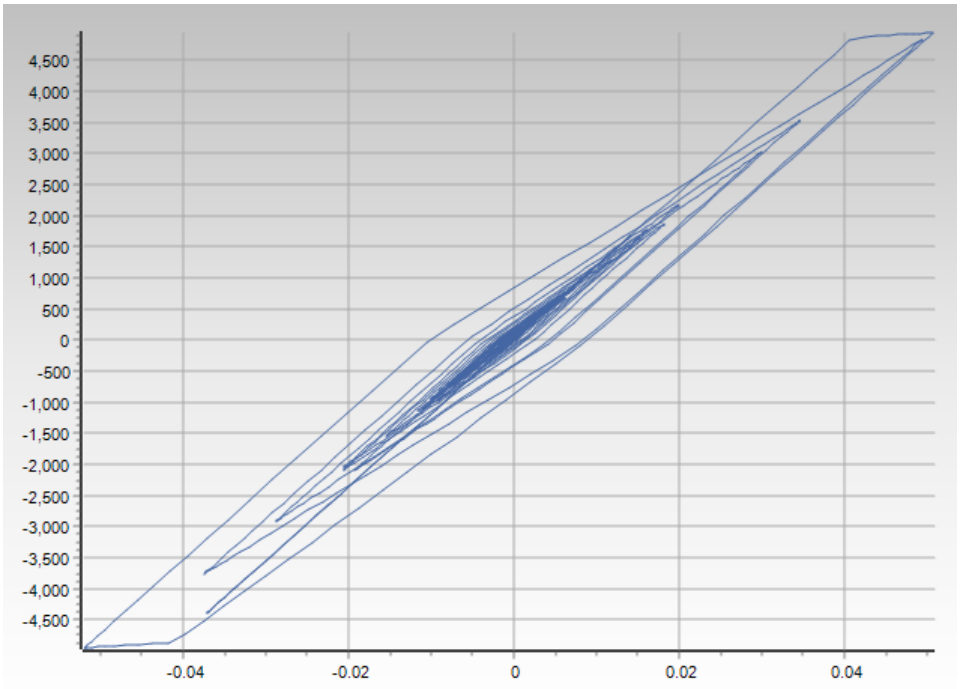

Figure III-F.7: Peak-oriented hysteretic behaviour of the equivalent SDoF system subjected to one ground motion selected

It can be seen that the peak-oriented behaviour is represented clearly, that is to say when the horizontal axis is reached (load changes from positive to the negative side or vice versa), the reloading path always targets the previous maximum displacement.

III-F.2.3 Determination of target displacement

The peak displacement of the equivalent SDoF model for the i-th accelerogram $d^*_{t,i}$, is calculated as the maximum of the absolute values of the displacement time history. Then, the first way to determine the target displacement of the SDoF model d^*_t is by defining it as the median value of peak displacements of all accelerograms. The second one is by calculating the following expression [E.2]:

$$d_t^* = \exp\left(\frac{1}{N_a}\sum_{i=1}^{Na}\ln(d_{t,i}^*)\right) = 0.049m \qquad \text{(III-F.2.1)}$$

where N_a represents the number of accelerograms.

Recapping the 15 SDoF models assigned with the corresponding ground motion applied, the non-linear response analyses for the seismic action with a return period of 475 years can be executed once at the same time for the 15 models and obtain the target displacement. The figure below shows the target displacement $d_t^* = 0.052m$ resulting in the median value of the peak displacements for the X direction.

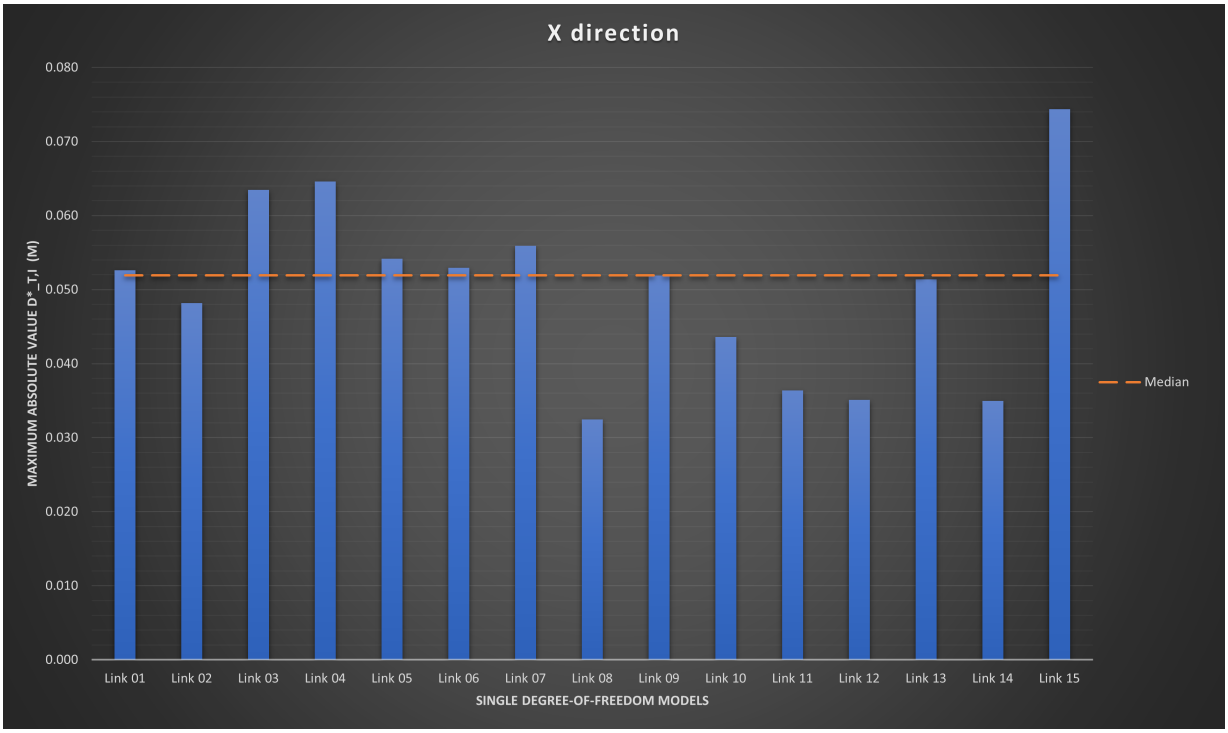

Figure III-F.8: Peak displacement of SDoF models for $T_R = 475\,years$

III-F.2.3.1 Target displacement comparison

Until now, four different methods to determine the target displacement of the equivalent SDoF system have been exposed, for the seismic action associated to a return period of 475 years: N2 method for the bilinear idealization according to EN1998-1-1:2004, N2 method for the trilinear idealization according to prEN1998-1-1: 2022, the median value of peak displacements in Annex E and the alternative expression III-F.2.1 of Annex E.

Table III-F.2: Target displacement d^* of the equivalent SDoF models for seismic demand with $T_R = 475$ years

Method	$d^*(m)$ [X direction]	$d^*(m)$ [Y direction]
EN1998-1-1:2004 [III-E.4.6]	0.054	0.059
prEN1998-1-1:2022 [III-E.4.8]	0.049	0.053
Annex E: median [III-F.8]	0.052	0.053
Annex E: Expression [III-F.2.1]	0.049	0.055

From the table III-F.2, it can be seen that for the case-study structure under the same seismic action the N2 method according to the current version of EC8 gives target displacements values larger than the ones obtained from the next generation of EC8. The difference from the second generation is about 9.3% and 10.2% smaller than the current version for the X and Y direction, respectively. This exhibits a significant underestimation of the performance point for the N2 method using the trilinear idealization (second generation). If the current bilinear idealization values are compared with the ones resulting from DTHA as the median value of peak displacements (Annex E), a better fitting is found for the X direction with just 3.7% difference and the same contrast (10.2%) for the Y direction. Again, if the EC8 current version results are taken as reference, the expression III-F.2.1 given in Annex E has the same difference for the X direction and much smaller dispersion (6.8%) for the Y direction as when compared with the N2 method of the second generation.

If a comparison were to focus on the methods given in the second generation of Eurocode 8, it seems that calculating the target displacements with the median value of peak displacements provided in Annex E is in good agreement with the N2 method, with only a small difference 6.1% in the X direction and identical results in the Y direction. The results that come out of the expression III-F.2.1 are the same as with the N2 method for the X direction and a 3.8% difference in the Y direction. As the Dynamic Time History Analysis (DTHA) is a method more complex and powerful compared to the N2 method, it can be proved then that the N2 method is a procedure with high reliability for the target displacement determination.

III-F.2.3.2 SDoF model vs MDoF comparison

Another interesting comparison between the equivalent SDoF model and the multi-degree-of-freedom structure can be performed, taking as reference the SDoF results for reference scaling factor $SF = 1.0$ with its corresponding spectral acceleration. The DTHA for this condition can be carried out for all the accelerograms and compare the MDoF system results with the ones obtained in the equivalent SDoF model.

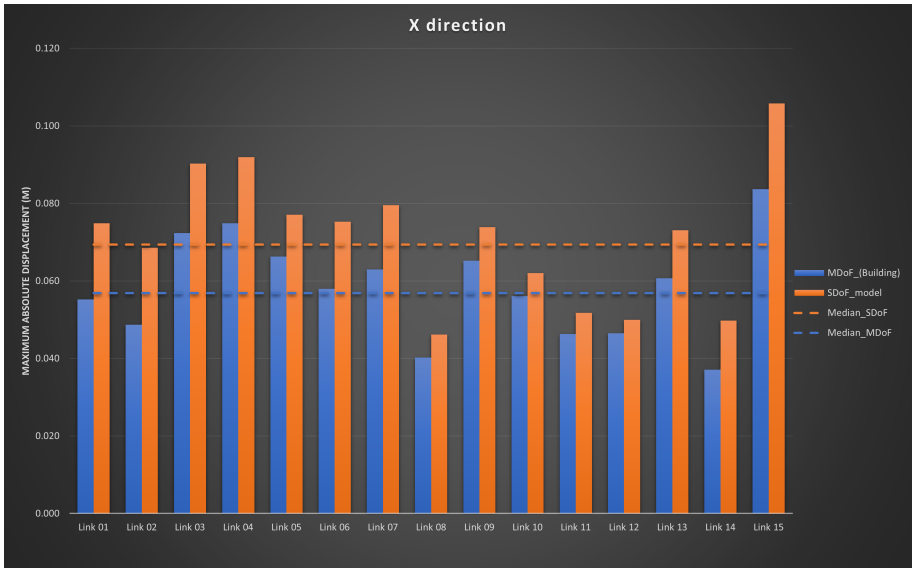

(a)

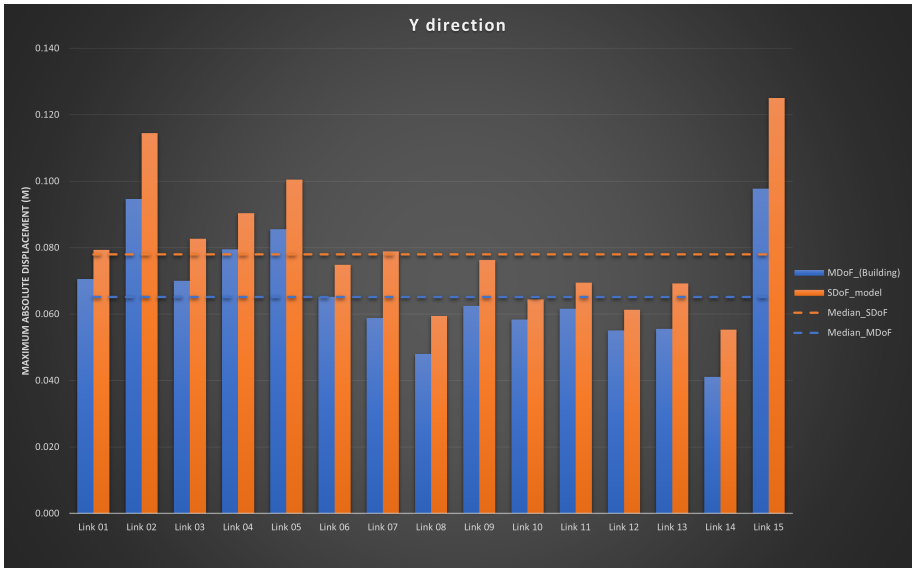

(b)

Figure III-F.9: (a) Maximum absolute displacements comparison in X direction (b) Maximum absolute displacements comparison in Y direction

Table III-F.3: Target displacement of the equivalent SDoF models vs MDoF models in global coordinates d_n for seismic demand with $T_R = 475$ years

Models	$d_n(m)$ [X direction]	$d_n(m)$ [Y direction]
Equivalent SDoF	0.069	0.078
Multi-degree-of-freedom (MDoF)	0.057	0.065

Note that until this section, previous target displacement calculations are computed in terms of the SDoF models d^*, so if a comparison with the entire building (i.e. MDoF system) needs to be made, a transformation to global coordinates is necessary through the expression: $d_n = \Gamma \cdot d^*$. It can be seen in figure III-F.9 that the magnitudes of the MDoF system are larger than the equivalent SDoF models, and they do not represent a conflict since the last one is an idealization

of the structure and in most cases, will be more conservative than when the whole building response is assessed.

III-F.2.4 Target displacements for seismic demand associated to Near collapse limit state (NC)

In the current edition of EC8 is also possible to evaluate structure performance for different seismic actions associated with other limit states using as reference the Significant Damage limit states (SD) shown in section III-D.3. This can be achieved by multiplying the reference seismic action by a scaling factor, called importance factor, γ_I, which may be computed as $\gamma_I = (T_{LR}/T_L)^{(-1/k)}$. Where $T_{LR} = 475\,years$ for Significant Damage limit state (SD), as the reference period, $T_L = 1600\,years$ in case of Near Collapse limit state (NC) [12], and $k = 3$ as recommended value.

The resulting response spectrum for the Near Collapse limit state associated with a return period $T_R = 1600\,years$ and with $\gamma_I = 1.5$, is given by:

$$S_{e,NC} = \gamma_I \cdot S_{e,SD}$$

By applying the N2 method of the same structure, the target displacement for the NC can be computed. See figure III-F.10.

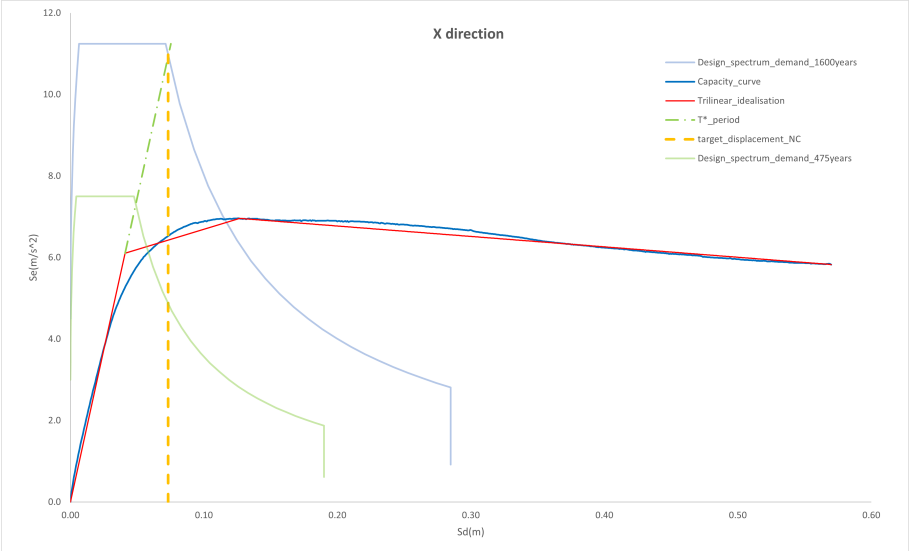

(a) X direction

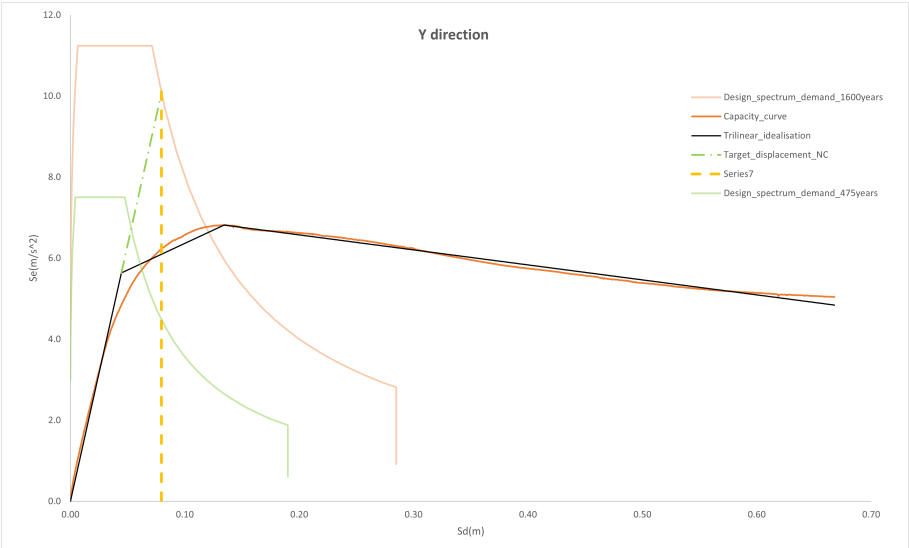

(b) Y direction

Figure III-F.10: Target displacement for seismic demand with return period $T_R = 1600\,years$

This target displacement obtained with the N2 method can be compared with the displacement at the Near Collapse state obtained in section III-E.5.3. This limit state for the SDoF system has been defined before, as the point where the chord rotation capacity of a vertical member (i.e. column) is reached.

In the second generation of EC8, part 3, the verification of the capacity implies the use of a safety factor $\gamma_{Rd,NC,d}$ (this safety factor is defined in [12] as the product of a factor $\gamma_{Rd,k} = 1.5$ and a shape factor $s_\gamma = 1$ for no circular sections). The resistance for the SDoF model for the Near Collapse limit state, in the X direction, is then given by:

$$d^*_{NC} = \frac{d^*_u}{\gamma_{Rd,NC,d}} = 0.239m \tag{III-F.2.2}$$

where $d^*_u = 0.358m$ is the point where the first column reaches its chord rotation capacity and $\gamma_{Rd,NC,d} = 1.5$ for no circular reinforced concrete sections.

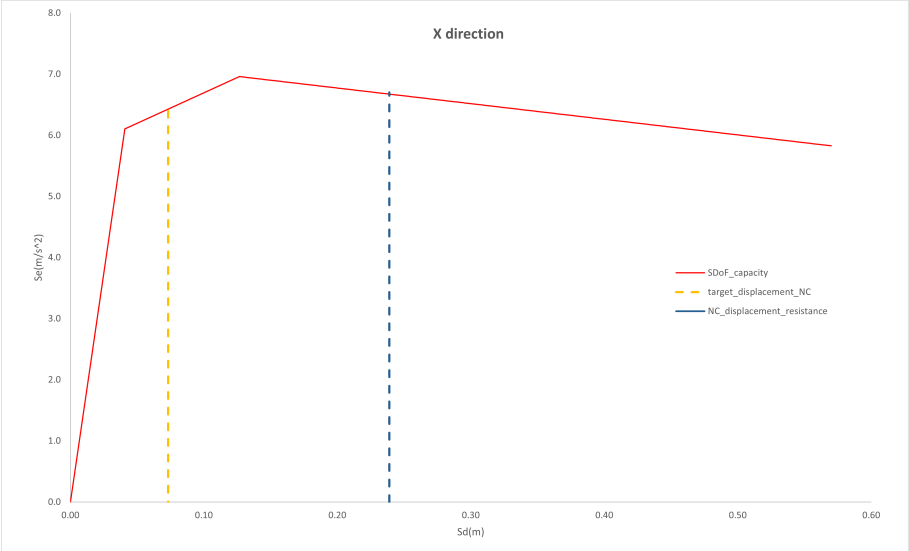

(a) X direction

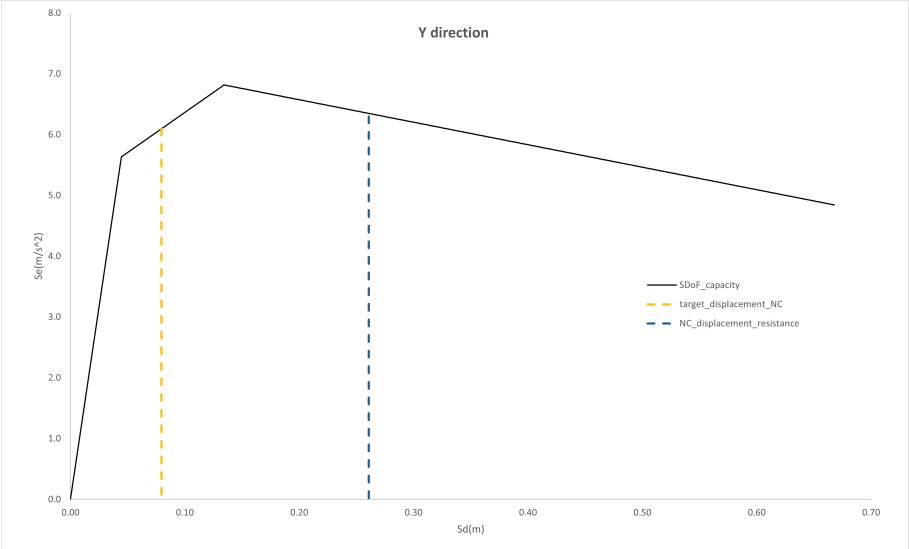

(b) Y direction

Figure III-F.11: Target displacement d^*_{NC} and resistance in terms of d^* for the Near Collapse limit state with $T_R = 1600\,years$

In figure III-F.11 can be observed that the structure accomplishes the requirements in terms of displacement for the Near Collapse limit state, with a verification ratio Capacity/Demand greater than 3 for both directions (using $d^*_{NC} = 0.261m$ in the Y direction). It is necessary to clarify that a comparison has been made for the Near Collapse limit state as defined in the second generation of EC8, this is the reason why the return period T_R to this limit state is 1600 years [12] and not 2475 years as stated in the current version of EC8 [17].

III-F.2.5 Determination of limit-state S_e

The last procedure given in Annex E refers to the determination of the limit-state spectral acceleration through non-linear response-history analysis. The limit-state spectral acceleration $S_{e_L S}$ is defined in this annex as the median value of spectral acceleration at the fundamental vibration period of the structure (T^* in this case) which causes a designated limit state. It can be also understood as the measure of the resistance of the structure if is expressed through the level of

spectral acceleration. This spectral acceleration is required for the reliability-based verification format developed in the next chapter.

To obtain the limit-state spectral acceleration, a selection of at least 15 accelerograms conforming to the provisions given in Annex D (III-F.1) should be applied. Moreover, this measure $S_{e,LS}$ may be obtained by incremental dynamic analysis (IDA). IDA is a method where a response-history analysis of the system is repeated for increasing scaling factors of the same accelerogram until a predetermined condition is attained, in this case until the limit state under consideration is attained [8].

Similar to the target displacement determination, two different methods to estimate the limit-state spectral acceleration are given, one as the median of the values for all accelerograms and the other using the following formula [E.3]:

$$S_{e,LS} = \exp\left(\frac{1}{N_a}\sum_{i=1}^{Na}\ln(S_{e,LS,i})\right) \tag{III-F.2.3}$$

where $S_{e,LS,i}$ is the limit-state spectral acceleration for the i-th accelerogram.

III-F.2.5.1 Procedure adopted for the $S_{e,LS}$ determination

Although both methods given in this annex for the determination of the limit-state spectral acceleration imply performing the incremental dynamic analysis per each ground motion separately, the modelization with 15 SDoF models adopted in Seismostruct allows the scaling of the accelerograms by using linear regression with some simple mathematical modifications, and so this measure can be obtained in a more manageable way.

The first step is to run the non-linear response-history analysis in all SDoF models at the same time for different scaling factors (SF) starting from 1.0. This initial scaling factor corresponds to the spectral acceleration at the reference period $S_e(T^*)$ (equal to $0.51s$ in the X direction) for the No-collapse limit state (NC), defined in EC8, part 1, which is associated with a seismic action with a probability of exceedance of 10% in 50 years and return period of $T_R = 475$ years. As explained in section III-F.1.3, this limit state could also be considered as the Significant Damage limit state (SD) described in the current version of EC8, part 3.

Secondly, considering the previous seismic action mentioned as reference $S_{e,ref}(T^*)$, it can be ensured that the scaling factor (SF) is directly proportional to the spectral acceleration at a certain limit state: $SF \propto S_{e,SF}$. That is to say for a given SF which induces the structure to a certain limit state, the limit-state spectral acceleration is obtained as:

$$S_{e,SF} = SF \cdot S_{e,ref}(T^*) \tag{III-F.2.4}$$

where for the x direction $S_{e,ref}(0.51s) = 7.32\, m/s^2$

Once the DTHA is carried out for several scaling factors (SF), the absolute peak displacements (in this section called D^*) for each ground motion and corresponding SF are also obtained. Then a graph with $ln(D^*)$ in y-axis and $ln(S_{e,SF})$ in the x-axis can be plotted. This logarithmic transformation is aiming to have a linear regression curve more fitted with the data and thus an easy interpolation can be accomplished.

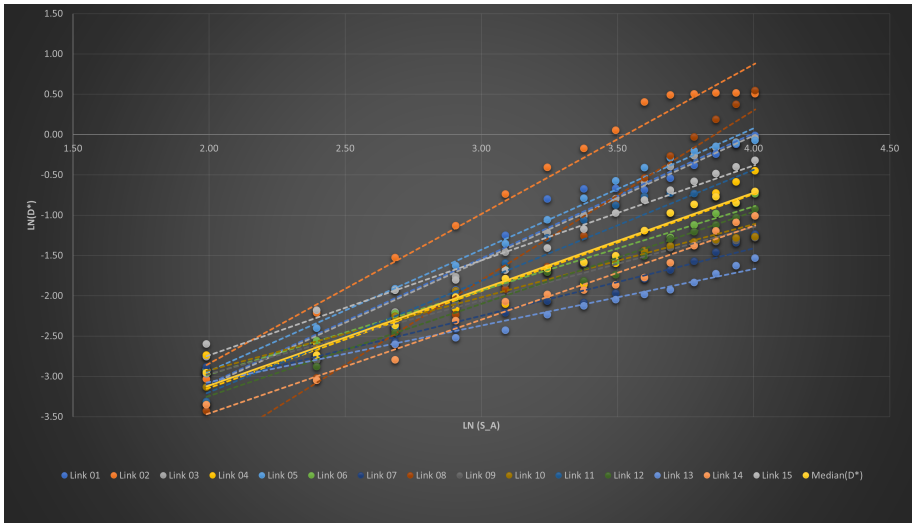

(a) X direction

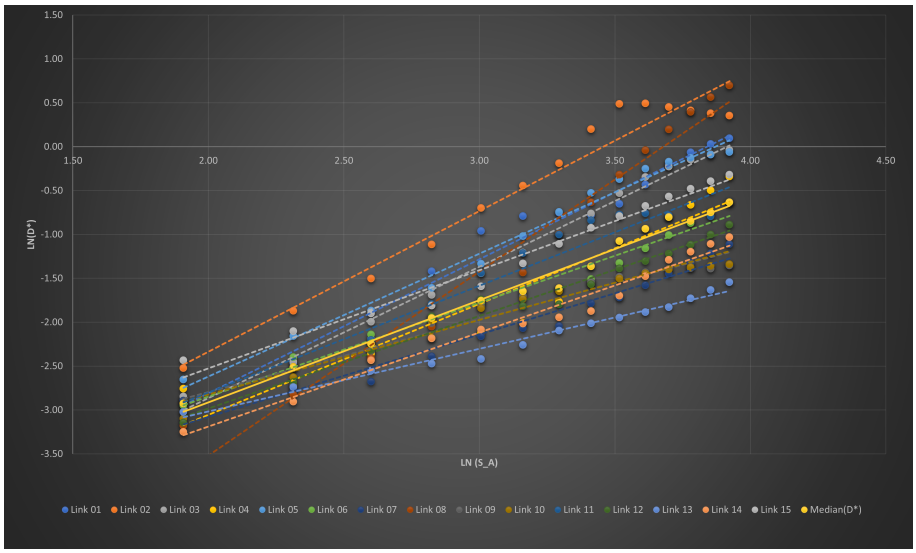

(b) Y direction

Figure III-F.12: LN of the absolute peak displacements D^* vs LN of the spectral accelerations $S_{e,SF}$

Figure III-F.12 shows the evolution of the peak absolute displacements per ground motion in function of the spectral accelerations, which correspond to each scaling factor; and also the median value of those peak absolute displacements, all of them expressed in logarithms terms. It is interesting to note the very good fitting of the median trend line (yellow solid line) with one of the ground motions associated in link 04 (yellow dashed line) for the X direction and link 06 (green dashed line) in the Y direction; which means that the median method to calculate the limit-state spectral acceleration is representative among the selected accelerograms that been previously scaled for the seismic action of that limit-state (i.e. SD and NC, for part 3 and part 1 of the EC8, respectively).

Having this median trend line is possible to get a mathematical expression for this line as linear regression, that allows the calculation of the limit-state spectral acceleration as illustrated in figure III-F.13. This expression follows the linear regression line can be obtained as the form: $y = a + b \cdot x$; where $y = \ln(D^*)$ and $x = \ln(S_{e,SF})$, and with the computation of the constants a and b, it results the following equation (X direction):

$$\ln(D^*) = 1.196 \cdot \ln(S_{e,SF}) - 5.506 \tag{III-F.2.5}$$

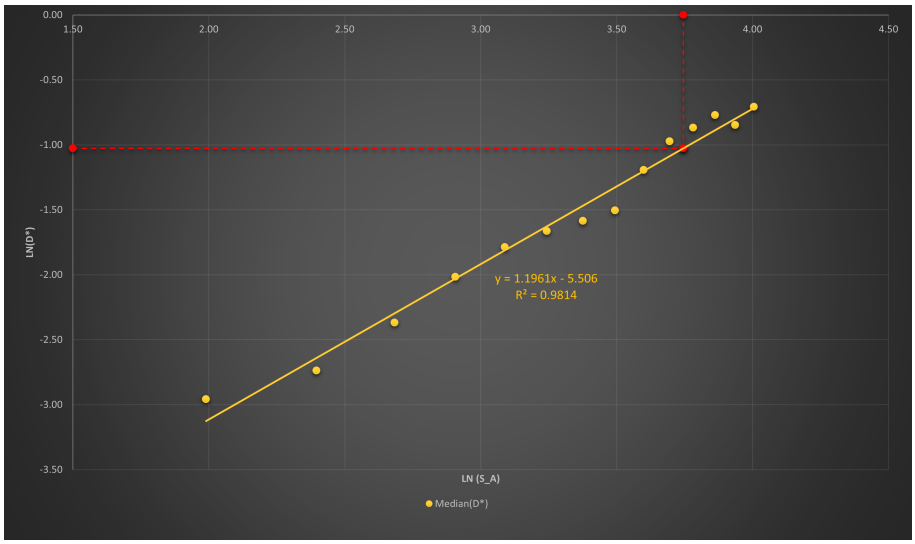

(a) X direction

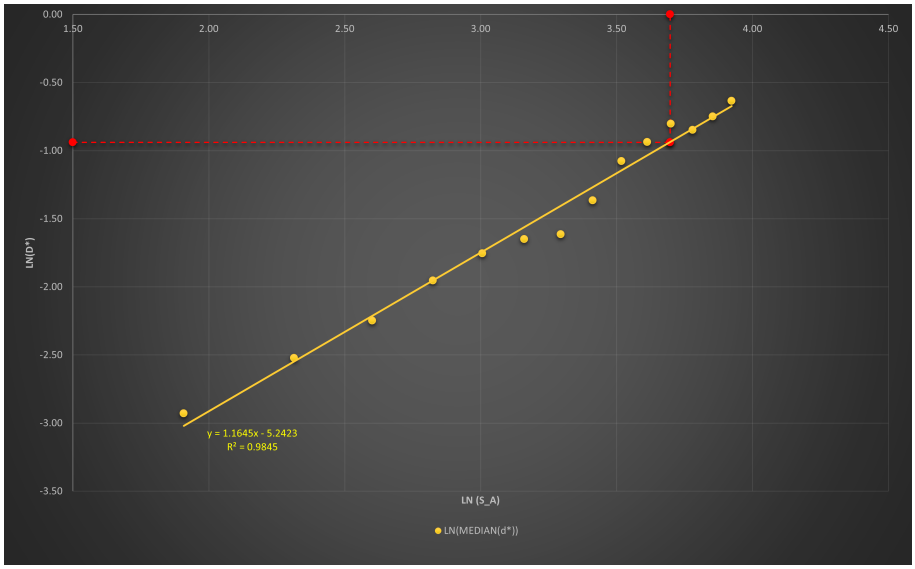

(b) Y direction

Figure III-F.13: *LN* of absolute peak displacements D^* median vs LN spectral accelerations $S_{e,SF}$

Now, the objective is to find the limit-state spectral acceleration which corresponds to the Near Collapse (NC) (i.e. the spectral acceleration that induces the target displacement for the Near Collapse limit state in the SDoF model). Reminding the discussion for the (NC) in section III-E.5.3, the displacement demand corresponding to that limit state is defined as the point where the first vertical element reaches its capacity (i.e. chord rotation failure in the column). So by expressing this displacement as $\ln(d^*) = \ln(0.358) = -1.026$, it is easy to compute the spectral acceleration by solving the equation and/or using a graphical interpolation as depicted in the previous figure.

$$ln(S_{e,NC}) = \exp\left(\frac{-1.026 - (-5.506)}{1.1961}\right) = 3.745 \tag{III-F.2.6}$$

Which also corresponds to the value by graphical interpolation, therefore, the limit-state spectral acceleration for the Near Collapse (NC) in X direction is:

$$S_{e,NC,x} = 42.32\, m/s^2$$

Following the same procedure for the Y direction, for the corresponding $T^* = 0.56s$ and Near collapse displacement $d^*_{NC} = 0.391m$, the limit-state spectral acceleration for the Near Collapse is then:

$$S_{e,NC,y} = 40.33\, m/s^2$$

Comparing both magnitudes, the last value (for Y direction) is then defined as the direction that controls the Near Collapse spectral acceleration for the current assessed building.

III-F.2.5.2 Alternative procedure to compute the target displacement

Similar to the method applied for the limit-state spectral acceleration, the target displacement for a seismic demand could also be calculated using a linear regression approximation, but in this case using the logarithmic transformation of the expression [E.2]. It is necessary then to compute the natural logarithmic with equation III-F.2.1 for each scale factor which corresponds to each reference spectral acceleration amplification.

Plots $\ln d^*_t$ in the vertical axis versus $\ln S_e$ in the horizontal axis are shown in figure III-F.14, with the corresponding linear regression equation (for x direction) resulting in:

$$ln(d^*_t) = 1.268 \cdot \ln(S_e) - 5.647 \qquad \text{(III-F.2.7)}$$

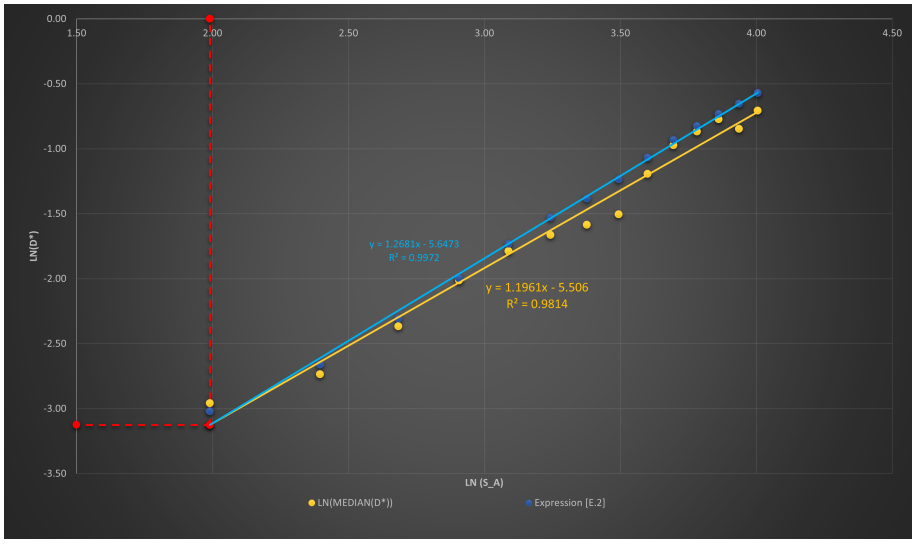

(a) X direction

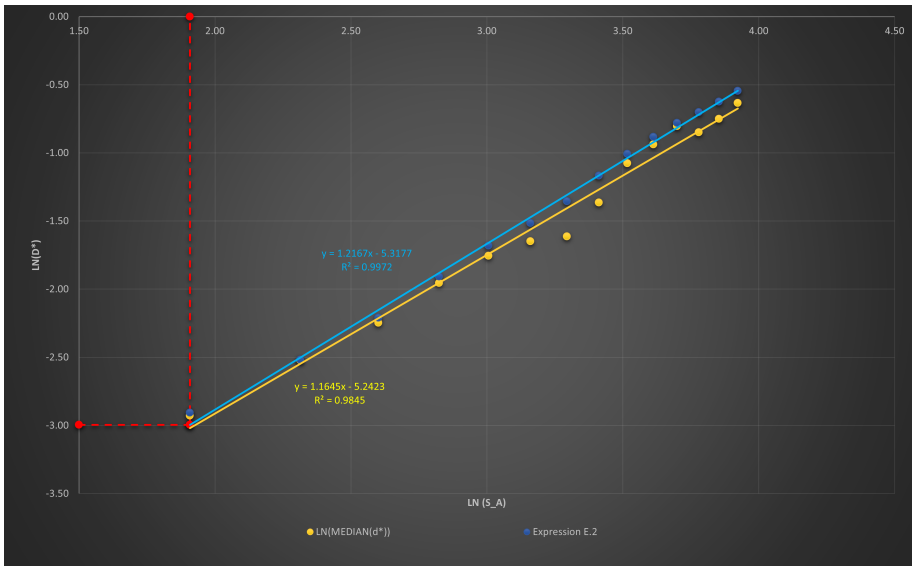

(b) Y direction

Figure III-F.14: LN of target displacement using expression [E.2] d_t^* median vs LN spectral accelerations $S_{e,SF}$

A graphical interpolation can be made to obtain the target displacement $d_t^* = 0.044m$ which corresponds to the $SF = 1$, with $S_e = 7.32m/s^2$, for the seismic action with return period $T_R = 475$ years. It may also be computed by substitution of equation III-F.2.7 (for x direction):

$$d_{t,x}^* = \left(\exp^{-5.647}\right) \cdot \left(7.32^{1.268}\right) = 0.044m$$

Applying the same concept in the other direction Y, with $S_e = 6.74m/s^2$, the following target displacement is obtained:

$$d_{t,y}^* = \left(\exp^{-5.318}\right) \cdot \left(6.74^{1.217}\right) = 0.050m$$

In figure III-F.14, can also be seen the consistency of both linear regression made in the logarithmic domain for the absolute peak displacements and spectral accelerations, which means dealing with displacements to get limit-state spectral accelerations or vice-versa gives acceptable results but less accurate. It is important to note that this alternative method for the target displacement determination is not presented in any version of EC8.

Part IV

Assessment of probability of failure

CHAPTER IV-G

SIMPLIFIED RELIABILITY-BASED VERIFICATION

IV-G.1. prEN1998-1-1: 2022: Annex F

The objective of this annex is to provide complementary and/or supplementary guidance to the performance requirements for different seismic actions. It may be used for a simplified verification of the performance of the structure in probabilistic terms, and also could be applied to design situations where uncertainties are outside the ranges that are covered by the partial factor (i.e. reduction/behaviour factors) design format [12].

IV-G.1.1 Reliability-based verification

Annex F expresses that for a given consequence class and a given limit state, the performance of a structure may be considered acceptable if the following inequality is satisfied [12]:

$$P_{LS} \leq P_{t,LS,CC} \tag{IV-G.1.1}$$

where P_{LS} is the annual probability of exceedance of a designated limit state and $P_{t,LS,CC}$ is the target annual probability of exceedance of a designated limit state for a given consequence class [12].

IV-G.1.2 Annual probability of exceedance P_{LS}

The annual probability of exceedance of a designated limit state may be calculated with the formula [F.2]:

$$P_{LS} = \int_0^\infty P(LS|S_e) \left| \frac{dH(S_e)}{dS_e} \right| dS_e$$

where S_e is the spectral acceleration at the fundamental period of the structure, $P(LS|S_e)$ is the probability that the ground motion with spectral acceleration S_e will cause an exceedance of the limit state LS and $H(S_e)$ is the seismic hazard function (i.e. the median of annual frequency of exceedance of S_e) [12].

Also to calculate the probability that the ground motion with S_e intensity will cause an exceedance of a given limit state, it may be assumed to be log-normally distributed, and is given by the formula (equation [F.3] in Annex F):

$$P(LS|S_e) = \Phi \left(\frac{\ln(S_e) - \ln(S_{e,LS})}{\beta_{Se,LS}} \right)$$

with Φ as the cumulative distribution function of the standardized Normal distribution, $S_{e,LS}$ as the median value of spectral accelerations which cause the designated limit state, and $\beta_{Se,LS}$ is the logarithmic standard deviation of spectral accelerations which causes the designated LS.

IV-G.1.3 Alternative procedure for P_{LS}

In absence of a hazard function, $H(S_e)$ may be assumed linear in the logarithmic domain and can be computed with the expression (equation [F.4] in annex F):

$$H(S_{e,LS}) = \frac{1}{T_{ref}} \left(\frac{S_{e,ref}}{S_{e,LS}} \right)^k \tag{IV-G.1.2}$$

In this case the P_{LS} could also be calculated according to the following formula (equation [F.5] in annex F):

$$P_{LS} = H(S_{e,LS}) \exp\left(0.5\, k^2\, \beta^2_{Se,LS}\right) \tag{IV-G.1.3}$$

where $H(S_{e,LS})$ is the median annual frequency of exceedance of $S_{e,LS}$; $S_{e,ref}$ is the value of S_e corresponding to the reference return period T_{ref} of seismic action for Significant Damage limit state (SD); k is the slope of the seismic hazard curve for $S_{e,ref}$ in the logarithmic domain; and $\beta_{Se,LS}$ is the logarithmic standard deviation of the limit-state spectral acceleration [12].

The calculation of $\beta_{Se,LS}$ may be obtained from the figure below (figure [F.1] in annex F):

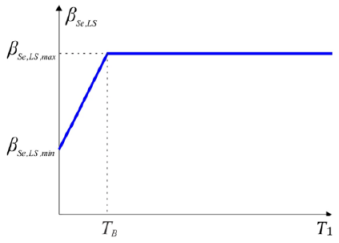

	OP and DL	SD and NC
$\beta_{Se,LS,min}$	0,30	0,40
$\beta_{Se,LS,max}$	0,40	0,60

Figure F.1 — $\beta_{Se,LS}$ as a function of the fundamental period of the structure T_1

Figure IV-G.1: Standard deviation for alternative procedure in P_{LS} calculation. Adapted form [12]

IV-G.1.4 Assessment of reliability for the current structure

For the present work, the annual probability of exceedance of the Near Collapse limit state (NC) is computed using the alternative procedure using the simplified expression to compute the median annual frequency of exceedance (equation IV-G.1.2).

Having calculated the limit-state spectral acceleration to the Near Collapse $S_{e,NC} = 42.32\, m/s^2$ (section III-F.2.5.1), defining the reference return period $T_{ref} = 475$ years associated to the seismic action of Significant Damage limit state where the corresponding reference spectral acceleration is $S_{e,ref} = 7.32\, m/s^2$ and using the recommended value of seismic hazard curve slope $k = 3$, the median annual frequency of exceedance of $S_{e,NC}$, for X direction, can be defined as follows:

$$H(S_{e,NC}) = \frac{1}{475} \cdot \left(\frac{7.32}{42.32} \right)^3 = 1.09 \times 10^{-5} \tag{IV-G.1.4}$$

Now, the annual probability of exceedance for the Near Collapse limit state (NC) can be calculated with equation IV-G.1.3. The logarithmic standard deviation of the Near Collapse spectral acceleration $S_{e,NC}$ should be obtained from the figure IV-G.1, assigning as the maximum value for the NC limit state $\beta_{Se,LS} = 0.6$.

So the value obtained for the annual probability of exceedance, for X direction, is given by:

$$P_{NC,x} = (1.09 \times 10^{-5}) \exp\left(0.5 \cdot (3)^2 \cdot (0.6)^2\right) = 5.50 \times 10^{-5} \quad \text{(IV-G.1.5)}$$

The target probability of exceedance of the Near Collapse limit state (NC) for structures of consequence class CC2 is $P_{t,NC,CC2} = 2 \times 10^{-4}$ [12]. Since the present structure is also categorized as CC2 according to the second generation of EC8, this criterion is accomplished.

$$P_{NC} = 5.5 \times 10^{-5} \leq P_{t,NC,CC2} = 2 \times 10^{-4}$$

Now, is necessary to evaluate the other direction Y, and to obtain which is the corresponding probability of exceedance.

Table IV-G.1: Comparison of annual probability of exceedance between both directions with seismic hazard curve slope $k = 3$ and deviation $\beta_{Se,NC} = 0.60$

Parameter	[X direction]	[Y direction]
Reference return period T_R (years)	475	475
Reference (SD) spectral acceleration $S_{e,ref}$ (m/s^2)	7.32	6.74
Near Collapse spectral acceleration $S_{e,NC}$ (m/s^2)	42.34	40.33
Median annual frequency of exceedance $H(S_{e,NC})$	1.09×10^{-5}	9.83×10^{-6}
Annual probability of exceedance P_{NC}	5.50×10^{-5}	4.97×10^{-5}

In table IV-G.1, the comparison shows the different parameters of the building for both directions with the conditions established in Annex F. In this comparison is proved that the X direction gives the higher annual probability of exceedance, contrary to section III-F.2.5.1 where the critical Near Collapse spectral acceleration $S_{e,NC}$ of the structure was controlled by the Y direction. The latter is consequent with the expression IV-G.1.3 which shows the inverse proportionality between the limit-state spectral acceleration and the annual probability of exceedance.

IV-G.2. Parametric evaluation of annual probability of exceedance for Near Collapse limit state P_{NC}

IV-G.2.1 P_{NC} in function of logarithmic standard deviation $\beta_{Se,NC}$

Several comparisons for the annual probability of exceedance for the NC limit state can be done. One of them is by varying the deviation $\beta_{Se,NC}$ for values from zero to the unity, as depicted below:

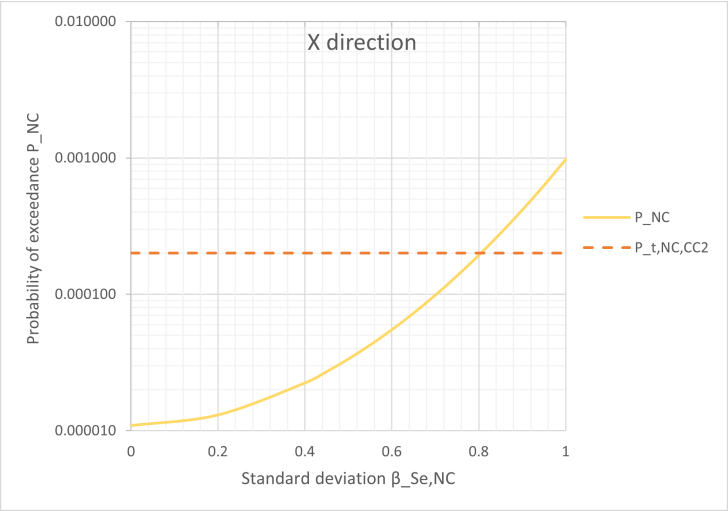

(a) X direction

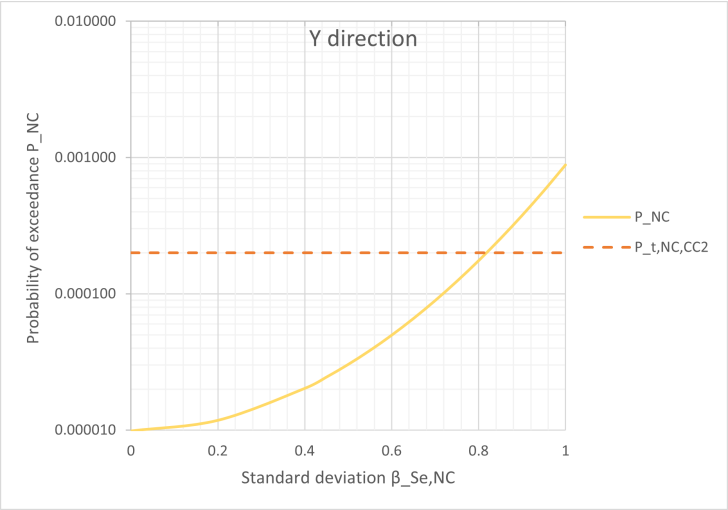

(b) Y direction

Figure IV-G.2: Probability of exceedance in function of logarithmic standard deviation with seismic hazard slope $k = 3$ and corresponding Near collapse spectral acceleration $S_{e,NC}$ for each direction

Although the values recommended in the second generation of EC8 have the lower limit equal to 0.4 for the Near Collapse limit state, a wider range of $\beta_{Se,NC}$ values are plotted in figure IV-G.2. It is shown that when the logarithmic standard deviation increases, the probability of exceedance also increases. The maximum probability of exceedance results, in both directions, when the $\beta_{Se,NC}$ goes to 1.0 and is approximately 1×10^{-3}; on the contrary, when the value of deviation is close to zero the minimum probability of exceedance is about 1×10^{-5}. It is also important to note that when the deviation is larger than $\beta_{Se,NC} = 0.8$, the probability of exceedance surpasses the target probability for the Near collapse limit state.

IV-G.2.2 P_{NC} in function of seismic hazard curve slope k

A second evaluation to see the evolution of the probability of exceedance is by testing different values of seismic hazard curve slope k (see figure IV-G.3).

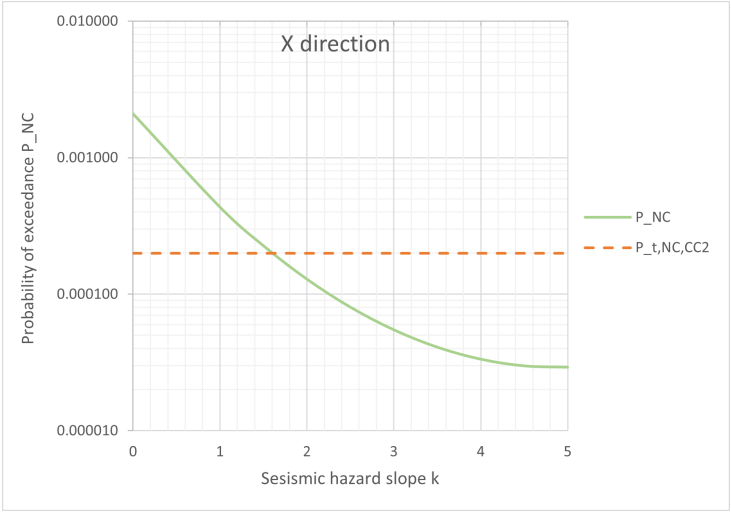

(a) X direction

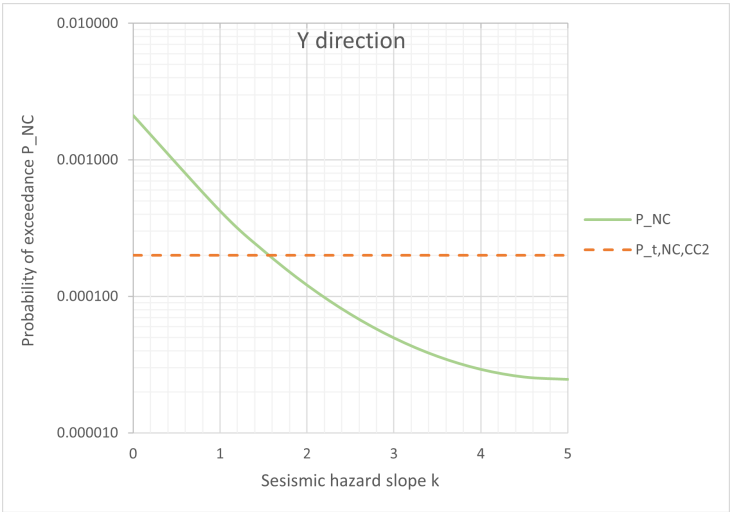

(b) Y direction

Figure IV-G.3: Probability of exceedance in function of seismic hazard curve slope with deviation $\beta_{Se,NC} = 0.60$ and corresponding Near collapse spectral acceleration $S_{e,NC}$ for each direction

Changing the values of k implies, of course, a variation in the median annual frequency of exceedance $H(S_{e,nc}$ besides the clear change in the probability of exceedance values. Compared with the variation of deviation of the previous section where the P_{NC} follows a curve in the

logarithmic domain, in this case, is also a curved line that includes a decline in the opposite direction and a threshold in $k = 1.6$. These plots also show that the probability of exceedance limit is not respected when the values of seismic hazard curve slope are lower than $k = 1.6$. It can be also proved that the probability of exceedance is inversely proportional to the seismic hazard slope.

IV-G.2.3 P_{NC} in function of Near Collapse displacement d^*_{NC}

Finally, and maybe the most interesting comparison results when the Near Collapse displacement of the structure is varying. Below, the variation of probability of exceedance P_{NC} with respect to those displacements d^*_{NC}, for X direction, is depicted in table IV-G.2.

Table IV-G.2: Variation of $S_{e,NC}$ and P_{NC} in function of the Near Collapse displacement d_{NC} for X direction

Displacement	$d^*(m)$	$S_{e,NC}\ (m/s^2)$	$H(S_{e,NC})$	P_{NC}
$(0.25)\times d^*_{NC}$	0.090	13.284	0.0003522	1.78×10^{-3}
$(0.33)\times d^*_{NC}$	0.118	16.755	0.0001755	8.87×10^{-4}
$(0.50)\times d^*_{NC}$	0.179	23.715	0.0000619	3.13×10^{-4}
$(0.67)\times d^*_{NC}$	0.240	30.290	0.000297	1.50×10^{-4}
d^*_{NC}	0.358	42.337	0.000109	5.50×10^{-5}
$(1.5)\times d^*_{NC}$	0.538	59.423	0.000039	1.99×10^{-5}
$(2)\times d^*_{NC}$	0.717	75.582	0.000019	9.66×10^{-6}
$(2.5)\times d^*_{NC}$	0.896	91.085	0.000011	5.52×10^{-6}

Figure IV-G.4 illustrates the variation of probability of exceedance P_{NC} when the Near Collapse displacement d^*_{NC} has different values, in both direction. The horizontal axis shows the variation of Near Collapse spectral acceleration $S_{e,NC}$, and since this limit-state spectral acceleration is a function of d^*_{NC}, the plot P_{NC} vs $S_{e,NC}$ can also be representative of the displacement variation.

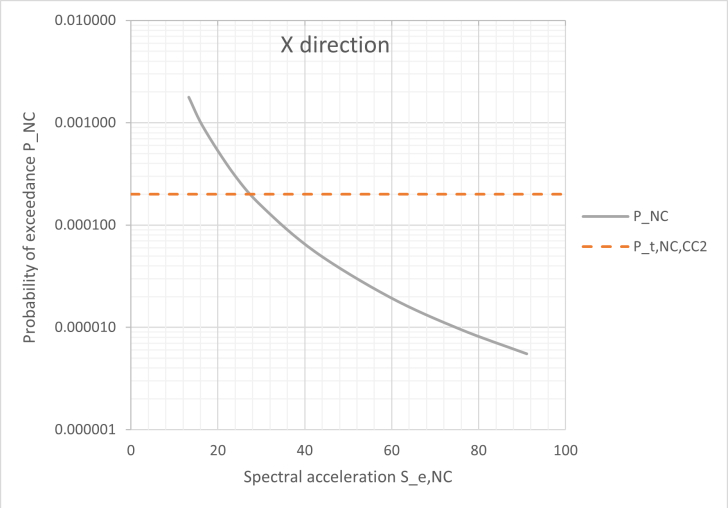

(a) X direction

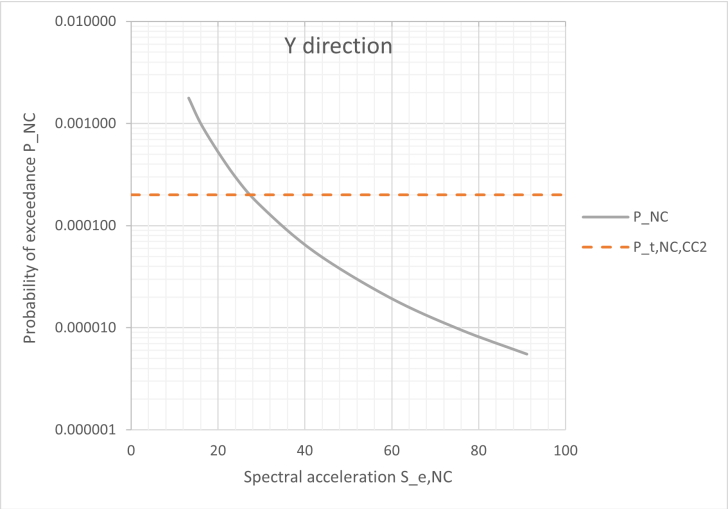

(b) Y direction

Figure IV-G.4: Probability of exceedance in function of Near Collapse displacement

Thanks to this graph, the lowest limit of the spectral acceleration in the Near Collapse limit state to satisfy the requirement of the probability of exceedance can be defined, taking place when $S_{e,NC} = 27.2\ m/s^2$, which corresponds to a NC displacement $d^*_{NC,x} = 0.21m$ for the X direction. That is to say that for lower values of Near Collapse displacements than 0.21m, P_{NC} is not satisfied for the X direction. Similarly, when the Near collapse displacement in the Y direction is lower than $d^*_{NC,y} = 0.58m$ the limit for the probability of exceedance is surpassed as well.
On the other hand, it is demonstrated that when the value of the NC displacement increases (and so does the NC spectral acceleration) the probability of exceedance decreases.

Part V

General conclusions

CONCLUSIONS

This project was focused in assess the performance of a given structure based on probabilistic terms following the guidance provided by the Annex F of the second generation of EC8.

The procedure for the evaluation of existing structures based on reliability described in the second generation of EC8 seeks to verify in a simplified way the performance of a structure in probabilistic terms. This assessment can be carried out for any type of structure regardless of the design concept for which it was conceived or the material it is made of.

In this research, a reinforced concrete building with a Wall-Equivalent Dual System in both directions has been designed according to the current version of EC8 and subsequently subjected to performance evaluation with the previously mentioned probabilistic approach. The final objective was to evaluate the probability of failure of this building in terms of annual probability of exceedance for the Near Collapse limit state (NC) and verify if it surpassed the limit set by the new generation of EC8.

The design of the reinforced concrete structure has been carried out successfully, complying with all the prescribed verifications following the current version of EC8. This included compliance with material requirements (concrete and reinforcing steel), concepts of the local capacity in the structural elements, and the limitations for the Ultimate Limit State (ULS) and the Service Limit State (SLS).

Within the methods presented according to the second generation of EC8 to determine the performance of the structure under study, in terms of displacement (i.e. target displacement), an acceptable variation (no more than 10%) was found when compared with the current version of EC8, which indicates that the results obtained are considered acceptable if the current version is set as a reference.

Regarding the reliability evaluation to which the structure was subjected, it can be concluded that it fully complies with the reliability limit (i.e. target reliability) for the Near Collapse limit state (NC) set by Annex F, both for the direction X as for direction Y. In general terms, the procedure can then be considered as its name indicates simplified, and accessible to apply.

Finally, after the parametric evaluation carried out to observe the evolution of the annual probability of exceedance in the case-study structure, the upper and lower limits of the variables deviation, seismic hazard curve slope and near collapse displacement were successfully determined and their corresponding distribution is in accordance with the mathematical expressions provided in Annex F of the second generation of EC8.

RECOMMENDATIONS

In this project, the design concepts applied for the building were idealized many times, specially for the design of longitudinal steel reinforcement distributed uniformly throughout the length of structural elements. However, in reality, structural designs are rarely so basic and homogeneous, so a point of improvement in future research would be to increase the complexity in the design phase so that the structures behave more realistically to the existing buildings. Of course, for that, a more solid base and more experience in the design of structures are needed, in this case, that of reinforced concrete structures.

It would also be convenient, perhaps for structures with a not-so-high degree of design difficulty, that when obtaining the results for certain performance and when determining that the structure is overdesigned, the redesign to reduce dimensions could be executed. This would provide the researcher (or student) with a more reality-based approach to structural design and optimization often achieved in structural design offices.

In terms of modeling the structure, a much more detailed comparison could be made if the IDA is run for the entire building and thus obtain the limit-state spectral acceleration of the MDoF system, and then compare and analyze the results with the procedure applied for the equivalent SDoF model suggested in EC8 2nd generation. Also, during the process of determining which hysteretic model to choose that reflects the behavior of the SDoF models in Seismostruct Software, it would be appropriate to delve into the numerous parameters that each of the hysteretic curves possesses. Probably, there are parameters within these hysteretic models that are not being clearly explained in the software help system, and their determination becomes complicated to apply them correctly later.

From the point of view of the applicability of the methods here examined, they could be expanded to larger structures, varying their seismic demand, and also to buildings with different lateral load resistance systems. This will allow knowing the reliability of these procedures for different conditions.

Part VI

Appendix

APPENDIX A

DESIGN SEISMIC ACTION

Table 3.1: Ground types

Ground type	Description of stratigraphic profile	Parameters		
		$v_{s,30}$ (m/s)	N_{SPT} (blows/30cm)	c_u (kPa)
A	Rock or other rock-like geological formation, including at most 5 m of weaker material at the surface.	> 800	–	–
B	Deposits of very dense sand, gravel, or very stiff clay, at least several tens of metres in thickness, characterised by a gradual increase of mechanical properties with depth.	360 – 800	> 50	> 250
C	Deep deposits of dense or medium-dense sand, gravel or stiff clay with thickness from several tens to many hundreds of metres.	180 – 360	15 - 50	70 - 250
D	Deposits of loose-to-medium cohesionless soil (with or without some soft cohesive layers), or of predominantly soft-to-firm cohesive soil.	< 180	< 15	< 70
E	A soil profile consisting of a surface alluvium layer with v_s values of type C or D and thickness varying between about 5 m and 20 m, underlain by stiffer material with v_s > 800 m/s.			
S_1	Deposits consisting, or containing a layer at least 10 m thick, of soft clays/silts with a high plasticity index (PI > 40) and high water content	< 100 (indicative)	–	10 - 20
S_2	Deposits of liquefiable soils, of sensitive clays, or any other soil profile not included in types A – E or S_1			

Figure A.1: Ground type

Table 4.3 Importance classes for buildings

Importance class	Buildings
I	Buildings of minor importance for public safety, e.g. agricultural buildings, etc.
II	Ordinary buildings, not belonging in the other categories.
III	Buildings whose seismic resistance is of importance in view of the consequences associated with a collapse, e.g. schools, assembly halls, cultural institutions etc.
IV	Buildings whose integrity during earthquakes is of vital importance for civil protection, e.g. hospitals, fire stations, power plants, etc.

Figure A.2: Important class

APPENDIX B

ELASTIC RESPONSE SPECTRA TYPES

Table 3.2: Values of the parameters describing the recommended Type 1 elastic response spectra

Ground type	S	T_B (s)	T_C (s)	T_D (s)
A	1,0	0,15	0,4	2,0
B	1,2	0,15	0,5	2,0
C	1,15	0,20	0,6	2,0
D	1,35	0,20	0,8	2,0
E	1,4	0,15	0,5	2,0

Figure B.1: Recommended values for type 1

Table 3.3: Values of the parameters describing the recommended Type 2 elastic response spectra

Ground type	S	T_B (s)	T_C (s)	T_D (s)
A	1,0	0,05	0,25	1,2
B	1,35	0,05	0,25	1,2
C	1,5	0,10	0,25	1,2
D	1,8	0,10	0,30	1,2
E	1,6	0,05	0,25	1,2

Figure B.2: Recommended values for type 2

Table 5.1: Basic value of the behaviour factor, q_o, for systems regular in elevation

STRUCTURAL TYPE	DCM	DCH
Frame system, dual system, coupled wall system	$3,0\alpha_u/\alpha_1$	$4,5\alpha_u/\alpha_1$
Uncoupled wall system	3,0	$4,0\alpha_u/\alpha_1$
Torsionally flexible system	2,0	3,0
Inverted pendulum system	1,5	2,0

Figure B.3: Behaviour factor q_o in function of type of structural system

APPENDIX C

RSA RESULTS FROM SEISMOSTRUCT

NODAL COORDINATES (m)					NODAL MASSES (ton)						
Node name	X	Y	Z		Node Name	[X]	[Y]	[Z]	[RX]	[RY]	[RZ]
n011	0.0	0.0	0.0	structural	n011	0.0000	0.0000	0.0000	0.0000	0.0000	0.0000
n012	0.0	7.0	0.0	structural	n012	0.0000	0.0000	0.0000	0.0000	0.0000	0.0000
n013	0.0	14.0	0.0	structural	n013	0.0000	0.0000	0.0000	0.0000	0.0000	0.0000
n021	6.0	0.0	0.0	structural	n021	0.0000	0.0000	0.0000	0.0000	0.0000	0.0000
n022	6.0	7.0	0.0	structural	n022	0.0000	0.0000	0.0000	0.0000	0.0000	0.0000
n023	6.0	14.0	0.0	structural	n023	0.0000	0.0000	0.0000	0.0000	0.0000	0.0000
n031	12.0	0.0	0.0	structural	n031	0.0000	0.0000	0.0000	0.0000	0.0000	0.0000
n032	12.0	7.0	0.0	structural	n032	0.0000	0.0000	0.0000	0.0000	0.0000	0.0000
n033	12.0	14.0	0.0	structural	n033	0.0000	0.0000	0.0000	0.0000	0.0000	0.0000
n041	18.0	0.0	0.0	structural	n041	0.0000	0.0000	0.0000	0.0000	0.0000	0.0000
n042	18.0	7.0	0.0	structural	n042	0.0000	0.0000	0.0000	0.0000	0.0000	0.0000
n043	18.0	14.0	0.0	structural	n043	0.0000	0.0000	0.0000	0.0000	0.0000	0.0000
n051	24.0	0.0	0.0	structural	n051	0.0000	0.0000	0.0000	0.0000	0.0000	0.0000
n052	24.0	7.0	0.0	structural	n052	0.0000	0.0000	0.0000	0.0000	0.0000	0.0000
n053	24.0	14.0	0.0	structural	n053	0.0000	0.0000	0.0000	0.0000	0.0000	0.0000
n111	0.0	0.0	3.0	structural	n111	12.3262	12.3262	0.0000	0.0000	0.0000	0.0000
n112	0.0	7.0	3.0	structural	n112	21.3374	21.3374	0.0000	0.0000	0.0000	0.0000
n113	0.0	14.0	3.0	structural	n113	12.3262	12.3262	0.0000	0.0000	0.0000	0.0000
n121	6.0	0.0	3.0	structural	n121	21.2997	21.2997	0.0000	0.0000	0.0000	0.0000
n122	6.0	7.0	3.0	structural	n122	39.2885	39.2885	0.0000	0.0000	0.0000	0.0000
n123	6.0	14.0	3.0	structural	n123	21.2997	21.2997	0.0000	0.0000	0.0000	0.0000
n131	12.0	0.0	3.0	structural	n131	21.3119	21.3119	0.0000	0.0000	0.0000	0.0000
n132	12.0	7.0	3.0	structural	n132	39.2885	39.2885	0.0000	0.0000	0.0000	0.0000
n133	12.0	14.0	3.0	structural	n133	21.3119	21.3119	0.0000	0.0000	0.0000	0.0000
n141	18.0	0.0	3.0	structural	n141	21.2997	21.2997	0.0000	0.0000	0.0000	0.0000
n142	18.0	7.0	3.0	structural	n142	39.2885	39.2885	0.0000	0.0000	0.0000	0.0000
n143	18.0	14.0	3.0	structural	n143	21.2997	21.2997	0.0000	0.0000	0.0000	0.0000
n151	24.0	0.0	3.0	structural	n151	12.3262	12.3262	0.0000	0.0000	0.0000	0.0000
n152	24.0	7.0	3.0	structural	n152	21.3374	21.3374	0.0000	0.0000	0.0000	0.0000
n153	24.0	14.0	3.0	structural	n153	12.3262	12.3262	0.0000	0.0000	0.0000	0.0000
n211	0.0	0.0	6.0	structural	n211	12.3262	12.3262	0.0000	0.0000	0.0000	0.0000
n212	0.0	7.0	6.0	structural	n212	21.3374	21.3374	0.0000	0.0000	0.0000	0.0000
n213	0.0	14.0	6.0	structural	n213	12.3262	12.3262	0.0000	0.0000	0.0000	0.0000
n221	6.0	0.0	6.0	structural	n221	21.2997	21.2997	0.0000	0.0000	0.0000	0.0000
n222	6.0	7.0	6.0	structural	n222	39.2885	39.2885	0.0000	0.0000	0.0000	0.0000
n223	6.0	14.0	6.0	structural	n223	21.2997	21.2997	0.0000	0.0000	0.0000	0.0000
n231	12.0	0.0	6.0	structural	n231	21.3119	21.3119	0.0000	0.0000	0.0000	0.0000
n232	12.0	7.0	6.0	structural	n232	39.2885	39.2885	0.0000	0.0000	0.0000	0.0000
n233	12.0	14.0	6.0	structural	n233	21.3119	21.3119	0.0000	0.0000	0.0000	0.0000
n241	18.0	0.0	6.0	structural	n241	21.2997	21.2997	0.0000	0.0000	0.0000	0.0000
n242	18.0	7.0	6.0	structural	n242	39.2885	39.2885	0.0000	0.0000	0.0000	0.0000
n243	18.0	14.0	6.0	structural	n243	21.2997	21.2997	0.0000	0.0000	0.0000	0.0000
n251	24.0	0.0	6.0	structural	n251	12.3262	12.3262	0.0000	0.0000	0.0000	0.0000
n252	24.0	7.0	6.0	structural	n252	21.3374	21.3374	0.0000	0.0000	0.0000	0.0000
n253	24.0	14.0	6.0	structural	n253	12.3262	12.3262	0.0000	0.0000	0.0000	0.0000

Figure C.1: Nodal coordinates and nodal masses (1/2)

n311	0.0	0.0	9.0	structural	n311	12.3262	12.3262	0.0000	0.0000	0.0000	0.0000
n312	0.0	7.0	9.0	structural	n312	21.3374	21.3374	0.0000	0.0000	0.0000	0.0000
n313	0.0	14.0	9.0	structural	n313	12.3262	12.3262	0.0000	0.0000	0.0000	0.0000
n321	6.0	0.0	9.0	structural	n321	21.2997	21.2997	0.0000	0.0000	0.0000	0.0000
n322	6.0	7.0	9.0	structural	n322	39.2885	39.2885	0.0000	0.0000	0.0000	0.0000
n323	6.0	14.0	9.0	structural	n323	21.2997	21.2997	0.0000	0.0000	0.0000	0.0000
n331	12.0	0.0	9.0	structural	n331	21.3119	21.3119	0.0000	0.0000	0.0000	0.0000
n332	12.0	7.0	9.0	structural	n332	39.2885	39.2885	0.0000	0.0000	0.0000	0.0000
n333	12.0	14.0	9.0	structural	n333	21.3119	21.3119	0.0000	0.0000	0.0000	0.0000
n341	18.0	0.0	9.0	structural	n341	21.2997	21.2997	0.0000	0.0000	0.0000	0.0000
n342	18.0	7.0	9.0	structural	n342	39.2885	39.2885	0.0000	0.0000	0.0000	0.0000
n343	18.0	14.0	9.0	structural	n343	21.2997	21.2997	0.0000	0.0000	0.0000	0.0000
n351	24.0	0.0	9.0	structural	n351	12.3262	12.3262	0.0000	0.0000	0.0000	0.0000
n352	24.0	7.0	9.0	structural	n352	21.3374	21.3374	0.0000	0.0000	0.0000	0.0000
n353	24.0	14.0	9.0	structural	n353	12.3262	12.3262	0.0000	0.0000	0.0000	0.0000
n411	0.0	0.0	12.0	structural	n411	12.3262	12.3262	0.0000	0.0000	0.0000	0.0000
n412	0.0	7.0	12.0	structural	n412	21.3374	21.3374	0.0000	0.0000	0.0000	0.0000
n413	0.0	14.0	12.0	structural	n413	12.3262	12.3262	0.0000	0.0000	0.0000	0.0000
n421	6.0	0.0	12.0	structural	n421	21.2997	21.2997	0.0000	0.0000	0.0000	0.0000
n422	6.0	7.0	12.0	structural	n422	39.2885	39.2885	0.0000	0.0000	0.0000	0.0000
n423	6.0	14.0	12.0	structural	n423	21.2997	21.2997	0.0000	0.0000	0.0000	0.0000
n431	12.0	0.0	12.0	structural	n431	21.3119	21.3119	0.0000	0.0000	0.0000	0.0000
n432	12.0	7.0	12.0	structural	n432	39.2885	39.2885	0.0000	0.0000	0.0000	0.0000
n433	12.0	14.0	12.0	structural	n433	21.3119	21.3119	0.0000	0.0000	0.0000	0.0000
n441	18.0	0.0	12.0	structural	n441	21.2997	21.2997	0.0000	0.0000	0.0000	0.0000
n442	18.0	7.0	12.0	structural	n442	39.2885	39.2885	0.0000	0.0000	0.0000	0.0000
n443	18.0	14.0	12.0	structural	n443	21.2997	21.2997	0.0000	0.0000	0.0000	0.0000
n451	24.0	0.0	12.0	structural	n451	12.3262	12.3262	0.0000	0.0000	0.0000	0.0000
n452	24.0	7.0	12.0	structural	n452	21.3374	21.3374	0.0000	0.0000	0.0000	0.0000
n453	24.0	14.0	12.0	structural	n453	12.3262	12.3262	0.0000	0.0000	0.0000	0.0000
n511	0.0	0.0	15.0	structural	n511	8.8644	8.8644	0.0000	0.0000	0.0000	0.0000
n512	0.0	7.0	15.0	structural	n512	16.0571	16.0571	0.0000	0.0000	0.0000	0.0000
n513	0.0	14.0	15.0	structural	n513	8.8644	8.8644	0.0000	0.0000	0.0000	0.0000
n521	6.0	0.0	15.0	structural	n521	16.0693	16.0693	0.0000	0.0000	0.0000	0.0000
n522	6.0	7.0	15.0	structural	n522	30.4546	30.4546	0.0000	0.0000	0.0000	0.0000
n523	6.0	14.0	15.0	structural	n523	16.0693	16.0693	0.0000	0.0000	0.0000	0.0000
n531	12.0	0.0	15.0	structural	n531	16.0754	16.0754	0.0000	0.0000	0.0000	0.0000
n532	12.0	7.0	15.0	structural	n532	30.4546	30.4546	0.0000	0.0000	0.0000	0.0000
n533	12.0	14.0	15.0	structural	n533	16.0754	16.0754	0.0000	0.0000	0.0000	0.0000
n541	18.0	0.0	15.0	structural	n541	16.0693	16.0693	0.0000	0.0000	0.0000	0.0000
n542	18.0	7.0	15.0	structural	n542	30.4546	30.4546	0.0000	0.0000	0.0000	0.0000
n543	18.0	14.0	15.0	structural	n543	16.0693	16.0693	0.0000	0.0000	0.0000	0.0000
n551	24.0	0.0	15.0	structural	n551	8.8644	8.8644	0.0000	0.0000	0.0000	0.0000
n552	24.0	7.0	15.0	structural	n552	16.0571	16.0571	0.0000	0.0000	0.0000	0.0000
n553	24.0	14.0	15.0	structural	n553	8.8644	8.8644	0.0000	0.0000	0.0000	0.0000

Figure C.2: Nodal coordinates and nodal masses (2/2)

NODAL DISPLACEMENTS X-Mode 2						
Node Name	X	Y	Z	RX	RY	RZ
n011	0.00000000	0.00000000	0.00000000	0.00000000	0.00000000	0.00000000
n012	0.00000000	0.00000000	0.00000000	0.00000000	0.00000000	0.00000000
n013	0.00000000	0.00000000	0.00000000	0.00000000	0.00000000	0.00000000
n021	0.00000000	0.00000000	0.00000000	0.00000000	0.00000000	0.00000000
n022	0.00000000	0.00000000	0.00000000	0.00000000	0.00000000	0.00000000
n023	0.00000000	0.00000000	0.00000000	0.00000000	0.00000000	0.00000000
n031	0.00000000	0.00000000	0.00000000	0.00000000	0.00000000	0.00000000
n032	0.00000000	0.00000000	0.00000000	0.00000000	0.00000000	0.00000000
n033	0.00000000	0.00000000	0.00000000	0.00000000	0.00000000	0.00000000
n041	0.00000000	0.00000000	0.00000000	0.00000000	0.00000000	0.00000000
n042	0.00000000	0.00000000	0.00000000	0.00000000	0.00000000	0.00000000
n043	0.00000000	0.00000000	0.00000000	0.00000000	0.00000000	0.00000000
n051	0.00000000	0.00000000	0.00000000	0.00000000	0.00000000	0.00000000
n052	0.00000000	0.00000000	0.00000000	0.00000000	0.00000000	0.00000000
n053	0.00000000	0.00000000	0.00000000	0.00000000	0.00000000	0.00000000
n111	-0.00000328	0.00000000	-0.00000021	0.00000001	-0.00000159	0.00000000
n112	-0.00000328	0.00000000	-0.00000006	0.00000000	-0.00000171	0.00000000
n113	-0.00000328	0.00000000	-0.00000021	-0.00000001	-0.00000159	0.00000000
n121	-0.00000328	0.00000000	-0.00000058	0.00000002	-0.00000068	0.00000000
n122	-0.00000328	0.00000000	0.00000004	0.00000000	-0.00000096	0.00000000
n123	-0.00000328	0.00000000	-0.00000058	-0.00000002	-0.00000068	0.00000000
n131	-0.00000328	0.00000000	0.00000000	0.00000000	-0.00000201	0.00000000
n132	-0.00000328	0.00000000	0.00000000	0.00000000	-0.00000107	0.00000000
n133	-0.00000328	0.00000000	0.00000000	0.00000000	-0.00000201	0.00000000
n141	-0.00000328	0.00000000	0.00000058	-0.00000002	-0.00000068	0.00000000
n142	-0.00000328	0.00000000	-0.00000004	0.00000000	-0.00000096	0.00000000
n143	-0.00000328	0.00000000	0.00000058	0.00000002	-0.00000068	0.00000000
n151	-0.00000328	0.00000000	0.00000021	-0.00000001	-0.00000159	0.00000000
n152	-0.00000328	0.00000000	0.00000006	0.00000000	-0.00000171	0.00000000
n153	-0.00000328	0.00000000	0.00000021	0.00000001	-0.00000159	0.00000000
n211	-0.00001118	0.00000000	-0.00000039	0.00000002	-0.00000246	0.00000000
n212	-0.00001118	0.00000000	-0.00000010	0.00000000	-0.00000268	0.00000000
n213	-0.00001118	0.00000000	-0.00000039	-0.00000002	-0.00000246	0.00000000
n221	-0.00001118	0.00000000	-0.00000109	0.00000004	-0.00000110	0.00000000
n222	-0.00001118	0.00000000	0.00000008	0.00000000	-0.00000154	0.00000000
n223	-0.00001118	0.00000000	-0.00000109	-0.00000004	-0.00000110	0.00000000
n231	-0.00001118	0.00000000	0.00000000	0.00000000	-0.00000310	0.00000000
n232	-0.00001118	0.00000000	0.00000000	0.00000000	-0.00000169	0.00000000
n233	-0.00001118	0.00000000	0.00000000	0.00000000	-0.00000310	0.00000000
n241	-0.00001118	0.00000000	0.00000109	-0.00000004	-0.00000110	0.00000000
n242	-0.00001118	0.00000000	-0.00000008	0.00000000	-0.00000154	0.00000000
n243	-0.00001118	0.00000000	0.00000109	0.00000004	-0.00000110	0.00000000
n251	-0.00001118	0.00000000	0.00000039	-0.00000002	-0.00000246	0.00000000
n252	-0.00001118	0.00000000	0.00000010	0.00000000	-0.00000268	0.00000000
n253	-0.00001118	0.00000000	0.00000039	0.00000002	-0.00000246	0.00000000

Figure C.3: Nodal displacements for mode 2 (1/2)

n311	-0.00002130	0.00000000	-0.00000052	0.00000003	-0.00000275	0.00000000
n312	-0.00002130	0.00000000	-0.00000014	0.00000000	-0.00000301	0.00000000
n313	-0.00002130	0.00000000	-0.00000052	-0.00000003	-0.00000275	0.00000000
n321	-0.00002130	0.00000000	-0.00000147	0.00000006	-0.00000118	0.00000000
n322	-0.00002130	0.00000000	0.00000010	0.00000000	-0.00000171	0.00000000
n323	-0.00002130	0.00000000	-0.00000147	-0.00000006	-0.00000118	0.00000000
n331	-0.00002130	0.00000000	0.00000000	0.00000000	-0.00000352	0.00000000
n332	-0.00002130	0.00000000	0.00000000	0.00000000	-0.00000190	0.00000000
n333	-0.00002130	0.00000000	0.00000000	0.00000000	-0.00000352	0.00000000
n341	-0.00002130	0.00000000	0.00000147	-0.00000006	-0.00000118	0.00000000
n342	-0.00002130	0.00000000	-0.00000010	0.00000000	-0.00000171	0.00000000
n343	-0.00002130	0.00000000	0.00000147	0.00000006	-0.00000118	0.00000000
n351	-0.00002130	0.00000000	0.00000052	-0.00000003	-0.00000275	0.00000000
n352	-0.00002130	0.00000000	0.00000014	0.00000000	-0.00000301	0.00000000
n353	-0.00002130	0.00000000	0.00000052	0.00000003	-0.00000275	0.00000000
n411	-0.00003195	0.00000000	-0.00000061	0.00000002	-0.00000284	0.00000000
n412	-0.00003195	0.00000000	-0.00000016	0.00000000	-0.00000309	0.00000000
n413	-0.00003195	0.00000000	-0.00000061	-0.00000002	-0.00000284	0.00000000
n421	-0.00003195	0.00000000	-0.00000171	0.00000005	-0.00000156	0.00000000
n422	-0.00003195	0.00000000	0.00000012	0.00000000	-0.00000185	0.00000000
n423	-0.00003195	0.00000000	-0.00000171	-0.00000005	-0.00000156	0.00000000
n431	-0.00003195	0.00000000	0.00000000	0.00000000	-0.00000350	0.00000000
n432	-0.00003195	0.00000000	0.00000000	0.00000000	-0.00000196	0.00000000
n433	-0.00003195	0.00000000	0.00000000	0.00000000	-0.00000350	0.00000000
n441	-0.00003195	0.00000000	0.00000171	-0.00000005	-0.00000156	0.00000000
n442	-0.00003195	0.00000000	-0.00000012	0.00000000	-0.00000185	0.00000000
n443	-0.00003195	0.00000000	0.00000171	0.00000005	-0.00000156	0.00000000
n451	-0.00003195	0.00000000	0.00000061	-0.00000002	-0.00000284	0.00000000
n452	-0.00003195	0.00000000	0.00000016	0.00000000	-0.00000309	0.00000000
n453	-0.00003195	0.00000000	0.00000061	0.00000002	-0.00000284	0.00000000
n511	-0.00004227	0.00000000	-0.00000064	0.00000005	-0.00000219	0.00000000
n512	-0.00004227	0.00000000	-0.00000017	0.00000000	-0.00000252	0.00000000
n513	-0.00004227	0.00000000	-0.00000064	-0.00000005	-0.00000219	0.00000000
n521	-0.00004227	0.00000000	-0.00000182	0.00000013	-0.00000018	0.00000000
n522	-0.00004227	0.00000000	0.00000013	0.00000000	-0.00000089	0.00000000
n523	-0.00004227	0.00000000	-0.00000182	-0.00000013	-0.00000018	0.00000000
n531	-0.00004227	0.00000000	0.00000000	0.00000000	-0.00000338	0.00000000
n532	-0.00004227	0.00000000	0.00000000	0.00000000	-0.00000129	0.00000000
n533	-0.00004227	0.00000000	0.00000000	0.00000000	-0.00000338	0.00000000
n541	-0.00004227	0.00000000	0.00000182	-0.00000013	-0.00000018	0.00000000
n542	-0.00004227	0.00000000	-0.00000013	0.00000000	-0.00000089	0.00000000
n543	-0.00004227	0.00000000	0.00000182	0.00000013	-0.00000018	0.00000000
n551	-0.00004227	0.00000000	0.00000064	-0.00000005	-0.00000219	0.00000000
n552	-0.00004227	0.00000000	0.00000017	0.00000000	-0.00000252	0.00000000
n553	-0.00004227	0.00000000	0.00000064	0.00000005	-0.00000219	0.00000000

Figure C.4: Nodal displacements for mode 2 (2/2)

NODAL DISPLACEMENTS Y-Mode 1						
Node Name	X	Y	Z	RX	RY	RZ
n011	0.00000000	0.00000000	0.00000000	0.00000000	0.00000000	0.00000000
n012	0.00000000	0.00000000	0.00000000	0.00000000	0.00000000	0.00000000
n013	0.00000000	0.00000000	0.00000000	0.00000000	0.00000000	0.00000000
n021	0.00000000	0.00000000	0.00000000	0.00000000	0.00000000	0.00000000
n022	0.00000000	0.00000000	0.00000000	0.00000000	0.00000000	0.00000000
n023	0.00000000	0.00000000	0.00000000	0.00000000	0.00000000	0.00000000
n031	0.00000000	0.00000000	0.00000000	0.00000000	0.00000000	0.00000000
n032	0.00000000	0.00000000	0.00000000	0.00000000	0.00000000	0.00000000
n033	0.00000000	0.00000000	0.00000000	0.00000000	0.00000000	0.00000000
n041	0.00000000	0.00000000	0.00000000	0.00000000	0.00000000	0.00000000
n042	0.00000000	0.00000000	0.00000000	0.00000000	0.00000000	0.00000000
n043	0.00000000	0.00000000	0.00000000	0.00000000	0.00000000	0.00000000
n051	0.00000000	0.00000000	0.00000000	0.00000000	0.00000000	0.00000000
n052	0.00000000	0.00000000	0.00000000	0.00000000	0.00000000	0.00000000
n053	0.00000000	0.00000000	0.00000000	0.00000000	0.00000000	0.00000000
n111	0.00000000	0.00000316	0.00000054	-0.00000116	0.00000001	0.00000000
n112	0.00000000	0.00000316	0.00000000	-0.00000195	0.00000000	0.00000000
n113	0.00000000	0.00000316	-0.00000054	-0.00000116	-0.00000001	0.00000000
n121	0.00000000	0.00000316	0.00000019	-0.00000152	0.00000002	0.00000000
n122	0.00000000	0.00000316	0.00000000	-0.00000116	0.00000000	0.00000000
n123	0.00000000	0.00000316	-0.00000019	-0.00000152	-0.00000002	0.00000000
n131	0.00000000	0.00000316	0.00000004	-0.00000173	0.00000000	0.00000000
n132	0.00000000	0.00000316	0.00000000	-0.00000110	0.00000000	0.00000000
n133	0.00000000	0.00000316	-0.00000004	-0.00000173	0.00000000	0.00000000
n141	0.00000000	0.00000316	0.00000019	-0.00000152	-0.00000002	0.00000000
n142	0.00000000	0.00000316	0.00000000	-0.00000116	0.00000000	0.00000000
n143	0.00000000	0.00000316	-0.00000019	-0.00000152	0.00000002	0.00000000
n151	0.00000000	0.00000316	0.00000054	-0.00000116	-0.00000001	0.00000000
n152	0.00000000	0.00000316	0.00000000	-0.00000195	0.00000000	0.00000000
n153	0.00000000	0.00000316	-0.00000054	-0.00000116	0.00000001	0.00000000
n211	0.00000000	0.00001089	0.00000101	-0.00000188	0.00000002	0.00000000
n212	0.00000000	0.00001089	0.00000000	-0.00000307	0.00000000	0.00000000
n213	0.00000000	0.00001089	-0.00000101	-0.00000188	-0.00000002	0.00000000
n221	0.00000000	0.00001089	0.00000036	-0.00000242	0.00000004	0.00000000
n222	0.00000000	0.00001089	0.00000000	-0.00000186	0.00000000	0.00000000
n223	0.00000000	0.00001089	-0.00000036	-0.00000242	-0.00000004	0.00000000
n231	0.00000000	0.00001089	0.00000007	-0.00000275	0.00000000	0.00000000
n232	0.00000000	0.00001089	0.00000000	-0.00000178	0.00000000	0.00000000
n233	0.00000000	0.00001089	-0.00000007	-0.00000275	0.00000000	0.00000000
n241	0.00000000	0.00001089	0.00000036	-0.00000242	-0.00000004	0.00000000
n242	0.00000000	0.00001089	0.00000000	-0.00000186	0.00000000	0.00000000
n243	0.00000000	0.00001089	-0.00000036	-0.00000242	0.00000004	0.00000000
n251	0.00000000	0.00001089	0.00000101	-0.00000188	-0.00000002	0.00000000
n252	0.00000000	0.00001089	0.00000000	-0.00000307	0.00000000	0.00000000
n253	0.00000000	0.00001089	-0.00000101	-0.00000188	0.00000002	0.00000000

Figure C.5: Nodal displacements for mode 1 (1/2)

n311	0.00000000	0.00002102	0.00000137	-0.00000208	0.00000004	0.00000000
n312	0.00000000	0.00002102	0.00000000	-0.00000356	0.00000000	0.00000000
n313	0.00000000	0.00002102	-0.00000137	-0.00000208	-0.00000004	0.00000000
n321	0.00000000	0.00002102	0.00000049	-0.00000277	0.00000006	0.00000000
n322	0.00000000	0.00002102	0.00000000	-0.00000217	0.00000000	0.00000000
n323	0.00000000	0.00002102	-0.00000049	-0.00000277	-0.00000006	0.00000000
n331	0.00000000	0.00002102	0.00000010	-0.00000317	0.00000000	0.00000000
n332	0.00000000	0.00002102	0.00000000	-0.00000205	0.00000000	0.00000000
n333	0.00000000	0.00002102	-0.00000010	-0.00000317	0.00000000	0.00000000
n341	0.00000000	0.00002102	0.00000049	-0.00000277	-0.00000006	0.00000000
n342	0.00000000	0.00002102	0.00000000	-0.00000217	0.00000000	0.00000000
n343	0.00000000	0.00002102	-0.00000049	-0.00000277	0.00000006	0.00000000
n351	0.00000000	0.00002102	0.00000137	-0.00000208	-0.00000004	0.00000000
n352	0.00000000	0.00002102	0.00000000	-0.00000356	0.00000000	0.00000000
n353	0.00000000	0.00002102	-0.00000137	-0.00000208	0.00000004	0.00000000
n411	0.00000000	0.00003189	0.00000160	-0.00000252	0.00000003	0.00000000
n412	0.00000000	0.00003189	0.00000000	-0.00000361	0.00000000	0.00000000
n413	0.00000000	0.00003189	-0.00000160	-0.00000252	-0.00000003	0.00000000
n421	0.00000000	0.00003189	0.00000057	-0.00000302	0.00000006	0.00000000
n422	0.00000000	0.00003189	0.00000000	-0.00000233	0.00000000	0.00000000
n423	0.00000000	0.00003189	-0.00000057	-0.00000302	-0.00000006	0.00000000
n431	0.00000000	0.00003189	0.00000012	-0.00000331	0.00000000	0.00000000
n432	0.00000000	0.00003189	0.00000000	-0.00000228	0.00000000	0.00000000
n433	0.00000000	0.00003189	-0.00000012	-0.00000331	0.00000000	0.00000000
n441	0.00000000	0.00003189	0.00000057	-0.00000302	-0.00000006	0.00000000
n442	0.00000000	0.00003189	0.00000000	-0.00000233	0.00000000	0.00000000
n443	0.00000000	0.00003189	-0.00000057	-0.00000302	0.00000006	0.00000000
n451	0.00000000	0.00003189	0.00000160	-0.00000252	-0.00000003	0.00000000
n452	0.00000000	0.00003189	0.00000000	-0.00000361	0.00000000	0.00000000
n453	0.00000000	0.00003189	-0.00000160	-0.00000252	0.00000003	0.00000000
n511	0.00000000	0.00004263	0.00000170	-0.00000102	0.00000007	0.00000000
n512	0.00000000	0.00004263	0.00000000	-0.00000353	0.00000000	0.00000000
n513	0.00000000	0.00004263	-0.00000170	-0.00000102	-0.00000007	0.00000000
n521	0.00000000	0.00004263	0.00000060	-0.00000225	0.00000011	0.00000000
n522	0.00000000	0.00004263	0.00000000	-0.00000137	0.00000000	0.00000000
n523	0.00000000	0.00004263	-0.00000060	-0.00000225	-0.00000011	0.00000000
n531	0.00000000	0.00004263	0.00000013	-0.00000280	0.00000000	0.00000000
n532	0.00000000	0.00004263	0.00000000	-0.00000111	0.00000000	0.00000000
n533	0.00000000	0.00004263	-0.00000013	-0.00000280	0.00000000	0.00000000
n541	0.00000000	0.00004263	0.00000060	-0.00000225	-0.00000011	0.00000000
n542	0.00000000	0.00004263	0.00000000	-0.00000137	0.00000000	0.00000000
n543	0.00000000	0.00004263	-0.00000060	-0.00000225	0.00000011	0.00000000
n551	0.00000000	0.00004263	0.00000170	-0.00000102	-0.00000007	0.00000000
n552	0.00000000	0.00004263	0.00000000	-0.00000353	0.00000000	0.00000000
n553	0.00000000	0.00004263	-0.00000170	-0.00000102	0.00000007	0.00000000

Figure C.6: Nodal displacements for mode 1 (2/2)

			Normalization to roof displacement	
Node name	Weight (KN)	Height: Z(m)	Mode 1:Y	Mode 2:X
n011	0.0000	0.0000	0.0000	0.0000
n012	0.0000	0.0000	0.0000	0.0000
n013	0.0000	0.0000	0.0000	0.0000
n021	0.0000	0.0000	0.0000	0.0000
n022	0.0000	0.0000	0.0000	0.0000
n023	0.0000	0.0000	0.0000	0.0000
n031	0.0000	0.0000	0.0000	0.0000
n032	0.0000	0.0000	0.0000	0.0000
n033	0.0000	0.0000	0.0000	0.0000
n041	0.0000	0.0000	0.0000	0.0000
n042	0.0000	0.0000	0.0000	0.0000
n043	0.0000	0.0000	0.0000	0.0000
n051	0.0000	0.0000	0.0000	0.0000
n052	0.0000	0.0000	0.0000	0.0000
n053	0.0000	0.0000	0.0000	0.0000
n111	120.9200	3.0000	0.0740	0.0776
n112	209.3200	3.0000	0.0740	0.0776
n113	120.9200	3.0000	0.0740	0.0776
n121	208.9500	3.0000	0.0740	0.0776
n122	385.4200	3.0000	0.0740	0.0776
n123	208.9500	3.0000	0.0740	0.0776
n131	209.0700	3.0000	0.0740	0.0776
n132	385.4200	3.0000	0.0740	0.0776
n133	209.0700	3.0000	0.0740	0.0776
n141	208.9500	3.0000	0.0740	0.0776
n142	385.4200	3.0000	0.0740	0.0776
n143	208.9500	3.0000	0.0740	0.0776
n151	120.9200	3.0000	0.0740	0.0776
n152	209.3200	3.0000	0.0740	0.0776
n153	120.9200	3.0000	0.0740	0.0776
n211	120.9200	6.0000	0.2556	0.2644
n212	209.3200	6.0000	0.2556	0.2644
n213	120.9200	6.0000	0.2556	0.2644
n221	208.9500	6.0000	0.2556	0.2644
n222	385.4200	6.0000	0.2556	0.2644
n223	208.9500	6.0000	0.2556	0.2644
n231	209.0700	6.0000	0.2556	0.2644
n232	385.4200	6.0000	0.2556	0.2644
n233	209.0700	6.0000	0.2556	0.2644
n241	208.9500	6.0000	0.2556	0.2644
n242	385.4200	6.0000	0.2556	0.2644
n243	208.9500	6.0000	0.2556	0.2644
n251	120.9200	6.0000	0.2556	0.2644
n252	209.3200	6.0000	0.2556	0.2644
n253	120.9200	6.0000	0.2556	0.2644

Figure C.7: Normalized displacements (1/2)

n311	120.9200	9.0000	0.4930	0.5038
n312	209.3200	9.0000	0.4930	0.5038
n313	120.9200	9.0000	0.4930	0.5038
n321	208.9500	9.0000	0.4930	0.5038
n322	385.4200	9.0000	0.4930	0.5038
n323	208.9500	9.0000	0.4930	0.5038
n331	209.0700	9.0000	0.4930	0.5038
n332	385.4200	9.0000	0.4930	0.5038
n333	209.0700	9.0000	0.4930	0.5038
n341	208.9500	9.0000	0.4930	0.5038
n342	385.4200	9.0000	0.4930	0.5038
n343	208.9500	9.0000	0.4930	0.5038
n351	120.9200	9.0000	0.4930	0.5038
n352	209.3200	9.0000	0.4930	0.5038
n353	120.9200	9.0000	0.4930	0.5038
n411	120.9200	12.0000	0.7482	0.7558
n412	209.3200	12.0000	0.7482	0.7558
n413	120.9200	12.0000	0.7482	0.7558
n421	208.9500	12.0000	0.7482	0.7558
n422	385.4200	12.0000	0.7482	0.7558
n423	208.9500	12.0000	0.7482	0.7558
n431	209.0700	12.0000	0.7482	0.7558
n432	385.4200	12.0000	0.7482	0.7558
n433	209.0700	12.0000	0.7482	0.7558
n441	208.9500	12.0000	0.7482	0.7558
n442	385.4200	12.0000	0.7482	0.7558
n443	208.9500	12.0000	0.7482	0.7558
n451	120.9200	12.0000	0.7482	0.7558
n452	209.3200	12.0000	0.7482	0.7558
n453	120.9200	12.0000	0.7482	0.7558
n511	86.9600	15.0000	1.0000	1.0000
n512	157.5200	15.0000	1.0000	1.0000
n513	86.9600	15.0000	1.0000	1.0000
n521	157.6400	15.0000	1.0000	1.0000
n522	298.7600	15.0000	1.0000	1.0000
n523	157.6400	15.0000	1.0000	1.0000
n531	157.7000	15.0000	1.0000	1.0000
n532	298.7600	15.0000	1.0000	1.0000
n533	157.7000	15.0000	1.0000	1.0000
n541	157.6400	15.0000	1.0000	1.0000
n542	298.7600	15.0000	1.0000	1.0000
n543	157.6400	15.0000	1.0000	1.0000
n551	86.9600	15.0000	1.0000	1.0000
n552	157.5200	15.0000	1.0000	1.0000
n553	86.9600	15.0000	1.0000	1.0000

Figure C.8: Normalized displacements (2/2)

	Mode 2:X			Mode 1:Y		
Node name	m_i*ϕ_i	m_i*ϕ_i^2	h_i*m_i*ϕ_i	m_i*ϕ_i	m_i*ϕ_i^2	h_i*m_i*ϕ_i
n011	0	0	0	0	0	0
n012	0	0	0	0	0	0
n013	0	0	0	0	0	0
n021	0	0	0	0	0	0
n022	0	0	0	0	0	0
n023	0	0	0	0	0	0
n031	0	0	0	0	0	0
n032	0	0	0	0	0	0
n033	0	0	0	0	0	0
n041	0	0	0	0	0	0
n042	0	0	0	0	0	0
n043	0	0	0	0	0	0
n051	0	0	0	0	0	0
n052	0	0	0	0	0	0
n053	0	0	0	0	0	0
n111	0.95631344	0.07419443	2.86894033	0.91265237	0.0675743	2.7379571
n112	1.65543736	0.12843512	4.96631208	1.57985736	0.11697527	4.73957207
n113	0.95631344	0.07419443	2.86894033	0.91265237	0.0675743	2.7379571
n121	1.6525109	0.12820808	4.9575327	1.57706451	0.11676848	4.73119352
n122	3.0481496	0.23648703	9.14444879	2.90907663	0.2153997	8.7272299
n123	1.6525109	0.12820808	4.9575327	1.57706451	0.11676848	4.73119352
n131	1.65346053	0.12828175	4.96038158	1.57797078	0.11683558	4.73391233
n132	3.0481496	0.23648703	9.14444879	2.90898446	0.21538605	8.72695339
n133	1.65346053	0.12828175	4.96038158	1.57797078	0.11683558	4.73391233
n141	1.6525109	0.12820808	4.9575327	1.57706451	0.11676848	4.73119352
n142	3.0481496	0.23648703	9.14444879	2.90907663	0.2153997	8.7272299
n143	1.6525109	0.12820808	4.9575327	1.57706451	0.11676848	4.73119352
n151	0.95631344	0.07419443	2.86894033	0.91265237	0.0675743	2.7379571
n152	1.65543736	0.12843512	4.96631208	1.57985736	0.11697527	4.73957207
n153	0.95631344	0.07419443	2.86894033	0.91265237	0.0675743	2.7379571
n211	3.25905276	0.861695	19.5543166	3.1502281	0.8051092	18.9013686
n212	5.64162069	1.49164702	33.8497242	5.45323851	1.39369353	32.719431
n213	3.25905276	0.861695	19.5543166	3.1502281	0.8051092	18.9013686
n221	5.63164751	1.48901011	33.7898851	5.44359834	1.39122977	32.66159
n222	10.3878916	2.74656315	62.3273495	10.0410243	2.56620181	60.2461457
n223	5.63164751	1.48901011	33.7898851	5.44359834	1.39122977	32.66159
n231	5.63488377	1.48986577	33.8093026	5.44672654	1.39202925	32.6803592
n232	10.3878916	2.74656315	62.3273495	10.0410243	2.56620181	60.2461457
n233	5.63488377	1.48986577	33.8093026	5.44672654	1.39202925	32.6803592
n241	5.63164751	1.48901011	33.7898851	5.44359834	1.39122977	32.66159
n242	10.3878916	2.74656315	62.3273495	10.0410243	2.56620181	60.2461457
n243	5.63164751	1.48901011	33.7898851	5.44359834	1.39122977	32.66159
n251	3.25905276	0.861695	19.5543166	3.1502281	0.8051092	18.9013686
n252	5.64162069	1.49164702	33.8497242	5.45323851	1.39369353	32.719431
n253	3.25905276	0.861695	19.5543166	3.1502281	0.8051092	18.9013686

Figure C.9: Calculations of modal participation factors (1/2)

n311	6.21048267	3.12911481	55.894344	6.07721623	2.99626464	54.6949461
n312	10.7507273	5.41669011	96.7565458	10.5200349	5.18671829	94.6803143
n313	6.21048267	3.12911481	55.894344	6.07721623	2.99626464	54.6949461
n321	10.7317223	5.40711455	96.5855008	10.5014377	5.17754928	94.5129396
n322	19.7952673	9.97372788	178.157406	19.3704944	9.55028178	174.33445
n323	10.7317223	5.40711455	96.5855008	10.5014377	5.17754928	94.5129396
n331	10.7378894	5.41022179	96.6410043	10.5074725	5.18052459	94.5672521
n332	19.7952673	9.97372788	178.157406	19.3704944	9.55028178	174.33445
n333	10.7378894	5.41022179	96.6410043	10.5074725	5.18052459	94.5672521
n341	10.7317223	5.40711455	96.5855008	10.5014377	5.17754928	94.5129396
n342	19.7952673	9.97372788	178.157406	19.3704944	9.55028178	174.33445
n343	10.7317223	5.40711455	96.5855008	10.5014377	5.17754928	94.5129396
n351	6.21048267	3.12911481	55.894344	6.07721623	2.99626464	54.6949461
n352	10.7507273	5.41669011	96.7565458	10.5200349	5.18671829	94.6803143
n353	6.21048267	3.12911481	55.894344	6.07721623	2.99626464	54.6949461
n411	9.31586979	7.04072869	111.790438	9.22223925	6.89991213	110.666871
n412	16.1263433	12.1879342	193.51612	15.9642631	11.9441721	191.571157
n413	9.31586979	7.04072869	111.790438	9.22223925	6.89991213	110.666871
n421	16.0978354	12.1663885	193.174025	15.9360417	11.9230573	191.2325
n422	29.6933657	22.4415901	356.320388	29.3949281	21.992752	352.739137
n423	16.0978354	12.1663885	193.174025	15.9360417	11.9230573	191.2325
n431	16.1070861	12.17338	193.285033	15.9451994	11.929909	191.342393
n432	29.6933657	22.4415901	356.320388	29.3949281	21.992752	352.739137
n433	16.1070861	12.17338	193.285033	15.9451994	11.929909	191.342393
n441	16.0978354	12.1663885	193.174025	15.9360417	11.9230573	191.2325
n442	29.6933657	22.4415901	356.320388	29.3949281	21.992752	352.739137
n443	16.0978354	12.1663885	193.174025	15.9360417	11.9230573	191.2325
n451	9.31586979	7.04072869	111.790438	9.22223925	6.89991213	110.666871
n452	16.1263433	12.1879342	193.51612	15.9642631	11.9441721	191.571157
n453	9.31586979	7.04072869	111.790438	9.22223925	6.89991213	110.666871
n511	8.86421031	8.86400062	132.963155	8.86442	8.86442	132.9663
n512	16.0567002	16.0563203	240.850502	16.05708	16.05708	240.8562
n513	8.86421031	8.86400062	132.963155	8.86442	8.86442	132.9663
n521	16.0689399	16.0685597	241.034098	16.06932	16.06932	241.0398
n522	30.45464	30.45464	456.8196	30.45464	30.45464	456.8196
n523	16.0689399	16.0685597	241.034098	16.06932	16.06932	241.0398
n531	16.0750497	16.0746695	241.125746	16.07543	16.07543	241.13145
n532	30.4539196	30.4531992	456.808794	30.45464	30.45464	456.8196
n533	16.0750497	16.0746695	241.125746	16.07543	16.07543	241.13145
n541	16.0689399	16.0685597	241.034098	16.06932	16.06932	241.0398
n542	30.45464	30.45464	456.8196	30.45464	30.45464	456.8196
n543	16.0689399	16.0685597	241.034098	16.06932	16.06932	241.0398
n551	8.86421031	8.86400062	132.963155	8.86442	8.86442	132.9663
n552	16.0567002	16.0563203	240.850502	16.05708	16.05708	240.8562
n553	8.86421031	8.86400062	132.963155	8.86442	8.86442	132.9663
Total	**796.169959**	**559.588533**	**9038.26705**	**785.781817**	**550.369368**	**8953.22536**

Figure C.10: Calculations of modal participation factors (2/2)

INTERNAL FORCES FOR STRUCTURAL ANALYSIS IN X DIRECTION								
Elm.Name	**End**		**F**	**V2**	**V3**	**Mt**	**M2**	**M3**
col252	-A-	Max	1004.6	-12.307	254.41	-1.6295	2453.5	-2.0383
		Min	776.99	-70.582	-447.73	-1.6296	-1344.8	-124.55
	-B-	Max	-776.99	70.582	447.73	1.6296	628.45	-34.691
		Min	-1004.6	12.307	-254.41	1.6295	-1157.3	-87.392
col231	-A-	Max	983.1	-37.036	1088.1	-1.6355	5971.1	-51.21
		Min	919.61	-54.337	-1206.3	-1.6356	-5316.7	-89.624
	-B-	Max	-919.61	54.337	1206.3	1.6356	2215.1	-59.819
		Min	-983.1	37.036	-1088.1	1.6355	-2515	-73.467
col212	-A-	Max	1004.6	70.582	447.73	-1.6295	1344.8	124.55
		Min	776.99	12.307	-254.41	-1.6296	-2453.5	2.0383
	-B-	Max	-776.99	-12.307	254.41	1.6296	1157.3	87.392
		Min	-1004.6	-70.582	-447.73	1.6295	-628.45	34.691
col552	-A-	Max	208.71	-21.242	43.114	-2.1295	147.49	-29.086
		Min	162.97	-105.7	-72.652	-2.1298	-146.25	-135.45
	-B-	Max	-162.97	105.7	72.652	2.1298	188.12	-34.619
		Min	-208.71	21.242	-43.114	2.1295	-100.75	-181.68
col152	-A-	Max	1244.7	-5.6061	298.33	-0.78836	3845.8	33.957
		Min	982.84	-38.089	-512.67	-0.78853	-2148.4	-77.653
	-B-	Max	-982.84	38.089	512.67	0.78853	1278.3	-36.157
		Min	-1244.7	5.6061	-298.33	0.78836	-2332.7	-51.234
col512	-A-	Max	208.71	105.7	72.652	-2.1295	146.25	135.45
		Min	162.97	21.242	-43.114	-2.1298	-147.49	29.086
	-B-	Max	-162.97	-21.242	43.114	2.1298	100.75	181.68
		Min	-208.71	-105.7	-72.652	2.1295	-188.12	34.619
col352	-A-	Max	747.71	-8.4587	200.44	-2.1574	1344.7	-4.1718
		Min	574.37	-78.069	-361.09	-2.1575	-728.91	-121.55
	-B-	Max	-574.37	78.069	361.09	2.1575	228.6	-21.015
		Min	-747.71	8.4587	-200.44	2.1574	-362.42	-112.85
col312	-A-	Max	747.71	78.069	361.09	-2.1574	728.91	121.55
		Min	574.37	8.4587	-200.44	-2.1575	-1344.7	4.1718
	-B-	Max	-574.37	-8.4587	200.44	2.1575	362.42	112.85
		Min	-747.71	-78.069	-361.09	2.1574	-228.6	21.015
col531	-A-	Max	207.09	-53.522	165.97	-2.1782	528.31	-69.256
		Min	193.96	-80.281	-193.22	-2.1788	-514.81	-102.9
	-B-	Max	-193.96	80.281	193.22	2.1788	576.93	-91.304
		Min	-207.09	53.522	-165.97	2.1782	-508.67	-137.95
col533	-A-	Max	207.09	80.281	193.22	-2.1782	514.81	102.9
		Min	193.96	53.522	-165.97	-2.1788	-528.31	69.256
	-B-	Max	-193.96	-53.522	165.97	2.1788	508.67	137.95
		Min	-207.09	-80.281	-193.22	2.1782	-576.93	91.304
col412	-A-	Max	481.19	74.596	254.19	-2.3373	305.9	116.1
		Min	369.75	10.333	-141.1	-2.3375	-540.11	16.162
	-B-	Max	-369.75	-10.333	141.1	2.3375	209.71	107.82
		Min	-481.19	-74.596	-254.19	2.3373	-314.77	14.709
col452	-A-	Max	481.19	-10.333	141.1	-2.3373	540.11	-16.162
		Min	369.75	-74.596	-254.19	-2.3375	-305.9	-116.1
	-B-	Max	-369.75	74.596	254.19	2.3375	314.77	-14.709
		Min	-481.19	10.333	-141.1	2.3373	-209.71	-107.82
col333	-A-	Max	735.58	56.644	957.87	-2.1693	2759.3	85.456
		Min	686.7	35.582	-856.94	-2.1694	-3129	48.683
	-B-	Max	-686.7	-35.582	856.94	2.1694	782.72	84.542
		Min	-735.58	-56.644	-957.87	2.1693	-715.9	57.997
col131	-A-	Max	1210.5	-19.934	1284.5	-0.76566	9721.1	-6.9163
		Min	1138.1	-29.528	-1411.7	-0.76591	-8728.7	-42.545
	-B-	Max	-1138.1	29.528	1411.7	0.76591	4950.3	-45.922
		Min	-1210.5	19.934	-1284.5	0.76566	-5561	-53
col431	-A-	Max	476.55	-34.532	584.45	-2.3554	1202.1	-53.818
		Min	444.75	-54.134	-657.25	-2.3557	-1054.6	-85.161
	-B-	Max	-444.75	54.134	657.25	2.3557	1082	-49.736

		Min	-476.55	34.532	-584.45	2.3554	-1011.1	-77.284
col112	-A-	Max	1244.7	38.089	512.67	-0.78836	2148.4	77.653
		Min	982.84	5.6061	-298.33	-0.78853	-3845.8	-33.957
	-B-	Max	-982.84	-5.6061	298.33	0.78853	2332.7	51.234
		Min	-1244.7	-38.089	-512.67	0.78836	-1278.3	36.157
col433	-A-	Max	476.55	54.134	657.25	-2.3554	1054.6	85.161
		Min	444.75	34.532	-584.45	-2.3557	-1202.1	53.818
	-B-	Max	-444.75	-34.532	584.45	2.3557	1011.1	77.284
		Min	-476.55	-54.134	-657.25	2.3554	-1082	49.736
col133	-A-	Max	1210.5	29.528	1411.7	-0.76566	8728.7	42.545
		Min	1138.1	19.934	-1284.5	-0.76591	-9721.1	6.9163
	-B-	Max	-1138.1	-19.934	1284.5	0.76591	5561	53
		Min	-1210.5	-29.528	-1411.7	0.76566	-4950.3	45.922
col233	-A-	Max	983.1	54.337	1206.3	-1.6355	5316.7	89.624
		Min	919.61	37.036	-1088.1	-1.6356	-5971.1	51.21
	-B-	Max	-919.61	-37.036	1088.1	1.6356	2515	73.467
		Min	-983.1	-54.337	-1206.3	1.6355	-2215.1	59.819
col331	-A-	Max	735.58	-35.582	856.94	-2.1693	3129	-48.683
		Min	686.7	-56.644	-957.87	-2.1694	-2759.3	-85.456
	-B-	Max	-686.7	56.644	957.87	2.1694	715.9	-57.997
		Min	-735.58	35.582	-856.94	2.1693	-782.72	-84.542
col511	-A-	Max	111.8	6.7994	52.911	-0.32637	11.425	6.758
		Min	56.632	-36.914	-9.4459	-0.32642	-60.334	-42.071
	-B-	Max	-56.632	36.914	9.4459	0.32642	12.665	10.581
		Min	-111.8	-6.7994	-52.911	0.32637	-74.592	-52.061
col353	-A-	Max	434.39	29.269	9.5834	-0.30448	53.381	37.841
		Min	215.59	-2.6966	-41.002	-0.3045	-14.759	-3.7619
	-B-	Max	-215.59	2.6966	41.002	0.3045	51.206	36.798
		Min	-434.39	-29.269	-9.5834	0.30448	-9.7107	-3.1182
col242	-A-	Max	1395.8	13.868	37.973	-0.23008	63.885	19.287
		Min	1394.9	-10.259	-47.975	-0.23008	-52.726	-14.286
	-B-	Max	-1394.9	10.259	47.975	0.23008	58.455	16.079
		Min	-1395.8	-13.868	-37.973	0.23008	-44.109	-11.876
col243	-A-	Max	941.34	46.243	69.845	-0.23013	60.588	62.333
		Min	459.91	30.581	-45.476	-0.23014	-91.561	38.956
	-B-	Max	-459.91	-30.581	45.476	0.23014	55.375	55.593
		Min	-941.34	-46.243	-69.845	0.23013	-86.545	39.018
col253	-A-	Max	589.21	26.834	3.8584	-0.22914	51.933	36.952
		Min	301.01	2.1918	-36.464	-0.22915	-9.6168	2.6688
	-B-	Max	-301.01	-2.1918	36.464	0.22915	41.07	31.475
		Min	-589.21	-26.834	-3.8584	0.22914	-0.24204	2.9185
col251	-A-	Max	558.26	4.8095	1.3323	-0.22914	55.744	7.1194
		Min	270.07	-19.832	-38.99	-0.22915	-5.8056	-27.164
	-B-	Max	-270.07	19.832	38.99	0.22915	43.7	5.1467
		Min	-558.26	-4.8095	-1.3323	0.22914	2.3883	-23.41
col411	-A-	Max	274.95	2.8214	39.9	-0.3322	12.534	3.918
		Min	135.05	-27.608	-10.053	-0.33222	-52.197	-36.647
	-B-	Max	-135.05	27.608	10.053	0.33222	13.12	3.2784
		Min	-274.95	-2.8214	-39.9	0.3322	-49.566	-33.756
col311	-A-	Max	434.39	2.6966	41.002	-0.30448	14.759	3.7619
		Min	215.59	-29.269	-9.5834	-0.3045	-53.381	-37.841
	-B-	Max	-215.59	29.269	9.5834	0.3045	9.7107	3.1182
		Min	-434.39	-2.6966	-41.002	0.30448	-51.206	-36.798
col453	-A-	Max	274.95	27.608	10.053	-0.3322	52.197	36.647
		Min	135.05	-2.8214	-39.9	-0.33222	-12.534	-3.918
	-B-	Max	-135.05	2.8214	39.9	0.33222	49.566	33.756
		Min	-274.95	-27.608	-10.053	0.3322	-13.12	-3.2784
col553	-A-	Max	111.8	36.914	9.4459	-0.32637	60.334	42.071
		Min	56.632	-6.7994	-52.911	-0.32642	-11.425	-6.758
	-B-	Max	-56.632	6.7994	52.911	0.32642	74.592	52.061
		Min	-111.8	-36.914	-9.4459	0.32637	-12.665	-10.581

col332	-A-	Max	1033.5	16.42	51.485	-0.30408	67.026	21.457
		Min	1033.5	-16.42	-51.485	-0.30408	-67.026	-21.457
	-B-	Max	-1033.5	16.42	51.485	0.30408	64.271	20.417
		Min	-1033.5	-16.42	-51.485	0.30408	-64.271	-20.417
col442	-A-	Max	650.4	17.999	43.818	-0.33043	82.718	23.378
		Min	649.06	-13.123	-64.39	-0.33044	-57.133	-17.057
	-B-	Max	-649.06	13.123	64.39	0.33044	81.48	22.522
		Min	-650.4	-17.999	-43.818	0.33043	-54.606	-16.408
col343	-A-	Max	690.44	47.752	87.605	-0.30446	74.458	60.63
		Min	325.7	27.2	-57.432	-0.30447	-112.05	33.234
	-B-	Max	-325.7	-27.2	57.432	0.30447	71.996	61.146
		Min	-690.44	-47.752	-87.605	0.30446	-111.34	36.116
col341	-A-	Max	704.3	-24.376	78.888	-0.30446	85.671	-29.433
		Min	339.56	-44.928	-66.149	-0.30447	-100.84	-56.829
	-B-	Max	-339.56	44.928	66.149	0.30447	83.011	-32.716
		Min	-704.3	24.376	-78.888	0.30446	-100.33	-57.746
col342	-A-	Max	1020.4	17.715	45.702	-0.30414	80.27	23.254
		Min	1019.7	-13.019	-62.302	-0.30414	-59.896	-17.095
	-B-	Max	-1019.7	13.019	62.302	0.30414	78.609	21.922
		Min	-1020.4	-17.715	-45.702	0.30414	-56.654	-16.107
col441	-A-	Max	446.52	-23.894	78.901	-0.33114	84.424	-31.081
		Min	211.41	-44.027	-65.065	-0.33115	-102.35	-57.777
	-B-	Max	-211.41	44.027	65.065	0.33115	81.494	-29.842
		Min	-446.52	23.894	-78.901	0.33114	-98.853	-54.497
col443	-A-	Max	437.4	46.766	87.864	-0.33113	72.789	61.44
		Min	202.3	26.633	-56.103	-0.33114	-113.98	34.744
	-B-	Max	-202.3	-26.633	56.103	0.33114	70.276	57.819
		Min	-437.4	-46.766	-87.864	0.33113	-110.07	33.164
col351	-A-	Max	410.54	11.857	6.2592	-0.30448	57.862	15.727
		Min	191.75	-20.108	-44.326	-0.3045	-10.278	-25.876
	-B-	Max	-191.75	20.108	44.326	0.3045	55.202	14.512
		Min	-410.54	-11.857	-6.2592	0.30448	-5.7147	-25.404
col321	-A-	Max	690.44	-27.2	57.432	-0.30446	112.05	-33.234
		Min	325.7	-47.752	-87.605	-0.30447	-74.458	-60.63
	-B-	Max	-325.7	47.752	87.605	0.30447	111.34	-36.116
		Min	-690.44	27.2	-57.432	0.30446	-71.996	-61.146
col313	-A-	Max	410.54	20.108	44.326	-0.30448	10.278	25.876
		Min	191.75	-11.857	-6.2592	-0.3045	-57.862	-15.727
	-B-	Max	-191.75	11.857	6.2592	0.3045	5.7147	25.404
		Min	-410.54	-20.108	-44.326	0.30448	-55.202	-14.512
col451	-A-	Max	259.2	11.594	6.6595	-0.3322	56.652	15.638
		Min	119.3	-18.835	-43.294	-0.33222	-8.0785	-24.927
	-B-	Max	-119.3	18.835	43.294	0.33222	53.765	13.929
		Min	-259.2	-11.594	-6.6595	0.3322	-8.9208	-23.106
col323	-A-	Max	704.3	44.928	66.149	-0.30446	100.84	56.829
		Min	339.56	24.376	-78.888	-0.30447	-85.671	29.433
	-B-	Max	-339.56	-24.376	78.888	0.30447	100.33	57.746
		Min	-704.3	-44.928	-66.149	0.30446	-83.011	32.716
col322	-A-	Max	1020.4	13.019	62.302	-0.30414	59.896	17.095
		Min	1019.7	-17.715	-45.702	-0.30414	-80.27	-23.254
	-B-	Max	-1019.7	17.715	45.702	0.30414	56.654	16.107
		Min	-1020.4	-13.019	-62.302	0.30414	-78.609	-21.922
col432	-A-	Max	659.82	16.488	52.656	-0.33016	67.541	21.505
		Min	659.82	-16.488	-52.656	-0.33016	-67.541	-21.505
	-B-	Max	-659.82	16.488	52.656	0.33016	66.735	20.54
		Min	-659.82	-16.488	-52.656	0.33016	-66.735	-20.54
col211	-A-	Max	589.21	-2.1918	36.464	-0.22914	9.6168	-2.6688
		Min	301.01	-26.834	-3.8584	-0.22915	-51.933	-36.952
	-B-	Max	-301.01	26.834	3.8584	0.22915	0.24204	-2.9185
		Min	-589.21	2.1918	-36.464	0.22914	-41.07	-31.475
col542	-A-	Max	288.38	22.395	51.545	-0.3287	93.177	26.359

		Min	284.76	-16.294	-78.423	-0.3287	-60.541	-19.142
	-B-	Max	-284.76	16.294	78.423	0.3287	106.8	30.749
		Min	-288.38	-22.395	-51.545	0.3287	-70.899	-22.407
col151	-A-	Max	693.29	0.37378	-0.35588	-0.093763	32.059	5.8061
		Min	361.4	-10.706	-20.213	-0.093784	-11.851	-12.82
	-B-	Max	-361.4	10.706	20.213	0.093784	19.53	-4.8504
		Min	-693.29	-0.37378	0.35588	0.093763	12.713	-14.484
col153	-A-	Max	728.72	13.811	0.80026	-0.093766	29.59	18.084
		Min	396.83	2.7309	-19.057	-0.093787	-14.32	-0.54154
	-B-	Max	-396.83	-2.7309	19.057	0.093787	19.051	17.136
		Min	-728.72	-13.811	-0.80026	0.093766	12.234	7.5027
col421	-A-	Max	437.4	-26.633	56.103	-0.33113	113.98	-34.744
		Min	202.3	-46.766	-87.864	-0.33114	-72.789	-61.44
	-B-	Max	-202.3	46.766	87.864	0.33114	110.07	-33.164
		Min	-437.4	26.633	-56.103	0.33113	-70.276	-57.819
col543	-A-	Max	187.43	63.114	110.89	-0.32981	78.703	72.575
		Min	81.477	34.761	-66.545	-0.32985	-129.98	40.756
	-B-	Max	-81.477	-34.761	66.545	0.32985	90.985	88.366
		Min	-187.43	-63.114	-110.89	0.32981	-152.8	47.884
col541	-A-	Max	191.9	-30.914	99.528	-0.3298	92.1	-36.438
		Min	85.953	-59.267	-77.912	-0.32984	-116.59	-68.258
	-B-	Max	-85.953	59.267	77.912	0.32984	106.58	-42.392
		Min	-191.9	30.914	-99.528	0.3298	-137.21	-82.874
col213	-A-	Max	558.26	19.832	38.99	-0.22914	5.8056	27.164
		Min	270.07	-4.8095	-1.3323	-0.22915	-55.744	-7.1194
	-B-	Max	-270.07	4.8095	1.3323	0.22915	-2.3883	23.41
		Min	-558.26	-19.832	-38.99	0.22914	-43.7	-5.1467
col143	-A-	Max	1178.3	24.788	30.778	-0.092538	30.138	27.508
		Min	620.65	17.451	-19.653	-0.092551	-41.715	12.303
	-B-	Max	-620.65	-17.451	19.653	0.092551	19.98	35.72
		Min	-1178.3	-24.788	-30.778	0.092538	-36.77	32.181
col121	-A-	Max	1178.3	-17.451	19.653	-0.092538	41.715	-12.303
		Min	620.65	-24.788	-30.778	-0.092551	-30.138	-27.508
	-B-	Max	-620.65	24.788	30.778	0.092551	36.77	-32.181
		Min	-1178.3	17.451	-19.653	0.092538	-19.98	-35.72
col122	-A-	Max	1783.8	4.591	20.587	-0.09312	29.142	7.839
		Min	1781.9	-6.1534	-17.791	-0.093121	-31.696	-10.481
	-B-	Max	-1781.9	6.1534	17.791	0.093121	16.228	3.87
		Min	-1783.8	-4.591	-20.587	0.09312	-20.803	-5.2126
col111	-A-	Max	728.72	-2.7309	19.057	-0.093766	14.32	0.54154
		Min	396.83	-13.811	-0.80026	-0.093787	-29.59	-18.084
	-B-	Max	-396.83	13.811	0.80026	0.093787	-12.234	-7.5027
		Min	-728.72	2.7309	-19.057	0.093766	-19.051	-17.136
col113	-A-	Max	693.29	10.706	20.213	-0.093763	11.851	12.82
		Min	361.4	-0.37378	0.35588	-0.093784	-32.059	-5.8061
	-B-	Max	-361.4	0.37378	-0.35588	0.093784	-12.713	14.484
		Min	-693.29	-10.706	-20.213	0.093763	-19.53	4.8504
col141	-A-	Max	1199	-16.447	27.977	-0.09254	34.11	-10.171
		Min	641.38	-23.784	-22.454	-0.092553	-37.743	-25.376
	-B-	Max	-641.38	23.784	22.454	0.092553	23.151	-31.751
		Min	-1199	16.447	-27.977	0.09254	-33.6	-35.29
col142	-A-	Max	1783.8	6.1534	17.791	-0.09312	31.696	10.481
		Min	1781.9	-4.591	-20.587	-0.093121	-29.142	-7.839
	-B-	Max	-1781.9	4.591	20.587	0.093121	20.803	5.2126
		Min	-1783.8	-6.1534	-17.791	0.09312	-16.228	-3.87
col123	-A-	Max	1199	23.784	22.454	-0.09254	37.743	25.376
		Min	641.38	16.447	-27.977	-0.092553	-34.11	10.171
	-B-	Max	-641.38	-16.447	27.977	0.092553	33.6	35.29
		Min	-1199	-23.784	-22.454	0.09254	-23.151	31.751
col132	-A-	Max	1793.9	5.669	18.329	-0.093089	29.634	9.4312
		Min	1793.9	-5.669	-18.329	-0.093089	-29.634	-9.4312

	-B-	Max	-1793.9	5.669	18.329	0.093089	17.109	5.0265
		Min	-1793.9	-5.669	-18.329	0.093089	-17.109	-5.0265
col522	-A-	Max	288.38	16.294	78.423	-0.3287	60.541	19.142
		Min	284.76	-22.395	-51.545	-0.3287	-93.177	-26.359
	-B-	Max	-284.76	22.395	51.545	0.3287	70.899	22.407
		Min	-288.38	-16.294	-78.423	0.3287	-106.8	-30.749
col551	-A-	Max	104.51	19.43	4.9809	-0.32638	65.493	20.9
		Min	49.341	-24.284	-57.376	-0.32643	-6.2667	-27.929
	-B-	Max	-49.341	24.284	57.376	0.32643	80.82	28.647
		Min	-104.51	-19.43	-4.9809	0.32638	-6.4375	-33.996
col523	-A-	Max	191.9	59.267	77.912	-0.3298	116.59	68.258
		Min	85.953	30.914	-99.528	-0.32984	-92.1	36.438
	-B-	Max	-85.953	-30.914	99.528	0.32984	137.21	82.874
		Min	-191.9	-59.267	-77.912	0.3298	-106.58	42.392
col232	-A-	Max	1410.6	12.804	41.066	-0.23018	55.943	17.678
		Min	1410.6	-12.804	-41.066	-0.23018	-55.943	-17.678
	-B-	Max	-1410.6	12.804	41.066	0.23018	48.78	14.973
		Min	-1410.6	-12.804	-41.066	0.23018	-48.78	-14.973
col423	-A-	Max	446.52	44.027	65.065	-0.33114	102.35	57.777
		Min	211.41	23.894	-78.901	-0.33115	-84.424	31.081
	-B-	Max	-211.41	-23.894	78.901	0.33115	98.853	54.497
		Min	-446.52	-44.027	-65.065	0.33114	-81.494	29.842
col513	-A-	Max	104.51	24.284	57.376	-0.32638	6.2667	27.929
		Min	49.341	-19.43	-4.9809	-0.32643	-65.493	-20.9
	-B-	Max	-49.341	19.43	4.9809	0.32643	6.4375	33.996
		Min	-104.51	-24.284	-57.376	0.32638	-80.82	-28.647
col521	-A-	Max	187.43	-34.761	66.545	-0.32981	129.98	-40.756
		Min	81.477	-63.114	-110.89	-0.32985	-78.703	-72.575
	-B-	Max	-81.477	63.114	110.89	0.32985	152.8	-47.884
		Min	-187.43	34.761	-66.545	0.32981	-90.985	-88.366
col241	-A-	Max	959.38	-28.426	63.177	-0.23013	69.373	-35.688
		Min	477.95	-44.088	-52.144	-0.23013	-82.777	-59.065
	-B-	Max	-477.95	44.088	52.144	0.23013	63.594	-36.792
		Min	-959.38	28.426	-63.177	0.23013	-78.326	-53.367
col223	-A-	Max	959.38	44.088	52.144	-0.23013	82.777	59.065
		Min	477.95	28.426	-63.177	-0.23013	-69.373	35.688
	-B-	Max	-477.95	-28.426	63.177	0.23013	78.326	53.367
		Min	-959.38	-44.088	-52.144	0.23013	-63.594	36.792
col222	-A-	Max	1395.8	10.259	47.975	-0.23008	52.726	14.286
		Min	1394.9	-13.868	-37.973	-0.23008	-63.885	-19.287
	-B-	Max	-1394.9	13.868	37.973	0.23008	44.109	11.876
		Min	-1395.8	-10.259	-47.975	0.23008	-58.455	-16.079
col532	-A-	Max	290.21	21.135	59.658	-0.32889	72.009	24.615
		Min	290.21	-21.135	-59.658	-0.32889	-72.009	-24.615
	-B-	Max	-290.21	21.135	59.658	0.32889	80.12	29.28
		Min	-290.21	-21.135	-59.658	0.32889	-80.12	-29.28
col413	-A-	Max	259.2	18.835	43.294	-0.3322	8.0785	24.927
		Min	119.3	-11.594	-6.6595	-0.33222	-56.652	-15.638
	-B-	Max	-119.3	11.594	6.6595	0.33222	8.9208	23.106
		Min	-259.2	-18.835	-43.294	0.3322	-53.765	-13.929
col221	-A-	Max	941.34	-30.581	45.476	-0.23013	91.561	-38.956
		Min	459.91	-46.243	-69.845	-0.23014	-60.588	-62.333
	-B-	Max	-459.91	46.243	69.845	0.23014	86.545	-39.018
		Min	-941.34	30.581	-45.476	0.23013	-55.375	-55.593
col422	-A-	Max	650.4	13.123	64.39	-0.33043	57.133	17.057
		Min	649.06	-17.999	-43.818	-0.33044	-82.718	-23.378
	-B-	Max	-649.06	17.999	43.818	0.33044	54.606	16.408
		Min	-650.4	-13.123	-64.39	0.33043	-81.48	-22.522
bmx611	-A-	Max	0.61432	0.0021755	15.219	3.3919	53.228	0.0031122
		Min	-7.3809	0.0020773	-12.52	1.7742	-44.121	0.0028642
	-B-	Max	7.3809	-0.0020773	12.52	-1.7742	16.887	0.0090712

		Min	-0.61432	-0.0021755	-15.219	-3.3919	-41.108	0.008768
bmx431	-A-	Max	6.9174	0.017716	94.323	1.9637	147.55	0.039796
		Min	-5.6683	0.017371	-70.385	1.0454	-196.08	0.039037
	-B-	Max	5.6683	-0.017371	70.385	-1.0454	119.92	0.027523
		Min	-6.9174	-0.017716	-94.323	-1.9637	-162.35	0.026974
bmy612	-A-	Max	1.934	-0.1522	29.322	1.421	11.968	-0.43067
		Min	-2.1169	-0.15231	-2.8186	-0.18963	-75.126	-0.43099
	-B-	Max	2.1169	0.15231	2.8186	0.18963	1.5616	-0.29987
		Min	-1.934	0.1522	-29.322	-1.421	-65.618	-0.30009
bmx423	-A-	Max	6.9174	0.017716	70.385	1.9637	162.35	0.027523
		Min	-5.6683	0.017371	-94.323	1.0454	-119.92	0.026974
	-B-	Max	5.6683	-0.017371	94.323	-1.0454	196.08	0.039796
		Min	-6.9174	-0.017716	-70.385	-1.9637	-147.55	0.039037
bmx613	-A-	Max	1.0895	0.0022631	17.086	-1.8102	46.832	0.0033708
		Min	-6.9057	0.0021649	-10.654	-3.428	-50.518	0.0031227
	-B-	Max	6.9057	-0.0021649	10.654	3.428	12.832	0.0093031
		Min	-1.0895	-0.0022631	-17.086	1.8102	-45.163	0.0089999
bmx521	-A-	Max	6.8088	-0.015638	58.438	-0.35072	191.97	-0.022424
		Min	-4.3443	-0.016091	-109.72	-1.103	-100.61	-0.02313
	-B-	Max	4.3443	0.016091	109.72	1.103	224.98	-0.037
		Min	-6.8088	0.015638	-58.438	0.35072	-121.46	-0.038014
bmy551	-A-	Max	0.62535	-0.012601	7.0386	1.1019	80.41	-0.019232
		Min	-1.0794	-0.012805	-34.116	-0.14559	-14.289	-0.019554
	-B-	Max	1.0794	0.012805	34.116	0.14559	83.347	-0.04125
		Min	-0.62535	0.012601	-7.0386	-1.1019	-19.497	-0.04191
bmy552	-A-	Max	0.13724	-0.012639	22.408	0.782	48.777	-0.04135
		Min	-1.5675	-0.012843	-18.747	-0.46547	-54.067	-0.04201
	-B-	Max	1.5675	0.012843	18.747	0.46547	41.209	-0.019316
		Min	-0.13724	0.012639	-22.408	-0.782	-53.49	-0.019637
bmx513	-A-	Max	1.2249	0.0047008	29.728	-0.77973	64.719	0.015097
		Min	-3.7344	0.0046371	-19.84	-1.3637	-86.244	0.014834
	-B-	Max	3.7344	-0.0046371	19.84	1.3637	46.384	0.011231
		Min	-1.2249	-0.0047008	-29.728	0.77973	-80.234	0.011129
bmx523	-A-	Max	6.1245	-0.015696	68.74	1.8175	174.11	-0.022524
		Min	-5.0286	-0.016149	-99.421	1.0652	-118.47	-0.02323
	-B-	Max	5.0286	0.016149	99.421	-1.0652	203.7	-0.037123
		Min	-6.1245	0.015696	-68.74	-1.8175	-142.74	-0.038137
bmx533	-A-	Max	6.8088	-0.015638	109.72	-0.35072	121.46	-0.037
		Min	-4.3443	-0.016091	-58.438	-1.103	-224.98	-0.038014
	-B-	Max	4.3443	0.016091	58.438	1.103	100.61	-0.022424
		Min	-6.8088	0.015638	-109.72	0.35072	-191.97	-0.02313
bmx541	-A-	Max	1.2249	0.0047008	19.84	-0.77973	80.234	0.011231
		Min	-3.7344	0.0046371	-29.728	-1.3637	-46.384	0.011129
	-B-	Max	3.7344	-0.0046371	29.728	1.3637	86.244	0.015097
		Min	-1.2249	-0.0047008	-19.84	0.77973	-64.719	0.014834
bmx543	-A-	Max	0.92392	0.0047208	23.09	1.7101	71.874	0.011273
		Min	-4.0353	0.0046572	-26.478	1.1261	-54.744	0.011171
	-B-	Max	4.0353	-0.0046572	26.478	-1.1261	76.405	0.015168
		Min	-0.92392	-0.0047208	-23.09	-1.7101	-74.559	0.014905
bmx531	-A-	Max	6.1245	-0.015696	99.421	1.8175	142.74	-0.037123
		Min	-5.0286	-0.016149	-68.74	1.0652	-203.7	-0.038137
	-B-	Max	5.0286	0.016149	68.74	-1.0652	118.47	-0.022524
		Min	-6.1245	0.015696	-99.421	-1.8175	-174.11	-0.02323
bmy611	-A-	Max	0.77077	-0.15208	11.976	0.65212	46.506	-0.29961
		Min	-3.2802	-0.15219	-20.164	-0.95854	-20.674	-0.29983
	-B-	Max	3.2802	0.15219	20.164	0.95854	50.281	-0.43038
		Min	-0.77077	0.15208	-11.976	-0.65212	-36.812	-0.4307
bmx443	-A-	Max	0.90561	-0.00020883	21.732	2.0373	63.324	-0.0010001
		Min	-4.7329	-0.00026482	-23.41	1.2092	-49.216	-0.0010991
	-B-	Max	4.7329	0.00026482	23.41	-1.2092	67.77	-0.00016925
		Min	-0.90561	0.00020883	-21.732	-2.0373	-72.481	-0.00038403

bmx433	-A-	Max	7.672	0.017714	104.1	-0.4007	127.09	0.039792
		Min	-4.9137	0.01737	-60.605	-1.319	-216.54	0.039034
	-B-	Max	4.9137	-0.01737	60.605	1.319	103.21	0.02752
		Min	-7.672	-0.017714	-104.1	0.4007	-179.05	0.026971
bmx441	-A-	Max	1.2315	-0.00020844	18.876	-0.96424	70.519	-0.00099695
		Min	-4.407	-0.00026443	-26.265	-1.7924	-42.022	-0.0010959
	-B-	Max	4.407	0.00026443	26.265	1.7924	76.567	-0.00017024
		Min	-1.2315	0.00020844	-18.876	0.96424	-63.684	-0.00038502
bmy451	-A-	Max	0.8608	0.012959	6.6153	1.0436	74.838	0.025582
		Min	-1.3774	0.012819	-32.05	-0.17842	-12.515	0.025367
	-B-	Max	1.3774	-0.012819	32.05	0.17842	79.004	0.036624
		Min	-0.8608	-0.012959	-6.6153	-1.0436	-19.239	0.036164
bmx511	-A-	Max	0.92392	0.0047208	26.478	1.7101	74.559	0.015168
		Min	-4.0353	0.0046571	-23.09	1.1261	-76.405	0.014905
	-B-	Max	4.0353	-0.0046571	23.09	-1.1261	54.744	0.011273
		Min	-0.92392	-0.0047208	-26.478	-1.7101	-71.874	0.011171
bmy512	-A-	Max	0.62535	-0.012601	34.116	1.1019	19.497	-0.04125
		Min	-1.0794	-0.012805	-7.0386	-0.14559	-83.347	-0.04191
	-B-	Max	1.0794	0.012805	7.0386	0.14559	14.289	-0.019232
		Min	-0.62535	0.012601	-34.116	-1.1019	-80.41	-0.019554
bmy452	-A-	Max	0.22146	0.012959	21.102	0.77312	47.078	0.036621
		Min	-2.0167	0.012819	-17.564	-0.44889	-51.164	0.036161
	-B-	Max	2.0167	-0.012819	17.564	0.44889	37.229	0.025584
		Min	-0.22146	-0.012959	-21.102	-0.77312	-50.124	0.025369
bmy511	-A-	Max	0.13724	-0.012639	18.747	0.782	53.49	-0.019316
		Min	-1.5675	-0.012843	-22.408	-0.46547	-41.209	-0.019637
	-B-	Max	1.5675	0.012843	22.408	0.46547	54.067	-0.04135
		Min	-0.13724	0.012639	-18.747	-0.782	-48.777	-0.04201
bmy251	-A-	Max	-0.092365	0.0607	2.4736	0.48625	45.342	0.12098
		Min	-1.3231	0.060626	-18.789	-0.13047	-2.7025	0.12088
	-B-	Max	1.3231	-0.060626	18.789	0.13047	44.843	0.17038
		Min	0.092365	-0.0607	-2.4736	-0.48625	-9.1707	0.17013
bmy252	-A-	Max	-0.43862	0.060665	12.853	0.45416	24.258	0.17029
		Min	-1.6694	0.060591	-8.4086	-0.16256	-29.755	0.17004
	-B-	Max	1.6694	-0.060591	8.4086	0.16256	16.103	0.1209
		Min	0.43862	-0.060665	-12.853	-0.45416	-31.942	0.1208
bmx243	-A-	Max	0.068728	0.00025768	13.341	1.6875	31.428	-0.0010239
		Min	-3.3799	0.0002266	-11.283	1.2326	-29.059	-0.0011131
	-B-	Max	3.3799	-0.0002266	11.283	-1.2326	31.757	0.0024733
		Min	-0.068728	-0.00025768	-13.341	-1.6875	-45.652	0.0023757
bmx641	-A-	Max	1.0895	0.0022631	10.654	-1.8102	45.163	0.0093031
		Min	-6.9057	0.0021649	-17.086	-3.428	-12.832	0.009
	-B-	Max	6.9057	-0.0021649	17.086	3.428	50.518	0.0033707
		Min	-1.0895	-0.0022631	-10.654	1.8102	-46.832	0.0031228
bmx633	-A-	Max	11.63	-0.20601	85.572	-0.33743	96.873	-0.46051
		Min	-6.7821	-0.20621	-42.225	-1.9942	-191.21	-0.46087
	-B-	Max	6.7821	0.20621	42.225	1.9942	63.581	-0.32234
		Min	-11.63	0.20601	-85.572	0.33743	-133.96	-0.32274
bmy311	-A-	Max	0.092357	0.037336	15.727	0.66335	43.096	0.072363
		Min	-1.7368	0.037217	-18.042	-0.37554	-33.503	0.072185
	-B-	Max	1.7368	-0.037217	18.042	0.37554	43.508	0.10685
		Min	-0.092357	-0.037336	-15.727	-0.66335	-41.987	0.10646
bmx321	-A-	Max	6.6033	0.050421	56.604	-0.43393	156.03	0.078324
		Min	-4.4059	0.050127	-90.611	-1.151	-96.828	0.077868
	-B-	Max	4.4059	-0.050127	90.611	1.151	188.29	0.11327
		Min	-6.6033	-0.050421	-56.604	0.43393	-118.27	0.11261
bmx631	-A-	Max	10.469	-0.2059	77.645	2.468	114.83	-0.46029
		Min	-7.9434	-0.2061	-50.152	0.81127	-173.25	-0.46065
	-B-	Max	7.9434	0.2061	50.152	-0.81127	75.743	-0.32213
		Min	-10.469	0.2059	-77.645	-2.468	-121.8	-0.32253
bmx313	-A-	Max	1.232	-0.0015209	22.497	-0.80404	56.798	-0.0038886

		Min	-3.7766	-0.0015633	-16.971	-1.4716	-66.017	-0.0040572
	-B-	Max	3.7766	0.0015633	16.971	1.4716	38.24	-0.0046179
		Min	-1.232	0.0015209	-22.497	0.80404	-59.968	-0.0047078
bmx311	-A-	Max	0.95079	-0.0015183	20.09	1.6928	64.229	-0.0038785
		Min	-4.0578	-0.0015607	-19.378	1.0253	-58.586	-0.004047
	-B-	Max	4.0578	0.0015607	19.378	-1.0253	44.288	-0.0046134
		Min	-0.95079	0.0015183	-20.09	-1.6928	-53.92	-0.0047034
bmy312	-A-	Max	0.6125	0.037341	27.549	0.89135	17.902	0.10687
		Min	-1.2167	0.037223	-6.2211	-0.14754	-67.593	0.10647
	-B-	Max	1.2167	-0.037223	6.2211	0.14754	11.959	0.072373
		Min	-0.6125	-0.037341	-27.549	-0.89135	-64.64	0.072195
bmx241	-A-	Max	0.25416	0.00023301	11.894	-1.106	35.024	-0.0010857
		Min	-3.1945	0.00020192	-12.73	-1.5609	-25.464	-0.001175
	-B-	Max	3.1945	-0.00020192	12.73	1.5609	36.263	0.002397
		Min	-0.25416	-0.00023301	-11.894	1.106	-41.146	0.0022993
bmy212	-A-	Max	-0.092366	0.0607	18.789	0.48625	9.1707	0.17038
		Min	-1.3231	0.060626	-2.4736	-0.13047	-44.843	0.17013
	-B-	Max	1.3231	-0.060626	2.4736	0.13047	2.7025	0.12098
		Min	0.092366	-0.0607	-18.789	-0.48625	-45.342	0.12088
bmx213	-A-	Max	0.25416	0.00023301	12.73	-1.106	41.146	0.002397
		Min	-3.1945	0.00020192	-11.894	-1.5609	-36.263	0.0022993
	-B-	Max	3.1945	-0.00020192	11.894	1.5609	25.464	-0.0010857
		Min	-0.25416	-0.00023301	-12.73	1.106	-35.024	-0.001175
bmy652	-A-	Max	0.77077	-0.15208	20.164	0.65212	36.812	-0.43038
		Min	-3.2802	-0.15219	-11.976	-0.95854	-50.281	-0.4307
	-B-	Max	3.2802	0.15219	11.976	0.95854	20.674	-0.29961
		Min	-0.77077	0.15208	-20.164	-0.65212	-46.506	-0.29983
bmx211	-A-	Max	0.068728	0.00025768	11.283	1.6875	45.652	0.0024733
		Min	-3.3799	0.0002266	-13.341	1.2326	-31.757	0.0023757
	-B-	Max	3.3799	-0.0002266	13.341	-1.2326	29.059	-0.0010239
		Min	-0.068728	-0.00025768	-11.283	-1.6875	-31.428	-0.0011131
bmy211	-A-	Max	-0.43862	0.060665	8.4086	0.45416	31.942	0.1209
		Min	-1.6694	0.060591	-12.853	-0.16256	-16.103	0.1208
	-B-	Max	1.6694	-0.060591	12.853	0.16256	29.755	0.17029
		Min	0.43862	-0.060665	-8.4086	-0.45416	-24.258	0.17004
bmy651	-A-	Max	1.934	-0.1522	2.8186	1.421	65.618	-0.29987
		Min	-2.1169	-0.15231	-29.322	-0.18963	-1.5616	-0.30009
	-B-	Max	2.1169	0.15231	29.322	0.18963	75.126	-0.43067
		Min	-1.934	0.1522	-2.8186	-1.421	-11.968	-0.43099
bmx231	-A-	Max	4.2078	0.082553	51.091	1.7962	91.701	0.18409
		Min	-3.2427	0.08235	-44.12	1.3505	-107.31	0.18361
	-B-	Max	3.2427	-0.08235	44.12	-1.3505	75.954	0.12961
		Min	-4.2078	-0.082553	-51.091	-1.7962	-86.829	0.12932
bmx233	-A-	Max	4.625	0.082579	56.387	-1.0016	80.612	0.18414
		Min	-2.8255	0.082376	-38.823	-1.4473	-118.4	0.18366
	-B-	Max	2.8255	-0.082376	38.823	1.4473	66.917	0.12966
		Min	-4.625	-0.082579	-56.387	1.0016	-95.867	0.12937
bmx223	-A-	Max	4.2078	0.082553	44.12	1.7962	86.829	0.12961
		Min	-3.2427	0.08235	-51.091	1.3505	-75.954	0.12932
	-B-	Max	3.2427	-0.08235	51.091	-1.3505	107.31	0.18409
		Min	-4.2078	-0.082553	-44.12	-1.7962	-91.701	0.18361
bmx221	-A-	Max	4.625	0.082579	38.823	-1.0016	95.867	0.12966
		Min	-2.8255	0.082376	-56.387	-1.4473	-66.917	0.12937
	-B-	Max	2.8255	-0.082376	56.387	1.4473	118.4	0.18414
		Min	-4.625	-0.082579	-38.823	1.0016	-80.612	0.18366
bmx643	-A-	Max	0.61432	0.0021755	12.52	3.3919	41.108	0.0090712
		Min	-7.3809	0.0020773	-15.219	1.7742	-16.887	0.0087681
	-B-	Max	7.3809	-0.0020773	15.219	-1.7742	44.121	0.0031121
		Min	-0.61432	-0.0021755	-12.52	-3.3919	-53.228	0.0028642
bmy411	-A-	Max	0.22146	0.012959	17.564	0.77312	50.124	0.025584
		Min	-2.0167	0.012819	-21.102	-0.44889	-37.229	0.025369

	-B-	Max	2.0167	-0.012819	21.102	0.44889	51.164	0.036621
		Min	-0.22146	-0.012959	-17.564	-0.77312	-47.078	0.036161
bmx411	-A-	Max	0.90561	-0.00020883	23.41	2.0373	72.481	-0.00016926
		Min	-4.7329	-0.00026482	-21.732	1.2092	-67.77	-0.00038402
	-B-	Max	4.7329	0.00026482	21.732	-1.2092	49.216	-0.0010001
		Min	-0.90561	0.00020883	-23.41	-2.0373	-63.324	-0.001099
bmx333	-A-	Max	6.6033	0.050421	90.611	-0.43393	118.27	0.11327
		Min	-4.4059	0.050127	-56.604	-1.151	-188.29	0.11261
	-B-	Max	4.4059	-0.050127	56.604	1.151	96.828	0.078324
		Min	-6.6033	-0.050421	-90.611	0.43393	-156.03	0.077868
bmx341	-A-	Max	1.232	-0.0015209	16.971	-0.80404	59.968	-0.0046179
		Min	-3.7766	-0.0015633	-22.497	-1.4716	-38.24	-0.0047078
	-B-	Max	3.7766	0.0015633	22.497	1.4716	66.017	-0.0038886
		Min	-1.232	0.0015209	-16.971	0.80404	-56.798	-0.0040572
bmx343	-A-	Max	0.95079	-0.0015183	19.378	1.6928	53.92	-0.0046134
		Min	-4.0578	-0.0015607	-20.09	1.0253	-44.288	-0.0047034
	-B-	Max	4.0578	0.0015607	20.09	-1.0253	58.586	-0.0038785
		Min	-0.95079	0.0015183	-19.378	-1.6928	-64.229	-0.004047
bmy351	-A-	Max	0.6125	0.037341	6.2211	0.89135	64.64	0.072373
		Min	-1.2167	0.037223	-27.549	-0.14754	-11.959	0.072195
	-B-	Max	1.2167	-0.037223	27.549	0.14754	67.593	0.10687
		Min	-0.6125	-0.037341	-6.2211	-0.89135	-17.902	0.10647
bmy352	-A-	Max	0.092357	0.037336	18.042	0.66335	41.987	0.10685
		Min	-1.7368	0.037217	-15.727	-0.37554	-43.508	0.10646
	-B-	Max	1.7368	-0.037217	15.727	0.37554	33.503	0.072363
		Min	-0.092357	-0.037336	-18.042	-0.66335	-43.096	0.072185
bmx621	-A-	Max	11.63	-0.20601	42.225	-0.33743	133.96	-0.32234
		Min	-6.782	-0.20621	-85.572	-1.9942	-63.581	-0.32274
	-B-	Max	6.782	0.20621	85.572	1.9942	191.21	-0.46051
		Min	-11.63	0.20601	-42.225	0.33743	-96.873	-0.46087
bmx323	-A-	Max	5.9622	0.050405	65.067	1.7135	141.54	0.078295
		Min	-5.0471	0.050111	-82.148	0.99646	-111.32	0.077839
	-B-	Max	5.0471	-0.050111	82.148	-0.99646	170.63	0.11324
		Min	-5.9622	-0.050405	-65.067	-1.7135	-135.93	0.11258
bmx331	-A-	Max	5.9622	0.050405	82.148	1.7135	135.93	0.11324
		Min	-5.0471	0.050111	-65.067	0.99646	-170.63	0.11258
	-B-	Max	5.0471	-0.050111	65.067	-0.99646	111.32	0.078295
		Min	-5.9622	-0.050405	-82.148	-1.7135	-141.54	0.077839
bmx421	-A-	Max	7.672	0.017714	60.605	-0.4007	179.05	0.02752
		Min	-4.9137	0.01737	-104.1	-1.319	-103.21	0.026971
	-B-	Max	4.9137	-0.01737	104.1	1.319	216.54	0.039792
		Min	-7.672	-0.017714	-60.605	0.4007	-127.09	0.039034
bmx413	-A-	Max	1.2315	-0.00020844	26.265	-0.96424	63.684	-0.00017025
		Min	-4.407	-0.00026443	-18.876	-1.7924	-76.567	-0.00038501
	-B-	Max	4.407	0.00026443	18.876	1.7924	42.022	-0.00099696
		Min	-1.2315	0.00020844	-26.265	0.96424	-70.519	-0.0010959
bmy412	-A-	Max	0.8608	0.012959	32.05	1.0436	19.239	0.036624
		Min	-1.3774	0.012819	-6.6153	-0.17842	-79.004	0.036164
	-B-	Max	1.3774	-0.012819	6.6153	0.17842	12.515	0.025582
		Min	-0.8608	-0.012959	-32.05	-1.0436	-74.838	0.025367
bmx623	-A-	Max	10.469	-0.2059	50.152	2.468	121.8	-0.32213
		Min	-7.9434	-0.2061	-77.645	0.81127	-75.743	-0.32253
	-B-	Max	7.9434	0.2061	77.645	-0.81127	173.25	-0.46029
		Min	-10.469	0.2059	-50.152	-2.468	-114.83	-0.46065
bmx532	-A-	Max	-0.80154	0.0047603	30.272	0.27529	74.763	0.0095125
		Min	-0.84472	0.003973	-25.944	0.19421	-82.627	0.0073231
	-B-	Max	0.84472	-0.003973	25.944	-0.19421	70.523	0.017145
		Min	0.80154	-0.0047603	-30.272	-0.27529	-86.899	0.014926
bmx222	-A-	Max	-0.072447	0.00067462	14.213	0.15329	43.077	0.0023581
		Min	-0.34084	0.00037565	-15.311	0.077101	-38.938	0.0015147
	-B-	Max	0.34084	-0.00037565	15.311	-0.077101	42.666	0.0014198

		Min	0.072447	-0.00067462	-14.213	-0.15329	-40.656	0.00058879
bmx422	-A-	Max	-0.46132	0.000067476	24.657	0.29469	80.518	0.000013389
		Min	-0.92198	-0.00044487	-28.318	0.13821	-66.692	-0.0013992
	-B-	Max	0.92198	0.00044487	28.318	-0.13821	78.061	0.00036449
		Min	0.46132	-0.000067476	-24.657	-0.29469	-71.387	-0.0010921
bmx522	-A-	Max	-0.80154	0.0047603	25.944	0.27529	86.899	0.017145
		Min	-0.84472	0.003973	-30.272	0.19421	-70.523	0.014926
	-B-	Max	0.84472	-0.003973	30.272	-0.19421	82.627	0.0095125
		Min	0.80154	-0.0047603	-25.944	-0.27529	-74.763	0.0073231
bmx332	-A-	Max	-0.36602	-0.0010565	24.769	0.24275	63.131	-0.001844
		Min	-0.69596	-0.0015028	-21.914	0.12916	-68.38	-0.0031004
	-B-	Max	0.69596	0.0015028	21.914	-0.12916	59.588	-0.0040722
		Min	0.36602	0.0010565	-24.769	-0.24275	-70.324	-0.0053153
bmx622	-A-	Max	-0.35623	0.0014418	12.851	0.32402	54.464	0.0051017
		Min	-1.9487	0.0011309	-19.111	-0.05401	-30.959	0.0042859
	-B-	Max	1.9487	-0.0011309	19.111	0.05401	52.559	0.0029746
		Min	0.35623	-0.0014418	-12.851	-0.32402	-41.008	0.0020446
bmx322	-A-	Max	-0.36602	-0.0010565	21.914	0.24275	70.324	-0.0040722
		Min	-0.69596	-0.0015028	-24.769	0.12916	-59.588	-0.0053153
	-B-	Max	0.69596	0.0015028	24.769	-0.12916	68.38	-0.001844
		Min	0.36602	0.0010565	-21.914	-0.24275	-63.131	-0.0031004
bmx632	-A-	Max	-0.35623	0.0014418	19.111	0.32402	41.008	0.0029746
		Min	-1.9487	0.0011309	-12.851	-0.05401	-52.559	0.0020446
	-B-	Max	1.9487	-0.0011309	12.851	0.05401	30.959	0.0051017
		Min	0.35623	-0.0014418	-19.111	-0.32402	-54.464	0.0042859
bmx432	-A-	Max	-0.46132	0.000067476	28.318	0.29469	71.387	0.00036449
		Min	-0.92198	-0.00044487	-24.657	0.13821	-78.061	-0.0010921
	-B-	Max	0.92198	0.00044487	24.657	-0.13821	66.692	0.000013389
		Min	0.46132	-0.000067476	-28.318	-0.29469	-80.518	-0.0013992
bmx232	-A-	Max	-0.072447	0.00067462	15.311	0.15329	40.656	0.0014198
		Min	-0.34084	0.00037565	-14.213	0.077101	-42.666	0.00058879
	-B-	Max	0.34084	-0.00037565	14.213	-0.077101	38.938	0.0023581
		Min	0.072447	-0.00067462	-15.311	-0.15329	-43.077	0.0015147
bmy542	-A-	Max	-1.0604	0.0032097	5.6576	-0.14502	47.055	0.0089781
		Min	-1.9227	0.0029963	-13.225	-1.6398	-13.652	0.0083127
	-B-	Max	1.9227	-0.0029963	13.225	1.6398	40.23	0.012206
		Min	1.0604	-0.0032097	-5.6576	0.14502	-23.688	0.011463
bmy631	-A-	Max	-1.1772	-0.095176	13.048	3.5257	2.636	-0.41295
		Min	-2.9761	-0.095569	1.7608	-2.8909	-39.705	-0.41419
	-B-	Max	2.9761	0.095569	-1.7608	2.8909	-14.257	-0.21521
		Min	1.1772	0.095176	-13.048	-3.5257	-46.414	-0.21657
bmy642	-A-	Max	-2.3128	0.0055985	6.7602	-0.31809	28.95	0.01338
		Min	-3.573	0.0053934	-6.4299	-3.2464	-13.354	0.012575
	-B-	Max	3.573	-0.0053934	6.4299	3.2464	13.487	0.023591
		Min	2.3128	-0.0055985	-6.7602	0.31809	-31.264	0.023001
bmy632	-A-	Max	-1.1772	-0.095176	-1.7608	3.5257	46.414	-0.21521
		Min	-2.9761	-0.095569	-13.048	-2.8909	14.257	-0.21657
	-B-	Max	2.9761	0.095569	13.048	2.8909	39.705	-0.41295
		Min	1.1772	0.095176	1.7608	-3.5257	-2.636	-0.41419
bmx612	-A-	Max	1.6593	-0.16989	32.1	1.8495	41.032	-0.62438
		Min	-4.4506	-0.17014	-10.154	-0.79451	-94.541	-0.62499
	-B-	Max	4.4506	0.17014	10.154	0.79451	15.828	-0.32701
		Min	-1.6593	0.16989	-32.1	-1.8495	-85.22	-0.32779
bmx642	-A-	Max	1.6593	-0.16989	10.154	1.8495	85.22	-0.32701
		Min	-4.4506	-0.17014	-32.1	-0.79451	-15.828	-0.32779
	-B-	Max	4.4506	0.17014	32.1	0.79451	94.541	-0.62438
		Min	-1.6593	0.16989	-10.154	-1.8495	-41.032	-0.62499
bmy622	-A-	Max	-2.4183	0.0054689	8.3455	3.2189	24.018	0.012965
		Min	-3.6785	0.0052638	-4.8446	0.29056	-18.286	0.01216
	-B-	Max	3.6785	-0.0052638	4.8446	-0.29056	7.9564	0.02315
		Min	2.4183	-0.0054689	-8.3455	-3.2189	-36.794	0.02256

bmy641	-A-	Max	-2.4183	0.0054688	4.8446	3.2189	36.794	0.02315
		Min	-3.6785	0.0052638	-8.3455	0.29056	-7.9564	0.022561
	-B-	Max	3.6785	-0.0052638	8.3455	-0.29056	18.286	0.012965
		Min	2.4183	-0.0054688	-4.8446	-3.2189	-24.018	0.01216
bmy621	-A-	Max	-2.3128	0.0055985	6.4299	-0.31809	31.264	0.023591
		Min	-3.573	0.0053934	-6.7602	-3.2464	-13.487	0.023001
	-B-	Max	3.573	-0.0053934	6.7602	3.2464	13.354	0.01338
		Min	2.3128	-0.0055985	-6.4299	0.31809	-28.95	0.012575
bmx542	-A-	Max	1.8787	-0.018072	15.766	1.2411	122.51	-0.032437
		Min	-2.5428	-0.018832	-45.648	-0.3352	-36.98	-0.034771
	-B-	Max	2.5428	0.018832	45.648	0.3352	133.12	-0.068764
		Min	-1.8787	0.018072	-15.766	-1.2411	-51.311	-0.070689
bmy322	-A-	Max	-1.2937	-0.0019668	8.1748	1.6681	24.972	-0.0048675
		Min	-2.0271	-0.0021036	-6.3534	0.053181	-21.586	-0.0052877
	-B-	Max	2.0271	0.0021036	6.3534	-0.053181	16.961	-0.0081126
		Min	1.2937	0.0019668	-8.1748	-1.6681	-32.367	-0.0085965
bmy321	-A-	Max	-1.2069	-0.0019777	8.2278	0.12299	25.937	-0.0081492
		Min	-1.9403	-0.0021145	-6.3005	-1.492	-23.392	-0.0086331
	-B-	Max	1.9403	0.0021145	6.3005	1.492	15.646	-0.0049029
		Min	1.2069	0.0019777	-8.2278	-0.12299	-30.912	-0.0053231
bmx312	-A-	Max	1.4614	0.042749	34.52	1.1321	55.886	0.15723
		Min	-2.6558	0.042337	-17.279	-0.36083	-100.78	0.15621
	-B-	Max	2.6558	-0.042337	17.279	0.36083	40.875	0.082168
		Min	-1.4614	-0.042749	-34.52	-1.1321	-92.53	0.080882
bmy331	-A-	Max	-0.39503	0.023903	12.181	2.4304	7.2791	0.10322
		Min	-1.4367	0.023139	-0.97326	-1.892	-39.082	0.10085
	-B-	Max	1.4367	-0.023139	0.97326	1.892	-0.85562	0.054538
		Min	0.39503	-0.023903	-12.181	-2.4304	-41.311	0.051874
bmx342	-A-	Max	1.4614	0.042749	17.279	1.1321	92.53	0.082168
		Min	-2.6558	0.042337	-34.52	-0.36083	-40.875	0.080882
	-B-	Max	2.6558	-0.042337	34.52	0.36083	100.78	0.15723
		Min	-1.4614	-0.042749	-17.279	-1.1321	-55.886	0.15621
bmy341	-A-	Max	-1.2937	-0.0019668	6.3534	1.6681	32.367	-0.0081126
		Min	-2.0271	-0.0021036	-8.1748	0.053181	-16.961	-0.0085965
	-B-	Max	2.0271	0.0021036	8.1748	-0.053181	21.586	-0.0048675
		Min	1.2937	0.0019668	-6.3534	-1.6681	-24.972	-0.0052877
bmy332	-A-	Max	-0.39503	0.023903	0.97326	2.4304	41.311	0.054538
		Min	-1.4367	0.023139	-12.181	-1.892	0.85562	0.051874
	-B-	Max	1.4367	-0.023139	12.181	1.892	39.082	0.10322
		Min	0.39503	-0.023903	-0.97326	-2.4304	-7.2791	0.10085
bmy242	-A-	Max	-1.7367	-0.001537	6.8238	0.095237	11.962	-0.0032678
		Min	-2.2027	-0.0016111	-2.0794	-1.0279	-16.485	-0.0034855
	-B-	Max	2.2027	0.0016111	2.0794	1.0279	1.7622	-0.0068744
		Min	1.7367	0.001537	-6.8238	-0.095237	-28.551	-0.00715
bmy222	-A-	Max	-1.7908	-0.0015071	7.9762	1.1312	8.3116	-0.0031763
		Min	-2.2568	-0.0015812	-0.92696	0.0080668	-20.136	-0.003394
	-B-	Max	2.2568	0.0015812	0.92696	-0.0080668	-2.1937	-0.0067684
		Min	1.7908	0.0015071	-7.9762	-1.1312	-32.507	-0.007044
bmy221	-A-	Max	-1.7367	-0.001537	2.0794	0.095237	28.551	-0.0068744
		Min	-2.2027	-0.0016111	-6.8238	-1.0279	-1.7622	-0.00715
	-B-	Max	2.2027	0.0016111	6.8238	1.0279	16.485	-0.0032678
		Min	1.7367	0.001537	-2.0794	-0.095237	-11.962	-0.0034855
bmx212	-A-	Max	0.39324	0.066822	19.78	0.73205	43.682	0.24489
		Min	-2.3288	0.066537	-13.253	-0.24616	-56.495	0.24417
	-B-	Max	2.3288	-0.066537	13.253	0.24616	30.532	0.12932
		Min	-0.39324	-0.066822	-19.78	-0.73205	-54.271	0.12843
bmy231	-A-	Max	-0.74505	0.038199	5.7186	1.5963	12.339	0.16532
		Min	-1.4219	0.037617	-2.5217	-1.2588	-16.774	0.16351
	-B-	Max	1.4219	-0.037617	2.5217	1.2588	4.3045	0.086793
		Min	0.74505	-0.038199	-5.7186	-1.5963	-20.969	0.084762
bmx242	-A-	Max	0.39324	0.066822	13.253	0.73205	54.271	0.12932

		Min	-2.3288	0.066537	-19.78	-0.24616	-30.532	0.12843
	-B-	Max	2.3288	-0.066537	19.78	0.24616	56.495	0.24489
		Min	-0.39324	-0.066822	-13.253	-0.73205	-43.682	0.24417
bmy241	-A-	Max	-1.7908	-0.0015071	0.92696	1.1312	32.507	-0.0067684
		Min	-2.2568	-0.0015812	-7.9762	0.0080668	2.1937	-0.007044
	-B-	Max	2.2568	0.0015812	7.9762	-0.0080668	20.136	-0.0031763
		Min	1.7908	0.0015071	-0.92696	-1.1312	-8.3116	-0.003394
bmy232	-A-	Max	-0.74505	0.038199	2.5217	1.5963	20.969	0.086793
		Min	-1.4219	0.037617	-5.7186	-1.2588	-4.3045	0.084762
	-B-	Max	1.4219	-0.037617	5.7186	1.2588	16.774	0.16532
		Min	0.74505	-0.038199	-2.5217	-1.5963	-12.339	0.16351
bmy521	-A-	Max	-1.0604	0.0032097	13.225	-0.14502	23.688	0.012206
		Min	-1.9227	0.0029963	-5.6576	-1.6398	-40.23	0.011463
	-B-	Max	1.9227	-0.0029963	5.6576	1.6398	13.652	0.0089781
		Min	1.0604	-0.0032097	-13.225	0.14502	-47.055	0.0083126
bmx512	-A-	Max	1.8787	-0.018072	45.648	1.2411	51.311	-0.068764
		Min	-2.5428	-0.018832	-15.766	-0.3352	-133.12	-0.070689
	-B-	Max	2.5428	0.018832	15.766	0.3352	36.98	-0.032437
		Min	-1.8787	0.018072	-45.648	-1.2411	-122.51	-0.034771
bmy442	-A-	Max	-1.3973	-0.0005808	6.6688	0.019484	38.752	-0.0013088
		Min	-2.2512	-0.00075492	-10.391	-1.8184	-16.144	-0.0018531
	-B-	Max	2.2512	0.00075492	10.391	1.8184	29.832	-0.0025243
		Min	1.3973	0.0005808	-6.6688	-0.019484	-27.87	-0.0031295
bmy522	-A-	Max	-1.1727	0.0032446	8.068	1.8952	39.419	0.0090762
		Min	-2.0351	0.0030312	-10.815	0.40043	-21.288	0.0084107
	-B-	Max	2.0351	-0.0030312	10.815	-0.40043	31.958	0.012339
		Min	1.1727	-0.0032446	-8.068	-1.8952	-31.96	0.011595
bmy541	-A-	Max	-1.1727	0.0032446	10.815	1.8952	31.96	0.012338
		Min	-2.0351	0.0030312	-8.068	0.40043	-31.958	0.011595
	-B-	Max	2.0351	-0.0030312	8.068	-0.40043	21.288	0.0090762
		Min	1.1727	-0.0032446	-10.815	-1.8952	-39.419	0.0084108
bmy532	-A-	Max	-0.2837	-0.0077712	-1.9482	2.6533	60.824	-0.016834
		Min	-1.3983	-0.0091199	-18.193	-2.007	10.384	-0.021502
	-B-	Max	1.3983	0.0091199	18.193	2.007	59.251	-0.034456
		Min	0.2837	0.0077712	1.9482	-2.6533	2.4737	-0.038689
bmy531	-A-	Max	-0.2837	-0.0077712	18.193	2.6533	-2.4737	-0.034456
		Min	-1.3983	-0.0091199	1.9482	-2.007	-59.251	-0.038689
	-B-	Max	1.3983	0.0091199	-1.9482	2.007	-10.384	-0.016834
		Min	0.2837	0.0077712	-18.193	-2.6533	-60.824	-0.021502
bmx442	-A-	Max	1.6515	0.014561	17.463	1.3205	110.14	0.028311
		Min	-3.0145	0.014103	-40.998	-0.41538	-40.381	0.02687
	-B-	Max	3.0145	-0.014103	40.998	0.41538	119.45	0.053229
		Min	-1.6515	-0.014561	-17.463	-1.3205	-57.413	0.052105
bmy421	-A-	Max	-1.3973	-0.00058081	10.391	0.019484	27.87	-0.0025243
		Min	-2.2512	-0.0007549	-6.6688	-1.8184	-29.832	-0.0031295
	-B-	Max	2.2512	0.0007549	6.6688	1.8184	16.144	-0.0013089
		Min	1.3973	0.00058081	-10.391	-0.019484	-38.752	-0.0018531
bmx412	-A-	Max	1.6515	0.014561	40.998	1.3205	57.413	0.053229
		Min	-3.0145	0.014103	-17.463	-0.41538	-119.45	0.052105
	-B-	Max	3.0145	-0.014103	17.463	0.41538	40.381	0.028311
		Min	-1.6515	-0.014561	-40.998	-1.3205	-110.14	0.02687
bmy342	-A-	Max	-1.2069	-0.0019777	6.3005	0.12299	30.912	-0.0049029
		Min	-1.9403	-0.0021145	-8.2278	-1.492	-15.646	-0.0053231
	-B-	Max	1.9403	0.0021145	8.2278	1.492	23.392	-0.0081492
		Min	1.2069	0.0019777	-6.3005	-0.12299	-25.937	-0.0086331
bmy422	-A-	Max	-1.4917	-0.0005812	8.854	2.02	31.808	-0.0013101
		Min	-2.3456	-0.00075529	-8.2063	0.18208	-23.088	-0.0018543
	-B-	Max	2.3456	0.00075529	8.2063	-0.18208	22.354	-0.0025256
		Min	1.4917	0.0005812	-8.854	-2.02	-35.348	-0.0031308
bmy441	-A-	Max	-1.4917	-0.00058118	8.2063	2.02	35.348	-0.0025256
		Min	-2.3456	-0.00075531	-8.854	0.18208	-22.354	-0.0031308

	-B-	Max	2.3456	0.00075531	8.854	-0.18208	23.088	-0.00131
		Min	1.4917	0.00058118	-8.2063	-2.02	-31.808	-0.0018544
bmy432	-A-	Max	-0.49348	0.0086017	-0.14776	2.7633	51.747	0.019943
		Min	-1.7047	0.0077538	-15.259	-2.133	5.3149	0.016986
	-B-	Max	1.7047	-0.0077538	15.259	2.133	48.961	0.036829
		Min	0.49348	-0.0086017	0.14776	-2.7633	-4.3397	0.034189
bmy431	-A-	Max	-0.49348	0.0086017	15.259	2.7633	4.3397	0.036829
		Min	-1.7047	0.0077538	0.14776	-2.133	-48.961	0.034189
	-B-	Max	1.7047	-0.0077538	-0.14776	2.133	-5.3149	0.019943
		Min	0.49348	-0.0086017	-15.259	-2.7633	-51.747	0.016986

INTERNAL FORCES FOR STRUCTURAL ANALYSIS IN Y DIRECTION								
Elm.Name	**End**		**F**	**V2**	**V3**	**Mt**	**M2**	**M3**
col252	-A-	Max	924.95	-32.703	1041.6	-2.1719	7069.6	-44.916
		Min	856.66	-50.186	-1298.9	-2.1722	-5591.4	-81.668
	-B-	Max	-856.66	50.186	1298.9	2.1722	2623	-53.137
		Min	-924.95	32.703	-1041.6	2.1719	-3329.4	-68.947
col231	-A-	Max	1057.2	-16.852	265.55	-2.1799	2129.3	-6.3928
		Min	845.54	-74.521	-422.79	-2.18	-1257	-134.44
	-B-	Max	-845.54	74.521	422.79	2.18	509.2	-43.897
		Min	-1057.2	16.852	-265.55	2.1799	-909.85	-89.389
col212	-A-	Max	924.95	50.186	1298.9	-2.1719	5591.4	81.668
		Min	856.66	32.703	-1041.6	-2.1722	-7069.6	44.916
	-B-	Max	-856.66	-32.703	1041.6	2.1722	3329.4	68.947
		Min	-924.95	-50.186	-1298.9	2.1719	-2623	53.137
col552	-A-	Max	192.7	-50.803	173.08	-2.8409	490.86	-66.314
		Min	178.98	-76.142	-212.8	-2.842	-488.29	-98.225
	-B-	Max	-178.98	76.142	212.8	2.842	539.74	-86.089
		Min	-192.7	50.803	-173.08	2.8409	-423.15	-130.21
col152	-A-	Max	1153	-16.975	1209.1	-1.0503	11121	-5.1063
		Min	1074.5	-26.72	-1494.2	-1.0509	-8859.8	-38.589
	-B-	Max	-1074.5	26.72	1494.2	1.0509	5315.6	-41.434
		Min	-1153	16.975	-1209.1	1.0503	-6721.3	-45.957
col512	-A-	Max	192.7	76.142	212.8	-2.8409	488.29	98.225
		Min	178.98	50.803	-173.08	-2.842	-490.86	66.314
	-B-	Max	-178.98	-50.803	173.08	2.842	423.15	130.21
		Min	-192.7	-76.142	-212.8	2.8409	-539.74	86.089
col352	-A-	Max	687.04	-32.822	828.83	-2.8766	3867.2	-45.254
		Min	635.04	-53.706	-1042.9	-2.877	-3044.8	-80.468
	-B-	Max	-635.04	53.706	1042.9	2.877	894.98	-53.156
		Min	-687.04	32.822	-828.83	2.8766	-1075.1	-80.705
col312	-A-	Max	687.04	53.706	1042.9	-2.8766	3044.8	80.468
		Min	635.04	32.822	-828.83	-2.877	-3867.2	45.254
	-B-	Max	-635.04	-32.822	828.83	2.877	1075.1	80.705
		Min	-687.04	-53.706	-1042.9	2.8766	-894.98	53.156
col531	-A-	Max	222.41	-22.303	35.599	-2.9066	165.76	-30.005
		Min	178.64	-111.5	-72.159	-2.9068	-147.17	-142.15
	-B-	Max	-178.64	111.5	72.159	2.9068	208.39	-36.882
		Min	-222.41	22.303	-35.599	2.9066	-117.29	-192.37
col533	-A-	Max	222.41	111.5	72.159	-2.9066	147.17	142.15
		Min	178.64	22.303	-35.599	-2.9068	-165.76	30.005
	-B-	Max	-178.64	-22.303	35.599	2.9068	117.29	192.37
		Min	-222.41	-111.5	-72.159	2.9066	-208.39	36.882
col412	-A-	Max	442.18	52.104	734.35	-3.1176	1253	81.122
		Min	408.75	32.825	-583.27	-3.1183	-1567	51.14
	-B-	Max	-408.75	-32.825	583.27	3.1183	804.5	75.228
		Min	-442.18	-52.104	-734.35	3.1176	-943.76	47.296
col452	-A-	Max	442.18	-32.825	583.27	-3.1176	1567	-51.14
		Min	408.75	-52.104	-734.35	-3.1183	-1253	-81.122
	-B-	Max	-408.75	52.104	734.35	3.1183	943.76	-47.296
		Min	-442.18	32.825	-583.27	3.1176	-804.5	-75.228
col333	-A-	Max	792.62	81.217	339.48	-2.8926	636.45	128.36
		Min	629.66	11.009	-204.96	-2.8927	-1130	5.7826
	-B-	Max	-629.66	-11.009	204.96	2.8927	269.82	115.51
		Min	-792.62	-81.217	-339.48	2.8926	-179.76	27.027
col131	-A-	Max	1295.1	-8.7405	319.81	-1.0203	3428.4	34.651
		Min	1053.5	-40.721	-489.04	-1.0204	-2106.6	-84.112
	-B-	Max	-1053.5	40.721	489.04	1.0204	1169.6	-37.663
		Min	-1295.1	8.7405	-319.81	1.0203	-1983.8	-61.259
col431	-A-	Max	513.64	-11.663	137.64	-3.1421	437.33	-17.251

		Min	407.65	-77.004	-234.87	-3.1422	-239.68	-121.73
	-B-	Max	-407.65	77.004	234.87	3.1422	360.99	-17.597
		Min	-513.64	11.663	-137.64	3.1421	-266.94	-109.42
col112	-A-	Max	1153	26.72	1494.2	-1.0503	8859.8	38.589
		Min	1074.5	16.975	-1209.1	-1.0509	-11121	5.1063
	-B-	Max	-1074.5	-16.975	1209.1	1.0509	6721.3	45.957
		Min	-1153	-26.72	-1494.2	1.0503	-5315.6	41.434
col433	-A-	Max	513.64	77.004	234.87	-3.1421	239.68	121.73
		Min	407.65	11.663	-137.64	-3.1422	-437.33	17.251
	-B-	Max	-407.65	-11.663	137.64	3.1422	266.94	109.42
		Min	-513.64	-77.004	-234.87	3.1421	-360.99	17.597
col133	-A-	Max	1295.1	40.721	489.04	-1.0203	2106.6	84.112
		Min	1053.5	8.7405	-319.81	-1.0204	-3428.4	-34.651
	-B-	Max	-1053.5	-8.7405	319.81	1.0204	1983.8	61.259
		Min	-1295.1	-40.721	-489.04	1.0203	-1169.6	37.663
col233	-A-	Max	1057.2	74.521	422.79	-2.1799	1257	134.44
		Min	845.54	16.852	-265.55	-2.18	-2129.3	6.3928
	-B-	Max	-845.54	-16.852	265.55	2.18	909.85	89.389
		Min	-1057.2	-74.521	-422.79	2.1799	-509.2	43.897
col331	-A-	Max	792.62	-11.009	204.96	-2.8926	1130	-5.7826
		Min	629.66	-81.217	-339.48	-2.8927	-636.45	-128.36
	-B-	Max	-629.66	81.217	339.48	2.8927	179.76	-27.027
		Min	-792.62	11.009	-204.96	2.8926	-269.82	-115.51
col511	-A-	Max	138.88	51.895	32.064	-0.43546	-10.878	57.177
		Min	31.988	-86.233	9.909	-0.43555	-36.306	-97.219
	-B-	Max	-31.988	86.233	-9.909	0.43555	-14.389	75.155
		Min	-138.88	-51.895	-32.064	0.43546	-45.457	-122.68
col353	-A-	Max	519.75	66.029	-6.6138	-0.40599	29.939	85.889
		Min	138.19	-36.403	-23.696	-0.40602	7.1886	-47.819
	-B-	Max	-138.19	36.403	23.696	0.40602	30.497	82.498
		Min	-519.75	-66.029	6.6138	0.40599	9.667	-45.021
col242	-A-	Max	1395.5	42.617	7.8913	-0.30664	23.071	59.288
		Min	1395.2	-37.807	-17.893	-0.30665	-11.912	-52.623
	-B-	Max	-1395.2	37.807	17.893	0.30665	22.558	49.391
		Min	-1395.5	-42.617	-7.8913	0.30664	-8.2118	-43.791
col243	-A-	Max	845.4	61.92	31.69	-0.30671	7.155	86.687
		Min	549.82	15.62	-5.1017	-0.30672	-41.051	15.69
	-B-	Max	-549.82	-15.62	5.1017	0.30672	5.8547	71.23
		Min	-845.4	-61.92	-31.69	0.30671	-39.759	24.12
col253	-A-	Max	699.77	55.449	-9.2288	-0.30539	30.464	77.058
		Min	200.77	-24.095	-22.536	-0.30541	10.583	-34.18
	-B-	Max	-200.77	24.095	22.536	0.30541	27.009	64.345
		Min	-699.77	-55.449	9.2288	0.30539	12.944	-27.269
col251	-A-	Max	658.5	33.425	-12.595	-0.30539	35.544	47.225
		Min	159.5	-46.119	-25.903	-0.30542	15.663	-64.013
	-B-	Max	-159.5	46.119	25.903	0.30542	30.514	38.016
		Min	-658.5	-33.425	12.595	0.30539	16.449	-53.598
col411	-A-	Max	331.66	34.638	22.93	-0.44313	-7.9833	46.373
		Min	83.608	-62.355	5.7824	-0.44318	-30.19	-83.017
	-B-	Max	-83.608	62.355	-5.7824	0.44318	-6.7566	41.962
		Min	-331.66	-34.638	-22.93	0.44313	-28.287	-75.995
col311	-A-	Max	519.75	36.403	23.696	-0.40599	-7.1886	47.819
		Min	138.19	-66.029	6.6138	-0.40602	-29.939	-85.889
	-B-	Max	-138.19	66.029	-6.6138	0.40602	-9.667	45.021
		Min	-519.75	-36.403	-23.696	0.40599	-30.497	-82.498
col453	-A-	Max	331.66	62.355	-5.7824	-0.44313	30.19	83.017
		Min	83.608	-34.638	-22.93	-0.44318	7.9833	-46.373
	-B-	Max	-83.608	34.638	22.93	0.44318	28.287	75.995
		Min	-331.66	-62.355	5.7824	0.44313	6.7566	-41.962

col553	-A-	Max	138.88	86.233	-9.909	-0.43546	36.306	97.219
		Min	31.988	-51.895	-32.064	-0.43555	10.878	-57.177
	-B-	Max	-31.988	51.895	32.064	0.43555	45.457	122.68
		Min	-138.88	-86.233	9.909	0.43546	14.389	-75.155
col332	-A-	Max	1033.5	54.732	15.446	-0.40546	20.108	71.523
		Min	1033.5	-54.732	-15.446	-0.40546	-20.108	-71.523
	-B-	Max	-1033.5	54.732	15.446	0.40546	19.281	68.056
		Min	-1033.5	-54.732	-15.446	0.40546	-19.281	-68.056
col442	-A-	Max	649.93	55.123	5.9452	-0.44078	33.77	71.607
		Min	649.53	-48.618	-26.517	-0.44079	-8.1854	-63.175
	-B-	Max	-649.53	48.618	26.517	0.44079	33.85	68.961
		Min	-649.93	-55.123	-5.9452	0.44078	-6.9759	-60.806
col343	-A-	Max	617.94	67.516	39.99	-0.40597	9.3748	87.575
		Min	393.57	8.3767	-6.9107	-0.40598	-50.707	7.5563
	-B-	Max	-393.57	-8.3767	6.9107	0.40598	8.2486	84.621
		Min	-617.94	-67.516	-39.99	0.40597	-51.268	13.774
col341	-A-	Max	636.43	-4.6113	28.367	-0.40597	24.325	-2.4872
		Min	412.06	-63.751	-18.534	-0.40597	-35.756	-82.506
	-B-	Max	-412.06	63.751	18.534	0.40597	22.936	-9.2415
		Min	-636.43	4.6113	-28.367	0.40597	-36.581	-80.088
col342	-A-	Max	1020.1	54.353	7.9008	-0.40554	31.212	71.355
		Min	1019.9	-48.091	-24.501	-0.40554	-10.838	-63.142
	-B-	Max	-1019.9	48.091	24.501	0.40554	31.267	67.258
		Min	-1020.1	-54.353	-7.9008	0.40554	-9.3119	-59.505
col441	-A-	Max	402.56	-5.0124	29.029	-0.44173	23.545	-5.9663
		Min	258.42	-61.993	-18.186	-0.44174	-37.581	-81.668
	-B-	Max	-258.42	61.993	18.186	0.44174	22.829	-6.7984
		Min	-402.56	5.0124	-29.029	0.44173	-36.442	-76.431
col443	-A-	Max	390.39	65.647	40.984	-0.44172	8.0232	86.555
		Min	246.25	8.6667	-6.2306	-0.44173	-53.103	10.853
	-B-	Max	-246.25	-8.6667	6.2306	0.44173	7.8652	80.862
		Min	-390.39	-65.647	-40.984	0.44172	-51.406	11.23
col351	-A-	Max	487.94	48.617	-11.046	-0.40599	35.914	63.775
		Min	106.38	-53.815	-28.129	-0.40602	13.164	-69.934
	-B-	Max	-106.38	53.815	28.129	0.40602	35.824	60.212
		Min	-487.94	-48.617	11.046	0.40599	14.994	-67.307
col321	-A-	Max	617.94	-8.3767	6.9107	-0.40597	50.707	-7.5563
		Min	393.57	-67.516	-39.99	-0.40598	-9.3748	-87.575
	-B-	Max	-393.57	67.516	39.99	0.40598	51.268	-13.774
		Min	-617.94	8.3767	-6.9107	0.40597	-8.2486	-84.621
col313	-A-	Max	487.94	53.815	28.129	-0.40599	-13.164	69.934
		Min	106.38	-48.617	11.046	-0.40602	-35.914	-63.775
	-B-	Max	-106.38	48.617	-11.046	0.40602	-14.994	67.307
		Min	-487.94	-53.815	-28.129	0.40599	-35.824	-60.212
col451	-A-	Max	310.64	46.341	-10.31	-0.44313	36.135	62.008
		Min	62.593	-50.653	-27.458	-0.44317	13.928	-67.381
	-B-	Max	-62.593	50.653	27.458	0.44317	33.888	56.168
		Min	-310.64	-46.341	10.31	0.44313	12.357	-61.789
col323	-A-	Max	636.43	63.751	18.534	-0.40597	35.756	82.506
		Min	412.06	4.6113	-28.367	-0.40597	-24.325	2.4872
	-B-	Max	-412.06	-4.6113	28.367	0.40597	36.581	80.088
		Min	-636.43	-63.751	-18.534	0.40597	-22.936	9.2415
col322	-A-	Max	1020.1	48.091	24.501	-0.40554	10.838	63.142
		Min	1019.9	-54.353	-7.9008	-0.40554	-31.212	-71.355
	-B-	Max	-1019.9	54.353	7.9008	0.40554	9.3119	59.505
		Min	-1020.1	-48.091	-24.501	0.40554	-31.267	-67.258
col432	-A-	Max	659.82	54.959	15.797	-0.44043	20.262	71.683
		Min	659.82	-54.959	-15.797	-0.44043	-20.262	-71.683
	-B-	Max	-659.82	54.959	15.797	0.44043	20.021	68.468

		Min	-659.82	-54.959	-15.797	0.44043	-20.021	-68.468
col211	-A-	Max	699.77	24.095	22.536	-0.30539	-10.583	34.18
		Min	200.77	-55.449	9.2288	-0.30541	-30.464	-77.058
	-B-	Max	-200.77	55.449	-9.2288	0.30541	-12.944	27.269
		Min	-699.77	-24.095	-22.536	0.30539	-27.009	-64.345
col542	-A-	Max	287.11	68.552	6.0562	-0.43857	39.376	80.649
		Min	286.03	-60.411	-32.934	-0.43859	-6.7397	-71.02
	-B-	Max	-286.03	60.411	32.934	0.43859	44.606	94.158
		Min	-287.11	-68.552	-6.0562	0.43857	-8.7038	-83.029
col151	-A-	Max	808.07	13.353	-7.2838	-0.12491	17.296	27.987
		Min	234.8	-22.654	-13.669	-0.12496	3.7317	-33.252
	-B-	Max	-234.8	22.654	13.669	0.12496	17.574	6.0703
		Min	-808.07	-13.353	7.2838	0.12491	14.828	-24.525
col153	-A-	Max	855.32	26.79	-5.7439	-0.12491	14.007	40.265
		Min	282.05	-9.2171	-12.129	-0.12496	0.44279	-20.974
	-B-	Max	-282.05	9.2171	12.129	0.12496	16.936	28.057
		Min	-855.32	-26.79	5.7439	0.12491	14.19	-2.5382
col421	-A-	Max	390.39	-8.6667	6.2306	-0.44172	53.103	-10.853
		Min	246.25	-65.647	-40.984	-0.44173	-8.0232	-86.555
	-B-	Max	-246.25	65.647	40.984	0.44173	51.406	-11.23
		Min	-390.39	8.6667	-6.2306	0.44172	-7.8652	-80.862
col543	-A-	Max	164.06	88.078	53.575	-0.44008	6.8037	100.77
		Min	103.34	11.084	-5.4243	-0.4401	-62.562	14.004
	-B-	Max	-103.34	-11.084	5.4243	0.4401	7.0284	123.83
		Min	-164.06	-88.078	-53.575	0.44008	-74.054	14.257
col541	-A-	Max	170.03	-5.9503	38.408	-0.44007	24.679	-8.2417
		Min	109.32	-82.944	-20.592	-0.44009	-44.687	-95.01
	-B-	Max	-109.32	82.944	20.592	0.44009	27.831	-6.9293
		Min	-170.03	5.9503	-38.408	0.44007	-53.252	-116.5
col213	-A-	Max	658.5	46.119	25.903	-0.30539	-15.663	64.013
		Min	159.5	-33.425	12.595	-0.30542	-35.544	-47.225
	-B-	Max	-159.5	33.425	-12.595	0.30542	-16.449	53.598
		Min	-658.5	-46.119	-25.903	0.30539	-30.514	-38.016
col143	-A-	Max	1066.6	32.459	13.976	-0.12329	4.6804	44.635
		Min	725.42	10.114	-1.9213	-0.1233	-17.577	-4.1163
	-B-	Max	-725.42	-10.114	1.9213	0.1233	0.21935	38.19
		Min	-1066.6	-32.459	-13.976	0.12329	-18.062	29.853
col121	-A-	Max	1066.6	-10.114	1.9213	-0.12329	17.577	4.1163
		Min	725.42	-32.459	-13.976	-0.1233	-4.6804	-44.635
	-B-	Max	-725.42	32.459	13.976	0.1233	18.062	-29.853
		Min	-1066.6	10.114	-1.9213	0.12329	-0.21935	-38.19
col122	-A-	Max	1783.1	16.867	7.1545	-0.12406	7.8484	28.773
		Min	1782.5	-18.948	-4.3587	-0.12407	-10.403	-32.292
	-B-	Max	-1782.5	18.948	4.3587	0.12407	3.2673	14.244
		Min	-1783.1	-16.867	-7.1545	0.12406	-7.8419	-16.032
col111	-A-	Max	855.32	9.2171	12.129	-0.12491	-0.44279	20.974
		Min	282.05	-26.79	5.7439	-0.12496	-14.007	-40.265
	-B-	Max	-282.05	26.79	-5.7439	0.12496	-14.19	2.5382
		Min	-855.32	-9.2171	-12.129	0.12491	-16.936	-28.057
col113	-A-	Max	808.07	22.654	13.669	-0.12491	-3.7317	33.252
		Min	234.8	-13.353	7.2838	-0.12496	-17.296	-27.987
	-B-	Max	-234.8	13.353	-7.2838	0.12496	-14.828	24.525
		Min	-808.07	-22.654	-13.669	0.12491	-17.574	-6.0703
col141	-A-	Max	1094.2	-8.7766	10.245	-0.1233	9.9716	6.9559
		Min	753.07	-31.121	-5.6526	-0.1233	-12.286	-41.795
	-B-	Max	-753.07	31.121	5.6526	0.1233	4.4429	-29.281
		Min	-1094.2	8.7766	-10.245	0.1233	-13.839	-37.618
col142	-A-	Max	1783.1	18.948	4.3587	-0.12406	10.403	32.292
		Min	1782.5	-16.867	-7.1545	-0.12407	-7.8484	-28.773

	-B-	Max	-1782.5	16.867	7.1545	0.12407	7.8419	16.032
		Min	-1783.1	-18.948	-4.3587	0.12406	-3.2673	-14.244
col123	-A-	Max	1094.2	31.121	5.6526	-0.1233	12.286	41.795
		Min	753.07	8.7766	-10.245	-0.1233	-9.9716	-6.9559
	-B-	Max	-753.07	-8.7766	10.245	0.1233	13.839	37.618
		Min	-1094.2	-31.121	-5.6526	0.1233	-4.4429	29.281
col132	-A-	Max	1793.9	18.897	5.4987	-0.12402	8.8901	31.437
		Min	1793.9	-18.897	-5.4987	-0.12402	-8.8901	-31.437
	-B-	Max	-1793.9	18.897	5.4987	0.12402	5.1326	16.755
		Min	-1793.9	-18.897	-5.4987	0.12402	-5.1326	-16.755
col522	-A-	Max	287.11	60.411	32.934	-0.43857	6.7397	71.02
		Min	286.03	-68.552	-6.0562	-0.43859	-39.376	-80.649
	-B-	Max	-286.03	68.552	6.0562	0.43859	8.7038	83.029
		Min	-287.11	-60.411	-32.934	0.43857	-44.606	-94.158
col551	-A-	Max	129.15	68.749	-15.867	-0.43547	43.189	76.048
		Min	22.259	-69.379	-38.021	-0.43556	17.762	-78.348
	-B-	Max	-22.259	69.379	38.021	0.43556	53.766	99.261
		Min	-129.15	-68.749	15.867	0.43547	22.698	-98.57
col523	-A-	Max	170.03	82.944	20.592	-0.44007	44.687	95.01
		Min	109.32	5.9503	-38.408	-0.44009	-24.679	8.2417
	-B-	Max	-109.32	-5.9503	38.408	0.44009	53.252	116.5
		Min	-170.03	-82.944	-20.592	0.44007	-27.831	6.9293
col232	-A-	Max	1410.6	42.679	12.32	-0.30679	16.783	58.925
		Min	1410.6	-42.679	-12.32	-0.30679	-16.783	-58.925
	-B-	Max	-1410.6	42.679	12.32	0.30679	14.634	49.911
		Min	-1410.6	-42.679	-12.32	0.30679	-14.634	-49.911
col423	-A-	Max	402.56	61.993	18.186	-0.44173	37.581	81.668
		Min	258.42	5.0124	-29.029	-0.44174	-23.545	5.9663
	-B-	Max	-258.42	-5.0124	29.029	0.44174	36.442	76.431
		Min	-402.56	-61.993	-18.186	0.44173	-22.829	6.7984
col513	-A-	Max	129.15	69.379	38.021	-0.43547	-17.762	78.348
		Min	22.259	-68.749	15.867	-0.43556	-43.189	-76.048
	-B-	Max	-22.259	68.749	-15.867	0.43556	-22.698	98.57
		Min	-129.15	-69.379	-38.021	0.43547	-53.766	-99.261
col521	-A-	Max	164.06	-11.084	5.4243	-0.44008	62.562	-14.004
		Min	103.34	-88.078	-53.575	-0.4401	-6.8037	-100.77
	-B-	Max	-103.34	88.078	53.575	0.4401	74.054	-14.257
		Min	-164.06	11.084	-5.4243	0.44008	-7.0284	-123.83
col241	-A-	Max	869.47	-12.749	22.804	-0.30671	18.862	-11.334
		Min	573.89	-59.049	-13.988	-0.30672	-29.344	-82.331
	-B-	Max	-573.89	59.049	13.988	0.30672	16.808	-21.155
		Min	-869.47	12.749	-22.804	0.30671	-28.805	-68.264
col223	-A-	Max	869.47	59.049	13.988	-0.30671	29.344	82.331
		Min	573.89	12.749	-22.804	-0.30672	-18.862	11.334
	-B-	Max	-573.89	-12.749	22.804	0.30672	28.805	68.264
		Min	-869.47	-59.049	-13.988	0.30671	-16.808	21.155
col222	-A-	Max	1395.5	37.807	17.893	-0.30664	11.912	52.623
		Min	1395.2	-42.617	-7.8913	-0.30665	-23.071	-59.288
	-B-	Max	-1395.2	42.617	7.8913	0.30665	8.2118	43.791
		Min	-1395.5	-37.807	-17.893	0.30664	-22.558	-49.391
col532	-A-	Max	290.21	70.452	17.897	-0.43883	21.603	82.051
		Min	290.21	-70.452	-17.897	-0.43883	-21.603	-82.051
	-B-	Max	-290.21	70.452	17.897	0.43883	24.036	97.601
		Min	-290.21	-70.452	-17.897	0.43883	-24.036	-97.601
col413	-A-	Max	310.64	50.653	27.458	-0.44313	-13.928	67.381
		Min	62.593	-46.341	10.31	-0.44317	-36.135	-62.008
	-B-	Max	-62.593	46.341	-10.31	0.44317	-12.357	61.789
		Min	-310.64	-50.653	-27.458	0.44313	-33.888	-56.168
col221	-A-	Max	845.4	-15.62	5.1017	-0.30671	41.051	-15.69

		Min	549.82	-61.92	-31.69	-0.30672	-7.155	-86.687
	-B-	Max	-549.82	61.92	31.69	0.30672	39.759	-24.12
		Min	-845.4	15.62	-5.1017	0.30671	-5.8547	-71.23
col422	-A-	Max	649.93	48.618	26.517	-0.44078	8.1854	63.175
		Min	649.53	-55.123	-5.9452	-0.44079	-33.77	-71.607
	-B-	Max	-649.53	55.123	5.9452	0.44079	6.9759	60.806
		Min	-649.93	-48.618	-26.517	0.44078	-33.85	-68.961
bmx611	-A-	Max	-2.1907	0.0029224	6.1305	4.9033	23.014	0.0042376
		Min	-4.7348	0.0027712	-4.0554	0.25062	-11.769	0.0037752
	-B-	Max	4.7348	-0.0027712	4.0554	-0.25062	-0.30342	0.012128
		Min	2.1907	-0.0029224	-6.1305	-4.9033	-22.562	0.011743
bmx431	-A-	Max	2.5422	0.023567	36.552	2.73	33.957	0.052922
		Min	-1.5592	0.023413	-15.877	0.4943	-75.662	0.052623
	-B-	Max	1.5592	-0.023413	15.877	-0.4943	26.376	0.036635
		Min	-2.5422	-0.023567	-36.552	-2.73	-63.234	0.036346
bmy612	-A-	Max	6.4835	-0.20299	65.706	1.0763	102.18	-0.57438
		Min	-6.2873	-0.20323	-36.141	0.30978	-173.64	-0.57509
	-B-	Max	6.2873	0.20323	36.141	-0.30978	71.3	-0.39999
		Min	-6.4835	0.20299	-65.706	-1.0763	-141.75	-0.40039
bmx423	-A-	Max	2.5422	0.023567	15.877	2.73	63.234	0.036635
		Min	-1.5592	0.023413	-36.552	0.4943	-26.376	0.036346
	-B-	Max	1.5592	-0.023413	36.552	-0.4943	75.662	0.052922
		Min	-2.5422	-0.023567	-15.877	-2.73	-33.957	0.052623
bmx613	-A-	Max	-1.5566	0.0030099	8.6205	-0.2988	14.48	0.0044961
		Min	-4.1006	0.0028588	-1.5654	-4.9515	-20.303	0.0040338
	-B-	Max	4.1006	-0.0028588	1.5654	4.9515	-5.7132	0.01236
		Min	1.5566	-0.0030099	-8.6205	0.2988	-27.972	0.011975
bmx521	-A-	Max	3.2015	-0.02105	-0.30127	0.30887	95.623	-0.030183
		Min	-0.48688	-0.021218	-54.427	-1.5238	1.7044	-0.030484
	-B-	Max	0.48688	0.021218	54.427	1.5238	111.2	-0.049805
		Min	-3.2015	0.02105	0.30127	-0.30887	-0.55958	-0.050144
bmy551	-A-	Max	2.5604	-0.016632	49.837	0.83259	187.89	-0.02539
		Min	-2.8612	-0.017147	-80.827	0.33638	-112.77	-0.026151
	-B-	Max	2.8612	0.017147	80.827	-0.33638	200.08	-0.054443
		Min	-2.5604	0.016632	-49.837	-0.83259	-126.45	-0.056153
bmy552	-A-	Max	1.9191	-0.01667	65.206	0.5127	165.51	-0.054544
		Min	-3.5025	-0.017185	-65.458	0.016495	-161.02	-0.056253
	-B-	Max	3.5025	0.017185	65.458	-0.016495	148.69	-0.025474
		Min	-1.9191	0.01667	-65.206	-0.5127	-151.97	-0.026234
bmx513	-A-	Max	-0.40286	0.0063148	14.21	-0.16967	13.985	0.020285
		Min	-2.006	0.0061427	-3.2357	-1.858	-38.798	0.019636
	-B-	Max	2.006	-0.0061427	3.2357	1.858	4.1348	0.015079
		Min	0.40286	-0.0063148	-14.21	0.16967	-40.777	0.014761
bmx523	-A-	Max	2.2671	-0.021108	13.444	2.4771	71.792	-0.030283
		Min	-1.4213	-0.021276	-40.682	0.64442	-22.127	-0.030584
	-B-	Max	1.4213	0.021276	40.682	-0.64442	82.801	-0.049927
		Min	-2.2671	0.021108	-13.444	-2.4771	-28.958	-0.050266
bmx533	-A-	Max	3.2015	-0.02105	54.427	0.30887	0.55958	-0.049805
		Min	-0.48688	-0.021218	0.30127	-1.5238	-111.2	-0.050144
	-B-	Max	0.48688	0.021218	-0.30127	1.5238	-1.7044	-0.030183
		Min	-3.2015	0.02105	-54.427	-0.30887	-95.623	-0.030484
bmx541	-A-	Max	-0.40286	0.0063148	3.2357	-0.16967	40.777	0.015079
		Min	-2.006	0.0061427	-14.21	-1.858	-4.1348	0.014761
	-B-	Max	2.006	-0.0061427	14.21	1.858	38.798	0.020285
		Min	0.40286	-0.0063148	-3.2357	0.16967	-13.985	0.019636
bmx543	-A-	Max	-0.80442	0.0063348	7.5715	2.3202	29.624	0.015121
		Min	-2.4076	0.0061628	-9.8741	0.63178	-15.288	0.014803
	-B-	Max	2.4076	-0.0061628	9.8741	-0.63178	25.671	0.020356
		Min	0.80442	-0.0063348	-7.5715	-2.3202	-27.112	0.019707

bmx531	-A-	Max	2.2671	-0.021108	40.682	2.4771	28.958	-0.049927
		Min	-1.4213	-0.021276	-13.444	0.64442	-82.801	-0.050266
	-B-	Max	1.4213	0.021276	13.444	-0.64442	22.127	-0.030283
		Min	-2.2671	0.021108	-40.682	-2.4771	-71.792	-0.030584
bmy611	-A-	Max	4.9412	-0.20288	48.361	0.30737	116.24	-0.39973
		Min	-7.8296	-0.20311	-53.487	-0.45913	-96.803	-0.40013
	-B-	Max	7.8296	0.20311	53.487	0.45913	140.49	-0.57409
		Min	-4.9412	0.20288	-48.361	-0.30737	-135.33	-0.57481
bmx443	-A-	Max	-1.0751	-0.00024362	7.4352	2.8874	25.493	-0.0012573
		Min	-2.861	-0.00039411	-8.1601	0.44078	-13.786	-0.0015505
	-B-	Max	2.861	0.00039411	8.1601	-0.44078	20.204	-0.00010697
		Min	1.0751	0.00024362	-7.4352	-2.8874	-27.851	-0.00065657
bmx433	-A-	Max	3.5629	0.023566	49.595	0.36555	6.6719	0.052918
		Min	-0.53849	0.023411	-2.8339	-1.8701	-102.95	0.05262
	-B-	Max	0.53849	-0.023411	2.8339	1.8701	4.0968	0.036631
		Min	-3.5629	-0.023566	-49.595	-0.36555	-85.514	0.036342
bmx441	-A-	Max	-0.6404	-0.00024324	3.6266	-0.11412	35.088	-0.0012541
		Min	-2.4263	-0.00039371	-11.969	-2.5608	-4.1904	-0.0015473
	-B-	Max	2.4263	0.00039371	11.969	2.5608	31.937	-0.00010798
		Min	0.6404	0.00024324	-3.6266	0.11412	-16.118	-0.00065754
bmy451	-A-	Max	3.4148	0.017469	47.252	0.7812	174.92	0.034422
		Min	-3.7246	0.017095	-76.34	0.28242	-104.35	0.033876
	-B-	Max	3.7246	-0.017095	76.34	-0.28242	191.52	0.049431
		Min	-3.4148	-0.017469	-47.252	-0.7812	-122.46	0.048178
bmx511	-A-	Max	-0.80442	0.0063348	9.8741	2.3202	27.112	0.020356
		Min	-2.4076	0.0061627	-7.5715	0.63178	-25.671	0.019707
	-B-	Max	2.4076	-0.0061627	7.5715	-0.63178	15.288	0.015121
		Min	0.80442	-0.0063348	-9.8741	-2.3202	-29.624	0.014803
bmy512	-A-	Max	2.5604	-0.016632	80.827	0.83259	126.45	-0.054443
		Min	-2.8612	-0.017147	-49.837	0.33638	-200.08	-0.056153
	-B-	Max	2.8612	0.017147	49.837	-0.33638	112.77	-0.02539
		Min	-2.5604	0.016632	-80.827	-0.83259	-187.89	-0.026151
bmy452	-A-	Max	2.5687	0.017469	61.738	0.51072	159.59	0.049428
		Min	-4.5708	0.017095	-61.854	0.011945	-154.39	0.048175
	-B-	Max	4.5708	-0.017095	61.854	-0.011945	137.31	0.034424
		Min	-2.5687	-0.017469	-61.738	-0.51072	-141.95	0.033878
bmy511	-A-	Max	1.9191	-0.01667	65.458	0.5127	151.97	-0.025474
		Min	-3.5025	-0.017185	-65.206	0.016495	-148.69	-0.026234
	-B-	Max	3.5025	0.017185	65.206	-0.016495	161.02	-0.054544
		Min	-1.9191	0.01667	-65.458	-0.5127	-165.51	-0.056253
bmy251	-A-	Max	1.3397	0.080977	25.23	0.34936	101.22	0.16136
		Min	-2.6412	0.08077	-43.518	0.11404	-54.124	0.16107
	-B-	Max	2.6412	-0.08077	43.518	-0.11404	107.67	0.22734
		Min	-1.3397	-0.080977	-25.23	-0.34936	-66.977	0.22663
bmy252	-A-	Max	0.87942	0.080942	35.609	0.31727	87.081	0.22725
		Min	-3.1015	0.080735	-33.138	0.081948	-87.562	0.22654
	-B-	Max	3.1015	-0.080735	33.138	-0.081948	71.981	0.16128
		Min	-0.87942	-0.080942	-35.609	-0.31727	-83.364	0.16099
bmx243	-A-	Max	-1.1499	0.0003509	5.3701	2.1796	10.751	-0.0013734
		Min	-2.2229	0.00028054	-2.8306	0.78254	-9.5787	-0.0015083
	-B-	Max	2.2229	-0.00028054	2.8306	-0.78254	5.1002	0.0033409
		Min	1.1499	-0.0003509	-5.3701	-2.1796	-20.494	0.0030768
bmx641	-A-	Max	-1.5566	0.0030099	1.5654	-0.2988	27.972	0.01236
		Min	-4.1006	0.0028588	-8.6205	-4.9515	5.7132	0.011975
	-B-	Max	4.1006	-0.0028588	8.6205	4.9515	20.303	0.0044962
		Min	1.5566	-0.0030099	-1.5654	0.2988	-14.48	0.0040338
bmx633	-A-	Max	5.6977	-0.27494	43.566	0.71505	-3.5497	-0.61458
		Min	-0.43971	-0.27509	2.4323	-2.8883	-96.797	-0.61484
	-B-	Max	0.43971	0.27509	-2.4323	2.8883	-5.693	-0.43018

		Min	-5.6977	0.27494	-43.566	-0.71505	-68.754	-0.43052
bmy311	-A-	Max	2.0322	0.049934	54.712	0.43164	124.35	0.096734
		Min	-3.8464	0.049617	-53.861	0.027969	-121.93	0.096277
	-B-	Max	3.8464	-0.049617	53.861	-0.027969	134.18	0.14295
		Min	-2.0322	-0.049934	-54.712	-0.43164	-140.68	0.14188
bmx321	-A-	Max	2.9791	0.067171	4.7936	0.21532	71.788	0.10436
		Min	-0.56072	0.067048	-41.619	-1.6129	-7.7586	0.10414
	-B-	Max	0.56072	-0.067048	41.619	1.6129	86.364	0.15089
		Min	-2.9791	-0.067171	-4.7936	-0.21532	-10.457	0.15064
bmx631	-A-	Max	4.1264	-0.27483	32.988	3.5205	20.417	-0.61436
		Min	-2.0109	-0.27498	-8.1455	-0.082781	-72.83	-0.61461
	-B-	Max	2.0109	0.27498	8.1455	0.082781	10.536	-0.42998
		Min	-4.1264	0.27483	-32.988	-3.5205	-52.525	-0.43031
bmx313	-A-	Max	-0.43789	-0.0019987	9.8502	-0.095247	14.809	-0.0050832
		Min	-2.0131	-0.0021174	-3.522	-2.1067	-26.503	-0.0055251
	-B-	Max	2.0131	0.0021174	3.522	2.1067	4.9143	-0.0061063
		Min	0.43789	0.0019987	-9.8502	0.095247	-28.658	-0.0063355
bmx311	-A-	Max	-0.81272	-0.0019961	6.6413	2.4016	24.715	-0.005073
		Min	-2.3879	-0.0021148	-6.7308	0.39024	-16.597	-0.005515
	-B-	Max	2.3879	0.0021148	6.7308	-0.39024	12.978	-0.0061019
		Min	0.81272	0.0019961	-6.6413	-2.4016	-20.595	-0.0063311
bmy312	-A-	Max	2.7221	0.04994	66.533	0.65964	108.58	0.14297
		Min	-3.1565	0.049622	-42.04	0.25596	-166.29	0.1419
	-B-	Max	3.1565	-0.049622	42.04	-0.25596	93.215	0.096744
		Min	-2.7221	-0.04994	-66.533	-0.65964	-153.07	0.096286
bmx241	-A-	Max	-0.90289	0.00032622	3.4421	-0.61379	15.543	-0.0014353
		Min	-1.9758	0.00025586	-4.7586	-2.0109	-4.7867	-0.0015701
	-B-	Max	1.9758	-0.00025586	4.7586	2.0109	11.105	0.0032646
		Min	0.90289	-0.00032622	-3.4421	0.61379	-14.489	0.0030005
bmy212	-A-	Max	1.3397	0.080977	43.518	0.34936	66.977	0.22734
		Min	-2.6412	0.08077	-25.23	0.11404	-107.67	0.22663
	-B-	Max	2.6412	-0.08077	25.23	-0.11404	54.124	0.16136
		Min	-1.3397	-0.080977	-43.518	-0.34936	-101.22	0.16107
bmx213	-A-	Max	-0.90289	0.00032622	4.7586	-0.61379	14.489	0.0032646
		Min	-1.9758	0.00025586	-3.4421	-2.0109	-11.105	0.0030005
	-B-	Max	1.9758	-0.00025586	3.4421	2.0109	4.7867	-0.0014353
		Min	0.90289	-0.00032622	-4.7586	0.61379	-15.543	-0.0015701
bmy652	-A-	Max	4.9412	-0.20288	53.487	0.30737	135.33	-0.57409
		Min	-7.8296	-0.20311	-48.361	-0.45913	-140.49	-0.57481
	-B-	Max	7.8296	0.20311	48.361	0.45913	96.803	-0.39973
		Min	-4.9412	0.20288	-53.487	-0.30737	-116.24	-0.40013
bmx211	-A-	Max	-1.1499	0.0003509	2.8306	2.1796	20.494	0.0033409
		Min	-2.2229	0.00028054	-5.3701	0.78254	-5.1002	0.0030768
	-B-	Max	2.2229	-0.00028054	5.3701	-0.78254	9.5787	-0.0013734
		Min	1.1499	-0.0003509	-2.8306	-2.1796	-10.751	-0.0015083
bmy211	-A-	Max	0.87942	0.080942	33.138	0.31727	83.364	0.16128
		Min	-3.1015	0.080735	-35.609	0.081948	-71.981	0.16099
	-B-	Max	3.1015	-0.080735	35.609	-0.081948	87.562	0.22725
		Min	-0.87942	-0.080942	-33.138	-0.31727	-87.081	0.22654
bmy651	-A-	Max	6.4835	-0.20299	36.141	1.0763	141.75	-0.39999
		Min	-6.2873	-0.20323	-65.706	0.30978	-71.3	-0.40039
	-B-	Max	6.2873	0.20323	65.706	-0.30978	173.64	-0.57438
		Min	-6.4835	0.20299	-36.141	-1.0763	-102.18	-0.57509
bmx231	-A-	Max	1.5936	0.10997	17.487	2.2177	25.186	0.24519
		Min	-0.76928	0.10989	-12.277	1.045	-37.114	0.24503
	-B-	Max	0.76928	-0.10989	12.277	-1.045	21.467	0.17267
		Min	-1.5936	-0.10997	-17.487	-2.2177	-29.337	0.17255
bmx233	-A-	Max	2.1516	0.10999	24.544	-0.58013	10.412	0.24525
		Min	-0.21128	0.10991	-5.22	-1.7528	-51.889	0.24508

	-B-	Max	0.21128	-0.10991	5.22	1.7528	9.4244	0.17272
		Min	-2.1516	-0.10999	-24.544	0.58013	-41.38	0.17259
bmx223	-A-	Max	1.5936	0.10997	12.277	2.2177	29.337	0.17267
		Min	-0.76928	0.10989	-17.487	1.045	-21.467	0.17255
	-B-	Max	0.76928	-0.10989	17.487	-1.045	37.114	0.24519
		Min	-1.5936	-0.10997	-12.277	-2.2177	-25.186	0.24503
bmx221	-A-	Max	2.1516	0.10999	5.22	-0.58013	41.38	0.17272
		Min	-0.21128	0.10991	-24.544	-1.7528	-9.4244	0.17259
	-B-	Max	0.21128	-0.10991	24.544	1.7528	51.889	0.24525
		Min	-2.1516	-0.10999	-5.22	0.58013	-10.412	0.24508
bmx643	-A-	Max	-2.1907	0.0029223	4.0554	4.9033	22.562	0.012128
		Min	-4.7348	0.0027712	-6.1305	0.25062	0.30342	0.011743
	-B-	Max	4.7348	-0.0027712	6.1305	-0.25062	11.769	0.0042376
		Min	2.1907	-0.0029223	-4.0554	-4.9033	-23.014	0.0037752
bmy411	-A-	Max	2.5687	0.017469	61.854	0.51072	141.95	0.034424
		Min	-4.5708	0.017095	-61.738	0.011945	-137.31	0.033878
	-B-	Max	4.5708	-0.017095	61.738	-0.011945	154.39	0.049428
		Min	-2.5687	-0.017469	-61.854	-0.51072	-159.59	0.048175
bmx411	-A-	Max	-1.0751	-0.00024363	8.1601	2.8874	27.851	-0.000107
		Min	-2.861	-0.0003941	-7.4352	0.44078	-20.204	-0.00065654
	-B-	Max	2.861	0.0003941	7.4352	-0.44078	13.786	-0.0012573
		Min	1.0751	0.00024363	-8.1601	-2.8874	-25.493	-0.0015504
bmx333	-A-	Max	2.9791	0.067171	41.619	0.21532	10.457	0.15089
		Min	-0.56072	0.067048	-4.7936	-1.6129	-86.364	0.15064
	-B-	Max	0.56072	-0.067048	4.7936	1.6129	7.7586	0.10436
		Min	-2.9791	-0.067171	-41.619	-0.21532	-71.788	0.10414
bmx341	-A-	Max	-0.43789	-0.0019987	3.522	-0.095247	28.658	-0.0061063
		Min	-2.0131	-0.0021174	-9.8502	-2.1067	-4.9143	-0.0063355
	-B-	Max	2.0131	0.0021174	9.8502	2.1067	26.503	-0.0050832
		Min	0.43789	0.0019987	-3.522	0.095247	-14.809	-0.0055251
bmx343	-A-	Max	-0.81272	-0.0019961	6.7308	2.4016	20.595	-0.0061019
		Min	-2.3879	-0.0021148	-6.6413	0.39024	-12.978	-0.0063311
	-B-	Max	2.3879	0.0021148	6.6413	-0.39024	16.597	-0.005073
		Min	0.81272	0.0019961	-6.7308	-2.4016	-24.715	-0.005515
bmy351	-A-	Max	2.7221	0.04994	42.04	0.65964	153.07	0.096744
		Min	-3.1565	0.049622	-66.533	0.25596	-93.215	0.096286
	-B-	Max	3.1565	-0.049622	66.533	-0.25596	166.29	0.14297
		Min	-2.7221	-0.04994	-42.04	-0.65964	-108.58	0.1419
bmy352	-A-	Max	2.0322	0.049934	53.861	0.43164	140.68	0.14295
		Min	-3.8464	0.049617	-54.712	0.027969	-134.18	0.14188
	-B-	Max	3.8464	-0.049617	54.712	-0.027969	121.93	0.096734
		Min	-2.0322	-0.049934	-53.861	-0.43164	-124.35	0.096277
bmx621	-A-	Max	5.6977	-0.27494	-2.4323	0.71505	68.754	-0.43018
		Min	-0.43971	-0.27509	-43.566	-2.8883	5.693	-0.43052
	-B-	Max	0.43971	0.27509	43.566	2.8883	96.797	-0.61458
		Min	-5.6977	0.27494	2.4323	-0.71505	3.5497	-0.61484
bmx323	-A-	Max	2.117	0.067156	16.076	2.3628	52.466	0.10433
		Min	-1.4228	0.067033	-30.337	0.53458	-27.081	0.10411
	-B-	Max	1.4228	-0.067033	30.337	-0.53458	62.815	0.15086
		Min	-2.117	-0.067156	-16.076	-2.3628	-34.006	0.15061
bmx331	-A-	Max	2.117	0.067156	30.337	2.3628	34.006	0.15086
		Min	-1.4228	0.067033	-16.076	0.53458	-62.815	0.15061
	-B-	Max	1.4228	-0.067033	16.076	-0.53458	27.081	0.10433
		Min	-2.117	-0.067156	-30.337	-2.3628	-52.466	0.10411
bmx421	-A-	Max	3.5629	0.023566	2.8339	0.36555	85.514	0.036631
		Min	-0.53849	0.023411	-49.595	-1.8701	-4.0968	0.036342
	-B-	Max	0.53849	-0.023411	49.595	1.8701	102.95	0.052918
		Min	-3.5629	-0.023566	-2.8339	-0.36555	-6.6719	0.05262
bmx413	-A-	Max	-0.6404	-0.00024324	11.969	-0.11412	16.118	-0.00010797

		Min	-2.4263	-0.00039372	-3.6266	-2.5608	-31.937	-0.00065755
	-B-	Max	2.4263	0.00039372	3.6266	2.5608	4.1904	-0.0012541
		Min	0.6404	0.00024324	-11.969	0.11412	-35.088	-0.0015473
bmy412	-A-	Max	3.4148	0.017469	76.34	0.7812	122.46	0.049431
		Min	-3.7246	0.017095	-47.252	0.28242	-191.52	0.048178
	-B-	Max	3.7246	-0.017095	47.252	-0.28242	104.35	0.034422
		Min	-3.4148	-0.017469	-76.34	-0.7812	-174.92	0.033876
bmx623	-A-	Max	4.1264	-0.27483	8.1455	3.5205	52.525	-0.42998
		Min	-2.0109	-0.27498	-32.988	-0.082781	-10.536	-0.43031
	-B-	Max	2.0109	0.27498	32.988	0.082781	72.83	-0.61436
		Min	-4.1264	0.27483	-8.1455	-3.5205	-20.417	-0.61461
bmx532	-A-	Max	-0.81664	0.0071662	10.597	0.44833	19.676	0.014934
		Min	-0.8296	0.0045421	-6.2682	0.17806	-27.54	0.0076364
	-B-	Max	0.8296	-0.0045421	6.2682	-0.17806	15.425	0.025196
		Min	0.81664	-0.0071662	-10.597	-0.44833	-31.801	0.017799
bmx222	-A-	Max	-0.16639	0.0011985	3.8796	0.28049	14.372	0.0039878
		Min	-0.2469	0.00020198	-4.9777	0.026519	-10.233	0.0011766
	-B-	Max	0.2469	-0.00020198	4.9777	-0.026519	13.503	0.0027243
		Min	0.16639	-0.0011985	-3.8796	-0.28049	-11.493	-4.5817E-05
bmx422	-A-	Max	-0.62255	0.00062049	6.1159	0.54947	28.995	0.0014972
		Min	-0.76074	-0.0010873	-9.7766	0.027879	-15.168	-0.0032114
	-B-	Max	0.76074	0.0010873	9.7766	-0.027879	25.754	0.0019776
		Min	0.62255	-0.00062049	-6.1159	-0.54947	-19.08	-0.0028776
bmx522	-A-	Max	-0.81664	0.0071662	6.2682	0.44833	31.801	0.025196
		Min	-0.8296	0.0045421	-10.597	0.17806	-15.425	0.017799
	-B-	Max	0.8296	-0.0045421	10.597	-0.17806	27.54	0.014934
		Min	0.81664	-0.0071662	-6.2682	-0.44833	-19.676	0.0076364
bmx332	-A-	Max	-0.4815	-0.0009534	8.4297	0.43721	17.102	-0.0011851
		Min	-0.58048	-0.0024412	-5.5751	0.058572	-22.351	-0.0053733
	-B-	Max	0.58048	0.0024412	5.5751	-0.058572	14.119	-0.0041539
		Min	0.4815	0.0009534	-8.4297	-0.43721	-24.855	-0.0082976
bmx622	-A-	Max	-0.91359	0.0022611	1.6644	0.81019	24.566	0.0077201
		Min	-1.3913	0.0012248	-7.9244	-0.4499	-1.0608	0.005001
	-B-	Max	1.3913	-0.0012248	7.9244	0.4499	19.811	0.0049498
		Min	0.91359	-0.0022611	-1.6644	-0.81019	-8.2597	0.0018499
bmx322	-A-	Max	-0.4815	-0.0009534	5.5751	0.43721	24.855	-0.0041539
		Min	-0.58048	-0.0024412	-8.4297	0.058572	-14.119	-0.0082976
	-B-	Max	0.58048	0.0024412	8.4297	-0.058572	22.351	-0.0011851
		Min	0.4815	0.0009534	-5.5751	-0.43721	-17.102	-0.0053733
bmx632	-A-	Max	-0.91359	0.0022611	7.9244	0.81019	8.2597	0.0049498
		Min	-1.3913	0.0012248	-1.6644	-0.4499	-19.811	0.0018499
	-B-	Max	1.3913	-0.0012248	1.6644	0.4499	1.0608	0.0077201
		Min	0.91359	-0.0022611	-7.9244	-0.81019	-24.566	0.005001
bmx432	-A-	Max	-0.62255	0.00062049	9.7766	0.54947	19.08	0.0019776
		Min	-0.76074	-0.0010873	-6.1159	0.027879	-25.754	-0.0028776
	-B-	Max	0.76074	0.0010873	6.1159	-0.027879	15.168	0.0014972
		Min	0.62255	-0.00062049	-9.7766	-0.54947	-28.995	-0.0032114
bmx232	-A-	Max	-0.16639	0.0011985	4.9777	0.28049	11.493	0.0027243
		Min	-0.2469	0.00020198	-3.8796	0.026519	-13.503	-4.5817E-05
	-B-	Max	0.2469	-0.00020198	3.8796	-0.026519	10.233	0.0039878
		Min	0.16639	-0.0011985	-4.9777	-0.28049	-14.372	0.0011766
bmy542	-A-	Max	-0.25645	0.0042136	21.535	-0.52947	99.558	0.011753
		Min	-2.6891	0.004097	-29.908	-1.17	-63.603	0.011413
	-B-	Max	2.6891	-0.004097	29.908	1.17	97.833	0.016056
		Min	0.25645	-0.0042136	-21.535	0.52947	-78.527	0.015628
bmy631	-A-	Max	0.92143	-0.12711	26.217	1.386	52.034	-0.55138
		Min	-5.0747	-0.12723	-11.408	-0.53894	-89.104	-0.55175
	-B-	Max	5.0747	0.12723	11.408	0.53894	23.258	-0.28757
		Min	-0.92143	0.12711	-26.217	-1.386	-83.929	-0.28797

bmy642	-A-	Max	-1.4507	0.0073614	16.81	-1.175	60.612	0.017479
		Min	-4.3998	0.0072826	-17.009	-2.3987	-43.366	0.017081
	-B-	Max	4.3998	-0.0072826	17.009	2.3987	51.65	0.031172
		Min	1.4507	-0.0073614	-16.81	1.175	-67.578	0.030919
bmy632	-A-	Max	0.92143	-0.12711	11.408	1.386	83.929	-0.28757
		Min	-5.0747	-0.12723	-26.217	-0.53894	-23.258	-0.28797
	-B-	Max	5.0747	0.12723	26.217	0.53894	89.104	-0.55138
		Min	-0.92143	0.12711	-11.408	-1.386	-52.034	-0.55175
bmx612	-A-	Max	-0.47913	-0.22649	17.311	5.1106	-6.4183	-0.8326
		Min	-2.3121	-0.22731	4.6352	-3.7029	-47.09	-0.83464
	-B-	Max	2.3121	0.22731	-4.6352	3.7029	-19.539	-0.43571
		Min	0.47913	0.22649	-17.311	-5.1106	-49.853	-0.43831
bmx642	-A-	Max	-0.47913	-0.22649	-4.6352	5.1106	49.853	-0.43571
		Min	-2.3121	-0.22731	-17.311	-3.7029	19.539	-0.43831
	-B-	Max	2.3121	0.22731	17.311	3.7029	47.09	-0.8326
		Min	0.47913	0.22649	4.6352	-5.1106	6.4183	-0.83464
bmy622	-A-	Max	-1.5914	0.0072318	18.925	2.362	54.031	0.017064
		Min	-4.5406	0.007153	-14.894	1.1382	-49.947	0.016666
	-B-	Max	4.5406	-0.007153	14.894	-1.1382	44.271	0.030732
		Min	1.5914	-0.0072318	-18.925	-2.362	-74.957	0.030478
bmy641	-A-	Max	-1.5914	0.0072318	14.894	2.362	74.957	0.030732
		Min	-4.5406	0.007153	-18.925	1.1382	-44.271	0.030478
	-B-	Max	4.5406	-0.007153	18.925	-1.1382	49.947	0.017064
		Min	1.5914	-0.0072318	-14.894	-2.362	-54.031	0.016666
bmy621	-A-	Max	-1.4507	0.0073614	17.009	-1.175	67.578	0.031172
		Min	-4.3998	0.0072826	-16.81	-2.3987	-51.65	0.030918
	-B-	Max	4.3998	-0.0072826	16.81	2.3987	43.366	0.017479
		Min	1.4507	-0.0073614	-17.009	1.175	-60.612	0.017081
bmx542	-A-	Max	0.33118	-0.023352	-5.7288	3.2315	66.69	-0.041014
		Min	-0.99525	-0.025887	-24.153	-2.0229	18.842	-0.048792
	-B-	Max	0.99525	0.025887	24.153	2.0229	68.568	-0.089758
		Min	-0.33118	0.023352	5.7288	-3.2315	13.239	-0.096173
bmy322	-A-	Max	-0.63629	-0.0026802	21.909	1.1987	66.14	-0.0066787
		Min	-2.7133	-0.0027474	-19.463	0.58127	-64.733	-0.0068595
	-B-	Max	2.7133	0.0027474	19.463	-0.58127	62.318	-0.01101
		Min	0.63629	0.0026802	-21.909	-1.1987	-79.867	-0.011274
bmy321	-A-	Max	-0.52067	-0.0026911	21.962	-0.34641	71.294	-0.011046
		Min	-2.5977	-0.0027583	-19.41	-0.96388	-70.891	-0.011311
	-B-	Max	2.5977	0.0027583	19.41	0.96388	56.814	-0.0067141
		Min	0.52067	0.0026911	-21.962	0.34641	-74.058	-0.0068949
bmx312	-A-	Max	0.020416	0.057466	16.39	3.0023	1.0527	0.21088
		Min	-1.2147	0.056094	0.85071	-1.9741	-45.947	0.20749
	-B-	Max	1.2147	-0.056094	-0.85071	1.9741	-5.8167	0.11093
		Min	-0.020416	-0.057466	-16.39	-3.0023	-45.838	0.10664
bmy331	-A-	Max	0.82021	0.031546	27.527	1.0072	61.367	0.13667
		Min	-2.6519	0.031317	-16.32	-0.28953	-93.17	0.13596
	-B-	Max	2.6519	-0.031317	16.32	0.28953	46.342	0.071532
		Min	-0.82021	-0.031546	-27.527	-1.0072	-88.509	0.070733
bmx342	-A-	Max	0.020416	0.057466	-0.85071	3.0023	45.838	0.11093
		Min	-1.2147	0.056094	-16.39	-1.9741	5.8167	0.10664
	-B-	Max	1.2147	-0.056094	16.39	1.9741	45.947	0.21088
		Min	-0.020416	-0.057466	0.85071	-3.0023	-1.0527	0.20749
bmy341	-A-	Max	-0.63629	-0.0026802	19.463	1.1987	79.867	-0.01101
		Min	-2.7133	-0.0027474	-21.909	0.58127	-62.318	-0.011274
	-B-	Max	2.7133	0.0027474	21.909	-0.58127	64.733	-0.0066787
		Min	0.63629	0.0026802	-19.463	-1.1987	-66.14	-0.0068595
bmy332	-A-	Max	0.82021	0.031546	16.32	1.0072	88.509	0.071532
		Min	-2.6519	0.031317	-27.527	-0.28953	-46.342	0.070733
	-B-	Max	2.6519	-0.031317	27.527	0.28953	93.17	0.13667

		Min	-0.82021	-0.031546	-16.32	-1.0072	-61.367	0.13596
bmy242	-A-	Max	-1.2866	-0.0020724	15.134	-0.2449	39.246	-0.0044234
		Min	-2.6349	-0.0021152	-10.773	-0.65339	-42.556	-0.0045505
	-B-	Max	2.6349	0.0021152	10.773	0.65339	31.853	-0.0092523
		Min	1.2866	0.0020724	-15.134	0.2449	-57.326	-0.0094119
bmy222	-A-	Max	-1.3586	-0.0020425	16.669	0.79107	34.382	-0.0043319
		Min	-2.7069	-0.0020853	-9.2368	0.38258	-47.42	-0.004459
	-B-	Max	2.7069	0.0020853	9.2368	-0.38258	26.581	-0.0091463
		Min	1.3586	0.0020425	-16.669	-0.79107	-62.598	-0.0093059
bmy221	-A-	Max	-1.2866	-0.0020724	10.773	-0.2449	57.326	-0.0092523
		Min	-2.6349	-0.0021152	-15.134	-0.65339	-31.853	-0.0094119
	-B-	Max	2.6349	0.0021152	15.134	0.65339	42.556	-0.0044234
		Min	1.2866	0.0020724	-10.773	0.2449	-39.246	-0.0045505
bmx212	-A-	Max	-0.55947	0.089372	8.2184	1.9541	8.62	0.3272
		Min	-1.3761	0.08842	-1.6913	-1.3066	-21.433	0.32482
	-B-	Max	1.3761	-0.08842	1.6913	1.3066	0.85117	0.17328
		Min	0.55947	-0.089372	-8.2184	-1.9541	-24.59	0.17033
bmy231	-A-	Max	0.044665	0.050635	15.332	0.6531	46.303	0.2195
		Min	-2.2117	0.05046	-12.135	-0.20342	-50.738	0.21895
	-B-	Max	2.2117	-0.05046	12.135	0.20342	33.791	0.11469
		Min	-0.044665	-0.050635	-15.332	-0.6531	-50.455	0.11408
bmx242	-A-	Max	-0.55947	0.089372	1.6913	1.9541	24.59	0.17328
		Min	-1.3761	0.08842	-8.2184	-1.3066	-0.85117	0.17033
	-B-	Max	1.3761	-0.08842	8.2184	1.3066	21.433	0.3272
		Min	0.55947	-0.089372	-1.6913	-1.9541	-8.62	0.32482
bmy241	-A-	Max	-1.3586	-0.0020425	9.2368	0.79107	62.598	-0.0091463
		Min	-2.7069	-0.0020853	-16.669	0.38258	-26.581	-0.0093059
	-B-	Max	2.7069	0.0020853	16.669	-0.38258	47.42	-0.0043319
		Min	1.3586	0.0020425	-9.2368	-0.79107	-34.382	-0.004459
bmy232	-A-	Max	0.044665	0.050635	12.135	0.6531	50.455	0.11469
		Min	-2.2117	0.05046	-15.332	-0.20342	-33.791	0.11408
	-B-	Max	2.2117	-0.05046	15.332	0.20342	50.738	0.2195
		Min	-0.044665	-0.050635	-12.135	-0.6531	-46.303	0.21895
bmy521	-A-	Max	-0.25645	0.0042136	29.908	-0.52947	78.527	0.016057
		Min	-2.6891	0.004097	-21.535	-1.17	-97.833	0.015628
	-B-	Max	2.6891	-0.004097	21.535	1.17	63.603	0.011753
		Min	0.25645	-0.0042136	-29.908	0.52947	-99.558	0.011413
bmx512	-A-	Max	0.33118	-0.023352	24.153	3.2315	-13.239	-0.089758
		Min	-0.99525	-0.025887	5.7288	-2.0229	-68.568	-0.096173
	-B-	Max	0.99525	0.025887	-5.7288	2.0229	-18.842	-0.041014
		Min	-0.33118	0.023352	-24.153	-3.2315	-66.69	-0.048792
bmy442	-A-	Max	-0.65496	-0.00084732	21.505	-0.49873	87.672	-0.0019951
		Min	-2.9621	-0.00092475	-25.956	-1.2329	-62.747	-0.0021872
	-B-	Max	2.9621	0.00092475	25.956	1.2329	83.641	-0.0035966
		Min	0.65496	0.00084732	-21.505	0.49873	-79.184	-0.0039167
bmy522	-A-	Max	-0.40633	0.0042485	24.751	1.5108	89.37	0.011852
		Min	-2.839	0.0041319	-26.692	0.87021	-73.791	0.011511
	-B-	Max	2.839	-0.0041319	26.692	-0.87021	86.797	0.016189
		Min	0.40633	-0.0042485	-24.751	-1.5108	-89.563	0.01576
bmy541	-A-	Max	-0.40633	0.0042485	26.692	1.5108	89.563	0.016189
		Min	-2.839	0.0041319	-24.751	0.87021	-86.797	0.01576
	-B-	Max	2.839	-0.0041319	24.751	-0.87021	73.791	0.011852
		Min	0.40633	-0.0042485	-26.692	-1.5108	-89.37	0.011511
bmy532	-A-	Max	1.0167	-0.010954	17.004	1.1302	119.67	-0.024522
		Min	-2.6987	-0.011358	-37.146	-0.26786	-48.462	-0.025922
	-B-	Max	2.6987	0.011358	37.146	0.26786	125.49	-0.047773
		Min	-1.0167	0.010954	-17.004	-1.1302	-63.767	-0.049043
bmy531	-A-	Max	1.0167	-0.010954	37.146	1.1302	63.767	-0.047773
		Min	-2.6987	-0.011358	-17.004	-0.26786	-125.49	-0.049043

	-B-	Max	2.6987	0.011358	17.004	0.26786	48.462	-0.024522
		Min	-1.0167	0.010954	-37.146	-1.1302	-119.67	-0.025922
bmx442	-A-	Max	0.018373	0.019931	-2.9981	3.4968	57.456	0.039258
		Min	-1.3814	0.018404	-20.536	-2.2896	12.3	0.034453
	-B-	Max	1.3814	-0.018404	20.536	2.2896	57.549	0.072355
		Min	-0.018373	-0.019931	2.9981	-3.4968	4.4894	0.068609
bmy421	-A-	Max	-0.65496	-0.00084733	25.956	-0.49873	79.184	-0.0035967
		Min	-2.9621	-0.00092473	-21.505	-1.2329	-83.641	-0.0039166
	-B-	Max	2.9621	0.00092473	21.505	1.2329	62.747	-0.0019951
		Min	0.65496	0.00084733	-25.956	0.49873	-87.672	-0.0021872
bmx412	-A-	Max	0.018373	0.019931	20.536	3.4968	-4.4894	0.072355
		Min	-1.3814	0.018404	2.9981	-2.2896	-57.549	0.068609
	-B-	Max	1.3814	-0.018404	-2.9981	2.2896	-12.3	0.039258
		Min	-0.018373	-0.019931	-20.536	-3.4968	-57.456	0.034453
bmy342	-A-	Max	-0.52067	-0.0026911	19.41	-0.34641	74.058	-0.0067141
		Min	-2.5977	-0.0027583	-21.962	-0.96388	-56.814	-0.0068949
	-B-	Max	2.5977	0.0027583	21.962	0.96388	70.891	-0.011046
		Min	0.52067	0.0026911	-19.41	0.34641	-71.294	-0.011311
bmy422	-A-	Max	-0.78083	-0.00084771	24.419	1.5017	78.411	-0.0019963
		Min	-3.088	-0.00092513	-23.042	0.76756	-72.009	-0.0021884
	-B-	Max	3.088	0.00092513	23.042	-0.76756	73.667	-0.003598
		Min	0.78083	0.00084771	-24.419	-1.5017	-89.157	-0.003918
bmy441	-A-	Max	-0.78083	-0.00084771	23.042	1.5017	89.157	-0.003598
		Min	-3.088	-0.00092513	-24.419	0.76756	-73.667	-0.003918
	-B-	Max	3.088	0.00092513	24.419	-0.76756	72.009	-0.0019963
		Min	0.78083	0.00084771	-23.042	-1.5017	-78.411	-0.0021885
bmy432	-A-	Max	0.91958	0.011138	17.482	1.1547	105.92	0.025372
		Min	-3.1177	0.010884	-32.889	-0.31416	-48.856	0.024484
	-B-	Max	3.1177	-0.010884	32.889	0.31416	111.15	0.048141
		Min	-0.91958	-0.011138	-17.482	-1.1547	-66.524	0.047349
bmy431	-A-	Max	0.91958	0.011138	32.889	1.1547	66.524	0.048141
		Min	-3.1177	0.010884	-17.482	-0.31416	-111.15	0.047349
	-B-	Max	3.1177	-0.010884	17.482	0.31416	48.856	0.025372
		Min	-0.91958	-0.011138	-32.889	-1.1547	-105.92	0.024484

APPENDIX D

DTHA RESULTS FROM SEISMOSTRUCT

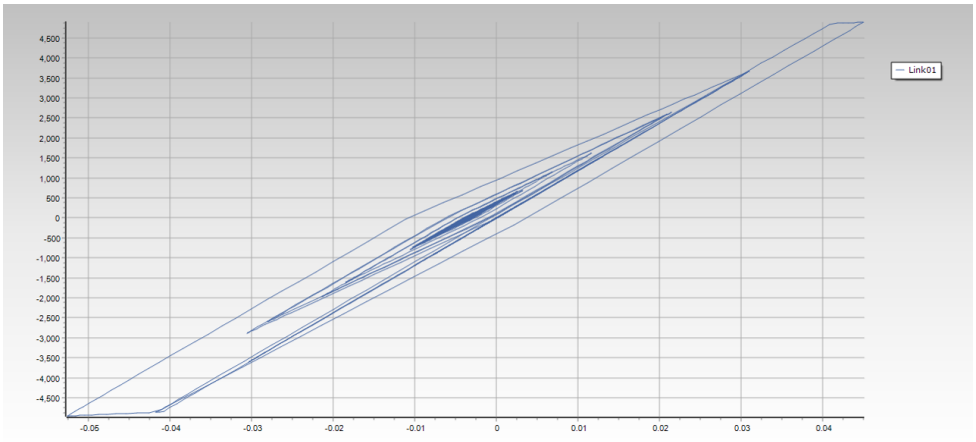

(a) Ground motion 01

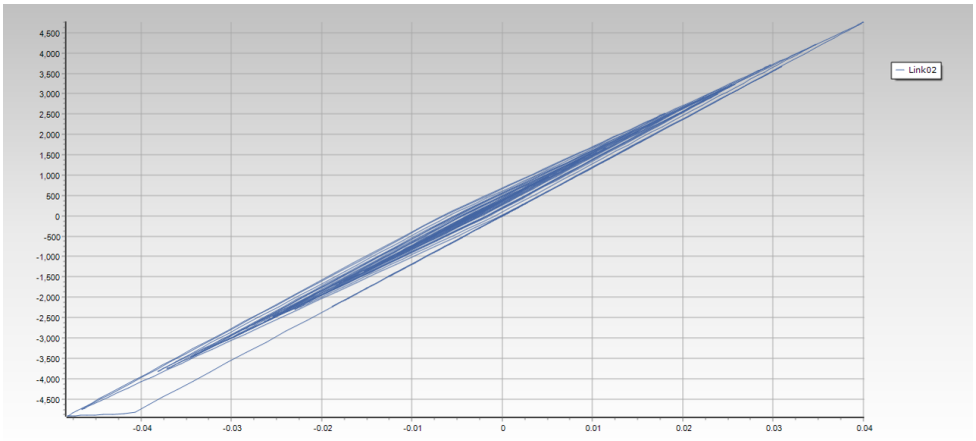

(b) Ground motion 02

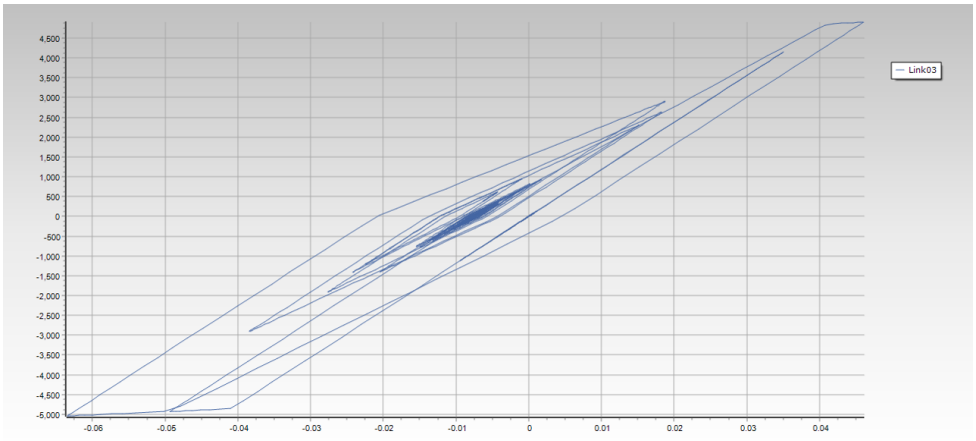

(c) Ground motion 03

Figure D.1: Hysteretic curves of SDoF systems for scaling factor $SF = 1.0$ in X direction

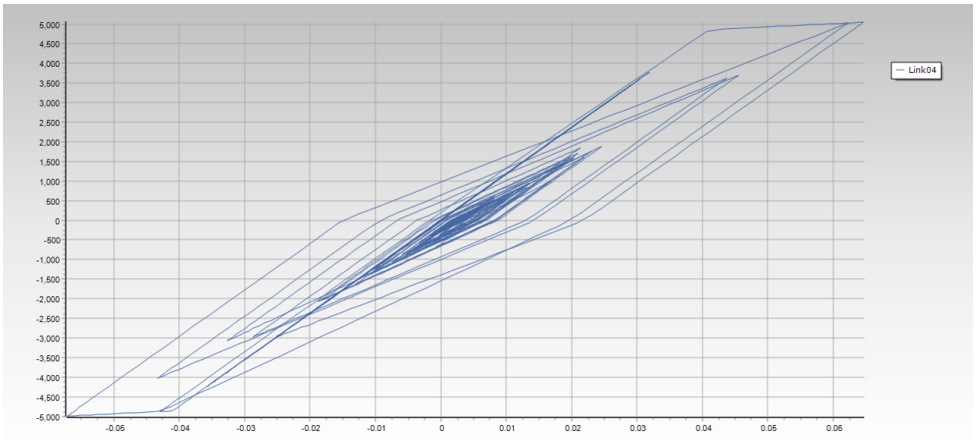

(a) Ground motion 04

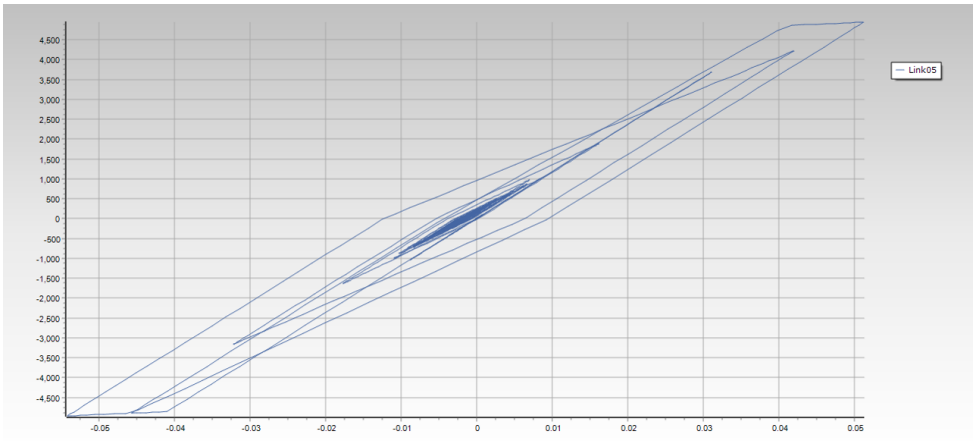

(b) Ground motion 05

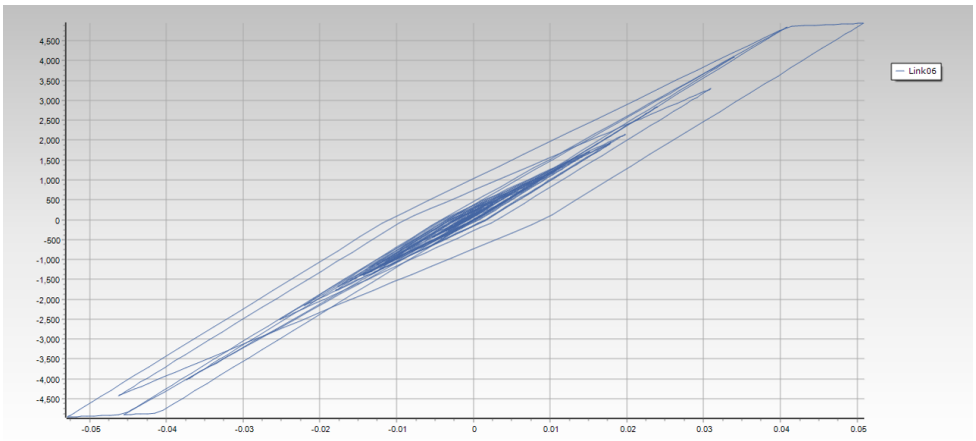

(c) Ground motion 06

Figure D.2: Hysteretic curves of SDoF systems for scaling factor $SF = 1.0$ in X direction

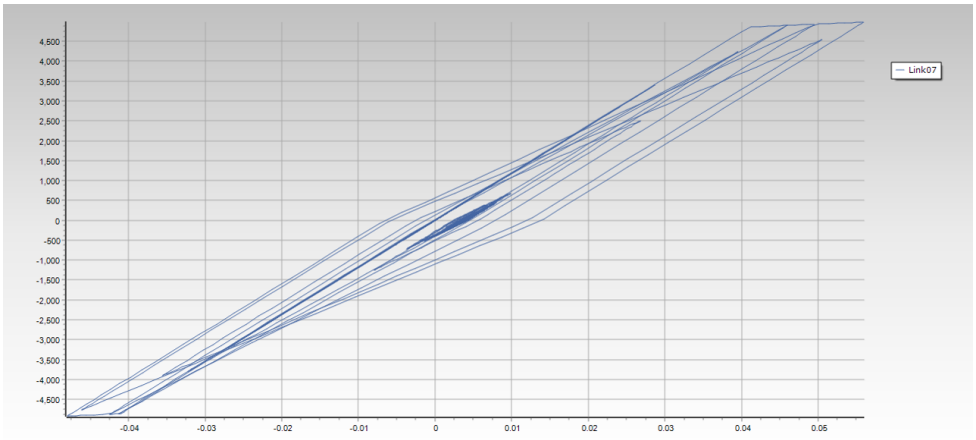

(a) Ground motion 07

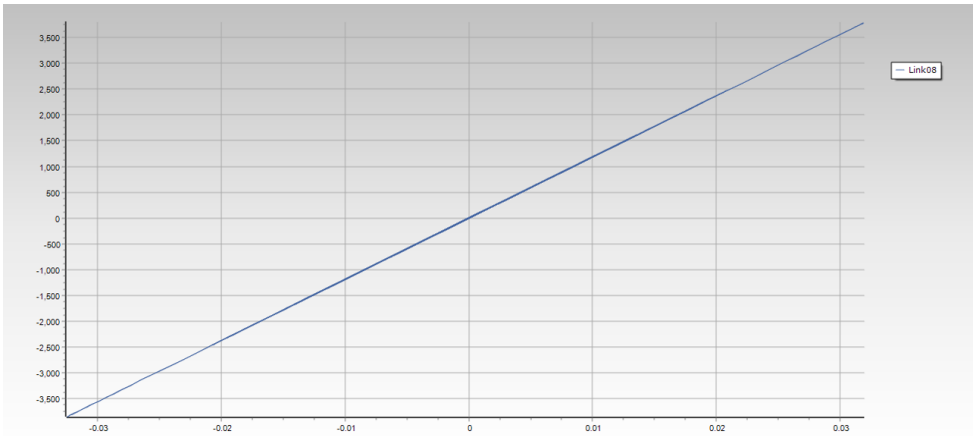

(b) Ground motion 08

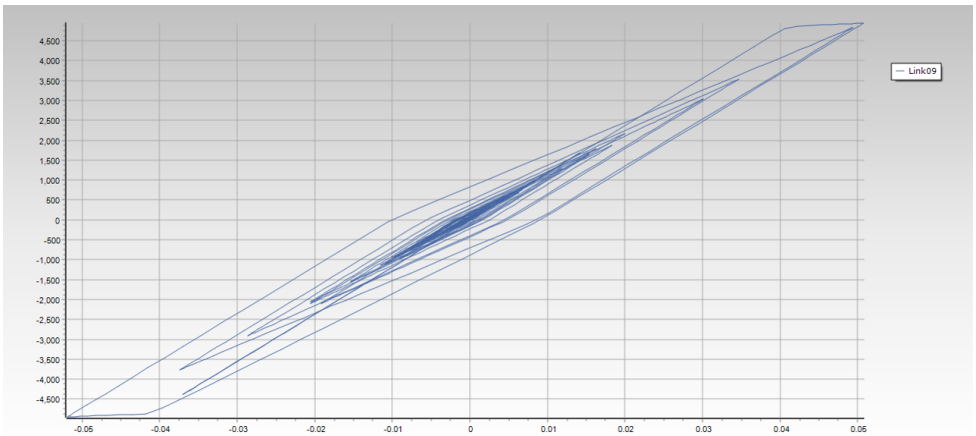

(c) Ground motion 09

Figure D.3: Hysteretic curves of SDoF systems for scaling factor $SF = 1.0$ in X direction

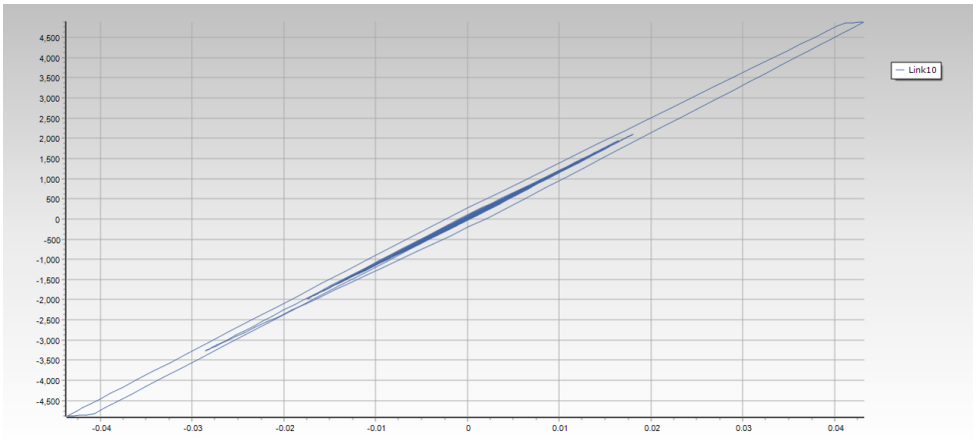

(a) Ground motion 10

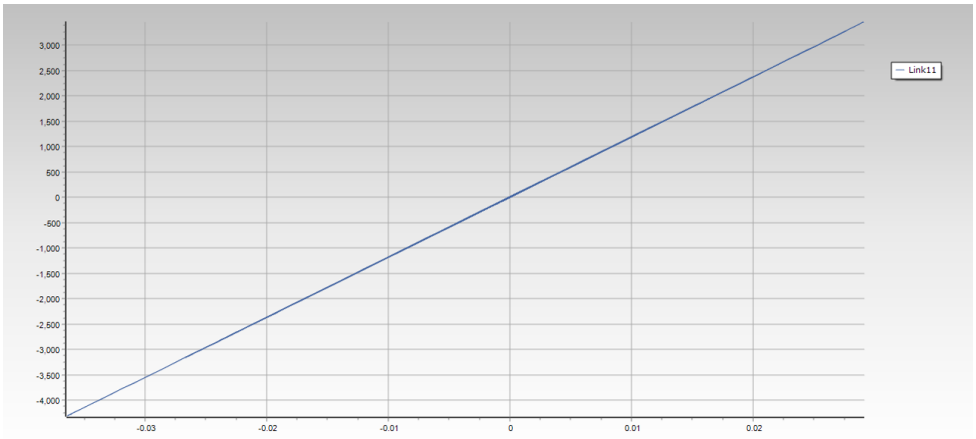

(b) Ground motion 11

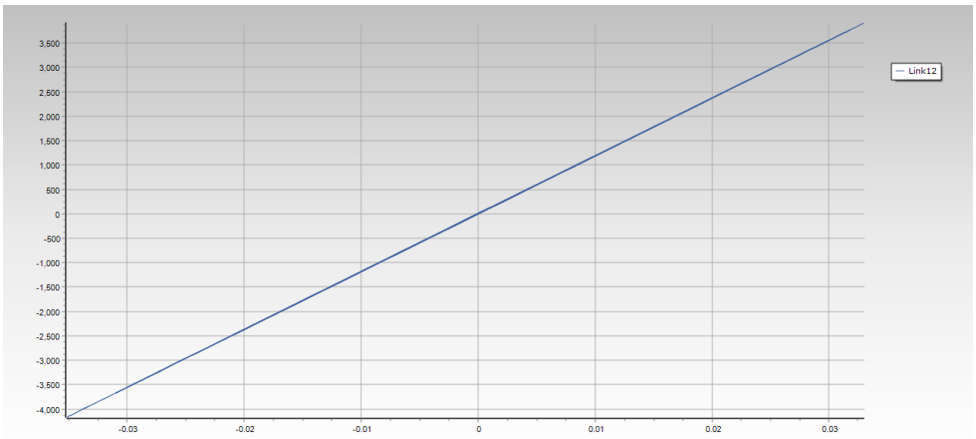

(c) Ground motion 12

Figure D.4: Hysteretic curves of SDoF systems for scaling factor $SF = 1.0$ in X direction

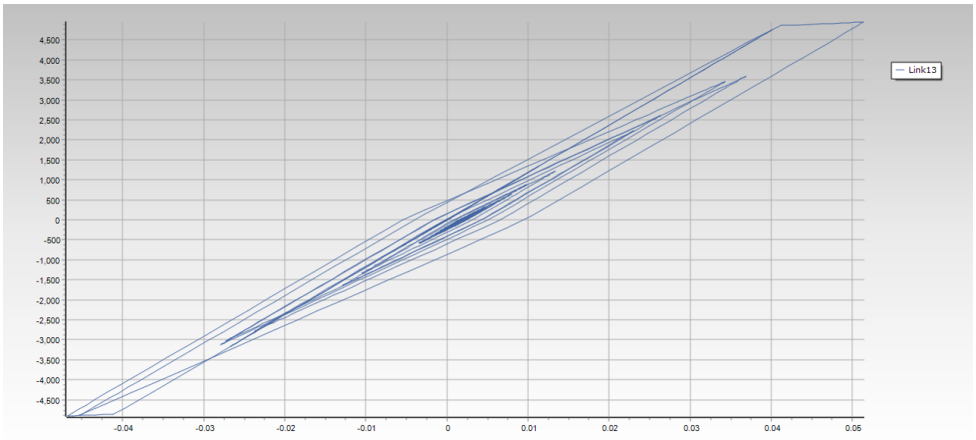

(a) Ground motion 13

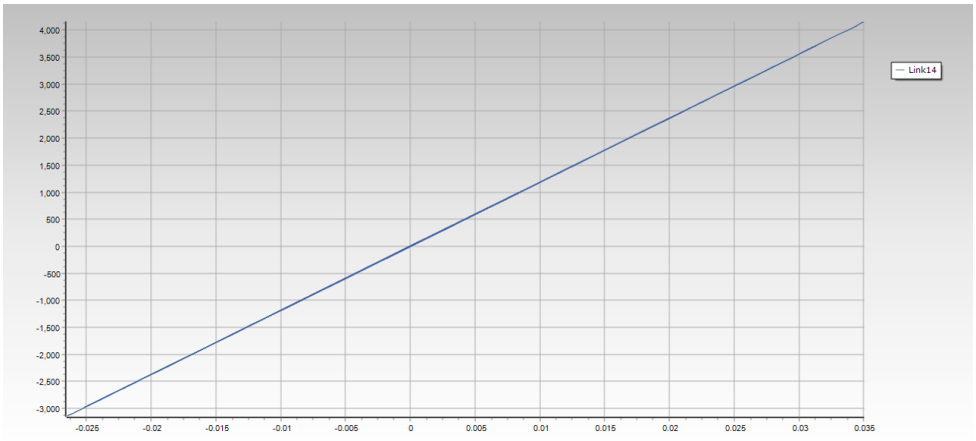

(b) Ground motion 14

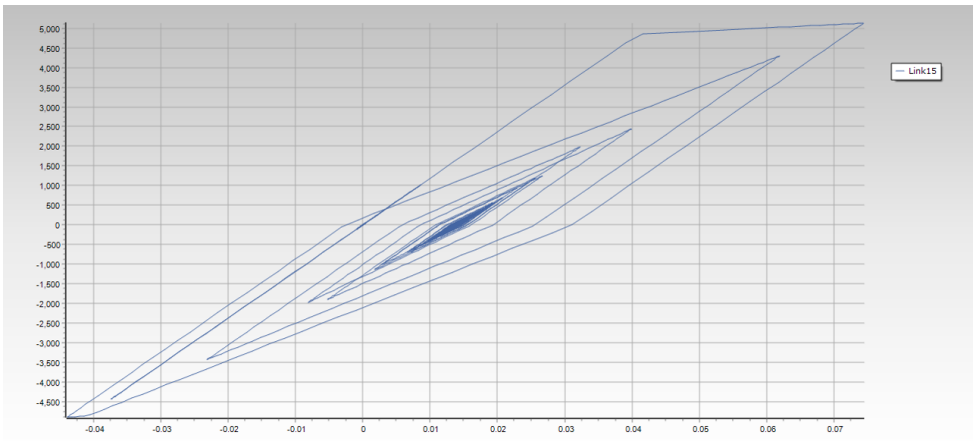

(c) Ground motion 15

Figure D.5: Hysteretic curves of SDoF systems for scaling factor $SF = 1.0$ in X direction

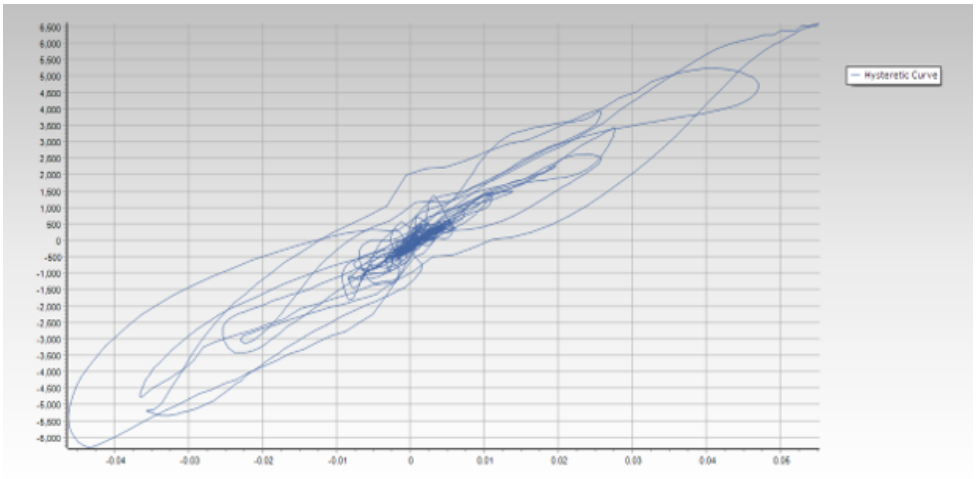

(a) Ground motion 01

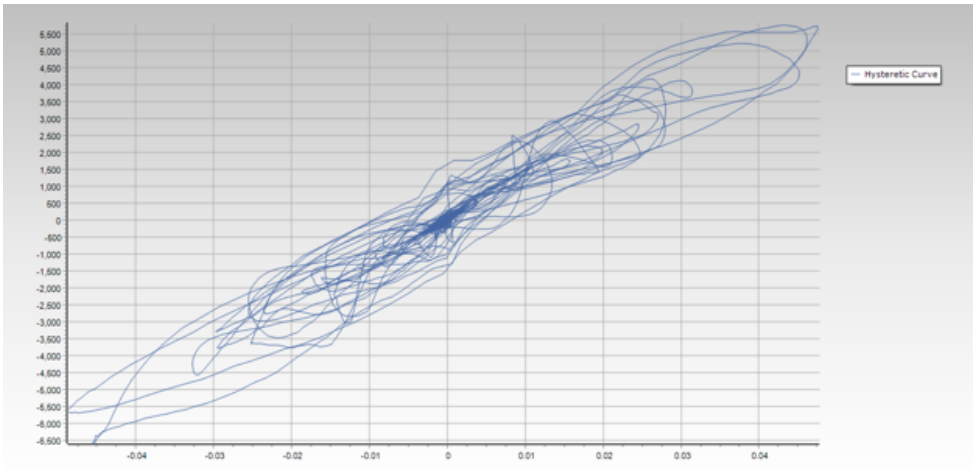

(b) Ground motion 02

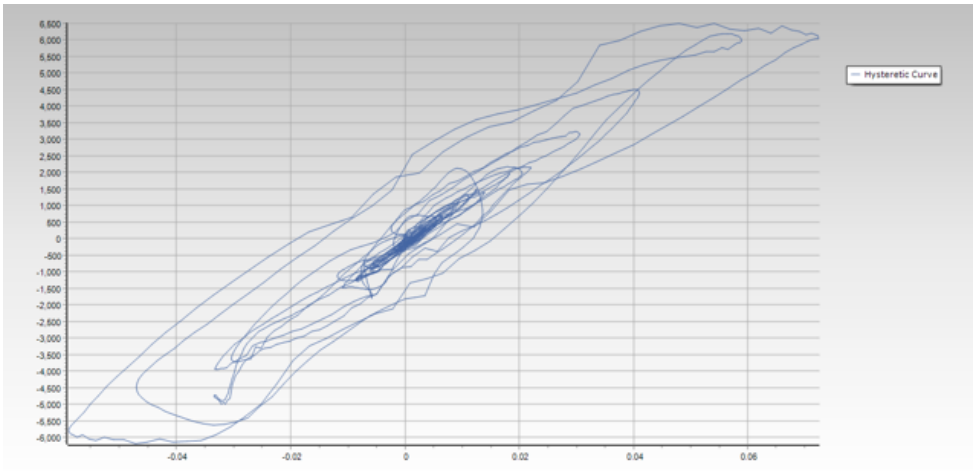

(c) Ground motion 03

Figure D.6: Hysteretic curves in MDoF (building) for scaling factor $SF = 1.0$ in X direction

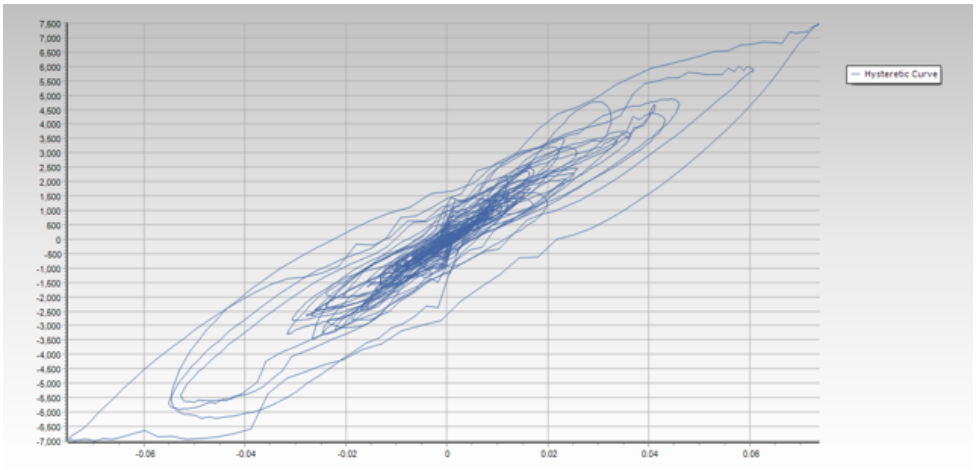

(a) Ground motion 04

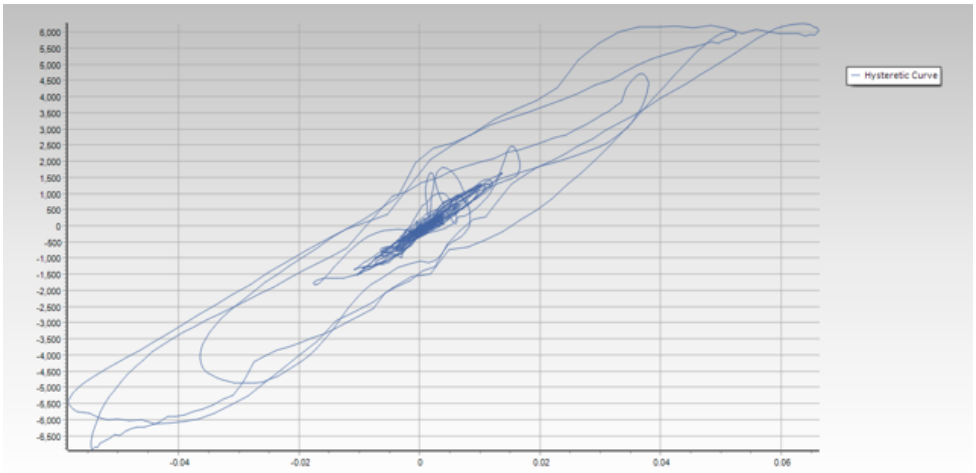

(b) Ground motion 05

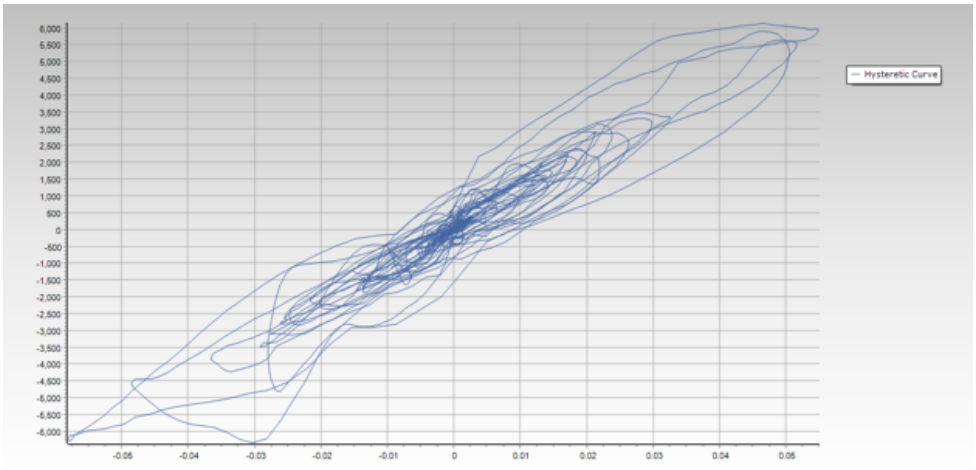

(c) Ground motion 06

Figure D.7: Hysteretic curves in MDoF (building) for scaling factor $SF = 1.0$ in X direction

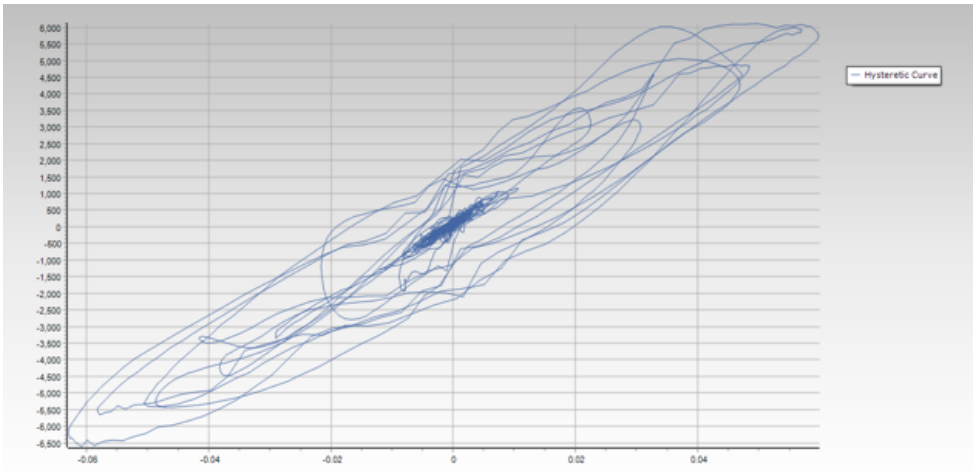

(a) Ground motion 07

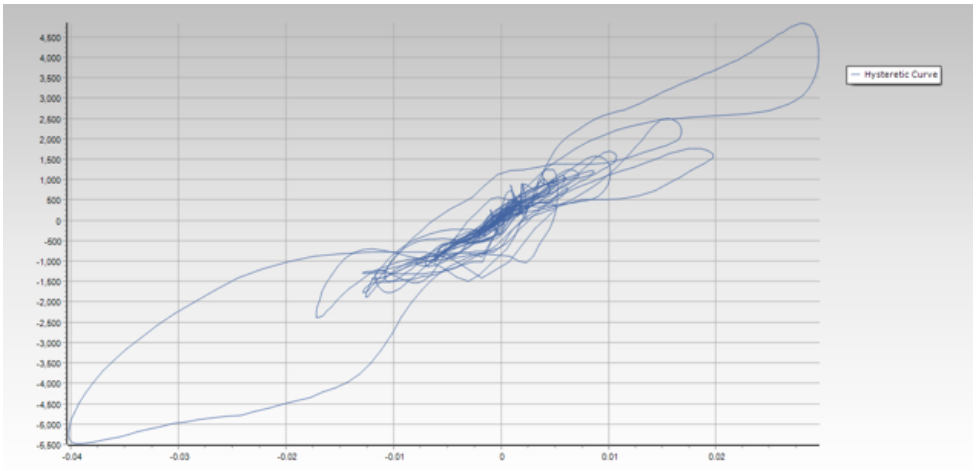

(b) Ground motion 08

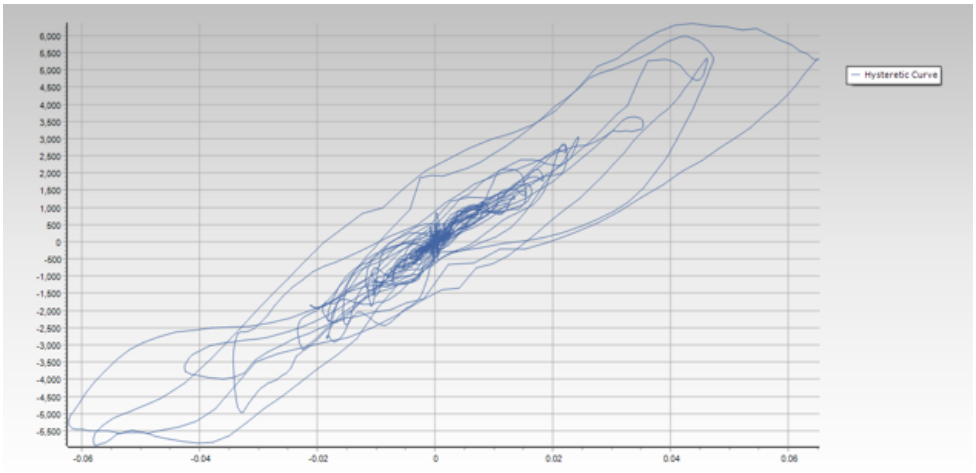

(c) Ground motion 09

Figure D.8: Hysteretic curves in MDoF (building) for scaling factor $SF = 1.0$ in X direction

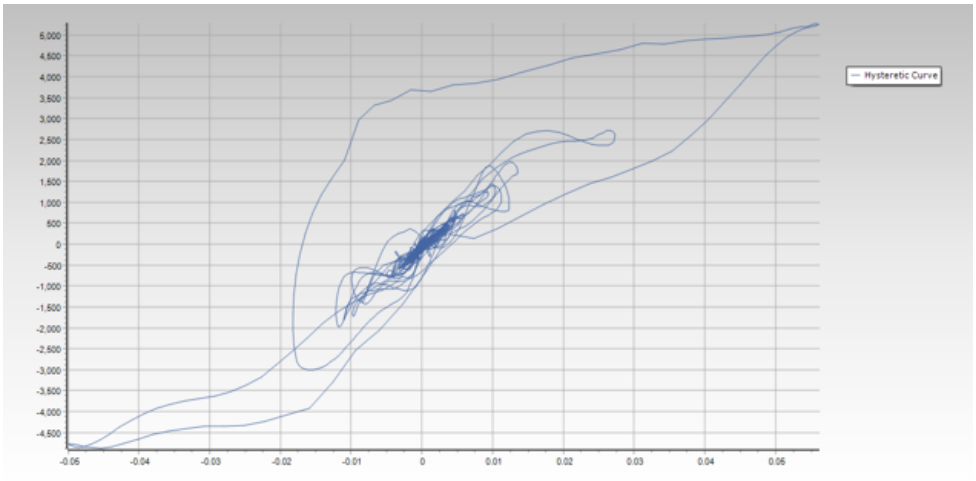

(a) Ground motion 10

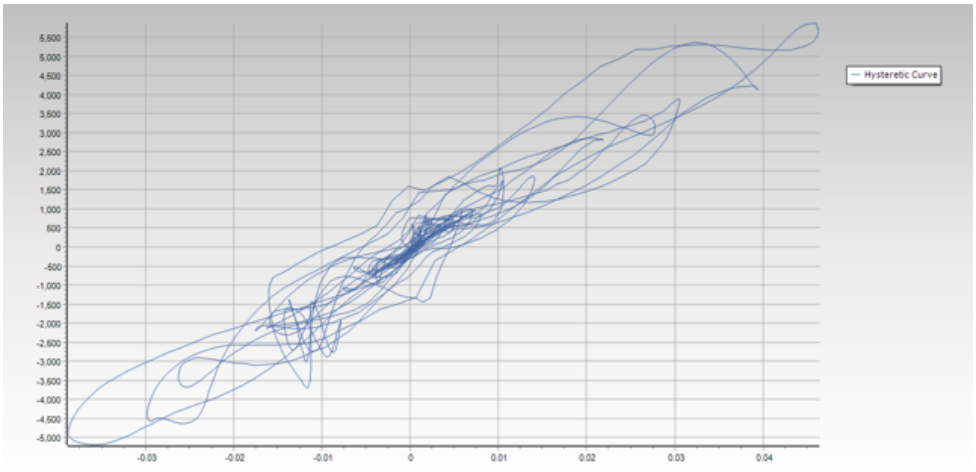

(b) Ground motion 11

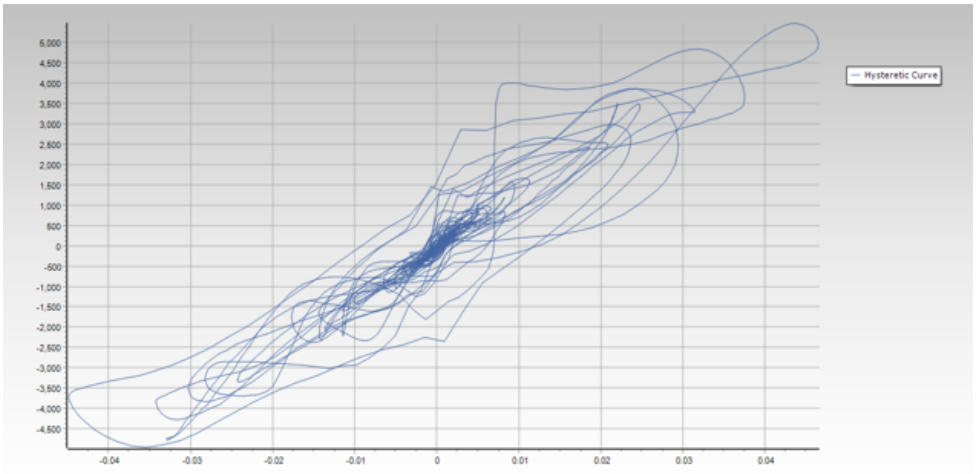

(c) Ground motion 12

Figure D.9: Hysteretic curves in MDoF (building) for scaling factor $SF = 1.0$ in X direction

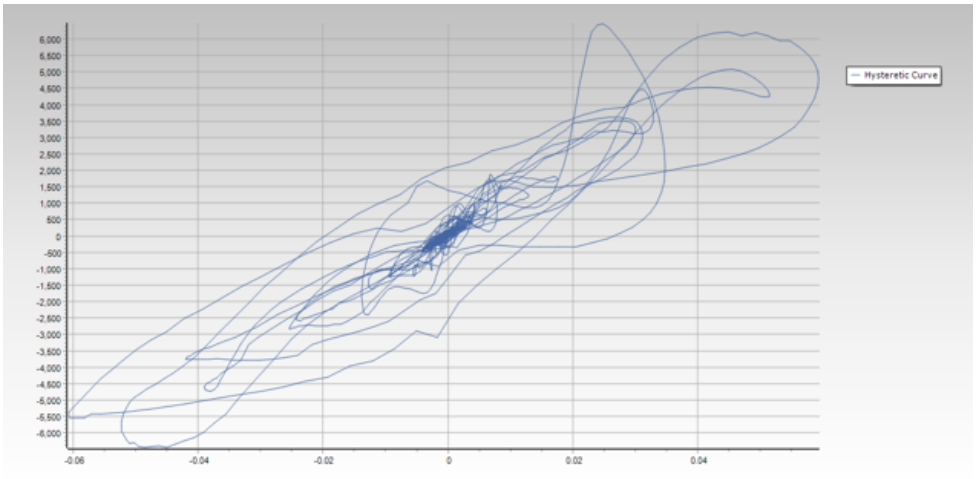

(a) Ground motion 13

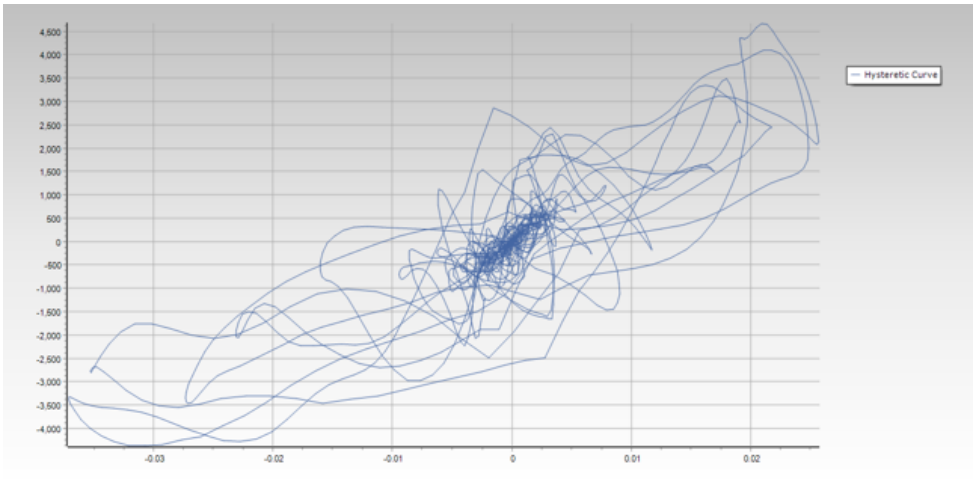

(b) Ground motion 14

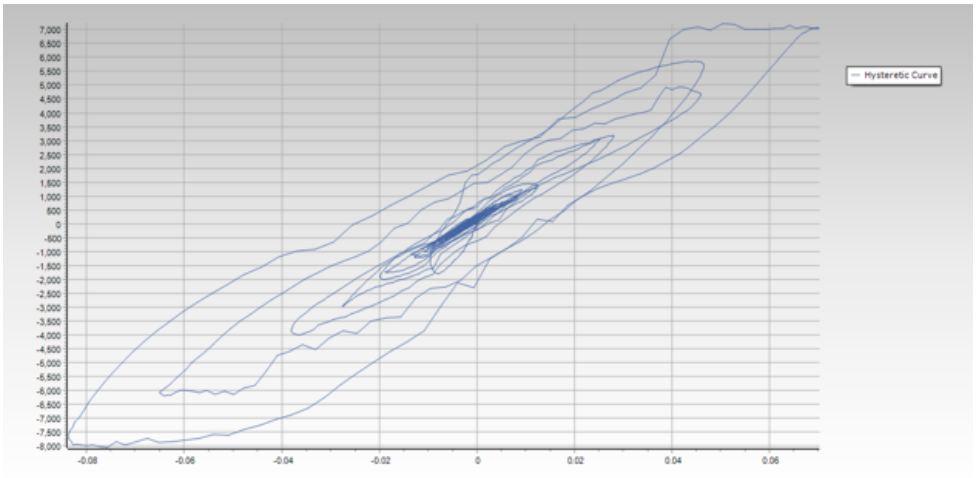

(c) Ground motion 15

Figure D.10: Hysteretic curves in MDoF (building) for scaling factor $SF = 1.0$ in X direction

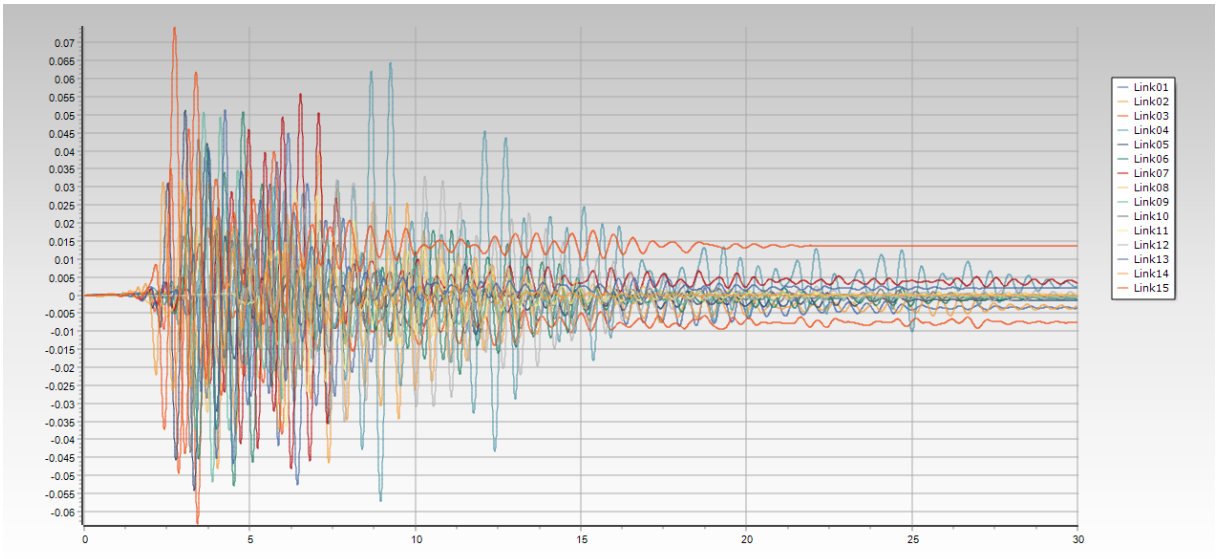

(a) X direction

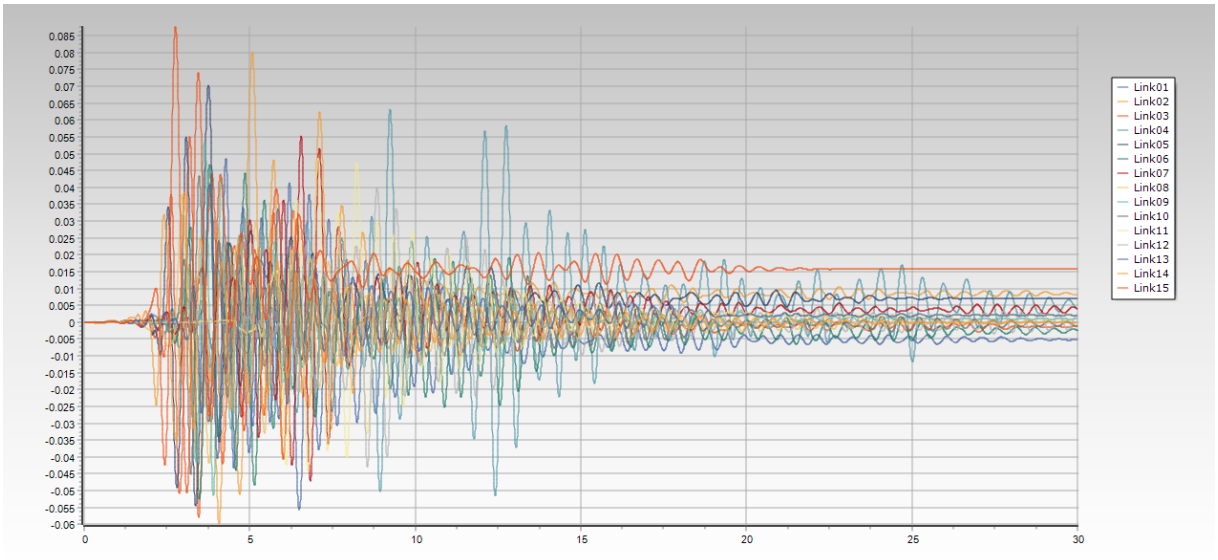

(b) Y direction

Figure D.11: DTHA results of SDoF systems for scaling factor $SF = 1.0$

BIBLIOGRAPHY

[1] J. Almeida. Lgciv2042. dynamic of structures (slides). *Université Catolique de Louvain. Belgium*, 2021-2022.

[2] J. Almeida. Lgciv2046. earthquake engineering (slides). *Université Catolique de Louvain. Belgium*, 2021-2022.

[3] J. Almeida and A. A. Correia. Displacement-based vs force-based formulations. concentrated vs distributed plasticity (slides). *UCLouvain and Laboratório Nacional de Engenharia civil. Italy*, 2021.

[4] Y. Bozorgnia and V. V. Bertero. *Earthquake engineering: from engineering seismology to performance-based engineering*. CRC press, 2004.

[5] A. K. Chopra. *Dynamics of structures*. Pearson Education India, 2007.

[6] A. Correia. Flexural design of reinforced concrete cross-sections (draf version). 2022.

[7] S. De Visscher, J. Saraiva Esteves Pacheco De Almeida, and A. Correia. Harmonisation des approches force et déplacement selon la seconde génération de l'eurocode 8: application aux ossatures en béton armé.

[8] M. Dolšek and P. Fajfar. In2-a simple alternative for ida. In *13th world conference on earthquake engineering*, pages 1–6, 2004.

[9] M. N. Fardis. *Seismic design, assessment and retrofitting of concrete buildings: based on EN-Eurocode 8*, volume 8. Springer, 2009.

[10] L. F. Ibarra, R. A. Medina, and H. Krawinkler. Hysteretic models that incorporate strength and stiffness deterioration. *Earthquake engineering & structural dynamics*, 34(12):1489–1511, 2005.

[11] D. G. Lignos and H. Krawinkler. Deterioration modeling of steel components in support of collapse prediction of steel moment frames under earthquake loading. *Journal of Structural Engineering-Reston*, 137(11):1291, 2011.

[12] C. S. N1141. pren1998-1-1:2022: Eurocode 8: Earthquake resistance design of structures (working draft). 2022.

[13] T. Paulay and M. N. Priestley. *Seismic design of reinforced concrete and masonry buildings*, volume 768. Wiley New York, 1992.

[14] B. Standard. Eurocode 2: Design of concrete structures—. *Part 1*, 2004.

[15] B. Standard et al. Eurocode. basis of structural design. *Eurocode 0*, 2002.

[16] E. Standard. Eurocode 8: Design of structures for earthquake resistance-part 1: general rules, seismic actions and rules for buildings. *Brussels: European Committee for Standardization*, 2005.

[17] E. Standard. Eurocode 8: Design of structures for earthquake resistance—part 3: Assessment and retrofitting of buildings. 2010.

[18] B. S. Taranath. *Structural analysis and design of tall buildings: Steel and composite construction*. CRC press, 2016.

[19] H. Varum, H. Maranhao, and J. Melo. Eurocodes balkan summer school: Eurocodes 2 and eurocode 8- design reinforced concrete buildings-worked examples (slides). 2021.

UNIVERSITÉ CATHOLIQUE DE LOUVAIN
École polytechnique de Louvain
Rue Archimède, 1 bte L6.11.01, 1348 Louvain-la-Neuve, Belgique | **www.uclouvain.be/epl**